

**DEVELOPMENT OF AN INTEGRATED AUTOMATIC IMAGE REGISTRATION
SCHEME**

BY

**AJAYI, Oluibukun Gbenga
PhD/SET/2015/782**

**DEPARTMENT OF SURVEYING AND GEOINFORMATICS
FEDERAL UNIVERSITY OF TECHNOLOGY
MINNA**

APRIL, 2019

**DEVELOPMENT OF AN INTEGRATED AUTOMATIC IMAGE REGISTRATION
SCHEME**

BY

**AJAYI, Oluibukun Gbenga
PhD/SET/2015/782**

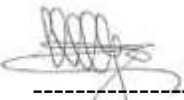
**A THESIS SUBMITTED TO THE POSTGRADUATE SCHOOL, FEDERAL
UNIVERSITY OF TECHNOLOGY, MINNA, NIGERIA, IN PARTIAL
FULFILLMENT OF THE REQUIREMENTS FOR THE AWARD OF THE DEGREE
OF DOCTOR OF PHILOSOPHY (PhD) IN SURVEYING AND GEOINFORMATICS**

APRIL, 2019

DECLARATION

I hereby declare that this thesis titled: “**Development of an Integrated Automatic Image Registration Scheme**” is a collection of my original research work and it has not been presented for any other qualification anywhere. Information from other sources (published or unpublished) has been duly acknowledged.

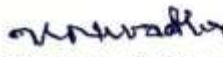
AJAYI, Oluibukun Gbenga
PhD/SET/2015/782
FEDERAL UNIVERSITY OF TECHNOLOGY
MINNA, NIGERIA


-----29/04/2019-
Signature & Date

CERTIFICATION

The thesis titled: “**Development of an Integrated Automatic Image Registration Scheme**”
by: AJAYI, Oluibukun Gbenga (PhD/SET/2015/782) meets the regulations governing the
award of the degree of PhD of the Federal University of Technology, Minna and it is approved
for its contribution to scientific knowledge and literary presentation.

Prof. I. J. Nwadiator
MAJOR SUPERVISOR

 29-4-2019
Signature & Date

Dr. I. C. Onuigbo
CO-SUPERVISOR

 29-4-2019
Signature & Date

Dr. O. A. Kemiki
CO-SUPERVISOR

 3/5/19
Signature & Date

Dr. Y. D. Opaluwa
HEAD OF DEPARTMENT

 3/5/19
Signature & Date

Prof. R. E. Olagunju
DEAN, SCHOOL OF ENVIRONMENTAL
TECHNOLOGY

 23-05-2019
Signature & Date

Engr. Prof. S. Sadiku
DEAN OF POSTGRADUATE SCHOOL

 22/07/19
Signature & Date

DEDICATION

This Thesis is dedicated to God, to my Parents, Elder Michael Oke Ajayi and Mrs Comfort Bolatito Ajayi, who are very keen about education, and to everyone in the pursuit of knowledge.

ACKNOWLEDGEMENTS

I give all the glory to God, who did not just create me but also sent His only begotten Son, Jesus Christ to redeem my soul and for also giving me the divine strength and enablement to embark on the journey of life and this academic pursuit.

I am highly grateful to my Major Supervisor, Professor Ifeanyi Jonathan Nwadiakor and my co supervisors, Dr. Ifeanyi Chukwudi Onuigbo and Dr. Olurotimi Adebawale Kemiki for their guidance, patience, constructive comments and consistent fatherly encouragements. Drinking from your wells of deep wisdom, resourcefulness and mentorship is indeed a great and rare privilege. I cannot but express my deep appreciation to the Head, Department of Surveying and Geoinformatics, Dr. Yusuf Drisu Opaluwa for his mentorship. You have been used by God to be a guide to me from the commencement of this programme and I am sincerely grateful.

I also acknowledge the kind gesture of the Commonwealth Association of Surveying and Land Economy (CASLE) who in collaboration with the Faculty of Environment and Technology (FET), University of the West of England (UWE), Bristol, United Kingdom, awarded me a scholarship for a brief academic visit to UWE. I am indeed grateful to the Pro Vice-Chancellor and Executive Dean; Professor Paul Olomolaiye, my academic host; Dr Mark Palmer and the entire members of the Faculty for making my stay very comfortable, resourceful and for giving me access to their research facilities which I used for most of the model experimentation and analysis of this research. I particularly appreciate their constructive comments which has helped in improving the quality of this thesis. I also appreciate the assistance of Surv. Kuta Abdullahi, who facilitated my access to the Photogrammetry Laboratory of Nottingham Geospatial Institute, University of Nottingham, United Kingdom where part of the model experimentation was also carried out.

I appreciate the Board of Trustees, Aubrey Barker Funds, under the Chairmanship of Professor Ian Dowman of University College London (UCL), United Kingdom, for the research grant awarded to me which was highly instrumental to the success of this research. I also appreciate the Surveyors Council of Nigeria (SURCON) and the Ekiti State Government, for the scholarship award given me to for this research. I cannot also forget the impact of the NEEDS assessment funds awarded to me by the management of the Federal University of Technology, Minna and I am indeed grateful for this. This research would have suffered great setbacks without these financial supports.

I also appreciate the effort of Mr. Omoware Bolarinwa, who was of great assistance to me during coding phase of this research and Professor A. M. Aibinu for his insights and guidance. I am grateful to Professor Ahmed Musa, Professor Y. A. Sanusi, Prof. (Mrs) S. N. Zubairu. Professor E. E. Udensi, Dr. R. A. Jimoh, Dr O. F. Adedayo, Dr. Luqman Oyewobi, Dr. B. J. Olawuyi, Dr. I. B. Mohammed and all the members of staff of the School of Environmental Technology who have contributed immensely to the success of this research. I am also grateful to Professor Joel Igbokwe, for his insightful comments and valuable contributions as the external examiner for this thesis.

I am particularly indebted to my Parents (Elder and Mrs M. O. Ajayi), for their undying love, prayers, unwavering support and the selfless sacrifice they paid to ensure that I am educated. The seeds sown are fast growing and bringing forth fruits. I thank my Siblings and In-laws for their fervent support and prayers.

Finally, my special gratitude goes to my darling and understanding Wife; Mrs Olufunmilola Oyenike Ajayi, and my lovely daughter; Gratia Ajayi for their kind understanding, relentless prayers, consistent support and encouragement. Thank you for the sacrifices you paid to ensure that this programme is successful, I am indeed grateful.

ABSTRACT

Photogrammetric applications in mapping and earth observation often result into series of overlapping image pairs that must be accurately fused together to obtain mosaics, which provide holistic and stereoscopic view of the geographical scene of interest, and also ensure accurate spatial details extraction. Manual approach to this fusion is time consuming, rigorous, and very prone to mismatch, hence, the need for the complete automation of the entire image registration process. This study presents the development of an integrated automatic image registration scheme which is aimed at improving the overall speed and accuracy of an image registration process. The Modified Harris and Stephens Corner Detector (MHCD), Speeded Up Robust Features (SURF) and Scale Invariant Feature Transform (SIFT) were independently implemented as the feature descriptors in the development of the image registration scheme. These feature descriptors were then individually integrated with epipolar constraints in the development of hybrid algorithms for fast and accurate automatic image registration. Other algorithms integrated in the development of the image registration scheme are the Random Sampling Consensus (RANSAC), which is a model fitting algorithm for exclusion of outliers from the extracted corresponding features, Sum of Absolute Difference (SAD) as the feature matching metric, Bilinear interpolation for image resampling and the eight-point algorithm for the estimation of fundamental matrix. The developed image registration algorithms were tested in two different registration campaigns using images extracted from Google Earth and image pairs acquired using a DJI Phantom 4 Unmanned Aerial vehicle (UAV), for the first and second campaigns respectively. The robustness of the image registration scheme was tested using the estimated speed, and the accuracy (using signed distances and Root Mean Square Errors (RMSE)) of the algorithms. The result of the first registration campaign shows that the integrated MHCD-epipolar algorithm, with RMSE of $6.645046828487534 \times 10^{-14}$, was more accurate and 4 times faster (with a speed of 463 milliseconds) than the conventional MHCD-based image registration algorithm while the integrated SURF-epipolar algorithm (with a speed of 1153 milliseconds) and SIFT-epipolar algorithm (with a speed of 1630 milliseconds) were 2.5 times and 2 times faster than the conventional SURF and SIFT-based image registration algorithms respectively. For the second registration campaign, the integrated MHCD-epipolar algorithm with a RMSE of $5.74974632623059 \times 10^{-14}$ also proved to be more accurate and approximately 4 times faster (with a speed of 1770 milliseconds) than the conventional MHCD algorithm (with a speed of 6649 milliseconds) while the integrated SURF-epipolar algorithm was more accurate (with a RMSE of $2.744940097552583 \times 10^{-13}$) and approximately 2 times faster (with a speed of 7055 milliseconds) than the conventional SURF algorithm (with a speed of 13109 milliseconds). The integrated SIFT-epipolar algorithm was also more accurate (with a RMSE of $1.1544770733452483 \times 10^{-13}$) and approximately 2 times faster (with a speed of 5923 milliseconds) than the conventional SIFT algorithm. The result obtained shows that the developed integrated epipolar correlation image registration algorithms outperformed the conventional feature descriptors in terms of speed and accuracy of the image registration. The research recommends that the integrated MHCD-epipolar correlation image registration algorithm should be adopted when both speed and accuracy of the image registration is of specific interest to Photogrammetrists and image registration analysts.

TABLE OF CONTENTS

Content	Page
Cover Page	i
Title page	ii
Declaration	iii
Certification	iv
Dedication	v
Acknowledgements	vi
Abstract	viii
Table of Contents	ix
List of Tables	xiv
List of Figures	xvi
List of Abbreviations	xx
List of Symbols	xxii
List of Appendices	xxv
CHAPTER ONE	1
1.0 INTRODUCTION	1
1.1 Background to the Study	1
1.2 Statement of the Problem	3
1.3 Aim and Objectives	5
1.4 Justification for the Study	6
1.5 Assumption and Delimitation to the Study	7
1.6 Scope of the Study	8

CHAPTER TWO	10
2.0 LITERATURE REVIEW	10
2.1 Theoretical Framework	12
2.1.1 Feature detection and extraction	12
2.1.2 Feature matching	16
2.1.3 Image resampling and interpolation	19
2.2 Geometric Transformation	20
2.2.1 Transformation functions	21
2.2.2 Mathematical expression of transformation elements	24
2.3 Optimization Techniques	27
2.4 Image Registration Approaches	30
2.5 Classification of Image Registration Algorithms	30
2.6 Classification of Image Registration According to Modalities	31
2.6.1 Monomodal registration	31
2.6.2 Multimodal image registration	32
2.7 The Concept of Epipolar Geometry	33
2.7.1 Fundamental matrix	36
2.7.1.1 Estimating fundamental matrix in terms of the essential matrix	37
2.7.1.2 Computing fundamental matrix from corresponding points	39
2.7.2 Coplanarity constraint from uncalibrated camera	42
2.7.2.1 Linearization of coplanarity condition equation	46
2.7.3 Camera calibration	58
2.7.3.1 Extrinsic parameters	58
2.7.3.2 Intrinsic parameters	60
2.7.3.3 Ideal perspective projection	60

2.8	Review of Related Studies on Epipolar Geometry	63
2.8.1	Principle and applications of epipolar image correlation	63
2.8.2	Automatic extraction of epipolar geometry and estimation of fundamental matrix	65
2.9	Review of Related Studies on Image Registration Applications	68
2.9.1	Evolution of image registration applications from inception till year 1999	68
2.9.2	Summary of the advances in image registration applications from 2000 - 2009	71
2.9.3	Summary of the advances in image registration from 2010 till date (2019)	75
2.10	Identified Research Gaps in Image Registration	81
	CHAPTER THREE	83
3.0	MATERIALS AND METHODS	83
3.1	Automatic Registration of Overlapping Images Using Three Different Feature Descriptors	83
3.1.1	Model formulation	84
3.1.2	Implementation of the feature detection and extraction algorithms	85
3.1.2.1	Modified Harris corner detection (MHCD) algorithm	86
3.1.2.2	Scale invariant feature transform algorithm (SIFT)	87
3.1.2.3	Speeded up robust feature (SURF) detection and extraction algorithm	89
3.1.3	Filtering of detected and extracted feature points	90
3.1.4	Feature matching	91
3.1.5	Model estimation	91
3.1.6	Image interpolation	91
3.2	Automatic Image Registration using Integrated Epipolar Correlation Algorithms	92
3.2.1	Epipolar correlation-based image registration model formulation	93
3.2.1.1	Epipolar image rectification of an un-calibrated stereo pairs	94
3.2.1.2	One dimensional automatic scanning and correspondence search	97
3.2.1.3	Formulation of transformation homography	98

3.2.1.4	Image registration using the inverse of the formulated	99
3.2.2	Estimation of fundamental matrix	100
3.3	Validation of Model and Performance Evaluation	101
3.4	Data Used for Model Experimentation	102
3.5	Model Packaging into Software Development	107
3.5.1	System specifications	108
3.5.2	Data specifications	109
CHAPTER FOUR		110
4.0	RESULTS AND DISCUSSION	110
4.1	Model Outlook	110
4.2	Automatic Image Registration Using Three Selected Feature Detection and Extraction Algorithms	111
4.2.1	Automatic image registration using Modified Harris Corner Detector (MHCD) (first registration campaign)	111
4.2.2	Automatic image registration using Scale Invariant Feature Transform (SIFT) (first registration campaign)	115
4.2.3	Automatic image registration using Speeded Up Robust Features (SURF) (first registration campaign)	118
4.3	Automatic Image Registration based on the Integrated Epipolar Correlation Algorithms	122
4.3.1	Integrated MHCD-epipolar correlation image registration scheme (first registration campaign)	123
4.3.2	Integrated SURF-epipolar correlation image registration scheme (first campaign)	125
4.3.3	Integrated SIFT-epipolar correlation image registration scheme (first registration campaign)	127
4.4	Performance Evaluation of the Developed Schemes using the Integrated Algorithms	129
4.4.1	Accuracy evaluation of the schemes using automatically extracted point correspondences (first registration campaign)	130
4.4.2	Accuracy evaluation of the schemes using measured conjugate point data	131

4.4.3	Performance evaluation of the schemes using processing run time	140
4.5	Second Image Registration Campaign	141
4.5.1	Automatic image registration using UAV acquired image pairs	141
4.5.2	Automatic image registration based on the integrated epipolar correlation algorithms (second image registration campaign)	151
4.6	Performance evaluation of the developed scheme using UAV images	155
4.6.1	Performance evaluation of the algorithms using processing time (second registration campaign)	164
4.7	Performance evaluation of the algorithms using PCs of different RAM configuration	165
CHAPTER FIVE		168
5.0	CONCLUSION AND RECOMMENDATIONS	168
5.1	Conclusions	168
5.1.1	Effect of feature descriptors on the developed image registration scheme	168
5.1.2	Effect of the developed integrated algorithms on the automatic image registration	169
5.1.3	Performance evaluation of the developed image registration scheme	170
5.2	Recommendations	171
5.3	Contributions to Knowledge	172
REFERENCES		173

LIST OF TABLES

Table		Page
2.1	Major characteristics of some of the widely-used feature detection and extraction algorithms	15
2.2	Weighted analysis of the qualities of selected feature descriptors	16
2.3	Matching methods	17
2.4	Mathematical Expression of Correlation-Based Similarity Measures	18
2.5	Characteristics of various types of 2D transformation functions	26
3.1	GCPs used for the first image registration campaign	106
3.2	GCPs used for the second image registration campaign	107
4.1	Image locations of measured conjugate points and their signed distances (MHCD)	134
4.2	Image locations of measured conjugate points and their signed distances (SIFT)	135
4.3	Image locations of measured conjugate points and their signed distances (SURF)	136
4.4	Image locations of measured conjugate points and their signed distances using MHCD-Epipolar correlation algorithm	137
4.5	Image locations of measured conjugate points and their signed distances using SURF-Epipolar correlation algorithm	138
4.6	Image locations of measured conjugate points and their signed distances using SIFT-epipolar correlation algorithm	139
4.7	Estimated processing run time of each of the automatic registration algorithms	140
4.8	Photo coordinates of measured conjugate points using MHCD (second image registration campaign)	158
4.9	Photo coordinates of measured conjugate points and their signed distances using SURF (second image registration campaign)	159
4.10	Photo coordinates of measured conjugate points and their signed distances using SIFT (second image registration campaign)	160
4.11	Coordinates of the conjugate points measured using MHCD-epipolar algorithm (second image registration campaign)	161
4.12	Coordinates of the conjugate points measured using SURF-epipolar algorithm (second image registration campaign)	162

4.13	Coordinates of the conjugate points measured using SIFT-epipolar algorithm (second image registration campaign)	163
4.14	Summary of the obtained RMSE and signed distances using the six algorithms	164
4.15	Estimated processing run time for each of the algorithms (second registration campaign)	165
4.16	Accuracy and estimated processing run time using a 4GB installed RAM PC	166
4.17	Accuracy and estimated processing run time using a 16GB installed RAM PC	167

LIST OF FIGURES

Figure		Page
2.1	Systematic review of literature	11
2.2	Basic automatic image registration process	12
2.3	Hierarchical formation of transformation types	27
2.4	Gradient based method of optimization techniques	28
2.5	Gradient free method of optimization techniques	29
2.6	Image registration approaches	30
2.7	Overview of image registration techniques classified according to modalities	33
2.8	Configuration epipolar geometry	35
2.9	Epipolar Geometry showing the epipolar lines (l and l'), epipoles (e_l and e_r), epipolar plane (π), origin of the camera frames (O_l and O_r) and the Baseline ($O_l O_r$)	35
2.10	Coplanarity condition	42
2.11	Expression of coplanarity condition with respect to a stereo pair	46
3.1	Process flow scheme for the automatic image registration model.	84
3.2	Flowchart of the feature-based auto-registration	85
3.3	Activity diagram of Harris corner detection algorithm	87
3.4	Activity diagram of Scale Invariant Feature Transform (SIFT) detector	88
3.5	Activity diagram for Speeded Up Robust Feature (SURF) detector	89
3.6	Activity diagram of Random Sampling Consensus (RANSAC) Model	90
3.7	Activity diagram for the implementation of bilinear interpolation model	92
3.8	Eight (8) point algorithm activity diagram for the estimation of fundamental matrix	101
3.9a	Image data of part of FUTMinna, Main campus, Minna (Base image)	104
3.9b	Image data of part of FUTMinna, Main campus, Minna (Search image)	104

3.10a	UAV acquired image of part of FUTMinna, Main Campus (Base image)	105
3.10b	UAV acquired image of part of FUTMinna, Main Campus (Search image)	105
4.1	Welcome page of the developed model	110
4.2	GUI of the developed model's working page showing the model's different modules	111
4.3	Associated image pairs containing the inliers and outliers (Using MHCD)	112
4.4	MHCD associated image pairs containing only the inliers (outliers excluded)	113
4.5	MHCD model's conjugate points register	113
4.6a	Mosaic generated using MHCD (displayed within the software environment)	114
4.6b	Mosaic generated using MHCD (exported out of the developed software)	114
4.7	Associated image pairs containing the inliers and outliers (Using SIFT Model)	116
4.8	SIFT's associated image pairs containing only the inliers (outliers excluded)	116
4.9	SIFT model's conjugate points register	117
4.10a	Mosaic generated in the developed software environment using SIFT	117
4.10b	Mosaic generated using SIFT Model	118
4.11	Associated image pairs containing the inliers and outliers (using SURF)	119
4.12	SURF's associated image pairs containing only the inliers (outliers excluded)	120
4.13	SURF Model's conjugate points register	120
4.14a	Mosaic generated in the developed software environment using SURF	121
4.14b	Mosaic generated using SURF Model	121
4.15	Integrated MHCD-Epipolar correlated inliers	124
4.16	Mosaic generated using integrated MHCD-epipolar correlation registration model	124
4.17	SURF-Epipolar correlated inliers	126
4.18	Mosaic generated using integrated SURF-epipolar correlation registration scheme	126
4.19	SIFT-Epipolar correlated inliers	128
4.20	Mosaic generated using integrated SIFT-epipolar correlation registration model	128

4.21	Engaging the stereo comparator	132
4.22	The rectified stereo pair	132
4.23	Coordinate input interface for keypoint measurement	133
4.24	Measured conjugate points	133
4.25	Associated image pairs using MHCD for the second registration campaign	143
4.26	Matched inliers using MHCD for the second registration campaigns	143
4.27	MHCD's conjugate point register for the second campaign	144
4.28	Mosaic generated using MHCD for the second registration campaign	144
4.29	Associated image pairs using SURF for the second registration campaign	145
4.30	Matched inliers using SURF for the second registration campaigns	146
4.31	SURF's conjugate point register for the second campaign	146
4.32	Mosaic generated using SURF for the second registration campaign	147
4.33	Associated image pairs using SIFT for the second registration campaign	148
4.34	Matched inliers using SIFT for the second registration campaigns	149
4.35	SIFT's conjugate point register for the second campaign	149
4.36	Mosaic generated using SIFT for the second registration campaign	150
4.37	Integrated MHCD-epipolar correlated inliers (second registration campaign)	151
4.38	Mosaic generated using integrated MHCD-epipolar model (second registration campaign)	152
4.39	Integrated SURF-epipolar correlated inliers (second registration campaign)	153
4.40	Mosaic generated using integrated SURF-epipolar scheme (second registration campaign)	153
4.41	Integrated SIFT-epipolar correlated inliers (second registration campaign)	154
4.42	Mosaic generated using integrated SIFT-epipolar scheme (second registration campaign)	155
4.43	The rectified stereo pair (second registration campaign)	156
4.44	Conjugate point measuring interface (second registration campaign)	157

LIST OF ABBREVIATIONS

Abbreviation	Meaning
MHCD	Modified Harris Corner Detector
SIFT	Scale Invariant Feature Transform
SURF	Speeded Up Robust Features
MSER	Maximally Stable Extremal Region
BRISK	Binary Robust Invariant Scalable Keypoint
ABRISK	Accelerated Binary Robust Invariant Scalable Keypoint
FREAK	Fast Retina Keypoint
RANSAC	Random Sampling Consensus
UAV	Unmanned Aerial Vehicle
SUSAN	Smallest Uni-Value Segment Assimilating Nucleus
FAST	Features from Accelerated Segment Test
PCA	Principal Component Analysis
DoG	Difference of Gaussian
SAD	Sum of Absolute Differences
ZSAD	Zero-mean Sum of Absolute Differences
LSAD	Locally scaled Sum of Absolute Differences
SSD	Sum of Squared Differences
ZSSD	Zero-mean Sum of Squared Differences
LSSD	Locally scaled Sum of Squared Differences
ZNCC	Zero-mean Normalized Cross Correlation
SHD	Sum of Hamming Distances
2D	Two Dimensional
3D	Three Dimensional

CV	Computer Vision
SVD	Singular Value Decomposition
LMedS	Least Median Square
LTS	Least Trimmed Squares
FFT	Fast Fourier Transformation
AHT	Adaptive Hough Transform
FHT	Fast Hough Transform
MI	Mutual Information
HAIR	High-Performance Automatic Image Registration
RMS	Root Mean Square
MIHT	Modified Iterated Hough Transform
TLS	Terrestrial Laser Scanner
MRF	Markov Random Field
LiDAR	Light Detection and Ranging
KL	Kozachenko – Leozenko entropy estimator
IRTK	Image Registration Toolkit
RMSD	Root Mean Square Deviation
DVFs	Displacement Vector Fields
UML	Unified Modelling Language
AIR	Automatic Image Registration
DIP	Digital Image Processing
DOF	Degrees of Freedom
SfM	Structure from Motion
GUI	Graphical User Interface
ARCHANGEL	Automatic Registration and Change Location

LIST OF SYMBOLS

Symbol	Meaning
f	Focal length
h	Two- dimensional (2D) spatial transformation
g	One-dimensional (1D) radiometric transformation
N_i	Number of iterations
a	Cosine function of the rotation angle
b	Sine function of the rotation angle
\bar{a}	The probability that any selected data point is an inlier
\bar{b}	The probability of observing an outlier
q	Minimum number of points needed
c	Camera constant
n	Number of points observed
w	Misclosure
w_i	Signed distance
P	Weight
E	Epipole
τ	Predefined threshold
F	Fundamental matrix
E	Essential matrix
K	Constant of reduction or increment of the length of a base line
I_1	Feature on the reference image
I_2	Corresponding feature on the moving or corresponding image
\vec{b}	Vector of the baseline

Φ	Minimized least squares solution
$\widehat{C}_{\hat{x}}$	Covariance matrix of the unknown
T	Translation matrix
R	Rotation matrix
S	Translation vector's skew symmetric matrix
S_b	Skew-symmetric (asymmetric) matrix of the base line
S_o	Object coordinate system
S_k	Camera coordinate system
Np	Total number of corresponding points
B	Camera model matrix
\otimes	Kroniker product
l, l'	epipolar lines
$[\cdot, \cdot, \cdot]$	Triple product
e_l, e_r	epipoles
π	Epipolar plane
O_l, O_r	Origin of the camera frames
$O_l O_r$	Base line
M, N	exposure stations
i, j	Pixel coordinates of the feature along the row and columns respectively
X, Y and Z	Axes of the object space
T_x, T_y	Translation along the x and y directions respectively
$svd(\widehat{F})$	Singular value decomposition of fundamental matrix
P', P''	Projection matrices of the first and second cameras respectively

R', R''	Orientation matrices of the first and second cameras respectively
X_O	Origin of the pin-hole camera
X_P	The location of the point in the object coordinate system
X'_o, X''_o	Projection centres of the first and second cameras respectively
${}^k X_P$	Euclidean coordinate (homogeneous coordinate)
K', K''	Calibration matrices of the first and second camera respectively
I_3	Identity matrix
${}^c X_{-p}$	Maps from the camera plane to the image plane
${}^c P_k$	Projective point in the image plane
${}^c K$	Calibration matrix for the ideal camera
k_u, k_v	Number of pixels per millimetre (width and height)
u_0, v_0	Centre projection
I_M, I_N	Images of the object P on the photograph
\bar{m}', \bar{m}''	Transformed corresponding pairs after rectification
H', H''	Transformation homographies
(x_M, y_M, z_M)	Axes of the principal point on the base image
(x_N, y_N, z_N)	Axes of the principal point on the corresponding image
$\overrightarrow{MP}, \overrightarrow{NP}$	Vectors on the image plane
\vec{l}_M, \vec{l}_N	Vectors of the ray of light from principal centre to the image
ω, φ and κ	Rotation angles of the rotation matrix R
$\beta^0, p_{Mi}^0, p_{Ni}^0, \theta^0$	Approximate values of the Taylor's expansion of $F(\beta, p_{Mi}, p_{Ni}, \theta)$
β	Coefficient of the baseline vector when the baseline vector is expressed in terms of one of its components b_x

LIST OF APPENDICES

Appendix		Page
A	Image coordinates of associated image pairs automatically obtained using Modified Harris Corner Detector algorithm on google earth image pairs	189
B	Image coordinates of associated image pairs automatically extracted using Scale Invariant Feature Transform algorithm on google earth image pairs	201
C	Image coordinates of associated image pairs automatically obtained using Speeded Up Robust Feature algorithm on google earth image pairs	231
D	Image coordinates of associated image pairs automatically obtained using Modified Harris Corner Detector algorithm on UAV acquired image pairs	248
E	Image coordinates of associated image pairs automatically obtained using Speeded Up Robust Features algorithm on UAV acquired image pairs	254
F	Image coordinates of associated image pairs automatically obtained using Scale Invariant Feature Transform algorithm on UAV acquired image pairs	272
G	Extract of java codes implemented for the developed image registration module	300

CHAPTER ONE

1.0

INTRODUCTION

1.1 Background to the Study

With the developments in technology, photogrammetric and remote sensing applications are fast gaining global acceptance in the geographical observation and monitoring of the earth surface (Chung-Hsien and Yu-Ching, 2017; Kleissl, 2013; Olaleye *et al.*, 2015; Rittavee *et al.*, 2009; Sindhu, 2014; Ting and Heng, 2016). These applications provide pictorial representations of a scene and they give an overview of a geographical scene of interest in the form of images which afford the observer or image analyst the opportunity to acquire accurate spatial or geometric information about the sphere of interest. Since the images of a large area or object are acquired in small patches, often there is the need to assemble and integrate those patches into larger pictures for wider view. Also, images are visual models of reality and unless they are registered onto the object, realistic measurements cannot be derived from them, hence, they must be mosaicked or fused together in order to ensure holistic representation and enable stereoscopic view of the desired geographical area of interest (Olaleye *et al.*, 2015). The process of fusing these image patches together is known as mosaicking or image-to-image registration.

Image registration is the process of registering an image to the object space (such as a map) or to another image (usually termed co-registration). It determines the relative orientation between two images. The aim of image co-registration is as follows: given two different representations of the same object (or geographical scene), find a transformation function which, when applied to one image, will align (or register) points in that image with their conjugate points in the other image of the same object (Calvin *et al.*, 2019). Mathematically, if there are two 2D datasets (images) of a defined area denoted by A_0 and A_1 where $A_0(x, y)$ and $A_1(x, y)$ each mapped to their respective

intensity values, then the mapping between these two images can be mathematically expressed as equations (1.0a) and (1.0b):

$$A_1(x, y) = g(A_0(h(x, y))) + w(x, y) \quad (1.0a)$$

$$\text{Approximately, } A_1(x, y) = g(A_0(h(x, y))) \text{ when } w(x, y)=0 \quad (1.0b)$$

where $w(x, y)$ is an error vector (residual) and it is said to be zero when there is a perfect correlation and/or registration, h is a two-dimensional (2D) spatial coordinate transformation, and g is a one-dimensional (1D) radiometric transformation.

The major issue in image registration is thus the task involved in finding the optimal or most efficient spatial and radiometric (intensity) transformation (h and g respectively) with specific emphasis on the spatial transformation. Establishing this spatial correspondence is a vital issue which arises in Digital Image Processing (DIP) especially when pixel by pixel comparison is to be made on more than one image which represents the same scene (Xiaolong and Siamak, 1999; Zhang *et al.*, 2014).

Though registration can be done by registering each image to the same map, direct image-to-image transformation is more common (co-registration). It is the process of establishing a spatial correspondence between two overlapping images such that the images' features on the image space correspond to their conjugate features in the object space (Xiaolong and Siamak, 1999), by determining the transformation that correlates the conjugate point in the two views of the overlapping image patches (Ajayi, 2014).

Generally, four (4) stages are involved in the registration of overlapping images. First, a decision has to be made on the type of primitive to be adopted. These primitives can be points, lines, or area/polygonal features. Once the primitive has been selected, correspondence or conjugate points must be established by devising a similarity measure, after which the mathematical relationship of the overlapping images will be established using a transformation function. This transformation

can either be orthogonal, affine, or projective transformation functions. Finally, a controlling model that provides solution to the registration problem is implemented by the implementation of these three stages (primitives, similarity measure and transformation function) (Al-Ruzouq, 2004).

The concept of adopting epipolar correlation for image registration can thus be simply highlighted as follows: For an image pair (first and second overlapping images), when a point lies in the first image, its corresponding point in the second image has to lie on the epipolar line corresponding to the first point. This fact establishes a mapping function or a correlation between points in the first image and lines in the second image and vice versa. The knowledge of this correspondence reduces the dimension of the space to 1D when searching for matching points in the whole image. This becomes important when an automatic detection of points is needed as it is in automatic registration of overlapping image pairs. The reduction of the space to 1D reduces considerably the search of matching points. This will reduce the search time, thereby making the registration process faster and at the same time, maintaining a high degree of accuracy by ensuring precise pixel-to-pixel matching (Zhou *et al.*, 2015).

This research therefore seeks to investigate the applicability and robustness of the use of epipolar based correlation algorithms in tandem with some other selected feature descriptors, for a fully automatic image co-registration process and to develop an integrated image registration scheme that will afford users the opportunity to select desired models based on the peculiarity of their image registration tasks.

1.2 Statement of the Research Problem

The accuracy requirement and the nature or properties of the images involved in image registration makes the process highly rigorous and tedious which often results in the solution of hundreds or thousands of mathematical equations (Zhengyou, 1998). Manual approaches to this problem have proved over time to be time consuming, highly prone to mis-match (outliers), computationally

complex (Kleissl, 2013), and as such, the complete automation of the entire registration process is one of the basic challenges of the present-day image registration experts (Jacqueline *et al.*, 2012; Olaleye *et al.*, 2015; Sindhu, 2014) especially with the advent of Unmanned Aerial Vehicles (UAVs). The best of most past efforts in achieving this task has only resulted in a semi-automatic (user assisted) model while completely automating the entire process of image registration remains a major issue.

Many mathematical models have been developed for each of the four (4) major processes or steps of automatic image registration. These steps are: (1) Feature detection and extraction (Lowe, 1999; Matas *et al.*, 2004), (2) Feature matching (David *et al.*, 1999), (3) Transformation model/parameter estimation (Strutz, 2016), and (4) Image transformation and resampling (Olaleye, 2010) which is used for the effectuation of the selected transformation function and resampling of the image pairs. These models offer individual users specific advantages based on the peculiarity or the prevailing circumstances of their image registration task (Lin and Labuz, 2013; Lowe, 2004). Though these models have individually displayed significant improvement in terms of either speed or accuracy, none of these algorithms has been known to offer dual advantages of speed and accuracy singularly. Integrating one or two of these existing algorithms together has proven to be an option for improving the accuracy without compromising the speed. Very little has been done in integrating some of these models into one package where users can make informed decisions on the type of feature descriptors to be used during their image registration tasks and which also ensures the optimization of the speed of the image registration.

Furthermore, apart from optimizing the image registration speed, finding a good similarity measure and ensuring precise image matching and correlation is pivotal for every image registration paradigm since small error in mismatch may have a very large impact on the accuracy of global change measurements (Dai, 2003). Though a couple of research efforts have been

invested in pursuing the realisation of these issues (Bay *et al.*, 2006; He *et al.*, 2008; Jan *et al.*, 2010), they still remain a major research problem in image registration (Jacqueline *et al.*, 2012) because no best-fit-approach has been found amongst users. In addressing these issues, research effort aimed at integrating epipolar constraints with a view to finding a good similarity measure and ensuring precise pixel-to-pixel match of conjugate features for the development of an integrated image registration scheme is germane and has remained largely unexplored basically due to the mathematical complexities and programming rigours involved in the integration and implementation process.

This research, therefore seeks to develop an integrated and a fully automated scheme for the entire processes involved in registering overlapping images with specific emphasis on the integration of epipolar correlation with some selected feature descriptors. Based on this problem, answers will be sought to the following research questions:

1. What are the effects of the choice of feature descriptors on the extracted corresponding features, the speed and accuracy of an automatic image registration scheme?
2. How will the development of an integrated epipolar correlation-based image registration algorithm improve the overall accuracy and speed of an image registration scheme?
3. How efficient are the developed and implemented algorithms for optimal registration of overlapping images?

1.3 Aim and Objectives

The aim of this research is to develop an integrated scheme for the automatic registration of overlapping image pairs with a view to optimizing the image registration process.

The pursued objectives are:

1. Examining the effect of different selected feature descriptors on the speed and accuracy of an automatic image registration scheme.

2. Development of an integrated epipolar correlation-based automatic image registration scheme.
3. Assessing the efficiency of the developed and implemented algorithms in optimal image registration.

1.4 Justification for the Study

The ultimate goal of current research efforts in digital photogrammetry is the complete automation of the entire image mapping and photogrammetric systems. An automatic image matching which is an integral part of image registration must be carried out if the inverse problem of recovering the original 3D scene information from overlapping pairs of images must be solved using an automated system. Different feature detection, description, extraction and matching models have been developed and implemented in the development of an automatic image registration scheme (Chung-Hsien and Yu-Ching, 2017; Olaleye *et al.*, 2015; Rittavee *et al.*, 2009; Shih-Ming, 2012; Ting and Heng, 2016; Zichun *et al.*, 2016). These models together with other models used at every stage of image registration process are of different characteristic features which make them suitable for different imaging conditions (Lin and Labuz, 2013; Lowe, 2004). Integrating these models together and packaging them into a user-friendly standalone software for the automatic registration of overlapping images will not only make them easily accessible for implementation by image analysts (He *et al.*, 2008), but will also provide a comprehensive image registration module for interdisciplinary applicability (Gang and Yun, 2005).

Also, optimization of the image registration process which improves both the speed and accuracy of the overall process is a major quest of image registration analysts (Al-Ruzouq, 2004; Lisa and Ghassan, 2003). Series of algorithms have been developed to optimize the different stages involved in image correlation and registration (Ashburner, 2007; Luong, 2009; Prachya, 1999; George and Siavash, 2000), but not much has been done to investigate the applicability and robustness of

epipolar correlation for image registration or automatic mosaic generation, and to also integrate some of the existing vector-based feature descriptors with epipolar correlation in the construction of a robust feature descriptor for a hybridized automatic image registration module.

Furthermore, apart from the easy accessibility and comprehensive applicability that a hybridized or integrated image registration module provides, the implementation of epipolar correlation model integrated with selected existing feature descriptors in the development of an automatic image registration scheme will also ensure the optimization of the overall speed of the image registration process and the accuracy of the registered image (He *et al.*, 2008) which makes it a very important tool for different applications such as earth monitoring, image processing, navigation, cartography and mapping, change detection, computer vision, medical imaging, metrology, and image fusion. More specifically, the developed scheme can be embedded in the image processing segment of an Unmanned Aerial System (UAS) for seamless and real-time registration of overlapping images acquired with the aid of an Unmanned Aerial Vehicle (UAV) during UAV flight missions.

1.5 Assumption and Delimitation to the Study

Only three feature descriptors were selected and implemented in this research for the development of the automatic image registration scheme because they are adjudged the most widely implemented feature descriptors (Panchal *et al.*, 2013; Dilipsinh *et al.*, 2014; Hassaballah *et al.*, 2016; Chung-Hsien and Yu-Ching, 2017) and they are also known to be invariant to noise, zoom, scale, rotation and illumination (Krishna and Varghese, 2015).

For the development of the integrated epipolar correlation-based image registration scheme, the study assumed an uncalibrated camera scenario and also limited the optimal functionality of the developed scheme to the co-registration of a single stereo pair at a time (pairwise). Also, the developed automatic image registration scheme was designed to optimally register image pairs

with $\geq 60\%$ overlap (side lap and end lap) and as such, image pairs with overlapping percentage (forward lap) that is less than 60% may be registered with considerable distortion. The developed model was also experimented with images extracted from google earth online image data repository and images acquired from a DJI Phantom 4 UAV only, to prove that the image registration software can register multimodal image pairs. Therefore, images from other sources were not experimented in the course of this study. Also, the software was primarily designed for image co-registration, hence, the registration of maps to images and vice versa were not experimented in this research.

Image pre-processing and post-processing techniques were not also applied to the image pairs before and after image registration because of the need to ensure that the performance of the developed and implemented image registration algorithms is not influenced by the enhancement or refinement introduced to the image pairs by the application of image pre-processing and post-processing techniques. Also, photogrammetrists now have access to metric and non-metric hybrid cameras equipped with an inbuilt intelligent system for the automatic enhancement of images at the instance of camera exposure or image data capture, hence, such images do not have to be subjected to the application of image pre-processing techniques since they have been ortho-rectified.

1.6 Scope of the Study

This research presents the functionality of some of the algorithms used at various stages of image registration methodology. Four basic stages of feature-based image registration have been presented which includes feature detection, feature matching, model estimation, resampling and estimation of transformation functions. The three selected vector-based feature detection and extraction algorithms implemented for this study are: (1) Scale Invariant Feature Transform

(SIFT), (2) Modified Harris and Stephens Corner Detector (MHCD) and (3) Speeded Up Robust Features (SURF).

The features detected and extracted by these three (3) feature detection and extraction algorithms were matched using the Sum of Absolute Differences (SAD) feature matching metric while Bilinear interpolation algorithm was implemented for the image resampling and interpolation. The outliers were excluded using both geometric and epipolar constraints (integrated approach) before the computation of transformation functions using projective transformation. The fundamental matrix of the epipolar correlation was estimated using the normalized eight-point algorithm while the modified Hartley method of image rectification was adopted for the auto-rectification of the unrectified stereo pairs.

For the model experimentation, two different image registration campaigns were adopted. For the first registration campaign, overlapping image pairs of part of the main campus of the Federal University of Technology, Minna, Nigeria, extracted from google earth online image data repository were used while a DJI phantom 4 UAV was deployed to acquire overlapping images also of part of the main campus of the Federal University of Technology, Minna, Nigeria. The images acquired from this flight mission were used to experiment the implemented models for the second registration campaign.

Finally, the algorithms were packaged into a user-friendly automatic image registration software which is equipped with an inbuilt semi-automatic stereo comparator and a module for automatic camera calibration.

CHAPTER TWO

2.0 LITERATURE REVIEW

The flow chart which shows the systematic dual approach that was adopted in conducting the literature review is presented in Figure 2.1. The figure highlights the summary of the details of the theories of both image registration and epipolar geometry on one hand and the documented applications showing the evolvement and advancement of both image registration and epipolar geometry on the other hand.

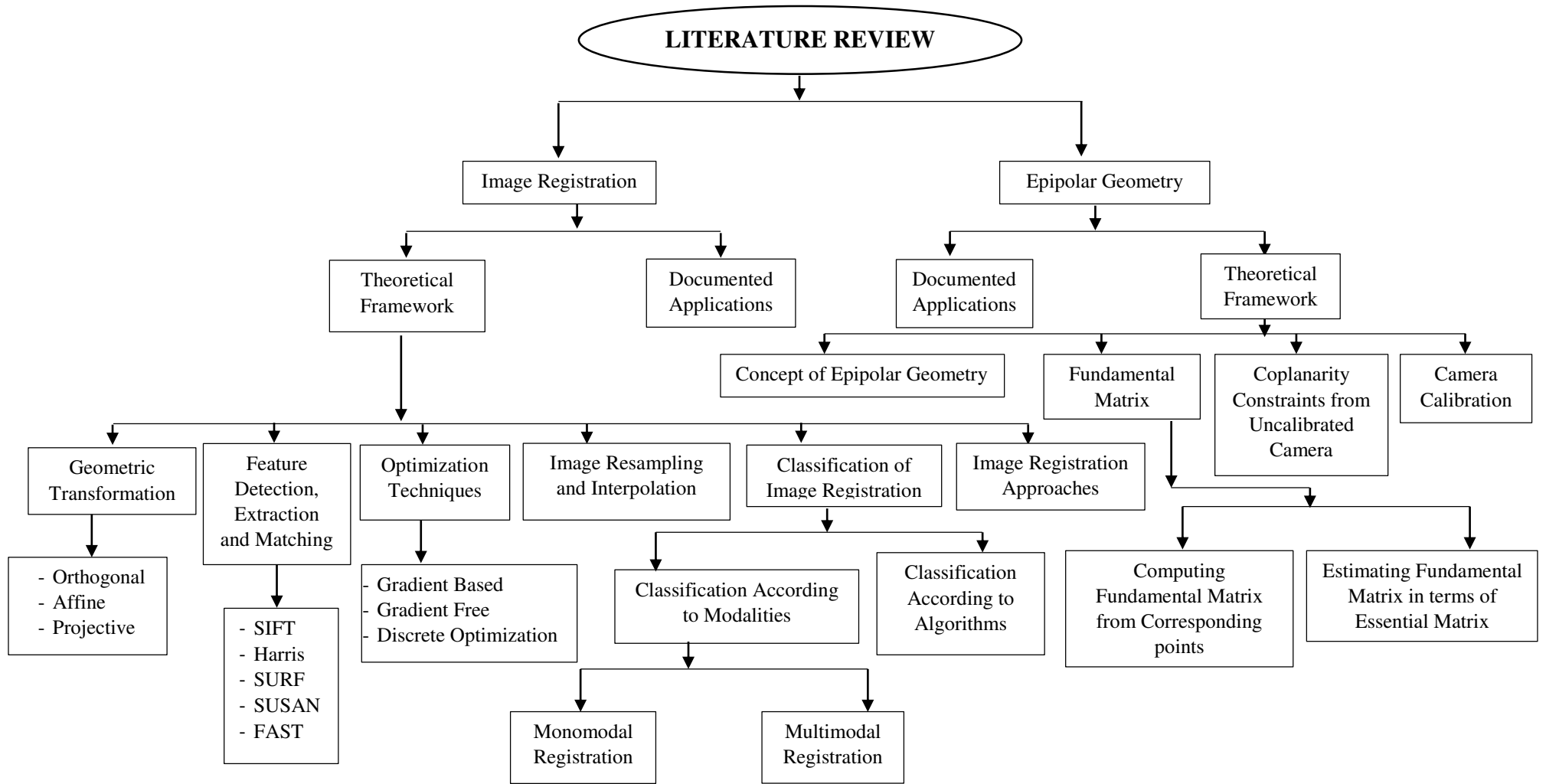


Figure 2.1: Systematic review of literature (Source: Author's Research)

2.1 Theoretical Framework

Basically, there are four major steps involved in the feature-based registration of overlapping images (Al-Ruzouq, 2004). These four basic steps are as follows (Figure 2.2):

1. Feature detection (extraction of features from each image).
2. Feature Matching (pairing of these images).
3. Transformation model/parameter.
4. Image Transformation and resampling.

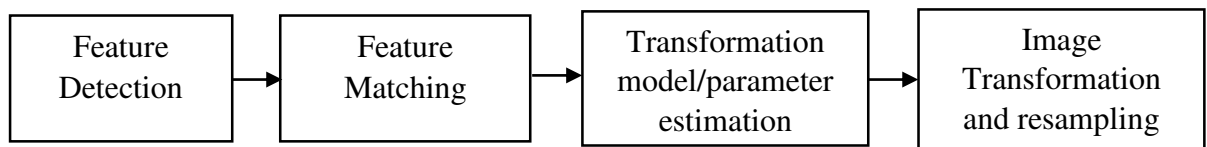


Figure 2.2: Basic automatic image registration process (Source: Author's Research)

Details of these four steps are as highlighted in subsections 2.1.1 and 2.1.2.

2.1.1 Feature detection and extraction

In image processing, images are generally represented by the features that can be extracted from them. These features are broadly categorised into two categories, namely, the global features and local features while the extraction of these image features can also be categorised into both high-level features and low-level features (Nixon and Aguado, 2008).

The global feature representation depicts the image as one multi-dimensional feature vector which describes the whole image. More specifically, the global feature representation approach produces one single vector with values that measure various part of the image such as tone, texture, pattern, shape (Hassaballah *et al.*, 2016). Though global feature representation is generally fast, simple to compute and requires small amount of memory, they are also notably limited. Specifically, they are variant to transformations and are very sensitive to occlusion and blurs. In local feature representation, images are distinctively represented based on their local structures using local features which are also known as key points or interest points and can be described as specific and

unique patterns that are distinct from the pixels within its neighbourhood (Tuytelaars and Mikolajczyk, 2007) and are generally associated with one or more properties of the image (Li *et al.*, 2015). They are points with a well-defined position in the image space, unambiguous mathematical description, and they are stable under perturbations such as variations in brightness (Mubarak, 1997). Examples of such features are regions, edges, and corners. When compared to global feature representation, the local features are notable for superior performance, distinctiveness and better stability (Jégou *et al.*, 2012) though they require significant amount of memory because many local features can be found on a single image. The advantages of local feature representation make it more suitable for object recognition and image matching (Hassaballah *et al.*, 2016).

Ideally, local features are expected to have the following qualities or characteristics: distinctiveness, locality, accuracy, quantity, efficiency, repeatability, invariance and robustness which attests to their less sensitivity to noise or blurs (Ehab and Murad, 2017). These qualities are also expected to be inherent in the formulation of feature detection and extraction algorithms which are the algorithms that detect and extract these features and prepares them for further applications in image registration. They are also referred to as feature descriptors which are described also as the methods that are used in the computation of abstractions of the information on an image pair, which is used in making informed decisions of the identity of every image point on an image whether there is an image feature of a particular type or not.

Feature-based descriptors are broadly categorised into:

1. Spatial relations (Tuytelaars, 2006).
2. Edge based (differentiation based) descriptors such as Canny and Sobel (Canny, 1986).
3. Corner based (gradient based) descriptors such as Harris and Stephens descriptors and its derivatives.

4. Corner based (template based) descriptors such as Features from Accelerated Segment Test (FAST), Smallest Uni-value Segment Assimilating Nucleus (SUSAN) and Binary Robust Independent Elementary Features (BRIEF) which belongs to the family of binary descriptors.
5. Corner based (contour based) descriptors such as hyperbola fitting.
6. Invariant descriptors (Kazhdan *et al.*, 2003; Tuytelaars, 2006) such as Scale Invariant Feature Transform (SIFT) algorithm developed by Lowe (2004) and Brown and Lowe (2007), Speeded Up Robust Features (SURF) descriptor proposed by Bay *et al.* (2008).
7. Blob (interest region) and salient regions such as the Maximally Stable Extremal Region (MSER) algorithm developed by Matas *et al.* (2004).
8. Blob (Key point) such as Fast Retina Key point (FREAK), and Binary Robust Invariant Scalable Key point (BRISK) and the Accelerated Binary Robust Invariant Scalable Key point (ABRISK) which detects binary features only. They are designed for tracking and not for image classification problem.

The major characteristics (advantages and disadvantages) of some of the widely-used feature descriptors are highlighted in Table 2.1 while Table 2.2 presents the weighted analysis of the major qualities, advantages and disadvantages of some of the commonly implemented feature descriptors (Chung-Hsien and Yu-Ching, 2017; Ehab and Murad, 2017; Kazhdan *et al.*, 2003; Krishna and Varghese, 2015; Lu *et al.*, 2018; Tuytelaars and Mikolajczyk, 2007), with weight allocated to each of them so as to identify the three most suitable descriptors which were implemented in this study.

Table 2.1: Major characteristics of some of the widely-used feature detection and extraction algorithms

S/N	Feature Descriptor	Characteristics
1	Modified Harris Corner Detector (MHCD)	MHCD is rotationally invariant. It can perform optimally in the absence of scale difference.
2	Smallest Uni-value Segment Assimilating Nucleus (SUSAN)	It is a corner detector with a mask that calculates the intensity differences to detect or find the corners. It is scale variant (not invariant to scale).
3	Features from Accelerated Segment Test (FAST)	It uses Bresenham circle of radius 3 (circle of 16 pixels) to classify whether a candidate is actually a corner. It is invariant to scale and rotation with great improvement in the execution or processing time in the absence of noise.
4	Speeded Up Robust Features (SURF)	It is basically time economical when compared to other models but at the expense of accuracy and extracted corresponding features.
5	Scale Invariant Feature Transform (SIFT)	It is invariant to rotation, affine transformation changes and illumination. It performs optimally in feature extraction but with a slow execution time.
6	Principal Component Analysis (PCA)-SIFT	It reduced SIFT's execution time for matching (executes faster) but was proved to be less effective in feature detection compared to SIFT.

Source: Modified after Dilipsinh *et al.* (2014).

Table 2.2: Weighted analysis of the qualities of selected feature descriptors

S/N	Features Detector	Invariance			Characteristics/ Qualities			
		Scale	Rotation	Zoom	Robustness	Repeatability	Localization	Efficiency
1	SIFT	†	†	†	⦿⦿⦿	⦿	⦿⦿⦿	⦿
2	SURF	†	†	†	⦿⦿⦿	⦿⦿⦿	⦿	⦿
3	MHCD	X	†	†	⦿⦿⦿	⦿⦿⦿	⦿⦿⦿	⦿⦿⦿
4	MSER	†	†	†	⦿	⦿⦿⦿	⦿⦿⦿	⦿⦿⦿
5	FAST	X	†	X	X	X	⦿⦿⦿	⦿⦿⦿
6	FREAK	†	†	X	⦿⦿⦿	⦿⦿⦿	X	X
7	SUSAN	X	†	X	⦿	⦿⦿⦿	⦿	⦿⦿⦿
8	Hessian	†	†	X	⦿	⦿	⦿	⦿
9	DoG	†	†	X	⦿	⦿	⦿	⦿
10	Hessian- Laplace	†	†	†	⦿⦿⦿	⦿⦿⦿	⦿⦿⦿	⦿

Key: Where † means Yes, X means No or None, ⦿ means good, ⦿⦿⦿ means better and ⦿⦿⦿⦿ means best.

2.1.2 Feature matching

Feature matching in digital image processing can be described as the determination of corresponding points or features between images. The image matching process is also subdivided into two broad methods which are the signal or area-based method (Cideciyan *et al.*, 1992; Li *et al.*, 1995; Walia and Suneja, 2010) and the feature-based method (Goshtasby *et al.*, 2003; Mason and Wong, 1992; Peli *et al.*, 1987; Schenk *et al.*, 1991). The signal or area-based method makes use of grey values only and does not require the detection of features while the feature-based method is further subdivided into the following primitives (Kerner *et al.*, 2016):

- i. Regions such as buildings (Canny, 1986), lakes (Cain *et al.*, 2001), shadows (Brivio *et al.*, 1992), urban areas (Brown, 1992) and forests (Bracewell, 1965).

- ii. Linear features such as line segments (Bro-Nielsen and Gramkow, 1996) and object contours (Brown, 1992).
- iii. Point features such as line intersections (Cain *et al.*, 2001), and high variance points (De-Castro and Morandi, 1987).

Table 2.3 presents a summary of characteristics of various matching methods as used in image registration.

Table 2.3: Matching methods

Matching method	Similarity measure	Matching entity/primitives
Area-based	Correlation, least-squares	Grey values
Feature-based	Cost function	Interest points such as points, edges, and regions
Relational	Cost function	Symbolic image description

Source: Potuckova (2004)

The area-based method is further subdivided into the following methods.

- i. Correlation-like methods (Normalized Cross correlation) which deals with intensity differences between multimodal images (Andronache *et al.*, 2008; Brown, 1992; Lin *et al.*, 2011). Sum of Absolute Difference (Scharstein and Szeliski, 2002), Sum of Squared Difference (Olaleye *et al.*, 2015), and Sum of Hamming Distances (Nzelibe, 2014).
- ii. Fourier methods (Bracewell, 1965).
- iii. Mutual Information methods (Alexander and Summers, 2003; Guoyan, 2010; Hassan *et al.*, 2014; Kuijper, 2004; Peter *et al.*, 2008; Pluim *et al.*, 2000; Pluim *et al.*, 2001).
- iv. Optimization methods.

Table 2.4 presents the summary of the mathematical expression of different similarity measures as used in image registration where I_1 is the feature on the reference image, I_2 defines the

corresponding feature on the search image, i and j describes the pixel coordinate of the feature along the row and columns respectively.

Table 2.4: Mathematical Expression of Correlation-Based Similarity Measures

Similarity Measure	Formula
Sum of Absolute Differences (SAD)	$\sum_{(i,j) \in W} I_1(i,j) - I_2(x+i, y+j) $
Zero-mean Sum of Absolute Differences (ZSAD)	$\sum_{(i,j) \in W} I_1(i,j) - \bar{I}_1(i,j) - I_2(x+i, y+j) + \bar{I}_2(x+i, y+j) $
Locally scaled Sum of Absolute Differences (LSAD)	$\sum_{(i,j) \in W} \left I_1(i,j) - \frac{\bar{I}_1(i,j)}{\bar{I}_2(x+i, y+j)} \bar{I}_2(x+i, y+j) \right $
Sum of Squared Differences (SSD)	$\sum_{(i,j) \in W} (I_1(i,j) - I_2(x+i, y+j))^2$
Zero-mean Sum of Squared Differences (ZSSD)	$\sum_{(i,j) \in W} (I_1(i,j) - \bar{I}_1(i,j) - I_2(x+i, y+j) + \bar{I}_2(x+i, y+j))^2$
Locally scaled Sum of Squared Differences (LSSD)	$\sum_{(i,j) \in W} (I_1(i,j) - \frac{\bar{I}_1(i,j)}{\bar{I}_2(x+i, y+j)} \bar{I}_2(x+i, y+j))^2$
Zero-mean Normalized Cross Correlation (ZNCC)	$\frac{\sum_{(i,j) \in W} (I_1(i,j) - \bar{I}_1(i,j)) \cdot (I_2(x+i, y+j) - \bar{I}_2(x+i, y+j))}{\sqrt{\sum_{(i,j) \in W} (I_1(i,j) - \bar{I}_1(i,j))^2 \cdot \sum_{(i,j) \in W} (I_2(x+i, y+j) - \bar{I}_2(x+i, y+j))^2}}$
Sum of Hamming Distances (SHD)	$\sum_{(i,j) \in W} I_1(i,j) \text{ bitwiseXOR } I_2(x+i, y+j)$

Source: Ajayi (2014), Scharstein and Szeliski (2002)

Detailed documentation of these similarity metrics and their mathematical expression are presented in Ajayi (2014), Bhavani (2005) and Bolarinwa (2017).

2.1.3 Image resampling and interpolation

Image resampling is the act of changing the pixel values sampled at each pixel coordinate in the image. Resampling is used to either increase the sample rate (make the image larger) or decrease it (make the image smaller). Interpolation on the other hand is the process of computing values between sampled points. Some of the major image resampling and interpolation algorithms used in image registration include: Nearest neighbour function, Bicubic Interpolation, Quadratic Splines (Banerjee *et al.*, 1995), Cubic B-Splines (Barrodale *et al.*, 1993), Higher-order B-Splines (Barrow *et al.*, 1977, Lehmann *et al.*, 2001), Gaussians (Appledorn, 1996; Bhattacharya and Sinha, 1997), and Truncated sinc-functions (Bracewell, 1965; The´venaz *et al.*, 2003) and Bilinear interpolation; which is one of the most widely used interpolation model because it strikes the best balance between accuracy and computational complexity and as such, was implemented in this study.

Bilinear interpolation extends the original linear interpolation for the interpolation of two variables (e.g., x and y) on a regular two-dimensional grid. This concept first performs the linear interpolation in one direction, and then repeats the same process again in the other direction. The interpolation is quadratic in the sampled location even though each step is linear in the sampled values and in the position.

Mathematically, suppose that the value of the unknown function f at the point $P = (x, y)$ is to be estimated, it is assumed that the value of f at the four points $Q_{11} = (x_1, y_1)$, $Q_{12} = (x_1, y_2)$, $Q_{21} = (x_2, y_1)$, and $Q_{22} = (x_2, y_2)$ is known. Hence, the linear interpolation is first performed along the x -direction which is described in equations (2.1) – (2.5):

$$f(R_1) \approx \frac{x_2 - x}{x_2 - x_1} f(Q_{11}) + \frac{x - x_1}{x_2 - x_1} f(Q_{21}) \quad (2.1)$$

where $R_1 = (x, y_1)$,

$$f(R_2) \approx \frac{x_2-x}{x_2-x_1} f(Q_{12}) + \frac{x-x_1}{x_2-x_1} f(Q_{22}) \quad (2.2)$$

where $R_2 = (x, y_2)$,

Also, interpolating in the y -direction yields:

$$f(P) \approx \frac{y_2-y}{y_2-y_1} f(R_1) + \frac{y-y_1}{y_2-y_1} f(R_2) \quad (2.3)$$

This results into the estimation of $f(x, y)$ as:

$$\begin{aligned} f(x, y) &\approx \frac{f(Q_{11})}{(x_2-x_1)(y_2-y_1)} (x_2-x)(y_2-y) + \frac{f(Q_{21})}{(x_2-x_1)(y_2-y_1)} (x-x_1)(y_2-y) + \\ &\frac{f(Q_{12})}{(x_2-x_1)(y_2-y_1)} (x_2-x)(y-y_1) + \frac{f(Q_{22})}{(x_2-x_1)(y_2-y_1)} (x-x_1)(y-y_1) = \\ &\frac{1}{(x_2-x_1)(y_2-y_1)} (f(Q_{11})(x_2-x)(y_2-y) + f(Q_{21})(x-x_1)(y_2-y) + f(Q_{12})(x_2-x)(y-y_1) \\ &+ f(Q_{22})(x-x_1)(y-y_1)) \end{aligned} \quad (2.4)$$

It should be noted that the same result will be also obtained if the interpolation is first performed along the y -direction before repeating the same process for the x -direction. The mathematical expression of the interpolation can be simplified to equation (2.5) if a coordinate system with four known points is chosen, such that f is given as $(0, 0)$, $(0, 1)$, $(1, 0)$, and $(1, 1)$.

$$f(x, y) \approx f(0,0)(1-x)(1-y) + f(1,0)x(1-y) + f(0,1)(1-x)y + f(1,1)xy \quad (2.5)$$

2.2 Geometric Transformation

The first task in achieving accurate registration is the selection of appropriate geometrical transformations which will be applied to one of the images in order to remove variations or distortions which results due to the multi-modality of the image acquisition. These geometrical transforms are basically categorised into rigid and non-rigid geometric transforms. The components of a rigid body transformation are translation and rotation while geometrical scaling

is sometimes necessary for photographic views based on the use of a lens system. These three components of rigid transformation together with intensity scaling have been explored by a number of researchers either individually or collectively. De-Castro *et al.* (1987), Peli *et al.* (1987), Venot and Leclerc (1984), and Yu *et al.* (1989) used translation only, while both rotation and translation were explored by De-Castro and Morandi (1987) and Junck *et al.* (1990). The combination of translation, rotation and geometric scaling was presented by Apicella *et al.* (1988) and Apicella *et al.* (1989) and the combination of these three elementary components together with intensity scaling were adopted by Herbin *et al.* (1989), Venot *et al.* (1986), and Venot *et al.* (1988). To compensate for more complex image acquisition distortions, non-rigid transformations are potent tools. Examples of non-rigid transformations include exponential warping (Yanagisawa *et al.*, 1984), bilinear polynomial warping (Fitzpatrick *et al.*, 1987; Mandava *et al.*, 1989) and higher degree polynomial warping (Steiner and Kirby, 1977; Van and Stein, 1977; Wong, 1977).

2.2.1 Transformation functions

One of the fundamental issues in image registration is the establishment of the transformation function that describes the mapping between the image pairs to be registered mathematically. In other words, given a pair of images (reference and input images), the transformation function tries to properly align the image pairs or overlay them. These transformation functions can be broadly categorised into global and local transforms. When all the pixels in the image pair are aligned using a given set of equations, it is referred to as global transformation while local transformation maps the image pairs based on their spatial location which results in several sets of equations for one map. Though local transforms are more computationally expensive when compared with global transforms, they often produce more accurate results (Fonseca and Manjunath, 1996).

The causes of geometric distortions vary considerably for different imaging systems based on different factors some of which include the scanning trajectory, imaging platform (airborne versus satellite), the image sensing device, and the total field of view. In order to filter these distortions,

several types of transformation functions have been developed, beginning with the 2-D similarity or orthogonal transformation. This transformation accurately matches image pairs with rigid-body distortion where the actual shape is not altered (Brown, 1992). It has four parameters and they include one rotation parameter, one scale parameter and two translation (in the x - and y -directions) parameters. It provides solution for parameters of the transformation function with a minimum of two tie points which implies that at least, only two tie points are required in order to accurately estimate the solution of the parameters of the 2-D transformation. It is however not advisable to use the minimum number of tie points that is required because it makes no provision for the monitoring of observation errors. The accuracy of the results can only be improved when many tie points that are properly densified or distributed across the images are used. The mathematical annotation of orthogonal transformation given in equation (2.6) while the reverse transformation can be achieved using equations (2.7a) and (2.7b). The equations allow us to establish a relationship between any point on the map and its corresponding point on the image.

$$\begin{bmatrix} x \\ y \end{bmatrix} = \begin{bmatrix} a & b \\ -b & a \end{bmatrix} \begin{bmatrix} u \\ v \end{bmatrix} + \begin{bmatrix} c \\ d \end{bmatrix} \quad (2.6)$$

$$\begin{bmatrix} u \\ v \end{bmatrix} = \frac{1}{|A|} \begin{bmatrix} a & -b \\ b & a \end{bmatrix} \begin{bmatrix} x & -c \\ y & -d \end{bmatrix} \quad (2.7a)$$

$$\text{Where } |A| = a^2 + b^2 \quad (2.7b)$$

Affine transformation is predominantly used in establishing the mapping function between two different coordinate systems. It has two more parameters than the 2-D similarity transformation making it six-parameters with additional allowance provided for two scale factors (in the x and y axis) and a non-orthogonality correction between them. It consists of the translation along the X and Y axis, the rotation, scale and skew. Generally, the more parameters included in the transformation function, the greater the ability to compensate for likely distortions between the two images. The estimation of the parameters of affine transform requires at least three tie points.

It preserves collinearity and ratios of distances but does not preserve orthogonality and angular relationships. It modifies the orthogonal type by using different scale factors in the x and y directions. It corrects for shrinkage by means of scale factor, applies the translation to the shift of the origin and also performs rotation through angle θ (plus a small angular correction for non-orthogonality to orient the axes in the u, v photo system) (Olaleye, 2010). Equation (2.8) presents the mathematical expression of affine transformation.

$$\begin{bmatrix} x \\ y \end{bmatrix} = \begin{bmatrix} a & b \\ c & d \end{bmatrix} \begin{bmatrix} u \\ v \end{bmatrix} + \begin{bmatrix} e \\ f \end{bmatrix} \quad (2.8)$$

Another notable type of transformation function is the projective transformation function. It is an eight-parameter (degrees of freedom) transformation, though with nine elements such as rotation, translation in X and Y directions and perspective distortion in homogeneous coordinates. It preserves collinearity but does not preserve parallelism. It maps quadrangle unto a square and ensures that concurrency, collinearity, order of contact (tangency, inflection and intersection) and cross ratio are all invariant (Olaleye, 2010). It is the most suitable choice of transformation type when the transformation takes place between two planes (Al-Ruzouq., 2004), and hence was the adopted transformation function used in the development of the automatic image registration scheme presented in this research to ensure that the scheme can register multimodal image pairs. Projective transformation allows the computation of the u, v coordinates of the points analytically after projecting them into a plane from another non-parallel plane which is expressed in equation (2.9):

$$\phi \begin{bmatrix} a, b, c, d \\ e, f, g, h \end{bmatrix} \quad \text{and can be written as (2.10):} \quad (2.9)$$

$$\begin{bmatrix} x \\ y \end{bmatrix} = \frac{1}{t} \begin{bmatrix} a & b \\ d & e \end{bmatrix} \begin{bmatrix} u \\ v \end{bmatrix} + \frac{1}{t} \begin{bmatrix} c \\ f \end{bmatrix} \quad (2.10)$$

$$\text{Where } t = gx + hy + 1 \quad (2.10a)$$

$$x = \frac{ax + by + 1}{gx + hy + 1} \quad (2.10b)$$

$$\text{And } y = \frac{dx + cy + 1}{gx + hy + 1} \quad (2.10c)$$

Although, these three transformation functions are the most commonly implemented transformation types, other higher order polynomials and surface splines have also been development to overcome the problems of significant geometric distortions. Details of these transforms are documented by Flusser (1994), Goshtasby (1988) and Goshtasby *et al.* (2003).

2.2.2 Mathematical expression of transformation elements

In describing the elements of the geometric transformation algorithms described in subsection 2.2.1, three major transformation conditions are considered and herein presented. These conditions are: (a) Transformation involving rotation only which involves both the object and the axes, (b) transformation involving rotation and scaling only and (c) transformation involving rotation, scaling and translation. Below is the mathematical expression of some of the elements in the transformation models highlighted above (Olaleye *et al.*, 2015):

Transformations Involving Only Rotations

$$x = u \cos \theta + v \sin \theta \quad (2.11a)$$

$$y = -u \sin \theta + v \cos \theta \quad (2.11b)$$

$$\text{In matrix notations, } \begin{bmatrix} x \\ y \end{bmatrix} = \begin{bmatrix} \cos \theta & \sin \theta \\ -\sin \theta & \cos \theta \end{bmatrix} \begin{bmatrix} u \\ v \end{bmatrix} \text{ - (when rotating the object)} \quad (2.11c)$$

$$\begin{bmatrix} x \\ y \end{bmatrix} = \begin{bmatrix} \cos \theta & -\sin \theta \\ \sin \theta & \cos \theta \end{bmatrix} \begin{bmatrix} u \\ v \end{bmatrix} \text{ - (When rotating the axes)} \quad (2.11d)$$

The orthogonality nature of the rotation matrices should be noted for analytical applications.

Transformations involving uniform scaling and rotation

$$x = u(s \cos \theta) + v(s \sin \theta) \quad (2.12a)$$

$$y = -u(s \sin \theta) + v(s \cos \theta) \quad (2.12b)$$

$$\begin{bmatrix} x \\ y \end{bmatrix} = s \begin{bmatrix} \cos \theta & \sin \theta \\ -\sin \theta & \cos \theta \end{bmatrix} \begin{bmatrix} u \\ v \end{bmatrix} \quad (2.12c)$$

$$\begin{bmatrix} x \\ y \end{bmatrix} = \begin{bmatrix} a & b \\ -b & a \end{bmatrix} \begin{bmatrix} u \\ v \end{bmatrix} \quad (2.12d)$$

$$\text{Where } s = \sqrt{a^2 + b^2} \quad (2.12e)$$

$$\theta = \tan^{-1}(b/a). \quad (2.12f)$$

Transformation involving Scaling, Rotation and Translation.

$$x = u(s \cos \theta) + v(s \sin \theta) + tx \quad (2.13a)$$

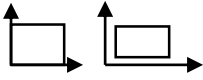
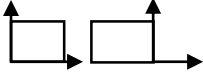
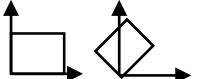

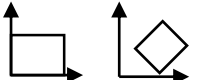
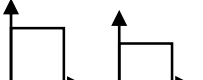

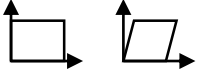
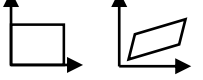
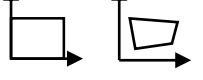
$$y = -u(s \sin \theta) + v(s \cos \theta) + ty. \quad (2.13b)$$

$$\begin{bmatrix} x \\ y \end{bmatrix} = s \begin{bmatrix} \cos \theta & \sin \theta \\ -\sin \theta & \cos \theta \end{bmatrix} \begin{bmatrix} u \\ v \end{bmatrix} + \begin{bmatrix} Tx \\ Ty \end{bmatrix} \quad (2.13c)$$

$$\begin{bmatrix} x \\ y \end{bmatrix} = sR \begin{bmatrix} u \\ v \end{bmatrix} + \begin{bmatrix} Tx \\ Ty \end{bmatrix} \quad (2.13d)$$

A summary of the mathematical expression and annotations, shapes and degrees of freedom of various transformation functions is presented in Table 2.5 while Figure 2.3 presents the structure of their hierarchical formation.

Table 2.5: Characteristics of various types of 2D transformation functions

2D Transformation	Figure	d.o.f	H	H
Translation		2	$\begin{bmatrix} 1 & 0 & t_x \\ 0 & 1 & t_y \\ 0 & 0 & 1 \end{bmatrix}$	$\begin{bmatrix} I & t \\ 0^T & 1 \end{bmatrix}$
Mirroring at y-axis		1	$\begin{bmatrix} 1 & 0 & 0 \\ 0 & -1 & 0 \\ 0 & 0 & 1 \end{bmatrix}$	$\begin{bmatrix} Z & 0 \\ 0^T & 1 \end{bmatrix}$
Rotation		1	$\begin{bmatrix} \cos\varphi & \sin\varphi & 0 \\ \sin\varphi & \cos\varphi & 0 \\ 0 & 0 & 1 \end{bmatrix}$	$\begin{bmatrix} R & 0 \\ 0^T & 1 \end{bmatrix}$
Motion		3	$\begin{bmatrix} \cos\varphi & \sin\varphi & t_x \\ \sin\varphi & \cos\varphi & t_y \\ 0 & 0 & 1 \end{bmatrix}$	$\begin{bmatrix} R & 0 \\ 0^T & 1 \end{bmatrix}$
Similarity		4	$\begin{bmatrix} a & -b & t_x \\ b & a & t_y \\ 0 & 0 & 1 \end{bmatrix}$	$\begin{bmatrix} \lambda R & 0 \\ 0^T & 1 \end{bmatrix}$
Scale difference		1	$\begin{bmatrix} 1 + m/2 & 0 & 0 \\ 0 & 1 - m/2 & 0 \\ 0 & 0 & 1 \end{bmatrix}$	$\begin{bmatrix} D & t \\ 0^T & 1 \end{bmatrix}$
Shear		1	$\begin{bmatrix} 1 & s/2 & 0 \\ s/2 & 1 & 0 \\ 0 & 0 & 1 \end{bmatrix}$	$\begin{bmatrix} S & t \\ 0^T & 1 \end{bmatrix}$
Asym. Shear		1	$\begin{bmatrix} 1 & s' & 0 \\ 0 & -1 & 0 \\ 0 & 0 & 1 \end{bmatrix}$	$\begin{bmatrix} S' & t \\ 0^T & 1 \end{bmatrix}$
Affinity		6	$\begin{bmatrix} a & b & c \\ d & e & f \\ 0 & 0 & 1 \end{bmatrix}$	$\begin{bmatrix} A & t \\ 0^T & 1 \end{bmatrix}$
Projectivity		8	$\begin{bmatrix} a & b & c \\ d & e & f \\ g & h & i \end{bmatrix}$	$\begin{bmatrix} A & t \\ P^T & 1/\lambda \end{bmatrix}$

Source: Bolarinwa (2017)

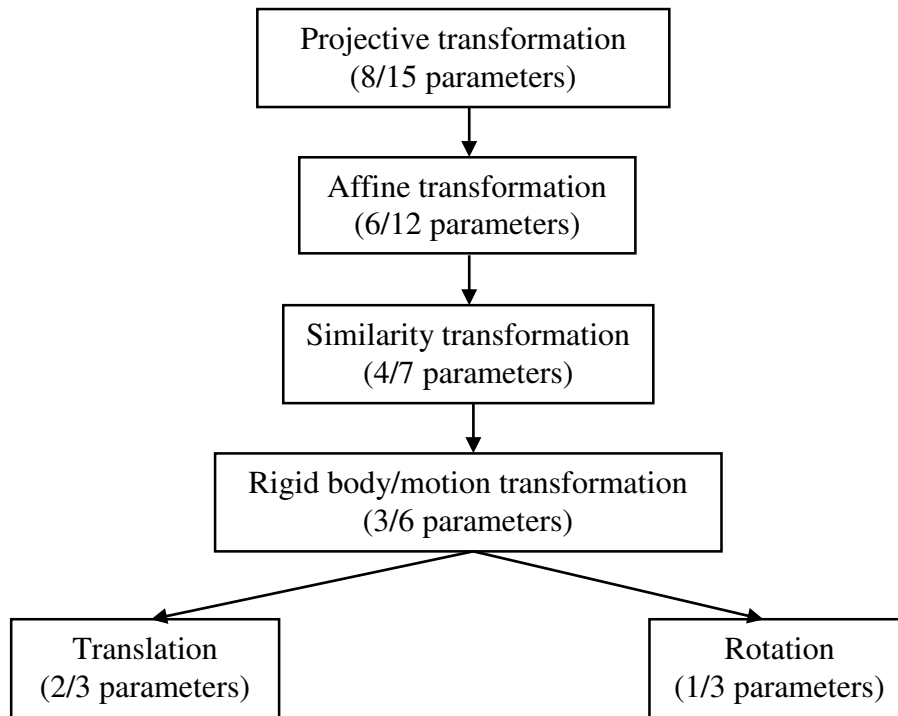


Figure 2.3: Hierarchical formation of transformation types (Source: Bolarinwa, 2017)

2.3 Optimization Techniques

The two major methods of determining the parameters of registration transformation functions are the direct computation method or the search method. Either way, different mathematical functions have been developed to ensure that optimal results are obtained by optimizing the transformation parameters iteratively (Maintz and Viergever, 1998). Darko *et al.* (2010) and Lisa and Ghassan (2003) gave a comprehensive review of iterative optimization, categorising these techniques into the following three major methods:

1. Gradient-based methods.
2. Gradient-free methods.
3. Discrete optimization.

The gradient based method can be further classified into deterministic and stochastic techniques (Klein, 2008) which can also be further sub-classified into the following techniques (see Figure 2.4):

1. Deterministic Techniques:

- i. Gradient descent technique (Klein *et al.*, 2009).
- ii. Quasi-Newton technique (Klein *et al.*, 2009).
- iii. Non-linear conjugate gradient technique.

2. Stochastic Techniques:

- i. Kiefer – Wolfowitz method (Kiefer and Wolfowitz, 1952).
- ii. Simultaneous Perturbation method.
- iii. Robbins – Monro Algorithm (Robbins and Monro, 1951).

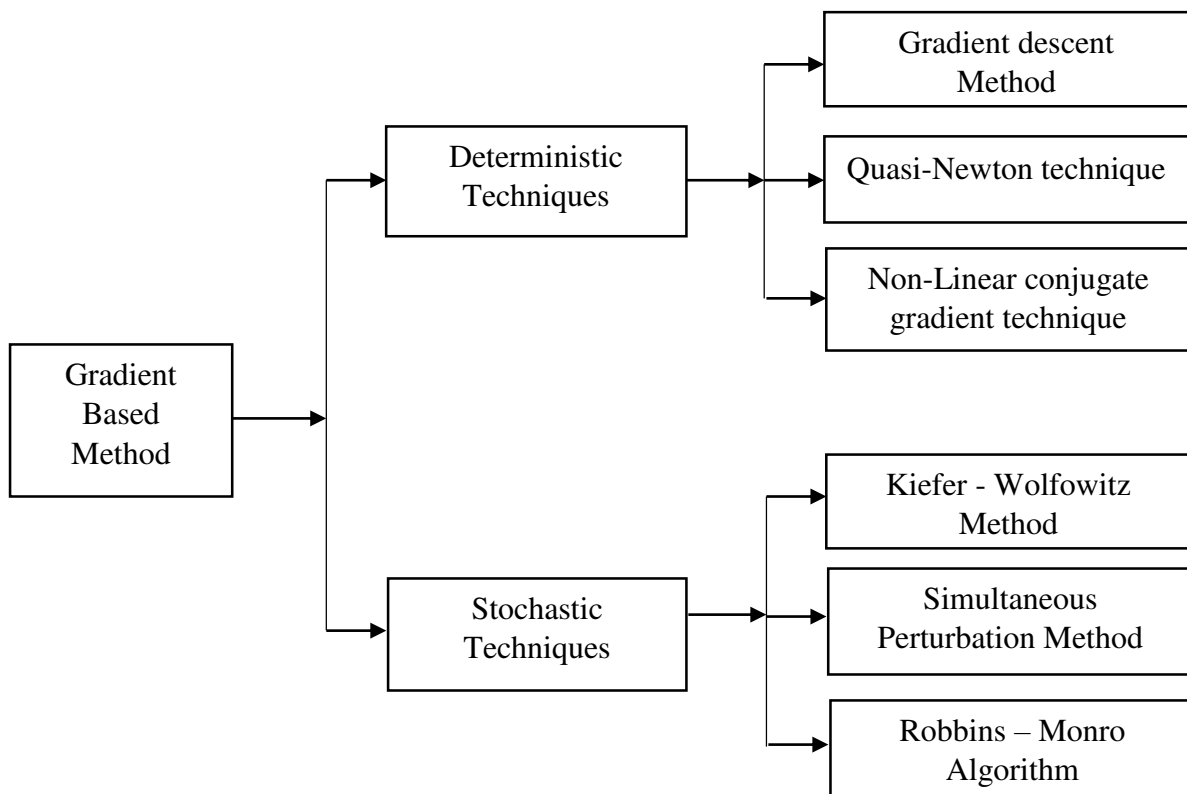


Figure 2.4: Gradient based method of optimization techniques (Source: Klein, 2008)

The gradient free approach makes few or no assumptions about the problem being optimized and can conduct searches in a very large solution space using some form of stochastic approach and it is often classified as follows:

1. Search based approaches:

- i. Powell’s conjugate gradient descent method (Maes *et al.*, 1996).

- ii. Simplex algorithm which is sometimes referred to as Nelder-Mead simplex, Downhill simplex or Amoeba method (Woods, 2009).
 - iii. Simulated Annealing (Liu *et al.*, 1994).
 - iv. DIRECT (Wachowiak and Peters, 2006).
2. Evolutionary Algorithms (Coello, 1998):
- i. Covariance Matrix Adaptation (Klein, 2008).
 - ii. Evolutionary Strategy.

Figure 2.5 presents the summary of the algorithms used in gradient free methods of optimization.

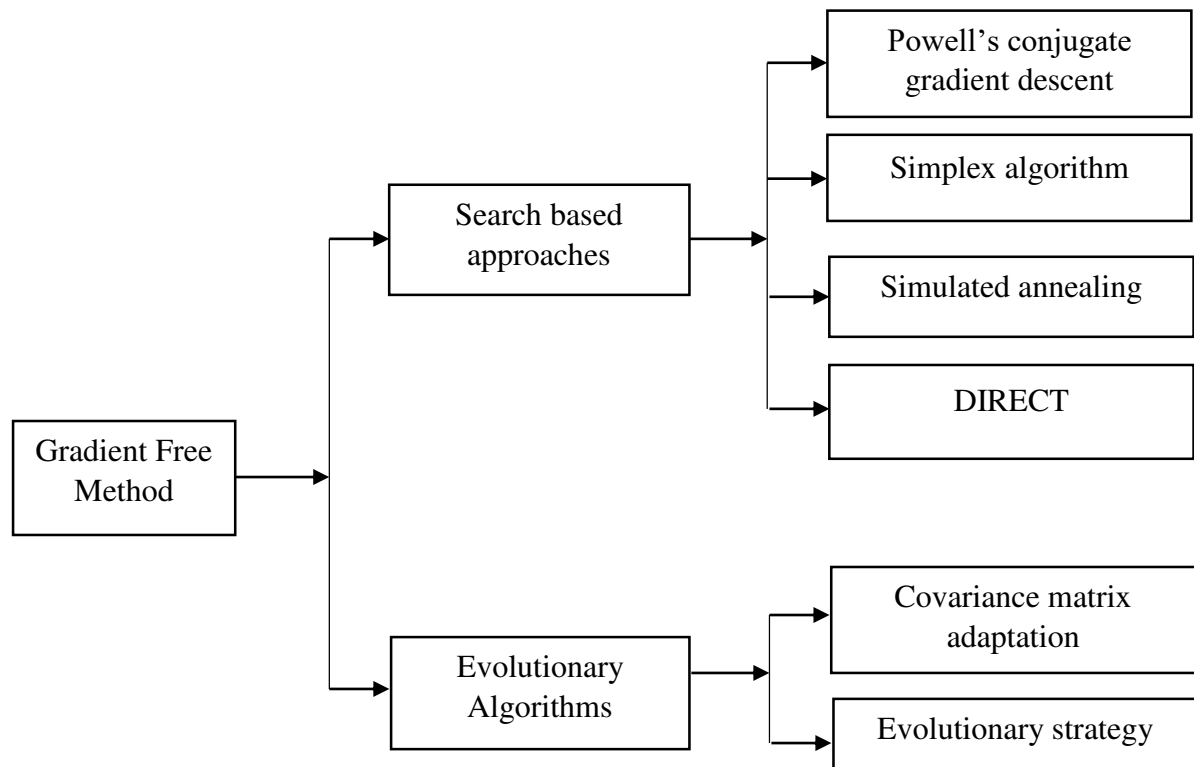


Figure 2.5: Gradient free method of optimization techniques (Source: Darko *et al.*, 2010)

A number of optimization algorithms and techniques have been reviewed and documented in Maintz and Viergever (1998) and Press *et al.* (1992).

2.4 Image Registration Approaches

Anil *et al.* (2014) presented a classification of image registration techniques according to the manner of image acquisition. These classes are (see Figure 2.6):

- i. Multiview (Different viewpoints).
- ii. Multi-temporal (Different times).
- iii. Multimodal or multi-sensoral analysis (Different sensors).
- iv. Scene to model registration.

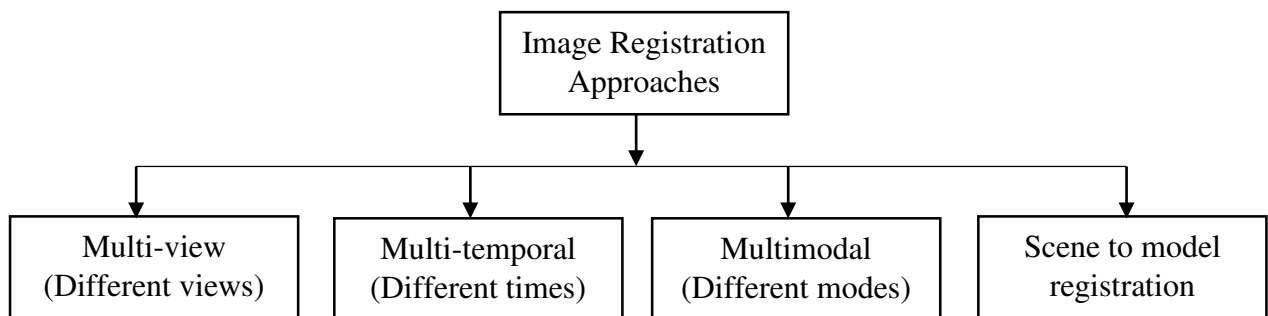


Figure 2.6: Image registration approaches (Source: Anil *et al.*, 2014)

Also, an overview of the techniques used in registration of overlapping images based on different classifications has been well documented by Barbara and Flusser (2003), Brown (1992), Dalley and Flynn (2002), Letser and Arrige (1999), Maintz *et al.*, (1998), Sindhu (2014), Sombir *et al.* (2014), van den Elsen *et al.* (1995), and Wan and Li (2003).

2.5 Classification of Image Registration Algorithms

The algorithms implemented at the various stages of an image registration paradigm must be considered in the development of an image registration system. Crum *et al.* (2004) and Dalley and Flynn (2002) classified image registration algorithms as:

- i. Intensity-based and feature – based classes.
- ii. Transformation algorithms.
- iii. Spatial frequency domain algorithms.
- iv. Single – multi – modality algorithms.

- v. Manual, semi-automatic and automatic algorithms.
- vi. Uncertainty algorithms.
- vii. Optimization algorithms.
- viii. Parametric and non-parametric algorithms.
- ix. Rigid and non-rigid algorithms.

2.6 Classification of Image Registration According to Modalities

The method or technique involved in the acquisition of images used for image registration is also an important factor in the development of an image registration paradigm (Makela *et al.*, 2002; Medha *et al.*, 2002; Wan and Li, 2003). There are two major modalities involved in image registration. These are:

1. Monomodal registration.
2. Multimodal registration.

2.6.1 Monomodal registration

Monomodal registration describes a model of registering overlapping images that depicts the same geographical features and are captured from the same camera source or sensor i.e. when the referenced and the sensed images to be registered together are from the same camera sensor. Well documented practical examples of the experimentation of monomodal registration can be found in Nemir *et al.* (2012) and Zhiyong *et al.* (2008). Monomodal image registration aids the finding and evaluation of the changes which appeared between the consecutive acquired images. Methods involved in monomodal image registration can be categorised into the following models: The transformation domain models (fourier transform methods, fourier transform to correct rotation method, and wavelet transform based image registration methods) and spatial domain models (contour-based image registration and combined approach of cross-correlation and features).

2.6.2 Multimodal image registration

Unlike monomodal image registration systems, a multimodal image registration system registers image pairs that stem from different modalities. It has the capability of registering images from different camera sensors (Frederick *et al.*, 1997; Gerlot and Bizais, 1987; Gerlot and Bizais, 1992).

Methods of multimodal image registration can be classified into five different methods (Mohammad and Somayeh, 2011). These include:

1. Information theory-based methods.
2. Discrete wavelet (Shuto *et al.*, 2006).
3. Intensity gradient (Eldad and Modersitzki, 2006).
4. Phase correction (Rania *et al.*, 2009).
5. Learning-based method (Diaa and Hany, 2007; Nahla and Monica, 2008).

The Information theory-based method can be further classified into four other sub-methods which include:

- a. Entropy (Meyer *et al.*, 2007).
- b. Mutual Information (MI) (Anand and James, 1998; Frederik *et al.*, 2003; Viola and Wells III, 1995; Wells III *et al.*, 1996; Xiang, 2014).
- c. Normalized Mutual Information (NMI).
- d. Kull back – Leibler Distance (Ho-Ming *et al.*, 2003).

Detailed notes on these aforementioned algorithms can be found in Mohammed and Somayeh (2011) while Figure 2.7 presents an overview of the classification of image registration according to image modalities.

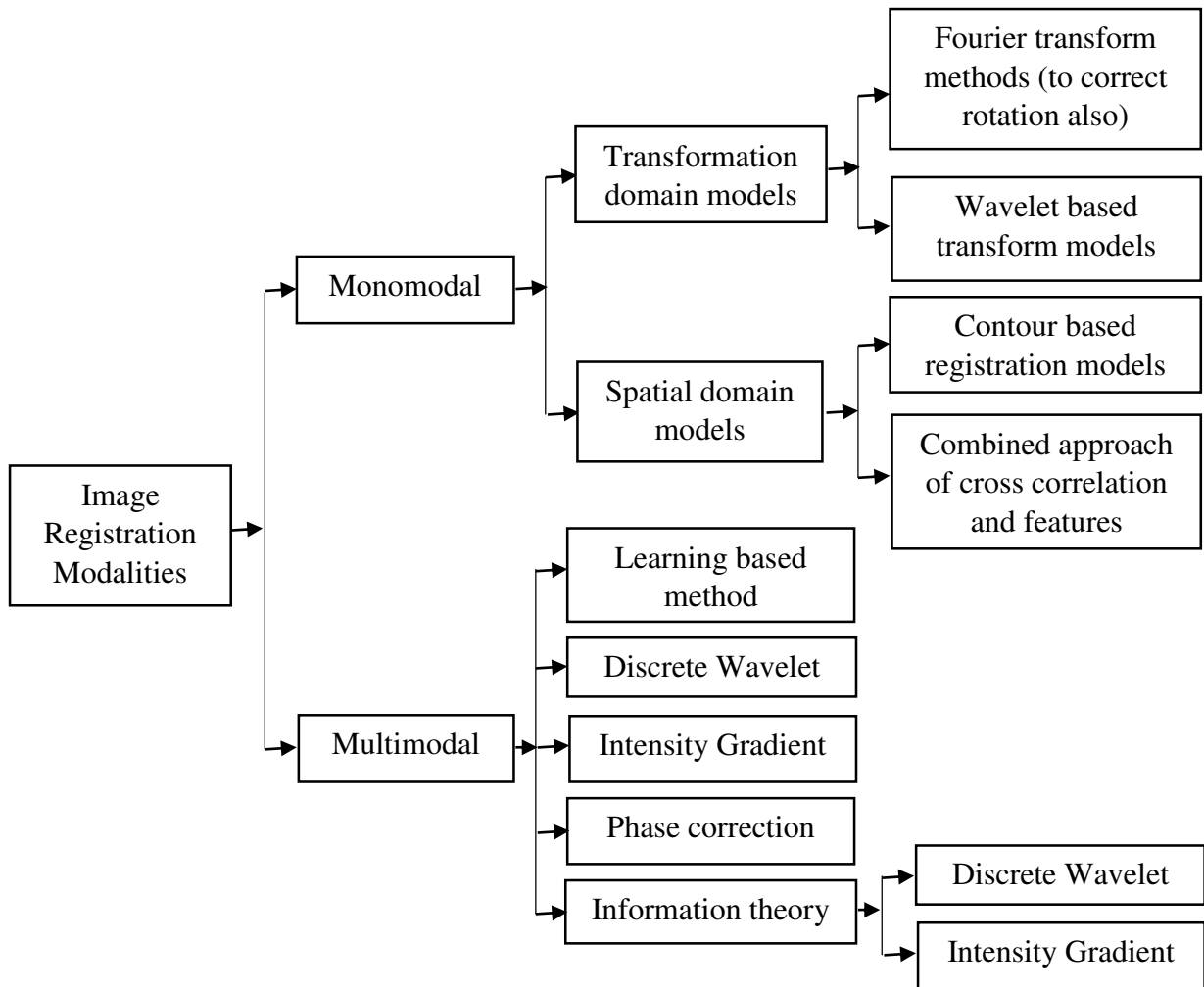


Figure 2.7: Overview of image registration techniques classified according to modalities

2.7 The Concept of Epipolar Geometry

Epipolar geometry can be described as the essential projective geometry between two different views. It is used to describe geometric relations in image pairs and enables efficient search for and prediction of corresponding points. It depends only on the intrinsic parameters of the cameras and their relative pose, and does not depend on the scene structure (Hartley & Zisserman, 2000; Olaleye, 2010). This intrinsic projective geometry is encoded in a 3x3 matrix referred to as the fundamental matrix $[F]$ (for the un-calibrated cameras), and the essential matrix $[E]$ (for the calibrated cameras). The F - matrix is a rank (2) matrix with seven (7) degrees of freedom (DOF) up to scale (five (5) pose and two (2) intrinsic). It can be computed from 2D image correspondences

(Feng and Hung, 2003). Thus, considering a point in 3D space, defined by location P (equation 2.14):

$$P = [X, Y, Z, 1]^T \quad (2.14)$$

The projected image of P (equation 2.14) in two different camera locations are given as equations (2.15) and (2.16):

$$P_l = [x_1, y_1, 1]^T \quad (2.15)$$

and

$$P_r = [x_2, y_2, 1]^T \quad (2.16)$$

And their vectors are given as equations (2.17) and (2.18) respectively:

$$p_l = [x_l \ y_l \ -f_l]^T \quad (2.17)$$

and

$$p_r = [x'r \ y'r \ -f_r]^T \quad (2.18)$$

Where P_l is one camera location of the projected image P and P_r is another camera location of P , then the epipolar constraint is given by equation (2.19), which is an expression of coplanarity constraint:

$$P_l^T F P_r = 0 \quad (2.19)$$

Where F is the fundamental matrix. Equations (2.13) and (2.14) represent the projections of P_l (equation 2.11) and P_r (equation 2.12) onto the two image planes, while f_l and f_r are the focal lengths of the two cameras and the points in the pixel coordinates corresponding to p_l and p_r are p_{xl} and p_{xr} . Figure 2.8 presents a diagrammatic illustration of epipolar geometry while Figure 2.9

shows the epipolar plane, epipolar line and the epipoles. The epipolar correlation method is a hybridised approach because it combines the feature-based (graph) method and the area-based methods (Nick and Heinz, 1996). It is a consequence of the coplanarity of the camera centres and scene point. That is, the corresponding points, camera centres and scene points all lie in a single plane referred to as the epipolar plane (Ludovico, 2011; Zhou *et al.*, 2015).

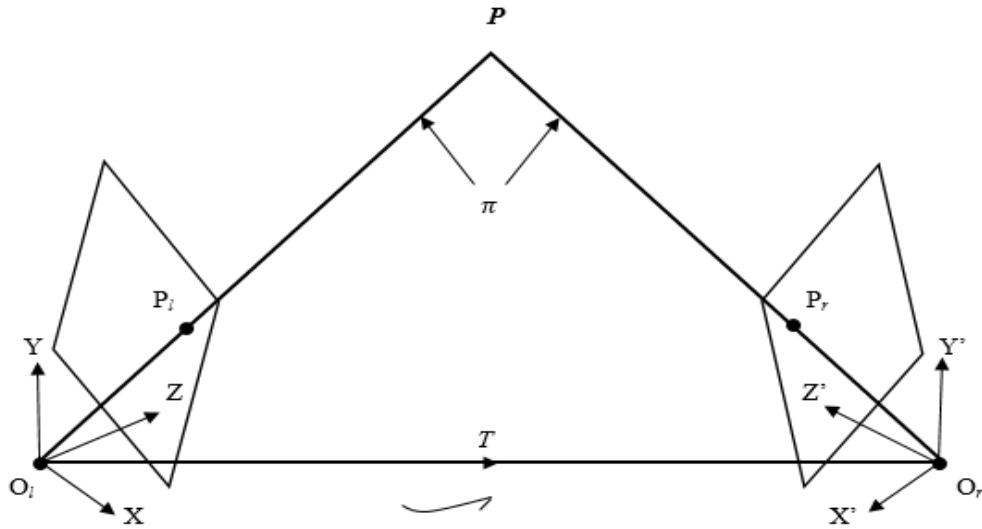


Figure 2.8: Configuration of epipolar geometry (Source: Zhou *et al.*, 2015).

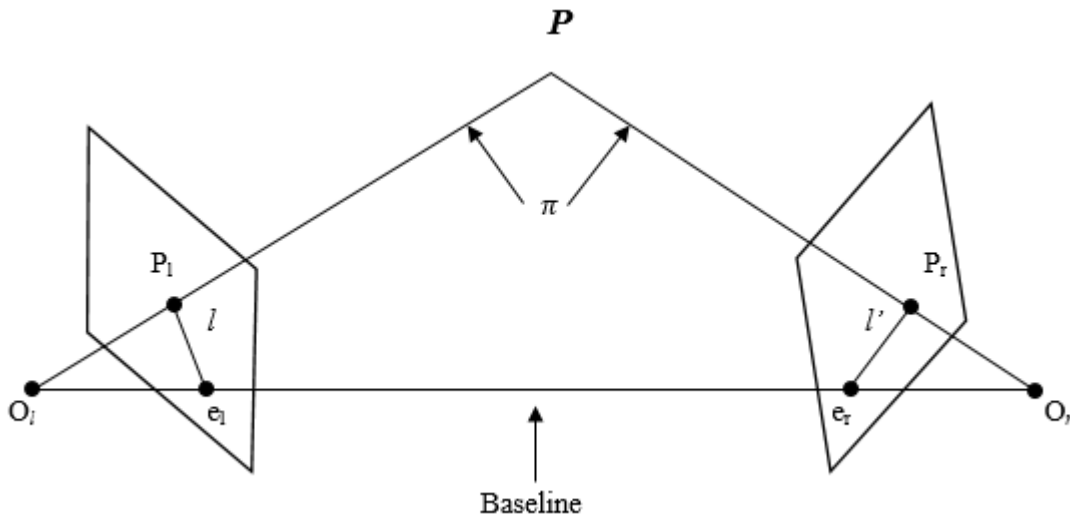


Figure 2.9: Epipolar geometry showing the epipolar lines (l and l'), epipoles (e_l and e_r), epipolar plane (π), origin of the camera frames (O_l and O_r) and the Baseline ($O_l O_r$) (Source: Author's Research).

2.7.1 Fundamental matrix

The fundamental matrix F is a matrix of array of fundamental solutions. Fundamental solutions are solutions that cannot be broken down any further and more specifically, one of those solutions cannot be expressed in terms of any of the other solutions; which means that they are all linearly independent. Fundamental matrix is a homogeneous and singular 3×3 matrix of the rank of two which encodes all the available relative orientation information for image pairs from uncalibrated cameras (cameras with unknown intrinsic parameters) without any information about the scene. It describes how image pairs are taken relative to each other and defines the relationship between the image pairs that constrains where the projection of points from the scene can occur in both image pairs. When many images are involved, F is depicted as F_{ij} and this yields the constraint $x_i'^T F_{ij} x_j'' = 0$ which means that $F = F_{12}$ where x_i', x_j'' are corresponding points. This is however different from F as used in Computer Vision (CV). In Computer Vision, $x_i''^T F_{ij} x_j' = 0$ which means that $F = F_{21} = F_{12}^T$. This implies that the transpose of the fundamental matrix as used in photogrammetry is what computer vision uses. This transposition needs to be taken into consideration when comparing algebraic expressions. The fundamental matrix can be easily computed from projection matrices, from corresponding points or expressed in terms of the essential matrix. It is basically defined by the calibration matrices of the two cameras, the rotation (orientation) matrices of the two cameras and the skew-symmetric matrix of the base line. It allows for the expression of coplanarity constraints (Hartley & Zisserman, 2000) as earlier shown in equation (2.19).

2.7.1.1 Estimating fundamental matrix in terms of the essential matrix

According to the law of coplanarity constraint, vectors P_l , P_r and T all lies on the same plane (see Figures 2.8 and 2.9), hence,

$$P_r^T T P_l = 0 \quad (2.20)$$

$$(P_l - T)^T T P_l = 0 \quad (2.21)$$

Expressing P_r in terms of P_l , translation T and rotation matrix R ,

$$P_r = R(P_l - T) \quad (2.22)$$

$$R^T P_r = (P_l - T) \quad (2.23)$$

Transposing both sides of equation (2.23) results into equation (2.24);

$$P_r^T R = (P_l - T)^T \quad (2.24)$$

Substituting equation (2.24) into equation (2.21) to obtain equation (2.25);

$$P_r^T R T P_l = 0 \quad (2.25)$$

Finding skew symmetric matrix S from the vector T and multiplying it with the vector P_l , equation (2.25) becomes;

$$P_r^T R S P_l = 0 \quad (2.26)$$

Where $S = \begin{bmatrix} 0 & -T_z & T_y \\ T_z & 0 & -T_x \\ -T_y & T_x & 0 \end{bmatrix}$

From equation (2.26), there are two matrices R and S where R is the rotation matrix and S is the translation vector's skew symmetric matrix. When these two matrices are multiplied, the essential matrix E is obtained.

$$RS = E \quad (2.27)$$

Substituting equation (2.27) into equation (2.26) gives equation (2.28):

$$P_r^T E P_l = 0 \quad (2.28)$$

But both P_l and P_r are three (3) dimensional and are in the object plane. When they are both expressed in the image plane, it results into fundamental matrix. In order to achieve this, the camera model must be applied to get the image plane from the world or object plane as follows:

$$X_l = B_l P_l \quad (2.29)$$

$$X_r = B_r P_r \quad (2.30)$$

Where B is the camera model matrix.

Solving for P_l and P_r from equations (2.29) and (2.30), equations (2.31) and (2.32) were obtained

$$B_l^{-1} X_l = P_l \quad (2.31)$$

$$B_r^{-1} X_r = P_r \quad (2.32)$$

Transposing equation (2.32),

$$X_r^T B_r^T = P_r^T \quad (2.33)$$

Substituting equations (2.31) and (2.33) into equation (2.32) yielded equation (2.34):

$$X_r^T B_r^T E B_l^{-1} X_l = 0 \quad (2.34)$$

This can also be re-written as:

$$X_r^T (B_r^T E B_l^{-1}) X_l = 0 \quad (2.35)$$

$$\text{When } F = B_r^T E B_l^{-1} \quad (2.36)$$

Substituting equation (2.36) into equation (2.35),

$$X_r^T F X_l = 0 \quad (2.37)$$

Equation (2.37) also defines the coplanarity constraint.

2.7.1.2 Computing fundamental matrix from corresponding points

The problem of estimating fundamental matrix from corresponding points can be defined as follows:

Given Np as the total number of corresponding points with each of the points having image coordinates $(x', y')_n, (x'', y'')_n$, when $n = 1, \dots, Np$, compute the Fundamental matrix F .

Recall that the coplanarity constraint is given as equation (2.38)

$$x'^T F x'' = 0 \quad (2.38)$$

For each point, the coplanarity constraint can be expressed as equation (2.39)

$$x_n'^T F x_n'' = 0 \quad (2.39)$$

when $n = 1, \dots, Np$

Equation (2.39) can be further expressed in homogeneous form to give equation (2.40).

$$[x_n', y_n', 1] \begin{bmatrix} F_{11} & F_{12} & F_{13} \\ F_{21} & F_{22} & F_{23} \\ F_{31} & F_{32} & F_{33} \end{bmatrix} \begin{bmatrix} x_n'' \\ y_n'' \\ 1 \end{bmatrix} = 0 \quad (2.40)$$

Where $\begin{bmatrix} F_{11} & F_{12} & F_{13} \\ F_{21} & F_{22} & F_{23} \\ F_{31} & F_{32} & F_{33} \end{bmatrix}$ are the 9 unknown parameters.

To solve for these unknown parameters, it should be noted that there is linear dependency between the known parameters (X' and X'') and the unknown parameters F . This becomes clearer when the product of this matrix (equation 2.40) in two vectors is computed, and this results in equation (2.41).

$$x_n'' F_{11} x_n' + x_n'' F_{21} y_n' + x_n'' F_{31} + \dots = 0 \quad (2.41)$$

Collecting like terms (of known and unknown elements), and fixing them into one vector each (vectors of known and unknown) produces a vector expressed as equation (2.42).

$$[x_n'' x_n', x_n'' y_n', x_n'', y_n' x_n', y_n' y_n', y_n'', x_n', y_n', 1] \cdot [F_{11}, F_{21}, F_{31}, F_{12}, F_{22}, F_{32}, F_{13}, F_{23}, F_{33}] = 0 \quad (2.42)$$

Where, $n = 1, 2, \dots, Np$.

Hence, the 3 x 3 matrix of equation (2.41) becomes a 9 x 1 matrix of equation (2.42).

Rewriting equation (2.42) as a product of vector a_n^T and vector f^T so as to compute the vector of unknowns, equation (2.42) becomes equation (2.43).

$$a_n^T \cdot f^T = 0, \quad n = 1, 2, \dots, Np \quad (2.43)$$

where $a_n^T = (x_n'' \otimes x_n')^T$ which is the kroniker product of the two individual elements, and

$f^T = \text{vec}F$ which converts the matrix F into a vector.

$$\text{Therefore, } (x_n'' \otimes x_n')^T \text{vec}F = 0, \quad n = 1, 2, \dots, Np \quad (2.44)$$

When equation (2.44) is expressed in a general form, it becomes;

$$X^T F y = (y \otimes X)^T \text{vec}F \quad (2.45)$$

If all points of Np are considered, a linear system will be directly obtained.

$$a_n^T \cdot f = 0, \quad n = 1, 2, \dots, Np \quad (2.46)$$

Where $f = \text{vec}F$

$$Af = 0 \quad (2.47a)$$

$$A = \begin{bmatrix} a_1^T \\ \dots \\ a_n^T \\ \dots \\ a_N^T \end{bmatrix}, \quad f = [F_{11}, F_{21}, F_{31}, F_{12}, F_{22}, F_{32}, F_{13}, F_{23}, F_{33}] \quad (2.47b)$$

Equation (2.47a) implies that the coplanarity constraint of all the individual pairs of corresponding points are encapsulated into one single equation where the unknowns are one vector (nine dimensional) and contains individual element of the fundamental matrix.

For the unknowns of matrix A to be computed, the system of linear equation must be solved, and in providing the solution of the linear system, Singular Value Decomposition (SVD) has been adopted. Recall that equation (2.43) can be characterized as a right-singular vector that corresponds to a singular value of A that is zero. Since vector f is a 9-dimensional vector, minimum of 8 corresponding points are needed instead of 9 because F matrix is a homogenous matrix and homogenous matrix has 8 degrees of freedom. Also, matrix A has a rank of at most 8.

Then, the vector f of A that corresponds to the smallest singular value is used to obtain F

$$A = UDV^T \quad (2.48)$$

Where $A = Np \times 9$, $D = Np \times 9$, $U = Np \times Np$ and $V = 9 \times 9$ dimensions.

From the F computed (equation 2.44), a matrix \hat{F} with rank 2 is enforced to get a matrix F with rank $F = 2$ while \hat{F} should approximate F computed as close as possible.

Then, the SVD of F is computed and used as follows:

$$F = UD^aV^T \quad (2.49)$$

$$F = Udiag(D_{11}, D_{22}, 0)V^T \quad (2.50)$$

$$svd(\hat{F}) = UDV^T, \text{ where } D_{11} \geq D_{22} \geq D_{33} \quad (2.51)$$

So, elements of the SVD are taken, and D modified by setting the smallest (closest to zero) element into zero so that a matrix F which is close to the initially computed matrix F as much as possible, and now, with rank 2 can be obtained.

$$\text{Finally, } F = UDV^T = U \begin{bmatrix} D_{11} & 0 & 0 \\ 0 & D_{22} & 0 \\ 0 & 0 & 0 \end{bmatrix} V^T \quad (2.52)$$

2.7.2 Coplanarity constraint from uncalibrated camera

In deriving the mathematical expression of coplanarity constraint from uncalibrated camera, it is important to define coplanarity equation in clear terms. Figure 2.10 presents a graphical expression of coplanarity constraints while equation (2.53) presents its mathematical expression.

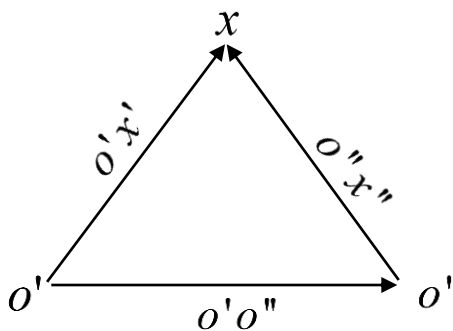


Figure 2.10: Coplanarity condition (Source: Author's Research)

Coplanarity can be expressed by:

$$[o'x' \quad o'o'' \quad o'x''] = 0 \quad (2.53)$$

Where x' and x'' refers to the same point (x) in space if the correspondences are correct. The main constraint which defines coplanarity is that these three vectors lie on the same plane in the 3D world or object space and this can be extracted using scalar triple product which consists of three vectors as shown in equation (2.53). The operator $[...]$ is the triple product which is expressed as the dot product of one of the vectors with the cross product of the remaining two vectors. i. e.,

$$[A, B, C] = (A \times B) \cdot C \quad (2.54)$$

This can be done basically by computing the vector that is orthogonal to A and B and using its dot product with the third vector C. What it basically does is that it computes the volume of the parallelepiped of the three vectors.

From equation (2.53) and figure (2.9), the directions of the vectors $o'x'$ and $o'x''$ can be derived from the image coordinates x', x'' .

$$x' = P'x \quad (2.55)$$

$$x'' = P''x \quad (2.56)$$

When P' and P'' are the projection matrices of the first and second cameras respectively.

$$P' = K' R' [I_3 / -X'_o] \quad (2.57)$$

$$P'' = K'' R'' [I_3 / -X''_o] \quad (2.58)$$

Where $[I_3 / -X''_o] = \begin{bmatrix} 1 & 0 & 0 & -X''_o \\ 0 & 1 & 0 & -Y''_o \\ 0 & 0 & 1 & -Z''_o \end{bmatrix}$, K' and K'' are the calibration matrices of the

first and second camera respectively (which is further expressed as equation (2.139) in subsection

2.7.3.2), R' and R'' are the orientation matrices, X'_o and X''_o are the projection centres and X is the 3D location of the point in the object space.

The normalized directions of the vectors $o'x'$ and $o''x''$ are:

$${}^nX' = (R')^{-1}(K')^{-1}x' = o'x' \quad (2.59)$$

$${}^nX'' = (R'')^{-1}(K'')^{-1}x'' = o''x'' \quad (2.60)$$

And the normalized projection gives

$${}^nX' = [I_3 / -X'_o]X \quad (2.61)$$

The base vector $o'o''$ directly results from the coordinates of the projection centres

$$b = B = X''_o - X'_o = o'o'' \quad (2.62)$$

Where X'_o and X''_o are the X, Y, Z coordinates of the first and second cameras respectively.

Substituting equations (2.59), (2.60) and (2.62) into equation (2.53), equation (2.63) was obtained as:

$$[{}^nX' \quad b \quad {}^nX''] = 0 \quad (2.63)$$

From the definition of triple scalar product,

$${}^nX' \cdot (b \times {}^nX'') = 0 \quad (2.64)$$

Equation (2.64) can thus be re-written as equation (2.65)

$${}^nX' S_b {}^nX'' = 0 \quad (2.65)$$

Where S_b is the skew-symmetric matrix of $b = \begin{bmatrix} 0 & -b_3 & b_2 \\ b_3 & 0 & -b_1 \\ -b_2 & b_1 & 0 \end{bmatrix}$. It is equal to the negative of its

transpose and it has a rank of 2. It has 3 Degrees of Freedom (DoF) and it is a singular matrix with vector b where b is the base line. It shows the direction of the first camera with respect to the second camera though there is ambiguity with respect to the scale. Also, Though the direction of the first camera with respect to the second camera is known, the distance between the two cameras is unknown.

Combining equations (2.59), (2.60) and (2.65) and replacing " X' " and " X'' ", yielded equation (2.66):

$$X'^T (K')^{-T} (R')^{-T} S_b (R'')^{-1} (K'')^{-1} X'' = 0 \quad (2.66)$$

$$\text{Let } F = (K')^{-T} (R')^{-T} S_b (R'')^{-1} (K'')^{-1} \quad (2.67)$$

Equation (2.67) can be further simplified as presented in equation (2.68).

$$F = (K')^{-T} R' S_b R''^T (K'')^{-1} \quad (2.68)$$

Where equation (2.68) is the general definition of the fundamental matrix (F) for uncalibrated cameras. It is basically defined by the calibration matrices of the two cameras (K' and K''), the rotation matrices (orientation) of the two cameras (R' and R'') and the skew-symmetric (asymmetric) matrix of the base line (S_b). It also allows for the expression of the coplanarity constraint i.e: substituting equation (2.67) into (2.66), to get equation (2.69):

$$X'^T F X'' = 0 \quad (2.69)$$

2.7.2.1 Linearization of coplanarity condition equation

Figure 2.11 presents the diagrammatic expression of the coplanarity condition with respect to a stereo pair, where (x_M, y_M, z_M) and (x_N, y_N, z_N) are the axes of the perspective centre projected on the image (principal point). In absolute conditions, this axis should superimpose on the fiducial centre but in most cases, it slightly drifts away from it. I_M and I_N are the images of the object P on the photo. \vec{l}_M and \vec{l}_N are vectors on the image plane. X, Y and Z are the axis of the object space.

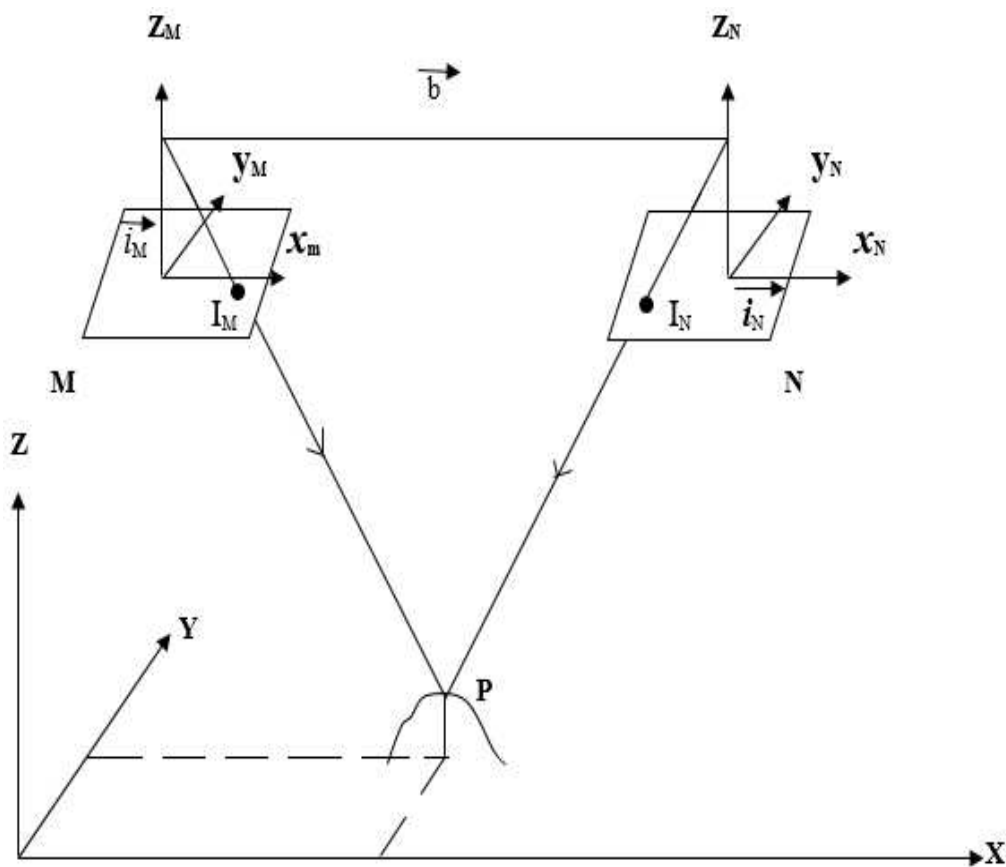


Figure 2.11: Expression of coplanarity condition with respect to a stereo pair (Source: Author's Research)

From Figure (2.11), coplanarity condition states that the baseline \vec{b} , and the corresponding position vectors $I_M = \vec{MP}$ and $I_N = \vec{NP}$, all lies on the same plane. P is the object and I_M and I_N are the images on the photograph at exposure stations M and N .

$$\vec{l}_M = \vec{MI}_M \quad (2.70a)$$

$$\vec{i}_N = \overrightarrow{MI_N} \quad (2.70b)$$

$x_M = \overrightarrow{MP}$ and $x_N = \overrightarrow{NP}$ are on the same plane with baseline \vec{b}

$$\text{Where } \vec{b} = \overrightarrow{MB} = \begin{bmatrix} b_x \\ b_y \\ b_z \end{bmatrix} \quad (2.71)$$

$$\vec{i}_M = \begin{bmatrix} x_m - x_0 \\ y_m - y_0 \\ -f \end{bmatrix} \text{ and } \vec{i}_N = \begin{bmatrix} x_b - x_0 \\ y_b - y_0 \\ -f \end{bmatrix} \quad (2.72)$$

Given that \vec{b} , \vec{i}_M and \vec{i}_N are coplanar as expressed in equation (2.73) which is the scalar triple product of equations (2.71) and (2.72).

$$\vec{b} \cdot (\vec{i}_M \times \vec{i}_N) = 0 \quad (2.73)$$

Expressing the components of \vec{i}_N in the camera reference system of M gives (2.74)

$$b^T [i_M \times] R i_N = 0 \quad (2.74)$$

Where R is the rotation matrix that turns camera N in line with camera M acting as in a relative orientation matrix.

If the length of the baseline is reduced by a constant value (say K), the intersecting property of the rays projected from the various exposure stations passing through their images remain unchanged, only that it does not target the real object but a model of the real object. This only increases the x, y, z, component of the baseline by a constant value.

$$K\vec{b} = K \begin{bmatrix} b_x \\ \beta_y \\ \beta_z \end{bmatrix} = \begin{bmatrix} Kb_x \\ K\beta_y \\ K\beta_z \end{bmatrix} \quad (2.75a)$$

Expressing the baseline vector by one of its components removes the constant value, which was done by factorizing b_x out of \vec{b} so that the \vec{b} will be expressed as a ratio of one of its components.

$$\vec{b} = b_x \begin{bmatrix} 1 \\ b_y/b_x \\ b_z/b_x \end{bmatrix} = b_x \begin{bmatrix} 1 \\ \beta_y \\ \beta_z \end{bmatrix} = b_x \beta \quad (2.75b)$$

Where:

$$(i_M \times) = i_M (i_M^T) = \begin{bmatrix} x_M - x_0 \\ y_M - y_0 \\ -f \end{bmatrix} \begin{bmatrix} x_M - x_0 & y_M - y_0 & -f \end{bmatrix} = \begin{bmatrix} 0 & f & (y_N - y_0) \\ -f & 0 & -(x_M - x_0) \\ -(y_N - y_0) & (x_M - x_0) & 0 \end{bmatrix} \quad (2.76a)$$

$$\text{Where: } (x_M - x_0)(x_M - x_0) = (y_M - y_0)(y_M - y_0) = -f(-f) = 0 \quad (2.76b)$$

$$(x_M - x_0)(y_M - y_0) = -f; (y_M - y_0)(-f) = (x_M - x_0) \text{ and}$$

$$-f(x_M - x_0) = (y_M - y_0); \quad (2.76c)$$

$$\text{Also } (y_M - y_0)(x_M - x_0) = f; (-f)(y_M - y_0) = -(x_M - x_0); \text{ and}$$

$$(x_M - x_0)(-f) = -(y_M - y_0); \quad (2.76d)$$

Thus, equation (2.74) can now be expressed as equation (2.77)

$$[1 \quad \beta_y \quad \beta_z] \begin{bmatrix} 0 & f & (y_N - y_0) \\ -f & 0 & -(x_M - x_0) \\ -(y_N - y_0) & (x_M - x_0) & 0 \end{bmatrix} R \begin{bmatrix} x_N - x_0 \\ y_N - y_0 \\ -f \end{bmatrix} = 0 \quad (2.77)$$

And when expanded further, results into equation (2.78)

$$\begin{aligned} & [-f\beta_y - \beta_z(y_N - y_0)][R_{11}(x_N - x_0) + R_{12}(y_N - y_0) - R_{13}f] + [f + \beta_z(x_M - x_0)][R_{21}(x_N - \\ & x_0) + R_{22}(y_N - y_0) - R_{23}f] + [y_N - y_0 - \beta_y(x_M - x_0)][R_{31}(x_N - x_0) + R_{32}(y_N - y_0) - \\ & R_{33}f] = 0 \end{aligned} \quad (2.78)$$

The above coplanarity equation can be reduced into a functional form as given in equation (2.79)

$$F(\beta_y, \beta_z, \omega, \varphi, \kappa, x_M, y_M, x_N, y_N) = \beta(\beta_y, \beta_z)^T [i_M(x_M, y_M) \times] R(\omega, \varphi, \kappa) i_N(x_N, y_N) = 0 \quad (2.79)$$

In order to find the linear approximation of the coplanarity equation (2.78), the least squares method was used and the details of the linearization process are as follows:

Taking the partial derivatives of every component of the coplanarity equation as in (2.78) results into the following equations:

Partial differentiation of the coplanarity equation (2.78) with respect to β_y :

$$\begin{aligned} \frac{\partial F(\beta_y, \beta_z, \omega, \varphi, \kappa, x_M, y_M, x_N, y_N)}{\partial \beta_y} &= \frac{\partial}{\partial \beta_y} [-f\beta_y - \beta_z(y_M - y_0)][R_{11}(x_N - x_0) + R_{12}(y_N - y_0) - \\ &R_{13}f] + \frac{\partial}{\partial \beta_y} [f + \beta_z(x_M - x_0)][R_{21}(x_N - x_0) + R_{22}(y_N - y_0) - R_{23}f] + \frac{\partial}{\partial \beta_y} [y_M - y_0 - \\ &\beta_y(x_M - x_0)][R_{31}(x_N - x_0) + R_{32}(y_N - y_0) - R_{33}f] = 0 \end{aligned} \quad (2.80a)$$

Solving equation (2.80a) further results into equation (2.80b):

$$\begin{aligned} \frac{\partial F(\beta_y, \beta_z, \omega, \varphi, \kappa, x_M, y_M, x_N, y_N)}{\partial \beta_y} &= [-f + 0][R_{11}(x_N - x_0) + R_{12}(y_N - y_0) - R_{13}f] + 0 + [0 - \\ &(x_M - x_0)][R_{31}(x_N - x_0) + R_{32}(y_N - y_0) - R_{33}f] = 0 \end{aligned} \quad (2.80b)$$

These further results into equation (2.80c) which is the partial derivative of equation (2.78) with respect to β_y :

$$\begin{aligned} \frac{\partial F(\beta_y, \beta_z, \omega, \varphi, \kappa, x_M, y_M, x_N, y_N)}{\partial \beta_y} &= -f[R_{11}(x_N - x_0) + R_{12}(y_N - y_0) - R_{13}f] \\ &-(x_M - x_0)[R_{31}(x_N - x_0) + R_{32}(y_N - y_0) - R_{33}f] = 0 \end{aligned} \quad (2.80c)$$

Partial differentiation of the coplanarity equation (2.78) with respect to β_z results into equation (2.81a):

$$\begin{aligned} \frac{\partial F(\beta_y, \beta_z, \omega, \varphi, \kappa, x_M, y_M, x_N, y_N)}{\partial \beta_z} &= \frac{\partial}{\partial \beta_z} [-f\beta_y - \beta_z(y_M - y_0)][R_{11}(x_N - x_0) + R_{12}(y_N - y_0) - \\ &R_{13}f] + \frac{\partial}{\partial \beta_z} [f + \beta_z(x_M - x_0)][R_{21}(x_N - x_0) + R_{22}(y_N - y_0) - R_{23}f] + \frac{\partial}{\partial \beta_z} [y_M - y_0 - \\ &\beta_\gamma(x_M - x_0)][R_{31}(x_N - x_0) + R_{32}(y_N - y_0) - R_{33}f] = 0 \end{aligned} \quad (2.81a)$$

Solving equation (2.81a) further results into equation (2.81b):

$$\begin{aligned} \frac{\partial F(\beta_y, \beta_z, \omega, \varphi, \kappa, x_M, y_M, x_N, y_N)}{\partial \beta_z} &= [0 - (y_M - y_0)][R_{11}(x_N - x_0) + R_{12}(y_N - y_0) - R_{13}f] + [0 + \\ &(x_M - x_0)][R_{21}(x_N - x_0) + R_{22}(y_N - y_0) - R_{23}f] + 0 = 0 \end{aligned} \quad (2.81b)$$

This results into equation (2.81c) which is the partial derivative of the coplanarity equation (2.78)

with respect to β_z :

$$\begin{aligned} \frac{\partial F(\beta_y, \beta_z, \omega, \varphi, \kappa, x_M, y_M, x_N, y_N)}{\partial \beta_z} &= -(y_M - y_0)[(R_{11}(x_N - x_0) + R_{12}(y_N - y_0) - R_{13}f] - (x_M - \\ &x_0)[R_{21}(x_N - x_0) + R_{22}(y_N - y_0) - R_{23}f] \end{aligned} \quad (2.81c)$$

In solving the partial differentiation of the coplanarity equation (2.78) with respect to x_M ,

$$\begin{aligned} \frac{\partial F(\beta_y, \beta_z, \omega, \varphi, \kappa, x_M, y_M, x_N, y_N)}{\partial x_M} &= \frac{\partial}{\partial x_M} [-f\beta_y - \beta_z(y_M - y_0)][R_{11}(x_N - x_0) + R_{12}(y_N - y_0) - \\ &R_{13}f] + \frac{\partial}{\partial x_M} [f + \beta_z(x_M - x_0)][R_{21}(x_N - x_0) + R_{22}(y_N - y_0) - R_{23}f] + \frac{\partial}{\partial x_M} [y_M - y_0 - \\ &\beta_\gamma(x_M - x_0)][R_{31}(x_N - x_0) + R_{32}(y_N - y_0) - R_{33}f] = 0 \end{aligned} \quad (2.82a)$$

Solving equation (2.82a) results into equation (2.82b):

$$\begin{aligned} \frac{\partial F(\beta_y, \beta_z, \omega, \varphi, \kappa, x_M, y_M, x_N, y_N)}{\partial x_M} &= 0 + [0 + \beta_z][R_{21}(x_N - x_0) + R_{22}(y_N - y_0) - R_{23}f] + [0 - \\ &\beta_\gamma][R_{31}(x_N - x_0) + R_{32}(y_N - y_0) - R_{33}f] = 0 \end{aligned} \quad (2.82b)$$

This results in equation (2.82c) which is the partial derivative of the coplanarity equation (2.78)

with respect to x_M :

$$\begin{aligned} \frac{\partial F}{\partial x_M} &= \beta_z [R_{21}(x_N - x_0) + R_{22}(y_N - y_0) - R_{23}f] - \\ &- \beta_\gamma [R_{31}(x_N - x_0) + R_{32}(y_N - y_0) - R_{33}f] \end{aligned} \quad (2.82c)$$

Partial differentiation of the coplanarity equation (2.78) with respect to y_M :

$$\begin{aligned} \frac{\partial F(\beta_y, \beta_z, \omega, \varphi, \kappa, x_M, y_M, x_N, y_N)}{\partial y_M} &= \frac{\partial}{\partial y_M} [-f\beta_y - \beta_z(y_M - y_0)] [R_{11}(x_N - x_0) + R_{12}(y_N - y_0) - \\ R_{13}f] &+ \frac{\partial}{\partial y_M} [f + \beta_z(x_M - x_0)] [R_{21}(x_N - x_0) + R_{22}(y_N - y_0) - R_{23}f] + \frac{\partial}{\partial y_M} [y_M - y_0 - \\ \beta_\gamma(x_M - x_0)] &[R_{31}(x_N - x_0) + R_{32}(y_N - y_0) - R_{33}f] = 0 \end{aligned} \quad (2.83a)$$

Solving equation (2.83a) further results into equation (2.83b):

$$\begin{aligned} \frac{\partial F(\beta_y, \beta_z, \omega, \varphi, \kappa, x_M, y_M, x_N, y_N)}{\partial y_M} &= [0 - \beta_z] [R_{11}(x_N - x_0) + R_{12}(y_N - y_0) - R_{13}f] + 0 + \\ [1] &[R_{31}(x_N - x_0) + R_{32}(y_N - y_0) - R_{33}f] = 0 \end{aligned} \quad (2.83b)$$

This results into equation (2.83c) which is the partial derivative of the coplanarity equation (2.78) with respect to y_M :

$$\begin{aligned} \frac{\partial F}{\partial y_M} &= -\beta_z [R_{11}(x_N - x_0) + R_{12}(y_N - y_0) - R_{13}f] + \\ y_M &[R_{31}(x_N - x_0) + R_{32}(y_N - y_0) - R_{33}f] \end{aligned} \quad (2.83c)$$

Partial differentiation of the coplanarity equation (2.78) with respect to x_N :

$$\begin{aligned} \frac{\partial F(\beta_y, \beta_z, \omega, \varphi, \kappa, x_M, y_M, x_N, y_N)}{\partial x_N} &= \frac{\partial}{\partial x_N} [-f\beta_y - \beta_z(y_M - y_0)] [R_{11}(x_N - x_0) + R_{12}(y_N - y_0) - \\ R_{13}f] &+ \frac{\partial}{\partial x_N} [f + \beta_z(x_M - x_0)] [R_{21}(x_N - x_0) + R_{22}(y_N - y_0) - R_{23}f] + \frac{\partial}{\partial x_N} [y_M - y_0 - \\ \beta_\gamma(x_M - x_0)] &[R_{31}(x_N - x_0) + R_{32}(y_N - y_0) - R_{33}f] = 0 \end{aligned} \quad (2.84a)$$

Solving equation (2.84a) further gives (2.84b):

$$\frac{\partial F(\beta_y, \beta_z, \omega, \varphi, \kappa, x_M, y_M, x_N, y_N)}{\partial x_N} = [-f\beta_y - \beta_z(y_M - y_0)][0 + R_{12}(1) - 0] + [f + \beta_z(x_M - x_0)][0 + R_{22}(1) - 0] + [y_M - y_0 - \beta_\gamma(x_M - x_0)][0 + R_{32}(1) - 0] = 0 \quad (2.84b)$$

This further result into equation (2.84c) which is the partial derivative of the coplanarity equation (2.78) with respect to x_N :

$$\frac{\partial F}{\partial x_N} = R_{11}[-f\beta_y - \beta_z(y_M - y_0)] + R_{21}[f + \beta_z(x_M - x_0) + R_{31}[(y_M - y_0) + \beta_\gamma(x_M - x_0)]] \quad (2.84c)$$

Partial differentiation of the coplanarity equation (2.78) with respect to y_N :

$$\begin{aligned} \frac{\partial F(\beta_y, \beta_z, \omega, \varphi, \kappa, x_M, y_M, x_N, y_N)}{\partial y_N} &= \frac{\partial}{\partial y_N} [-f\beta_y - \beta_z(y_M - y_0)][R_{11}(x_N - x_0) + R_{12}(y_N - y_0) - \\ &R_{13}f] + \frac{\partial}{\partial y_N} [f + \beta_z(x_M - x_0)][R_{21}(x_N - x_0) + R_{22}(y_N - y_0) - R_{23}f] + \frac{\partial}{\partial y_N} [y_M - y_0 - \\ &\beta_\gamma(x_M - x_0)][R_{31}(x_N - x_0) + R_{32}(y_N - y_0) - R_{33}f] = 0 \end{aligned} \quad (2.85a)$$

Solving equation (2.85a) further gives equation (2.85b):

$$\begin{aligned} \frac{\partial F(\beta_y, \beta_z, \omega, \varphi, \kappa, x_M, y_M, x_N, y_N)}{\partial y_N} &= [-f\beta_y - \beta_z(y_M - y_0)][0 + R_{12}(y_N - 0) - 0] + [f + \beta_z(x_M - \\ &x_0)][0 + R_{22}(y_N - 0) - 0] + [y_M - y_0 - \beta_\gamma(x_M - x_0)][0 + R_{32}(y_N - 0) - 0] = 0 \end{aligned} \quad (2.85b)$$

This further results in equation (2.85c) which is the partial derivative of the coplanarity equation (2.78) with respect to y_N :

$$\begin{aligned} \frac{\partial F}{\partial y_N} &= R_{21}[-f\beta_y - \beta_z(y_M - y_0)] + R_{22}[f + \beta_z(x_M - x_0) + R_{32}[(y_M - y_0) + \beta_\gamma(x_M - x_0)]] = \\ &R_{21}[-f\beta_y - \beta_z(y_M - y_0)] + R_{22}[f + \beta_z(x_M - x_0) + \\ &R_{32}[(y_M - y_0) + \beta_\gamma(x_M - x_0)]] \end{aligned} \quad (2.85c)$$

To get the partial derivatives with respect to the angles ω , φ and κ , we recall that

$R_\omega R^T = [w_\omega \times], R_\varphi R^T = [w_\varphi \times], R_\kappa R^T = [w_\kappa \times]$ are asymmetric matrices with axial vectors $w_\omega, w_\varphi, w_\kappa$, respectively, which in turn are the rows of the already given matrix W .

$$R^T = \begin{bmatrix} \cos \varnothing \cos \kappa & -\cos \varnothing \sin \kappa & \sin \varnothing \\ \cos \omega \sin \kappa + \sin \omega \sin \varnothing \cos \kappa & \cos \omega \cos \kappa - \sin \omega \sin \varnothing \sin \kappa & -\sin \omega \cos \varnothing \\ \sin \omega \sin \kappa - \cos \omega \sin \varnothing \cos \kappa & \sin \omega \cos \kappa - \cos \omega \sin \varnothing \sin \kappa & \cos \omega \cos \varnothing \end{bmatrix} \quad (2.85a)$$

Where the rotation matrix is (2.85b)

$$R = \begin{bmatrix} \cos \varphi \cos \kappa & \cos \omega \sin \kappa + \sin \omega \sin \varphi \cos \kappa & \sin \omega \sin \kappa - \cos \omega \sin \varphi \cos \kappa \\ -\cos \varphi \sin \kappa & \cos \omega \cos \kappa - \sin \omega \sin \varphi \sin \kappa & \sin \omega \cos \kappa - \cos \omega \sin \varphi \sin \kappa \\ \sin \varphi & -\sin \omega \cos \varphi & \cos \omega \cos \varphi \end{bmatrix} \quad (2.85b)$$

$R_\omega = [w_\omega \times]R, R_\varphi = [w_\varphi \times]R, R_\kappa = [w_\kappa \times]R$ and the required derivatives becomes equation (2.86)

$$\frac{\partial F}{\partial \omega} = \beta^T [i_M \times] R_\omega i_N = \beta^T [i_M \times] [w_\omega \times] R i_N \quad (2.86)$$

Applying scalar triple product, equations (2.87), (2.88) and (2.89) were obtained:

$$\frac{\partial F}{\partial \omega} = -\beta^T [i_M \times] [(R i_N) \times] w_\omega \quad (2.87)$$

$$\frac{\partial F}{\partial \varphi} \beta^T [i_M \times] R_\varphi i_N = \beta^T [i_M \times] [w_\varphi \times] R i_N = -\beta^T [i_M \times] [(R i_N) \times] w_\varphi \quad (2.88)$$

$$\frac{\partial F}{\partial \kappa} \beta^T [i_M \times] R_\kappa i_N = \beta^T [i_M \times] [w_\kappa \times] R i_N = -\beta^T [i_M \times] [(R i_N) \times] w_\kappa, \quad (2.89)$$

where the vectors $w_\omega, w_\varphi, w_\kappa$ are the same as in the case of the collinearity equations. By setting

$\theta = [\omega \varphi \kappa]^T$, the above derivatives can be summarized as equation (2.90).

$$\frac{\partial F}{\partial \theta} = -\beta^T [i_M \times] [(R i_N) \times] [w_\omega w_\varphi w_\kappa] \quad (2.90)$$

$$\frac{\partial F}{\partial \theta} = -\beta^T [i_M \times] [(R i_N) \times] W \quad (2.91)$$

Making use of the property

$$[i_M \times][(Ri_N) \times] = Ri_N i_M^T - (i_M^T Ri_N)I \quad (2.92)$$

The derivative is more easily computed as given in Equation (2.93)

$$\frac{\partial F}{\partial \theta} = -\beta^T [Ri_N i_M^T - (i_M^T Ri_N)I]W = [(i_M^T Ri_N) - (\beta^T Ri_N)i_M]^T W \quad (2.93)$$

Setting

$$P_N = \begin{bmatrix} P_{M1} \\ P_{M2} \\ P_{M3} \end{bmatrix} = Ri_N = \begin{bmatrix} (i_{M2}P_{N2} + i_{M3}P_{N3})\beta_1 - (\beta_2P_{N2} + \beta_3P_{N3})i_{M1} \\ (i_{M1}P_{N1} + i_{M3}P_{N3})\beta_2 - (\beta_1P_{N1} + \beta_3P_{N3})i_{M2} \\ (i_{M1}P_{N1} + i_{M2}P_{N2})\beta_3 - (\beta_1P_{N1} + \beta_2P_{N2})i_{M3} \end{bmatrix} \quad (2.94)$$

Substituting for the explicit values of i_{M1} , i_{M2} and i_{M3} ; where $i_M = \begin{bmatrix} x_M - x_0 \\ y_M - y_0 \\ -f \end{bmatrix}$ as in equation

(2.72)

$$P_N = \begin{bmatrix} [(y_M - y_0)P_{N2} - fP_{N3}]\beta_1 - (\beta_2P_{N2} + \beta_3P_{N3})(x_M - x_0) \\ [(x_M - x_0)P_{N1} - fP_{N3}]\beta_2 - (\beta_1P_{N1} + \beta_3P_{N3})(y_M - y_0) \\ [(x_M - x_0)P_{N1} + (y_M - y_0)P_{N2}]\beta_3 + (\beta_1P_{N1} + \beta_2P_{N2})f \end{bmatrix} \quad (2.95)$$

Using the notations:

$$P_M = \begin{bmatrix} x_M \\ y_M \end{bmatrix}, \quad (2.96a)$$

$$P_N = \begin{bmatrix} x_N \\ y_N \end{bmatrix}, \quad (2.96b)$$

$$\beta = \begin{bmatrix} \beta_x \\ \beta_y \end{bmatrix} \quad (2.96c)$$

We now linearized the coplanarity equation $F(\beta, p_{Mi}, p_{Ni}, \theta) = 0$ by Taylor's expansion around approximate values $\beta^0, p_{Mi}^0, p_{Ni}^0, \theta^0$, retaining only the first order terms as shown in equation (2.97):

$$F(\beta, p_{Mi}, p_{Ni}, \theta) = F(\beta^0, p_{Mi}^0, p_{Ni}^0, \theta^0) + \left(\frac{\partial F}{\partial \beta}\right)_0 (\beta - \beta^0) + \left(\frac{\partial F}{\partial p_M}\right)_0 (p_M - p_M^0) + \left(\frac{\partial F}{\partial p_N}\right)_0 (p_N - p_N^0) + \left(\frac{\partial F}{\partial \theta}\right)_0 (\theta - \theta^0) \quad (2.97)$$

Or with simpler notation as shown in equation (2.98):

$$F^0 + a_\beta^T \delta\beta + b_{p_M}^T \delta p_M + b_{p_N}^T \delta p_N + a_\theta^T \delta\theta = 0, \quad (2.98)$$

where:

$$F^0 = F(\beta^0, p_{Mi}^0, p_{Ni}^0, \theta^0) \quad (2.98a)$$

$$b_{p_M}^T = \left(\frac{\partial F}{\partial p_M}\right)_0 \quad (2.98b)$$

$$b_{p_N}^T = \left(\frac{\partial F}{\partial p_N}\right)_0 \quad (2.98c)$$

$$a_\theta^T = \left(\frac{\partial F}{\partial \theta}\right)_0 \quad (2.98d)$$

$$\delta\beta = \beta - \beta^0 \quad (2.98e)$$

$$\delta p_M = p_M - p_M^0 \quad (2.98f)$$

$$\delta p_N = p_N - p_N^0 \quad (2.98g)$$

$$\delta\theta = \theta - \theta^0 \quad (2.98h)$$

When n points are observed, then the linear conditions are satisfied and there will be series of observation for n rows.

$$F_j^0 + [a_{\beta.j}^T \quad a_{\theta.j}^T] \begin{bmatrix} \delta\beta \\ \delta\theta \end{bmatrix} + [b_{p_M.j}^T \quad b_{p_N.j}^T] \begin{bmatrix} \delta p_{Mj} \\ \delta p_{Nj} \end{bmatrix} = 0, \quad j = 1, 2, \dots, n \quad (2.99)$$

for $j = 1$

$$F_1^0 + [a_{\beta.1}^T \quad a_{\theta.1}^T] \begin{bmatrix} \delta\beta \\ \delta\theta \end{bmatrix} + [b_{p_M.1}^T \quad b_{p_N.1}^T] \begin{bmatrix} \delta p_{M1} \\ \delta p_{N1} \end{bmatrix} = 0 \quad (2.100)$$

for $j = n$

$$F_n^0 + [a_{\beta,n}^T \quad a_{\beta,\theta}^T] \begin{bmatrix} \delta\beta \\ \delta\theta \end{bmatrix} + [b_{p_{Mn}}^T \quad b_{p_{Nn}}^T] \begin{bmatrix} \delta P_{Mn} \\ \delta P_{Nn} \end{bmatrix} = 0 \quad (2.101)$$

Combining everything into one matrix gives the expression in matrix form as equation (2.102)

$$\begin{bmatrix} F_1^0 \\ \vdots \\ F_n^0 \end{bmatrix} + \begin{bmatrix} a_{\beta,1}^T & a_{\theta,1}^T \\ \vdots & \vdots \\ a_{\beta,n}^T & a_{\beta,\theta}^T \end{bmatrix} \begin{bmatrix} \delta\beta \\ \delta\theta \end{bmatrix} + \begin{bmatrix} b_{p_{M,1}}^T & b_{p_{N,1}}^T & \dots & 0 & 0 \\ \vdots & \vdots & \ddots & \vdots & \vdots \\ 0 & 0 & \dots & b_{p_{M,n}}^T & b_{p_{N,n}}^T \end{bmatrix} \begin{bmatrix} \delta P_{M1} \\ \delta P_{N1} \\ \vdots \\ \delta P_{Mn} \\ \delta P_{Nn} \end{bmatrix} = 0 \quad (2.103)$$

These equations are of the form:

$$f_0 + Mx + N(y - y_0) = 0 \quad (2.104)$$

where f_0 are the approximate condition values, x the unknown parameters and y the observed parameters. Taking into account that the observed values are $y^b = y + e$, where e are the observational errors, $y = y^b - e$ can be substituted in equation (2.104) to obtain equation (2.105).

$$f_0 + N(y^b - e - y_0) + Mx = 0 \quad (2.105)$$

$$f_0 + N(y^b - y_0) - Ne + Mx = w - Ne + Mx = 0 \quad (2.106)$$

Where $w = N(y^b - y_0)$

The quantities w are called the misclosures because they are a linear approximation to the actual condition misclosures. Hence,

$$f(x_0, y^b) \approx f(x_0, y_0) + \left(\frac{\partial F}{\partial y}\right)_0 (y^b - y_0) = f_0 + N(y^b - y_0), \quad (2.107)$$

the misclosure for each point being:

$$f(x_0, y^b)_i = F(\beta_0, \theta, P_M^b, P_N^b), \quad (2.108)$$

Where the observed values on the photographs M and N are

$$P_M^b = [x_M^b \quad y_M^b]^T \quad (2.109)$$

The least squares solution minimizes $e^T P e = \min$, under the condition that $w + Mx - Ne = 0$ is found by forming the Lagrangean (where P is the weight).

$$\Phi = e^T P e + 2k^T (w + Mx - Ne) \quad (2.110)$$

Taking the partial derivatives with respect to x , e and k and equating it to zero,

$$\frac{\partial \Phi}{\partial x} = 2\hat{k}^T M = 0 \quad \Rightarrow \quad M^T \hat{k} = 0 \quad (2.111)$$

$$\frac{\partial \Phi}{\partial e} = 2\hat{e}^T P - 2\hat{k}^T N = 0 \quad \Rightarrow \quad \hat{e} = P^{-1} N^T \hat{k} \quad (2.112)$$

$$\frac{\partial \Phi}{\partial w} = -2(w + M\hat{x} - N\hat{e})^T = 0 \quad \Rightarrow \quad w + M\hat{x} - N\hat{e} = 0 \quad (2.113)$$

Substituting $\hat{e} = P^{-1} N^T \hat{k}$ in $w + M\hat{x} - N\hat{e} = 0$ and $\hat{k} = (NP^{-1}N^T)^{-1}(M\hat{x} + w)$, i.e. the normal equations,

$$[M^T (NP^{-1}N^T)^{-1} M] = -M^T (NP^{-1}N^T)^{-1} w \quad (2.114)$$

The estimates of the errors can be found by combining $\hat{e} = P^{-1} N^T \hat{k}$ with $\hat{k} = (NP^{-1}N^T)^{-1}(M\hat{x} + w)$

$$c = P^{-1} N^T (NP^{-1}N^T)^{-1} (M\hat{x} + w) \quad (2.115)$$

The estimation is completed by computing $\hat{\sigma}^2$ as in equation (2.116)

$$\hat{\sigma}^2 = \frac{\hat{e}^T P \hat{e}}{f} \quad (2.116)$$

Where $f = 4n + n - (4n + 5) = n - 5$ are the degrees of freedom (number of observations $4n$ plus number of conditions n minus number of unknowns $4n + 5$ (5 in x and $4n$ in y)). The estimate of the covariance matrix of the unknowns is given by equation (2.117)

$$\widehat{C}_{\hat{x}} = \hat{\sigma}^2 [M^T (NP^{-1}N^T)^{-1} M]^{-1} \quad (2.117)$$

2.7.3 Camera calibration

Since epipolar geometry depends basically on the camera intrinsic parameters and relative pose, it is important to understand these parameters which are broadly described in camera calibration. Camera calibration is the process of finding the inside characteristics or parameters of a camera and the camera's location in space with respect to a fixed object. This is very essential when lens distortion is to be corrected or the size of object in world unit is to be measured. The characteristics inside the camera are known as the intrinsic parameters while the characteristics outside the camera are known as the extrinsic parameters. While the extrinsic parameter is basically the camera's location in the world space in relation to a fixed object, the intrinsic parameters include the lens distortion coefficients, camera focal length, pixel scaling factors and optical centre. The knowledge of these intrinsic parameters allows us to improve the quality of the image, correct for lens distortion and mapping of real-world distances to pixels, while the knowledge of the extrinsic parameters is a precursor for stereo calibration and solving the problem of structure from motion (SfM). Camera calibration is very important in several applications such as machine vision (for the measurement of the actual size of an object using images), robotics (to aid navigation systems), and 3D scene reconstruction (for recovery of the 3dimensional structure of the scene).

2.7.3.1 Extrinsic parameters

The extrinsic parameters describe the pose (position and heading) of the camera in the world space. It is a rigid body transformation that is invertible. Six parameters are needed to describe this transformation (Three (3) for pose X, Y, Z and three (3) for the orientation or heading where the camera is actually pointing to) which also implies that Six (6) degrees of freedom (dof) are involved. The major problem that extrinsic parameters seek to solve is as follows: Having a point P in the real world, where does this point end up with respect to the camera system.

$$X_p = [X_p, Y_p, Z_p]^T \quad (2.118)$$

Where $[X_p, Y_p, Z_p]^T$ is the coordinates of P in the world coordinate system.

The origin of the camera frame can also be defined as centre O of the projection. The coordinates of this projection can be expressed as shown in equation (2.119) which is the translation between the origin of the world frame and the camera frame.

$$X_o = [X_o, Y_o, Z_o]^T \quad (2.119)$$

The rotation R from the frame S_o (object coordinate system) to S_k (camera coordinate system) in the Euclidean coordinates yields equation (2.120):

$${}^k X_p = R(X_p - X_o) \quad (2.120)$$

where R is the rotation matrix, X_o is the origin of the pin-hole camera and X_p is the location of the point in the object coordinate system.

Expressing equation (2.120) as homogenous coordinate, we obtain:

$$\begin{bmatrix} {}^k X_p \\ 1 \end{bmatrix} = \begin{bmatrix} R & O \\ O^T & 1 \end{bmatrix} \begin{bmatrix} I_3 & -X_o \\ O^T & 1 \end{bmatrix} \begin{bmatrix} X_p \\ 1 \end{bmatrix} \quad (2.121)$$

Where: ${}^k X_p$ is the Euclidean coordinate, R is the rotation matrix, and I_3 is an identity matrix.

Solving equation (2.121) further, it results in equation (2.122);

$$\begin{bmatrix} {}^k X_p \\ 1 \end{bmatrix} = \begin{bmatrix} R & -RX_o \\ O^T & 1 \end{bmatrix} \begin{bmatrix} X_p \\ 1 \end{bmatrix} \quad (2.122)$$

$$\text{Finally, } {}^k X_p = {}^k H X_p \quad (2.123)$$

Where ${}^k H = \begin{bmatrix} R & -RX_o \\ O^T & 1 \end{bmatrix}$ and ${}^k X_p$ is the homogenous coordinate.

2.7.3.2 Intrinsic parameters

The intrinsic parameters describe the process of projecting points from the camera frame to the sensor. These parameters are contained in the calibration matrix of a calibrated camera which is used to convert from the image coordinates frame (which is measured in pixels) to the world coordinate frame (measured in millimetres). These parameters include: the centre of projection (x and y), the aspect ratio, focal length and the sensor skew. While the central projection (mapping from 3D to 2D world) is not invertible, mapping or transforming from the image plane to the sensor and from the sensor to the model deviations (given the knowledge of non-linear function) are both invertible.

2.7.3.3 Ideal Perspective Projection

Through the intercept theorem, the coordinates $[c_{x_p}, c_{y_p}]$ can be obtained from the point \bar{p} projected unto the image plane as expressed by equation (2.124).

$$\bar{p} = [c_{x_p}, c_{y_p}] \quad (2.124)$$

Therefore,

$$c_{x_p} = {}^k X_p = c \frac{{}^k X_p}{{}^k Z_p} \quad (2.125)$$

$$c_{y_p} = {}^k Y_p = c \frac{{}^k Y_p}{{}^k Z_p} \quad (2.126)$$

$$c = {}^k Z_p = c \frac{{}^k Z_p}{{}^k Z_p} \quad (2.127)$$

Where c is camera constant.

Expressing these equations in homogeneous coordinates,

$$\begin{bmatrix} {}^kU_p^- \\ {}^kV_p^- \\ {}^kW_p^- \\ {}^kT_p^- \end{bmatrix} = \begin{bmatrix} c & 0 & 0 & 0 \\ 0 & c & 0 & 0 \\ 0 & 0 & c & 0 \\ 0 & 0 & 1 & 0 \end{bmatrix} \begin{bmatrix} {}^kX_p \\ {}^kY_p \\ {}^kZ_p \\ 1 \end{bmatrix} \quad (2.128)$$

Dropping the third coordinate, the expression of equation (2.128) becomes equation (2.129);

$${}^cX_p^- = \begin{bmatrix} {}^cU_p^- \\ {}^cV_p^- \\ {}^cW_p^- \end{bmatrix} = \begin{bmatrix} c & 0 & 0 & 0 \\ 0 & c & 0 & 0 \\ 0 & 0 & 1 & 0 \end{bmatrix} \begin{bmatrix} {}^kX_p \\ {}^kY_p \\ {}^kZ_p \\ 1 \end{bmatrix} \quad (2.129)$$

$$\text{Therefore, } {}^cX_p^- = {}^cP_k {}^kX_p \quad (2.130)$$

Where ${}^cX_p^-$ maps from the camera plane to the image plane, ${}^cP_k = \begin{bmatrix} c & 0 & 0 & 0 \\ 0 & c & 0 & 0 \\ 0 & 0 & 1 & 0 \end{bmatrix}$, which is the

projective point in the image plane, and ${}^kX_p = \begin{bmatrix} {}^kX_p \\ {}^kY_p \\ {}^kZ_p \\ 1 \end{bmatrix}$, which maps from the real world unit to the

camera plane. Therefore,

$${}^cX = {}^cPX \quad (2.131)$$

And likewise,

$${}^cP = {}^cP_k {}^kH \quad (2.132)$$

Recall that ${}^kH = \begin{bmatrix} R & -RX_o \\ O^T & 1 \end{bmatrix}$, and ${}^cP_k = \begin{bmatrix} c & 0 & 0 & 0 \\ 0 & c & 0 & 0 \\ 0 & 0 & 1 & 0 \end{bmatrix}$, hence,

$${}^cP = \begin{bmatrix} c & 0 & 0 & 0 \\ 0 & c & 0 & 0 \\ 0 & 0 & 1 & 0 \end{bmatrix} \begin{bmatrix} R & -RX_o \\ O^T & 1 \end{bmatrix} \quad (2.133)$$

Thus, the calibration matrix for the ideal camera can be defined as:

$${}^cK = \begin{bmatrix} c & 0 & 0 \\ 0 & c & 0 \\ 0 & 0 & 1 \end{bmatrix} \quad (2.134)$$

Therefore, the overall mapping can be expressed as:

$${}^cP = {}^cK[R/-RX_o] \quad (2.135)$$

This can further be solved as:

$${}^cP = {}^cKR[I_3/-X_o] \quad (2.136)$$

where $[I_3/-X_o] = \begin{bmatrix} 1 & 0 & 0 & -X_o \\ 0 & 1 & 0 & -Y_o \\ 0 & 0 & 1 & -Z_o \end{bmatrix}$, cK is the calibration matrix, R is the rotation matrix and I_3

is an identity matrix.

Therefore, equation (2.136) can be defined as the overall mapping function. In like terms, equation (2.137) maps a point to the image plane.

$${}^cX = {}^cKR[I_3/-X_o]X \quad (2.137)$$

Equation (2.136) then yields;

$$\begin{bmatrix} {}^cU' \\ {}^cV' \\ {}^cW' \end{bmatrix} = \begin{bmatrix} c & 0 & 0 \\ 0 & c & 0 \\ 0 & 0 & 1 \end{bmatrix} \begin{bmatrix} r_{11} & r_{12} & r_{13} \\ r_{21} & r_{22} & r_{23} \\ r_{31} & r_{32} & r_{33} \end{bmatrix} \begin{bmatrix} X - X_o \\ Y - Y_o \\ Z - Z_o \end{bmatrix} \quad (2.138)$$

$$\text{Where } {}^c K = \begin{bmatrix} c & 0 & 0 \\ 0 & c & 0 \\ 0 & 0 & 1 \end{bmatrix}, R = \begin{bmatrix} r_{11} & r_{12} & r_{13} \\ r_{21} & r_{22} & r_{23} \\ r_{31} & r_{32} & r_{33} \end{bmatrix} \text{ and } [I_3 / -X_0] = \begin{bmatrix} X - X_0 \\ Y - Y_0 \\ Z - Z_0 \end{bmatrix}$$

The Euclidean coordinates of equation (2.138) results into the collinearity equation.

The calibration matrix (K) is further expressed as equation (2.139) with specific emphasis on the intrinsic parameters of the camera (Whitehead and Roth, 2004).

$$K = \begin{bmatrix} fk_u & -fk_u \cot(\theta) & u_0 \\ 0 & \frac{fk_v}{\sin(\theta)} & v_0 \\ 0 & 0 & 1 \end{bmatrix} \quad (2.139)$$

Where: f = focal length (in millimetres), k_u, k_v = Number of pixels per millimetre (width and height), and u_0, v_0 = centre projection.

2.8 Review of Related Studies on Epipolar Geometry

The documented applications which highlights the efforts of various researchers and advancements in epipolar geometry is broadly subdivided into two parts. The first part presents the summary of past research efforts on the principle and applications of epipolar image correlation (subsection 2.8.1) while the second part presents the summary of advancements in extraction of epipolar geometry and estimation of fundamental matrix (subsection 2.8.2).

2.8.1 Principle and applications of epipolar image correlation

Mosienko (1973) gave a brief description of the principle of epipolar image correlation along with a short theoretical background of different correlation techniques and some advantages and disadvantages of each of them. He also described the application of the epipolar principle to the analytical plotter AP/2C and the procedure followed in scanning a model. Results from scanning different models of different scales were given, which clearly showed the potential of a fairly

economical image correlation method and which can be used for a rapid production of orthophotographs. Image correlation was also defined as a comparison of two nearly identical images to obtain the best match possible between these images and measuring their respective positions on a pair of stereo photographs.

Kang (2008) gave a lucid discussion on the generation of epipolar images and corresponding point matching on such images using coaxial vehicle-based images which were taken along the optical axis where the epipolar lines of coaxial stereo pair were arranged in the direction of radial instead of nearly horizontal arrangement of stereo pair with horizontal baseline. Although the straight lines in raw image become arcs in epipolar image, the point features are still apparently clear and possible for 1D corresponding point matching. Moreover, matching in the epipolar images can improve the success rate. Also presented by Kang (2008) is a detailed description of the image matching algorithm which was employed in finding corresponding points between adjacent images.

Chen-Yu *et al.* (2013) employed the usage of epipolar geometry for the development of a new driver eye gaze estimation approach. SIFT image descriptor was used to find putative correspondences and then RANSAC algorithm was used to estimate fundamental matrix between the two views before modelling the distribution of reliable corresponding points across two views using affine transformation function. The experimental results showed that epipolar geometry with affine transformation can accurately estimate the gaze point of drivers and that it even proved to be more accurate than both the pure homography and epipolar line searching approaches. The implementation of the developed approach also proved to be very easy, simple and fast, without complicated facial model reconstruction and with the ability to achieve 19.91 pixels accuracy.

A model for the automatic matching of Synthetic Aperture Radar (SAR) images using similar corresponding epipolar line based on photogrammetry theory was developed by Xiaoman *et al.*

(2008). Results of the model's experimentation affirmed that the speed of the image matching is enhanced to a certain extent by enhancing search efficiency.

He *et al.* (2008) developed a novel algorithm which proposed the integration of similarity constraint and epipolar constraint. The algorithm first implements the Harris-Laplace detector combined with the SIFT descriptor before introducing the epipolar constraints. Experimental results showed that the developed algorithm is more robust than SIFT in terms of matching accuracy though at the cost of more computation time.

2.8.2 Automatic extraction of epipolar geometry and estimation of fundamental matrix

Zhengyou (1998) categorized the algorithms developed for the estimation of fundamental matrix into three distinct methods. These methods are: (1) The linear estimation methods (Seven-Point and Eight-Point Algorithms), (2) The iterative estimation and (3) The robust estimation approach (M-Estimator, Least Median Squares, and RANSAC) (Nister, 2003). Jing-Fu *et al.* (2007) examined the characteristics of these different methods and the algorithms categorized under each of them while Armanque *et al.* (2001) carried out a comparative survey of fifteen of these models with an attempt to suggest the most accurate and optimum algorithm amongst the fifteen (15). The eight-point algorithm which belongs to the linear estimation approach was adjudged the best because it is notable for its computational efficiency and implementation simplicity. It is however sensitive to the presence of outliers in the point correspondences and as such, prone to mismatch. This is also the major limitation of the iterative estimation approach. RANSAC and Least Median Square (LMedS) which belong to the robust estimation approach indeed perform more efficiently in the presence of outliers in the point correspondences, though they are computationally intensive and time consuming. Hartley (1997) later proposed a normalization approach which requires that the image data be normalized before imposing the eight-point algorithm on it for the establishment of point correspondences. In this approach, an attempt was made to ascertain the robustness and reliability of the estimated fundamental matrix in point correspondences using the normalized

eight-point algorithm (linear estimation approach) as compared to RANSAC and LMedS (robust estimation approaches).

Castillo and Jacobs (2009) developed a model for the automatic extraction of epipolar geometry from each pair of images using the method of Domke and Aloimonos (2006a), and Domke and Aloimonos (2006b) which requires no hand-picking of point selection.

Pellejero *et al.* (2004) developed a model which automatically computes homographies from matched line between two views and recover epipolar geometry using the computation results. Experimental results of the model showed that it works perfectly with both indoor and outdoor images so far a minimum of two planes containing sufficient lines are available within the scene.

Also, Jurgen (2011) presented a detailed review and model formulation of a robust procedure starting from Least Trimmed Squares (LTS) (Rousseeuw and van Driessen, 2006) as the initial estimator, it was implemented by David *et al.* (2014). Xu and Li (2000) implemented Least Median of Squares (LMedS) and data snooping technique to robustify surface matching algorithm. The efficiency of the LMedS estimator was improved using M-estimator. Simulative data was used to evaluate the efficiency and robustness of the proposed method. Result of the experiments showed that robust matching using LMedS estimator outperformed LTS and can detect local deformation that covers up to 50% of the surface and very small deformation can be detected too. The result also proved that this method is more superior to other methods of robustifying surface matching.

Estimation of epipolar geometry was formulated as a global optimization problem by Jinxiang and Song (1998). They also presented a genetic algorithm for parameter searching. Comparing with previous approaches, the experimental results obtained using both simulated and real images showed that the Genetic Approach (GA) is very robust to outliers. Also, it is more efficient than LMedS and RANSAC in terms of computational efficiency.

Feng and Hung (2003) proposed the development of a fundamental matrix estimation model which is robust even when outliers are present by searching for the inliers with the use of search engine known as the random minimum subset while Adrien and Peter (2004) also developed a seven-parameter model for the estimation of fundamental matrix non-linearly by updating the singular value decomposition on which its orthogonal representation was based. The output showed that the models converged faster than other models though they have higher tendencies of being more frequently trapped in local minima.

Torr and Zisserman (1997) proposed an algorithm for automatically establishing point correspondences between image pairs and the estimation of F-Matrix by imposing degradation on the images using lossy compression at Nine (9) different level which ranges from 90, 80...10. Four image pairs were evaluated for the model's experimentation. The model proved to be very robust at every imposed degradation level from 90 to 10.

Bing and Xiaoli (2013) proposed a fundamental estimation model based on improved Singular Value Decomposition (SVD). Jing-Fu *et al.* (2007) developed a model for computing fundamental matrix by modifying the RANSAC model. The developed model was implemented and its performance was tested by comparing its results with the results of eleven other algorithms using both real and simulated image data. The model outperformed the other eleven tested algorithms under different levels of outliers.

A survey of several methods of fundamental matrix estimation was conducted and presented by Armangue *et al.* (2001) and Diana (2005). Each of the investigated models was grouped under three major methods viz: (1) Linear estimation methods (2) Iterative methods of estimation (3) Robust methods of estimation. The experiments conducted using real and synthetic images revealed that though the linear methods converge quickly which makes them very fast, their sensitivity to outliers or noise makes their accuracy quite poor. The iterative estimation gave a better accuracy by at the expense of time consumption and they are unable to remove or exclude

outliers efficiently, while the robust estimation methods gave the most satisfactory results because they still perform optimally even when outliers are present. Diana (2005) implemented non-linear approach (bi-epipolar constraints method) and discovered that the method is not only time consuming but also prone to inaccurate estimation of fundamental matrices. Zhengyou (1998) also affirmed that linear methods are quite poor though relatively good results can be obtained when the image data is normalized before the fundamental matrix estimation and that LMedS is very robust in the face of outliers while Zhou *et al.* (2015) proposed a method of estimating F-matrix by using the epipolar geometry of linear features. The result obtained shows that the developed model proved to be more stable with improved accuracy when compared with RANSAC and LMedS.

2.9 Review of Related Studies on Image Registration Applications

This section is subdivided into three subsections. The first subsection (2.9.1) presents the summary of the evolution of image registration and its advancements from the inception till 1999, the second subsection (2.9.2) presents the summary of the advances in image registration applications from 2000 to year 2009 while the summary of the advances in image registration from 2010 to year 2019 is presented in the third subsection (2.9.3).

2.9.1 Evolution of image registration applications from inception till year 1999

One of the foremost and well documented research articles on automatic image registration can be traced to Anuta (1969) and Anuta (1970). These researches implemented Sum of Absolute Difference (SAD) as the similarity measure and Fast Fourier Transformation (FFT) function respectively in order to register multispectral video imagery and multitemporal digital imagery using FFT. This same similarity measure was applied by Barnea and Silverman (1992) for the optimization of the speed of digital image registration. It was also implemented by Michael and Shmuel (1991) in their attempt to improve image resolution by image registration and ensuring a quick convergence of the model. SAD proved to be very robust in terms of speed and accuracy.

Lesse *et al.* (1971) and Pratt (1974) used cross correlation as the similarity measure for image registration while Gruen (1985) emphasized new perspectives (multiphoton, multitemporal, multisensory, multipoint and simultaneous correlation/triangulation). The method provides for monitoring of quality, precision and reliability measures, guaranteeing high matching accuracy. The major demerit of the approach is that its solution vector converges at a very slow rate which even oscillates or converges to a false solution.

Bruce and Takeo (1981) developed a generalized registration algorithm which can extract depth information from Stereo images using a type of Newton-Raphson Iteration. The proposed technique proved to be very fast but its major drawback is that it requires considerable hand-guidance because it is not fully automated. An elastic matching algorithm developed by Burr (1981) was extended by Moshfeghi (1991) to adopt contour information in the registration of images of deformable anatomy using an iterative gaussian smoothed deformation model and calculating a displacement vector between each point in one contour and its nearest line segment from another contour. The technique was experimented on two dimensional CT and MR chest image slices and satisfactory results were obtained.

A simple pack detection algorithm using Multiresolution Hough transform and based on coarse-to-fine iterative search was proposed by Atiquzzaman (1992). The approach used two efficient implementations of the Hough transformation known as Adaptive Hough Transform (AHT) and Fast Hough Transform (FHT). A simple detection algorithm that requires small amount of computing power was used because of consideration of discretization errors. The model was experimented on both real-world images and simulations on synthetic images and it was discovered it reduces computation time, ensures faster convergence and very robust to noise in the image and discontinuities in the pattern though it is computationally complex.

Collignon *et al.* (1995) implemented a voxel similarity based (VB) registration algorithm which was earlier proposed by van den Elsen (1994). Experimental results showed that the developed system was completely automated with a subvoxel accuracy obtained. The model was also found to be robust in multi-modality situations and Mutual Information (MI) matching criterion was found to be a well-behaved multi-modality 3D registration criterion. Meanwhile, its claim of unimodality was not proved and as such cannot be affirmed, neither was the speed of the system documented.

The´venaz and Unser (1997) developed an optimizer for multiresolution image registration using Mutual Information (MI). The iteration strategy was inspired by the Marquardt-Levenberg algorithm. An image pyramid was computed using a developed framework based on a continuous polynomial spline representation of images. The framework was also used to set the optimizer in a multiresolution context. Experimental results proved that the optimizer adapted well to multiresolution processing and ensures better accuracy. Tseng *et al.* (1997) used Fourier descriptor and neural networks to match area features in the execution of image-to-image registration. Segmentation algorithm was used by Alpert *et al.* (1996) to develop an improved method for image registration. The algorithm produced robust accuracy and it enhanced processing speed even with its computational complexities.

Automatic Registration and Change Location (ARCHANGEL) algorithm was designed by Dowman (1998) for the registration of small-scale images and prompt extraction of polygons from them (primitive). The research affirmed that developing a fully automatic feature extraction which is robust enough for reliable automatic image registration is still a dream in the pipeline for image processing analysts and that only semi-automatic models are visible in the near future. Fitzpatrick and West (1998) emphasised on the retrospective registration techniques, volume-based and surface-based image registration in their review.

Xiaolong and Siamak (1999) developed a feature-based image registration module using image segmentation for the model's feature extraction and introducing thin and robust zero crossing for the improvement of the performance of the Laplacian of Gaussian operators. Registration accuracy of less than $\frac{1}{3}$ of a pixel was achieved during the experimentation of the model.

Prachya (1999) proposed a High-Performance Automatic Image Registration (HAIR) algorithm which reduces search data by using sub-images only with the aid of a new metric called 'registrability'.

2.9.2 Summary of the advances in image registration applications from 2000 - 2009

A Log-Polar robust image registration module was developed by George and Siavash (2000). The module based on affine transformation, accommodates within a wide latitude, changes in scaling and rotation angles which are arbitrary. Sub-pixel accuracy was achieved though recovery of perspective parameters was not investigated or experimented.

Attempt was made by Dare and Dowman (2000) in the development of a multiple feature extraction and matching technique model for the automatic registration of multimodal and multitemporal images. Due to its computational efficiency, tiling method was adopted instead of pyramid-based method. The model which seeks to combine multimodal and multi-temporal earth observation images in its design, produced an accuracy of less than 2 pixels RMS residual though with an increased volume of processing time.

Yoshinori *et al.* (2002) developed a non-photorealistic rendering method that creates an artistic effect and generates mosaic images using the site and edges of Voronoi diagrams and adopting key frame method to preserve coherence and to keep computational cost low. In providing a theoretical framework for defining image registration problem, a detailed discussion of an algorithm based on the idea of optic flow fields was presented (Peter and Senhill, 2003) while Modified Iterated Hough Transform (MIHT) was proposed and implemented by Ayman *et al.*

(2003). The model relied on the mathematical relationship between conjugate entities and it provides solution to problems arising from relief displacement and / or occlusions. This same transform was also adopted by Al-Ruzouq (2004) in the development of a semi-automated model for the registration of multisource satellite imagery. The model used linear features as primitives and edges as basis for change detection and it also implemented both 2D similarity and affine transformation functions. Real world data used for experimentation of the model proved its feasibility and robustness. While linear features proved to be better primitives than points, affine transformation function proved to be better than 2D Similarity. Manual digitisation was adopted without considering automatic extraction of straight lines.

Zwickels which is especially well suited for images of man-made structures was used to develop a novel method for affine invariant matching (Joachim *et al.*, 2004). Zwickels are sections defined by two intersecting line segments which divide the neighbourhood around the intersection point into two sectors. An affine invariant representation was computed using the information inside the smaller sector while the sector was rectified using the line information and to compute a histogram of the edge orientation as a descriptor vector. The experimentation of this proposed method using aerial and terrestrial images proved that the method avoids the problem of depth discontinuities and the features are insensitive against view point changes as well as illumination changes when compared to other affine invariant descriptors.

An algorithm that made use of a pairwise fine registration was proposed by Mian *et al.* (2004). The approach makes 3D modelling process simpler without compromising the accuracy. The results obtained from the qualitative accuracy assessment shows that the proposed method can favourably compete with other traditional methods of pairwise registration. Huzefa (2005) proposed a new class of similarity measure which is entropic graph-based estimate of Renyi's α -entropy. Quantitative comparisons of this model showed that both the entropic graph-based higher

dimensional estimate of α -Jensen difference had robust performance and lower registration errors in test cases of image registration as compared with the standard Shannon Mutual Information computed using pixel histograms.

Gang and Yun (2005) implemented the integration of feature based and area-based feature matching techniques (relaxation based and wavelet-based models) in order to mitigate the effect of the local distortions introduced by terrain relief. Using IKONOS and QuickBird image datasets, the experimental results showed that the proposed technique consumes more time for convergence when extracting features and establishing correspondence between conjugate features. Both matching methods were also combined by Thitipon *et al.* (2006) and the results obtained are similar to the results presented by Gang and Yun (2005).

Al-Manasir and Fraser (2006) used 3D similarity transformation function to develop a model which simultaneously registers overlapping Terrestrial Laser Scanner (TLS) point clouds. A 2mm level accuracy was attained in the registered point cloud through the proposed approach.

A novel architecture based on MI was proposed by Marnak *et al.* (2006) for dynamically-reconfigurable registration of overlapping images. Another novel, physically motivated curve/region descriptor suitable for the establishment of image correspondences in a geometrically invariant fashion was proposed by Marco (2006). The study also proposed new methods for the estimation of image transformation parameters and robustification of RANSAC in the presence of large quantities of outliers and of multiple models using point features as primitives. The model was experimented with biological images, satellite images and consumer photographs. The results showed that robustification procedure improved the estimates of the homographies that relate planar structures in image pairs and makes the results more stable across a larger set of values for the noise standard deviations. It also affirmed that sequential RANSAC without robustification is very sensitive to the selection of the noise threshold.

Diego (2006) reformulated the problem of image registration as an unconstrained optimization problem. It developed a simple algorithm based on the steepest descent method using Normalized cross correlation and mutual information as similarity measures. A simple algorithm was also developed for finding overlapping areas in the presence of rotation misalignment. The normalized cross correlation proved to be more efficient in terms of computational cost suitability for gradient based optimization methods when compared to the MI measure. Experiments were only based on simulated and not realistic conditions as noise corruption and illumination variations were not simulated. The model also successfully registered slight translational misalignment, however when the misalignment increases, the effect of the sensitivity to local minima becomes more pronounced.

Fischer and Modersikzi (2006) developed an intensity-based software for non-linear registration of images. Their research affirmed that intensity-based image registration allows for stable, fast and efficient scheme. A diffeomorphic image registration algorithm called DARTEL was described by Ashburner (2007). The optimization of the algorithm was performed using Levenberg - Marquardt strategy and the first and second derivatives used by the optimization was computed using a recursive approach.

Hector *et al.* (2008) developed a new similarity measure using kernel functions for the evaluation of random variables that are predictable. The method proved to be as robust as the MI methods.

Thirion's Demon was implemented by Nathan *et al.* (2009) while an adaptive polar transformation which solves the problem of conventional log-polar transform suffering from non-uniform sampling using Projective transformation function and Gabor feature extraction to accelerate the localization procedure was proposed by Rittavee *et al.* (2009). The algorithm was experimented on real images and the results demonstrated that the proposed approaches are very effective in the registration of images infested with occlusion.

Luong (2009) developed a model which concentrated more on non-rigid 2D monomodal image registration and also proposed a novel approach based on difference sampling, applied to the stochastic approach. Experimental results showed a better convergence of subsampling techniques and difference sampling technique when compared to traditional methods.

The Markov Random Field (MRF) formulation proposed by Ben *et al.* (2009) for linear image registration proved to be robust with respect to initial alignment, though its performance was not compared with other methods. The method was tested on 2D and 3D monomodal and series of multimodal registrations of brain image data and the average processing run time was computed to be 20 seconds (2D random study), 3 minutes (3D Random study) and 5 Minutes (3D Multimodal registration).

2.9.3 Summary of the advances in image registration from 2010 till date (2019)

Ludovico (2011) used Shi-Thomas algorithm as feature detector to detect interest points while Lukas-Kanade tracker was used together with phase correlation algorithm formed the feature matching strategy. Different biological samples, a middle density cell culture and a histological sample were used for the experimentation aimed at testing the effectiveness of the approach and it was discovered that the robustness of the geometrical model selection needs improvement or refinement.

Xiaofeng (2011) proposed a model for the fusion of LiDAR elevation data with imagery by integrating SIFT and Harris Corner detection feature algorithms with MI. It was also demonstrated experimentally that the MMI based algorithm works on the registration of the infrared system. It also showed that the performance, robustness, accuracy and efficiency of the developed model needs improvement.

Joseph *et al.* (2011) developed a scale-space model which was found to be easily generalized to handle translation and rotation and thus, it was embedded into a non-linear least squares method

for simultaneous translation, rotation and scale estimation. Studies on the performance metric of the proposed registration method to ascertain whether it improves convergence, speed and over all accuracy was not conducted.

Armagam *et al.* (2013) developed a framework which proved to be capable of naturally dealing with the cases where it is practically impossible to successfully match time consuming images. The results obtained proved that the developed framework is very robust when compared to previous approaches for large-area mosaicking. The approach proved to be robust to sensor failure when its performance was experimented using different image pairs.

A comparative analysis of SIFT and SURF was conducted by Panchal *et al.* (2013) and Vivek and Kanchan (2014). The experimental results showed that SIFT displayed better robustness by detecting and matching more features though more time was expended. Dilipsinh *et al.* (2014) also reviewed the characteristics of Harris Corner Detector, SUSAN, FAST which is SUSAN corner criterion based and uses a corner response function (CRF), SURF, SIFT and PCA- SIFT. The research examined the merits and drawbacks of each of the reviewed algorithms. Arun and Katiyar (2013) investigated the extent of improvement of these feature detection algorithms achievable by enhancing them with Wavelet Transform and the findings of the research proved that the enhanced models were more robust than the feature descriptors.

Juan (2013) conducted an overview of the recent advancements in multiple feature and multiple image registration paying more attention to the use of criteria derived from the total edge cost of the so-called entropic graphs and particularly, the use of Kozachenko - Leozenko entropy estimator (KL); a robust and numerically stable method that computes entropy of a sample based on the nearest neighbour distances between its elements. The study also presented a practical application of an elastic registration framework based on KL in cervical cancer prevention. The accuracy of the proposed algorithm was measured using semi-automatically extracted landmarks as ground

truth. The research manuscript also presented the results on how KL calculates higher – order MI for high dimensional multispectral images and how it outperforms other more widespread similarity criteria in alignment tasks. Using landmarks, the result showed a clear advantage of high order MI by achieving zero mis-registrations even at high initial displacements when the number of correct registrations using regular MI dropped below 50%. The landmarks were also used to compare the results of elastic image registration using high order joint entropy against those obtained using the Image Registration Toolkit (IRTK) and the generalised dual-bootstrap ICP. The results showed that the method can effectively compete with generalised dual-bootstrap ICP and a superior performance when compared to IRTK.

Daniel (2013) used Morphon for the development of a framework for registering non-parametric images using local structure tensors for controlling regularizations. The framework proved to have introduced improvements to the computational performance of the registration paradigm. A similarity measure which is robust on images with intensity inhomogeneities or pathologies was proposed by Stefan *et al.* (2014). Though time consuming, the similarity measure showed robustness as compared to Normalized Mutual Information (NMI) and the cosine squared measure of Haber and Modersitzki (2006).

A geometric based, user assisted, semi-automatic image registration algorithm was developed by Ajayi *et al.* (2014). The model was based on three transformation functions (orthogonal, affine and projective transformation functions), allowing users to select either of these three during the registration process. Root Mean Square Deviation (RMSD) was adopted for the accuracy assessment of the model. Experiments conducted on real world images extracted from google earth showed that the model reduces computational complexity without compromising the processing speed. It also showed that registration based on Projective transformation function outperformed the other two in terms of accuracy. The model's major drawback lies in the need for on-screen

selection of conjugate points (using points as primitives) by the user which makes it highly prone to geometric distortions and mismatch.

Md-Mashiur and Zadidul (2015) comparatively analysed three different methods used in image registration viz: pixel, wavelet and translation methods. The result of the analysis revealed that translation method gave the best accuracy and at a shorter processing time, followed by the wavelet method and then the pixel method.

Yeqing *et al.* (2015) developed a model by introducing a new similarity measure. The model was also found to be highly robust and accurate on natural images under spatially – varying intensity distortions. The approach is scalable to large data sets because of its low computational complexity but cannot handle large transformations and can only be used for off-line registration.

Olaleye *et al.* (2015) developed an image registration model which used the Speeded Up Robust Feature (SURF) algorithm for feature extraction, Sum of Squared Difference (SSD) for feature match, bilinear interpolation for image resampling and computation of non-integer coordinates, Random Sampling Consensus (RANSAC) for exclusion of outliers and computation of the transformation matrix. A novel accuracy measure which establishes the relationship between the total matched points (inliers and outliers) and the points voted for the final registration (inliers only) was also developed and embedded in the model. The model which was developed and packaged in MATLAB environment using Image Processing and Computer Vision Tool boxes was experimented using real world images extracted from Google Earth. Experimental results showed that the time taken by the registration process and the accuracy obtained are both directly proportional to the radiometric and geometric properties (e.g. resolution) of the image. It also showed that the projective-based transformation gave a more refined accuracy (approximately 75% - 84%) compared to affine (approximately 62%) and non-reflective similarity (approximately 20%) transformation functions. The automatic registration model registered two overlapping

images in an average of 42 - 62 seconds processing time on an 8gig RAM, Corei7, 1Terabyte hard disk HP Laptop computer.

An automatic system of registering remote sensing images was developed by Krishna and Varghese (2015) using SURF, MSER and PCA-SIFT for feature detection. The detected features were then matched to generate point correspondences using RANSAC to estimate an outlier free transformation and MI for fine-tuning the registration. The descriptors used are known to be variant to rotation, zoom, noise, illumination and scale. The experimental results proved that SIFT model gave a higher accuracy compared to SURF and MSER (which uses a low dimensional descriptor), though SURF proved to be 5 times faster than Hessian-Laplace, it failed when the rotation is large.

Zichun *et al.* (2016) demonstrated that the mesh-based methods have faster computational speed and better displacement vector fields (DVF), while Hiba (2016), Hipwell *et al.* (2016) and Feng *et al.* (2016) documented a review of the most commonly used image registration approaches in human and veterinary medicine.

A fast image matching algorithm for automatic registration of UAV acquired images was developed by Chung-Hsien and Yu-Ching (2017). The developed technique adopted the implementation of ABRISK and the spatial analysis of corresponding control points for image registration. The result obtained was compared with the SIFT algorithm and BRISK using images of different sizes and it was found to be 19.2 times and 312 times faster than SIFT for image sizes of 1000 x 1000 pixels and 4000 x 4000 pixels respectively. ABRISK was also found to be 4.7 times faster than BRISK.

Focussing on both model robustness and solver efficacy, Daoping & Ke (2018) investigated image registration by mapping one image to another in a variational framework by first proposing a new variational model with a special regularizer, based on quasi-conformal theory which can

quarantee that the registration map is diffeomorphic. An iterative method was then proposed to solve the resulting nonlinear optimization problem and prove the convergence of the method. Numerical experimentation of the approach demonstrated that the new model can ensure accurate diffeomorphic registration even when the deformation is large, though the model is not efficient with respect to speed, and can not handle 3D problems.

Fereshteh *et al.* (2018) proposed a multi-modal to mono-modal transformation method that facilitates direct application of well-founded mono-modal registration methods in order to obtain accurate alignment of multi-modal images in both cases, with full and partial overlap. The transformation facilitates recovering strong scales, rotations and translations. The effectiveness of the designed method was examined and compared with widely used information theory-based techniques using simulated and clinical human brain images with full data and the designed method outperformed the existing algorithms, though at the expense of time.

Alam *et al.* (2019) presented an automatic features based approach for the rigid and deformable registration of medical images using interested common sub-regions. In the presented approach, interested common sub-regions in the overlapping image pairs are detected automatically and registered locally. The local registration yielded the transformation parameters which were finally used for the global registration. In the experiments of rigid and deformable registrations, it was proved that the developed approach outperformed existing approach in terms of both the accuracy and time efficiency, especially with monomodal brain image registration while also boasting of good potentials for multimodal images of different human organs. The approach was never tested for earth observation or mapping purposes.

Also, a global optimization algorithm which requires the minimisation of a dissimilarity measure with multiple local minima was developed by Calvin *et al.* (2019) and applied to the problem of

identifying the best transformation for aligning two images. The developed algorithm proved to be more robust when compared with the simulated annealing algorithm.

Kai *et al.* (2019) developed a coarse-to-fine registration strategy for images with large resolution differences which consists of three phases viz: the feature base registration, normalized mutual information-based registration and direct registration between the original high and low resolution images. Ant Colony Optimization (ACO) for continuous domain was adopted for the optimization of the similarity metrics throughout the three phases. The experimentation of the strategy using multisensor image pairs with different resolution ratios showed that the method yielded sub-pixel registration accuracy of images with resolution differences from 1 to 50 times, though at the expense of processing time, which is the strategy's major drawback.

2.10 Identified Research Gaps in Image Registration

The following are the identified research issues or gaps in the automatic registration of overlapping images according to the reviewed literature.

- i. Finding a good similarity measure.
- ii. Optimal estimation of transformation and outlier rejection.
- iii. Constructing robust region descriptors which automatically extract windows of interest by decreasing processing time without compromising the accuracy.
- iv. Integration of registration algorithms for improved robustness and applicability.

From all the reviewed literature, it was discovered that research efforts aimed at exploring the applicability of epipolar correlation in the development of a more robust image registration model is still relatively unknown, and that none of the authors and their research foci considered the development of a user-friendly software for the automatic registration of overlapping images by implementing different algorithms used at different stages of the image registration scheme. This research therefore presents an integrated approach to automatic registration of overlapping images

which integrated some of the algorithms used in image registration in one software package with emphasis on epipolar correlation model which is a novel application for image registration. The epipolar correlation-based image co-registration scheme adopted the concept which integrates both geometric and epipolar constraints (He *et al.*, 2008). It also investigates their robustness with regards to processing time, and degree of accuracy. It is opined that exploring epipolar geometry in automatic registration of overlapping images will help in proffering solution to some of these highlighted research gaps most especially, issues (i) – (iii) while integrating the selected feature descriptors with epipolar correlation will address the gap identified in (iv).

CHAPTER THREE

3.0 MATERIALS AND METHODS

This chapter describes the methodology adopted in the course of this research. It also presents the details of the materials acquired and how they were used. It starts by introducing the model formulation adopted in realising the research objectives. Since one of the major issues of image registration is the simplification of computational complexities, activity diagrams which provide simplified schemes for the implemented algorithms used in the development of the integrated image registration software were also designed within the enterprise architecture software environment. The chapter concludes by highlighting the details of the overlapping image pairs used for the model experimentation, the performance evaluation of the developed software and the software's system specifications.

3.1 Automatic Registration of Overlapping Images Using Three Different Feature Descriptors

This section addresses the first objective of the research as highlighted in section 1.3. Feature based method of image registration which uses cost function as its similarity measure was adopted for the development of the image registration scheme. Three different feature detection and extraction algorithms were systematically selected and implemented for the development of an automatic image registration scheme. These algorithms are: (1) The SURF algorithm (Bay *et al.*, 2008), (2) The MHCD algorithm (Harris and Stephens, 1988) and (3) The SIFT algorithm (Lowe, 2004). The choice of these techniques was informed by their popular acceptance as they are regarded as the most implemented feature descriptors (Chung-Hsien and Yu-Ching, 2017) and they are known to be invariant to zoom, noise, scale, rotation and illumination (Krishna and Varghese, 2015).

3.1.1 Model formulation

The work flow of an ideal automatic image registration paradigm which was adopted in this study consists of four (4) major stages. Figure 3.1 presents the algorithmic components of these four stages.

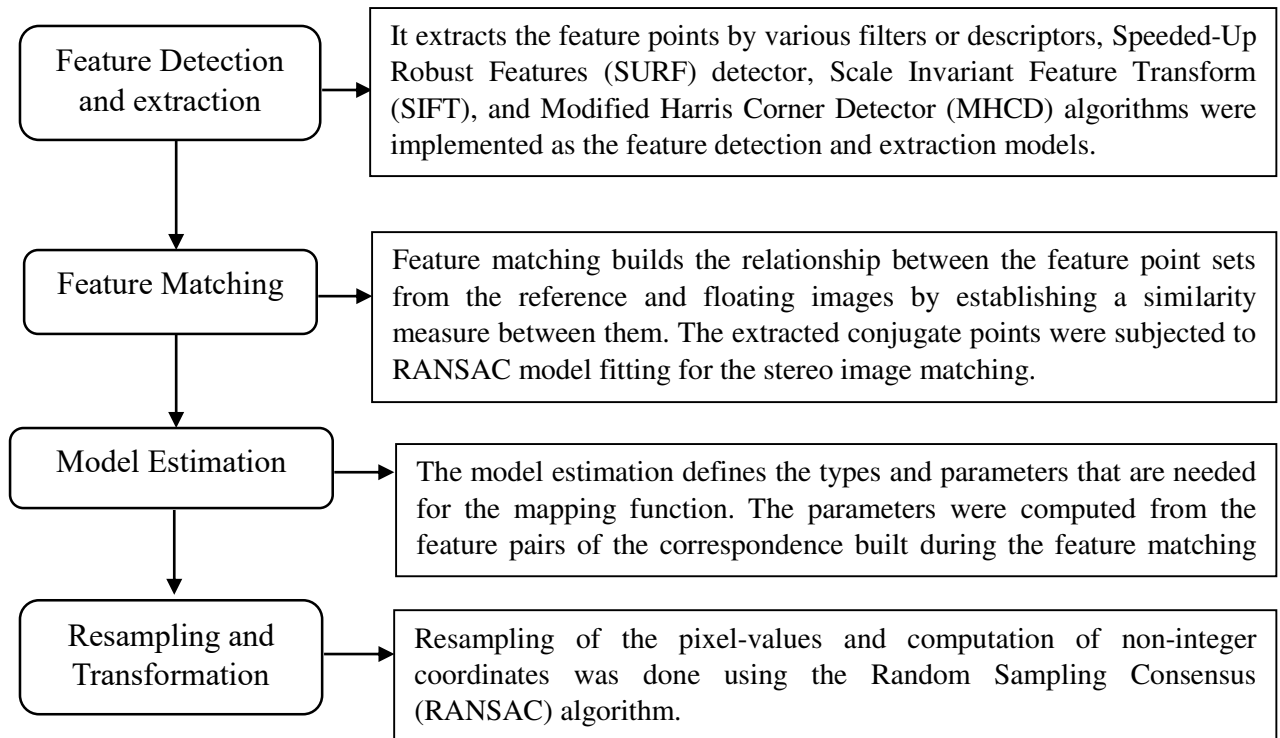


Figure 3.1: Process flow scheme for the automatic image registration model.

The implementation of these four basic stages involved in automatic image registration requires that they are subdivided into simpler steps. The process flow diagram for the feature--based registration algorithm is presented in Figure 3.2.

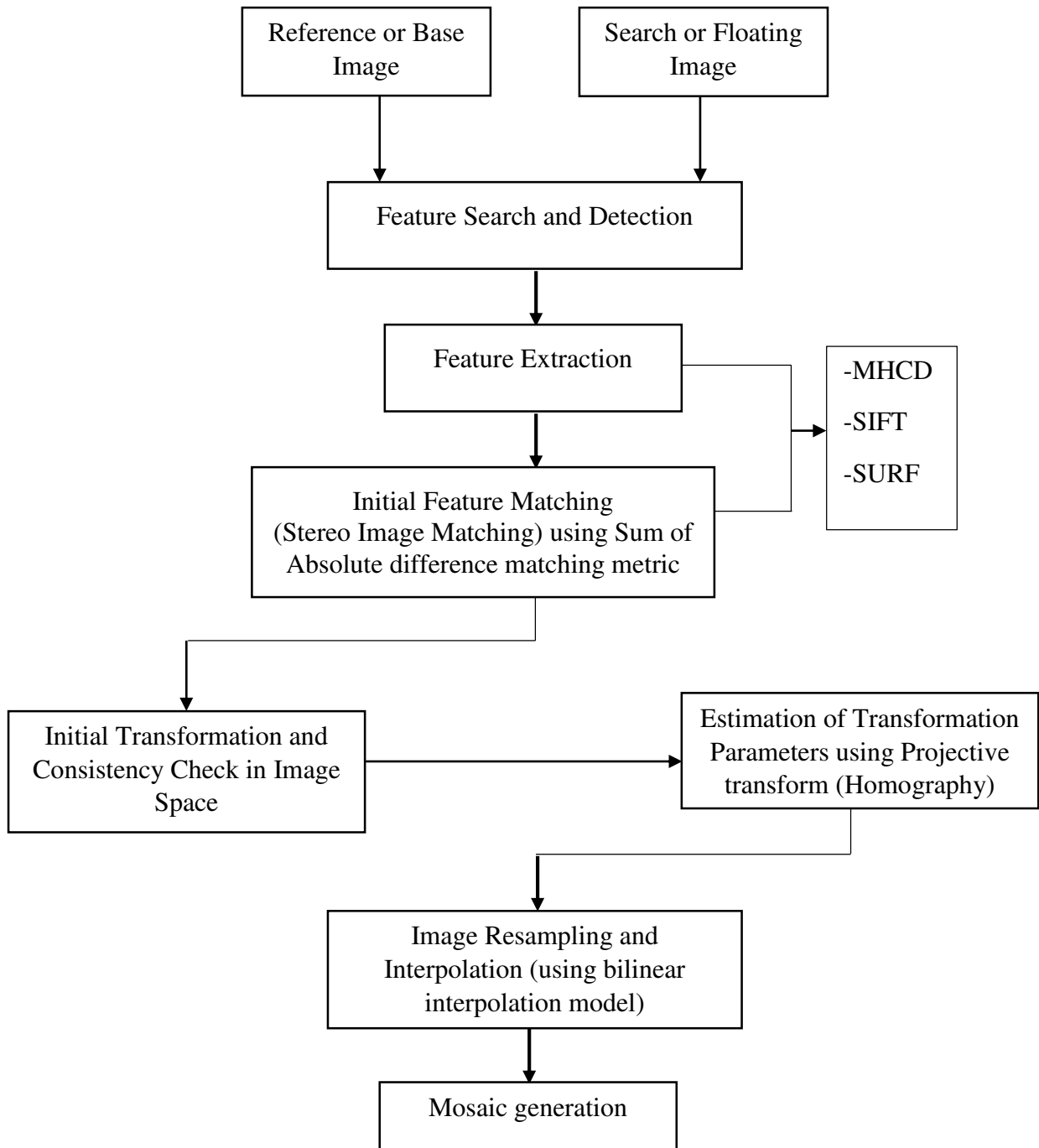


Figure 3.2: Flow diagram of the feature-based auto-registration

3.1.2 Implementation of the feature detection and extraction algorithms

The details of the step by step process of implementing each of the three (3) feature detection and extraction algorithms are presented in subsections 3.1.2.1 (Modified Harris corner detector), 3.1.2.2 (Scale Invariant Feature Transform) and 3.1.2.3 (Speeded Up Robust Features).

These three feature descriptors are the most popularly implemented models for various applications in Computer Vision and they are known to be very stable in the presence of outliers and noise, and in terms of matching accuracy (Bolarinwa, 2017; Dilipsinh *et al.*, 2014; Hassaballah *et al.*, 2016). Together with some other qualities, these descriptors are also known to be invariant to scaling and rotation as highlighted in Tables 2.1 and 2.2, subsection 2.1.1, and as such, they were implemented in this research.

In order to simplify the computational complexities of these algorithms, activity diagrams were also designed for each of them. Activity diagrams are very important diagrams in Unified Modelling Language (UML) which describes the dynamic aspect of the model implementation. They are graphical representations of both computational and organizational processes (workflows) which describe the step-by-step activities with expression of choice, iteration and concurrency. The activity diagram presents the description and the graphical illustration of the process flow of designing the major algorithms combined together to form the integrated Automatic Image Registration (AIR) model. These algorithms are involved in building an ideal image registration paradigm following the four (4) basic processes as discussed in Chapter 2, section 2.1. The activity diagram of each of the algorithms is segmented into three (3) compartments which describe the three major stages of the algorithm's implementation. The stages are: (i) the input, (ii) processing and (iii) output stages. They were designed within the Enterprise Architecture Software environment.

3.1.2.1 Modified Harris corner detection (MHCD) algorithm

The activity diagram depicting the algorithmic stages of implementing the Modified Harris Corner detection (MHCD) algorithm is presented in Figure 3.3 while the step-by-step procedure are as follows:

Step 1. Computation of horizontal and vertical derivatives of the stereo image.

- Step 2. Computation of three images corresponding to the three terms in matrix M .
- Step 3. Convolving these three images with a large Gaussian window.
- Step 4. Computation of scalar corner response using one of the corner response measure.
- Step 5. Finding local maxima above some predefined threshold as detected interest points.
- Step 6. Computation of SURF descriptor around detected interest points.
- Step 7. Matching the corresponding points based on the descriptor difference.
- Step 8. Filtering out the outliers from matched points using RANSAC algorithm.

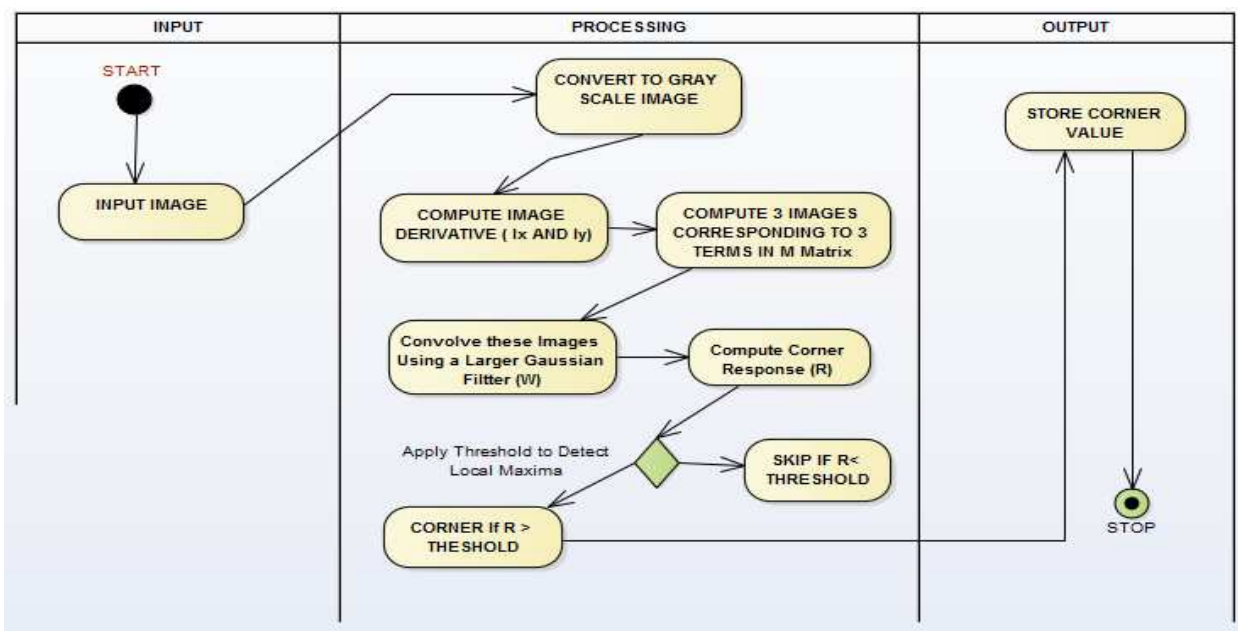


Figure 3.3: Activity diagram of Harris corner detection algorithm

3.1.2.2 Scale invariant feature transform algorithm (SIFT)

Figure 3.4 presents the activity diagram showing the implementation stages of the SIFT algorithm while the step by step procedure are as described in the following steps:

Step 1. Detection of Key points: Locally distinct points over different image pyramid levels were detected by:

- a. Applying Gaussian smoothing,
- b. Using Difference-of-Gaussians (DoG) to find extrema (over smoothing scales),

- c. Maxima suppression at edges.

Step 2. Computation of SIFT descriptor which transformed image content into features that are invariant to scaling, image translation, and rotation by:

- i. Computing image gradients in local 16x16 area at the selected scale
- ii. Creation of an array of orientation histograms; 8 orientations \times 4 \times 4 histogram array of 128 dimensions (yields best results).

Step 3. Matching of the corresponding points based on the descriptor difference.

Step 4. Filtering out outliers from matched points using RANSAC algorithm.

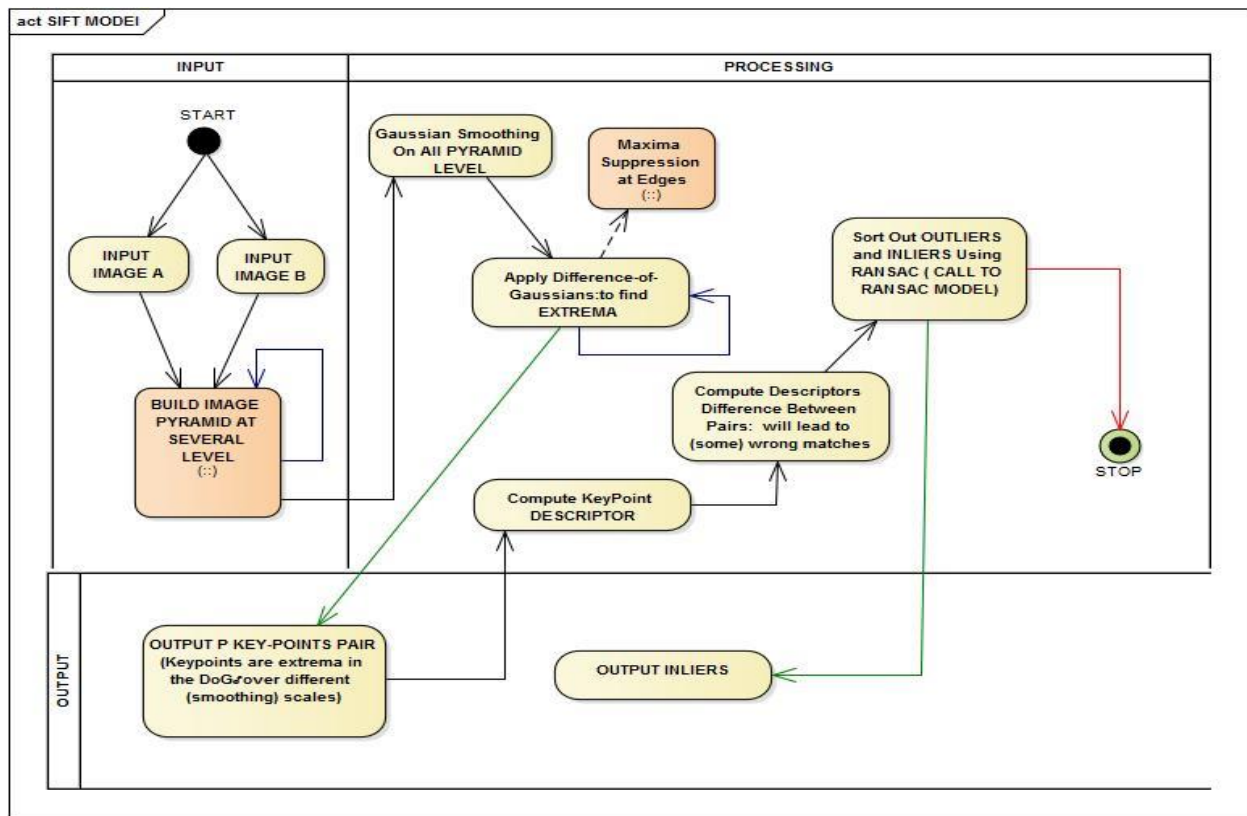


Figure 3.4: Activity diagram of Scale Invariant Feature Transform (SIFT) detector

3.1.2.3 Speeded up robust feature (SURF) detection and extraction algorithm

Figure 3.5 presents the activity diagram for the implementation of SURF algorithm while the following procedural steps are the details of the algorithm's implementation.

Step 1. Creation of an integral image,

Step 2. Extraction of key points by:

- a. Creating approximation of Hessian matrix.
- b. Calculating responses of kernel used.
- c. Finding local maxima across scale space.

Step 3. Determination of the SURF descriptor size to be used.

Step 4. Obtaining the dominant orientation.

Step 5. Extraction of the SURF descriptor.

Step 6. Matching the corresponding points based on the descriptor difference.

Step 7. Filtering out the outliers from matched points using RANSAC algorithm.

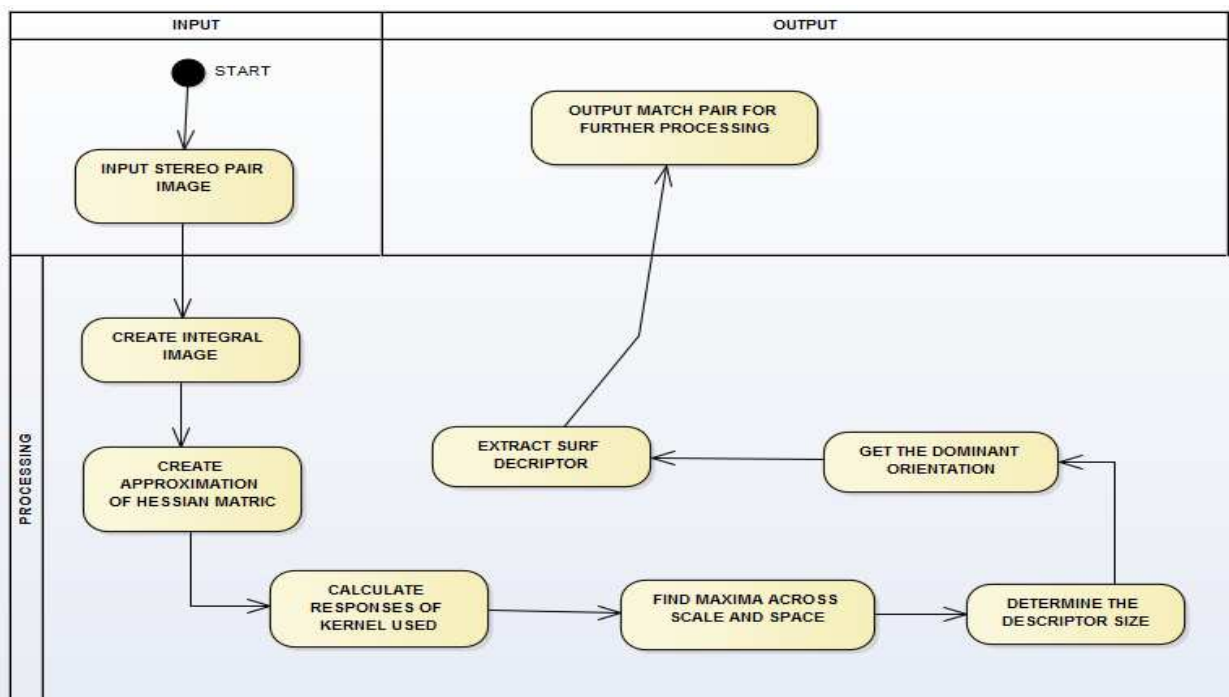


Figure 3.5: Activity diagram for Speeded Up Robust Feature (SURF) detector

3.1.3 Filtering of detected and extracted feature points

Having successfully detected and extracted the corresponding feature points automatically, it is very important to filter out points that are not accurately matched (outliers), because the presence of outliers in the registration scheme will result in registration errors. It is important that all outliers are filtered out or excluded from the entire matched points as much as possible such that only inliers (accurately matched points) are left and used for the final registration. In order to filter out these outliers, the Random Sampling Consensus (RANSAC) algorithm was used to fit the matched correspondences.

The algorithmic procedure of implementing RANSAC shall be discussed in further details in subsection 3.2.2 which addresses the model formulation of the epipolar correlation based image registration scheme because RANSAC was also used iteratively for the formulation of homography. Meanwhile, its activity diagram is presented in Figure 3.6.

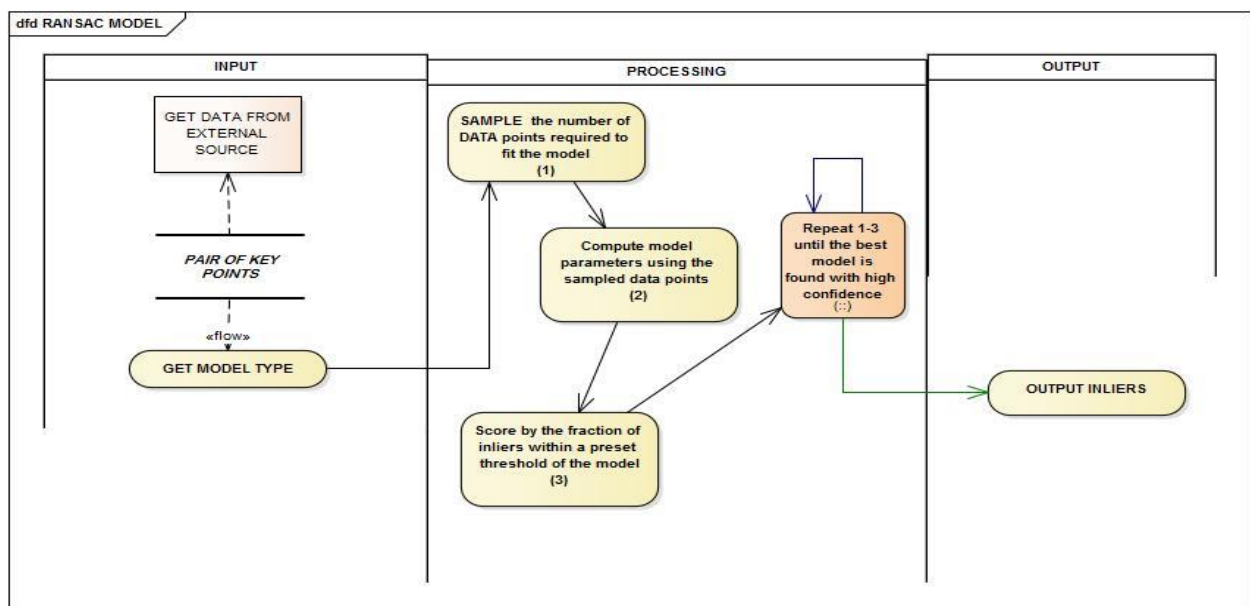


Figure 3.6: Activity diagram of Random Sampling Consensus (RANSAC) Model

3.1.4 Feature matching

Feature matching builds the relationship between the feature point sets from the reference and floating images. The establishment of the correspondence is based on the various feature descriptors and similarity measures. The string used to specify the feature matching is a metric which includes: Normalized Cross- Correlation (normxcorr), Sum of Squared Differences (SSD) and Sum of Absolute Differences (SAD). For this research, SAD was adopted which is a correlation-based method because of its proven robustness (Scharstein and Szeliski, 2002, Shmuel, 1991).

SAD is one of the simplest of all similarity measures and it is computed by the subtraction of pixels within a square neighbourhood between the reference image (I1) and the floating image (I2), after which the absolute differences within the square window is aggregated before proceeding with the optimization using the winner-take-all (WTA) strategy (Kanade *et al.*, 1997). In the event that the reference and floating images are perfectly matched, zero will be turned in as the resultant. The mathematical expression of this matching metric is as presented in Table 2.4, subsection 2.1.2 of Chapter two.

3.1.5 Model Estimation

The model estimation decides the types and parameters that are required for the mapping function. The parameters are computed from the feature pairs extracted from the correspondence established in feature matching. The mapping model was designed to be robust with respect to distortion and noise that may be inherent in the overlapping image pairs.

3.1.6 Image interpolation

Image interpolation algorithms are broadly categorised into non-adaptive and adaptive interpolation algorithms. Non-adaptive interpolation algorithms have an attribute of treating all pixels across the image equally during the interpolation which makes them more accurate because

they include more adjacent pixels. Adaptive interpolation algorithms on the other hand, are designed primarily to maximize artefact-free detail in enlarged photos, hence, some of the algorithms cannot be used for distortion or rotation of images. Bilinear interpolation algorithm which is a non-adaptive interpolation algorithm was implemented for the development of the automatic image registration scheme in this study because it strikes the best balance between accuracy and computational complexity which makes it one of the most widely used interpolation algorithm. The bilinear interpolation algorithm uses the average weight of two-pixel values that has been translated and follows a computational procedure of first zero padding the input matrix and translating it by the designated pixel value along the selected direction before creating the output matrix. The activity diagram of bilinear interpolation algorithm is presented in Figure 3.7.

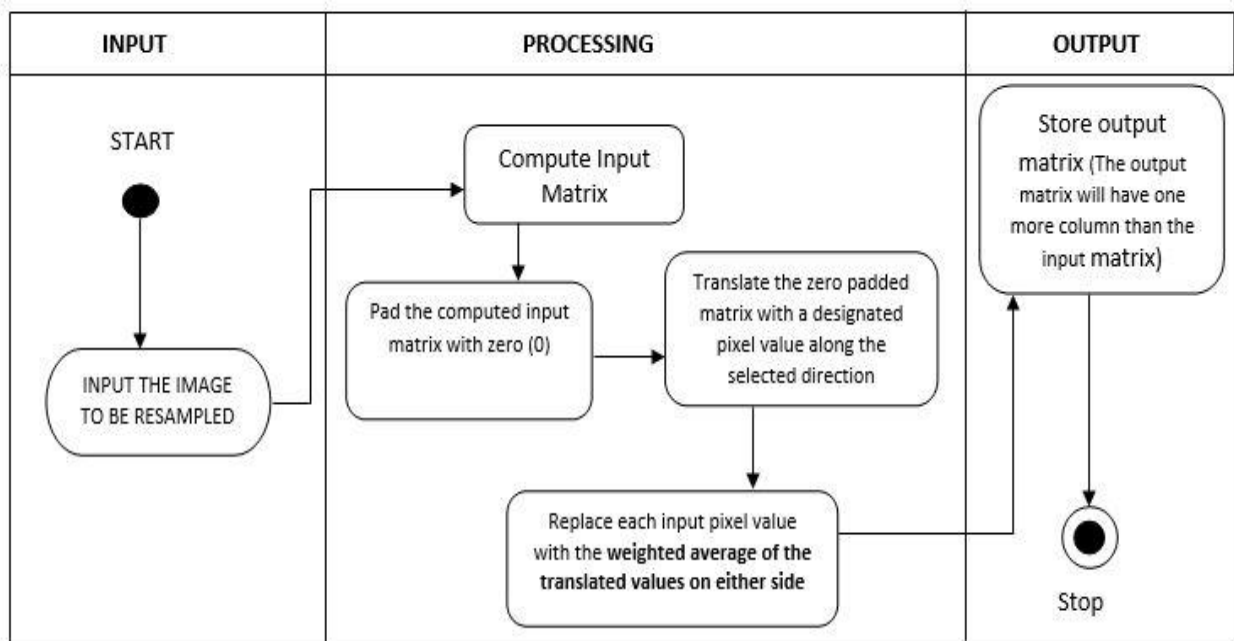


Figure 3.7: Activity diagram for the implementation of bilinear interpolation model

3.2 Automatic Image Registration using Integrated Epipolar Correlation Algorithms

In developing a new integrated image registration scheme, the robustness of epipolar correlation was explored in establishing point correspondences between a stereo pair by integrating it with each of the selected feature detection and extraction algorithms. The selected feature descriptors

were used to automatically extract corresponding or conjugate points from the overlapping image pairs which were used to estimate the epipolar geometry that exists between the image, assuming an uncalibrated camera. Since epipolar geometry is algebraically represented or depicted as the fundamental matrix, and fundamental matrix also defines coplanarity constraints, it is important to further examine the coplanarity condition which is always expressed as non-linear equation, and which must be linearized for analytical applications. Since coplanarity condition is an integral foundation of epipolar geometry and its application, the need for the linearization of the equation that expresses it is one of the major research problems in digital photogrammetry because of its computational complexities when compared to collinearity condition equation which is much simpler to linearize. A simplified approach using Taylor's series was adopted in the linear approximation of the coplanarity condition equation as presented in subsection 2.7.2.1.

3.2.1 Epipolar correlation-based image registration model formulation

For the formulation of integrated epipolar correlation image registration algorithms, the three feature descriptors and the Sum of Absolute Difference feature matching metric earlier used in addressing objective 1 and discussed in subsections 2.1.1 and 2.1.2 respectively were also used for the extraction and matching of conjugate features before they were subjected to RANSAC model fitting algorithm for filtering out or exclusion of outliers and retainment of conjugate features adjudged to be inliers only. The conjugate inliers were then used for the estimation of fundamental matrix using the normalized eight-point algorithm which was later used for the rectification of the stereopair. The Four (4) other major steps observed in formulating the epipolar stereo image registration model to address the second objective of this research are as follows:

1. Epipolar image rectification of un-calibrated stereo pairs.
2. 1D automatic scanning and search for corresponding points.
3. Formulation of transformation homography.
4. Image registration using inverse homography of the above formulation.

3.2.1.1 Epipolar image rectification of an un-calibrated stereo pairs

Stereo image rectification can be described as the process of transforming an image pair such that corresponding epipolar lines which are parallel to the x and y axis are made to coincide in such a way that measured coordinates on both images will have the same y – value with varying x – value. This type of transformation is known as projective rectification (Hartley, 1999).

The rectification process of stereo images can be subdivided into two major algorithmic approaches. While one algorithm adopted the usage of calibrated camera where the camera parameters are known and thus, the rectification becomes easier (Fusiello *et. al.*, 2000; Jawed *et. al.*, 2009), the other algorithm uses an uncalibrated camera (Hartley, 1992; Mallon and Whelan, 2005) where the camera intrinsic and extrinsic parameters are unknown, and hence, makes the rectification process more rigorous. This second algorithmic approach was adopted in this model formulation since the availability of calibrated camera in all imaging situations may not always be assured for image analysts. In doing so, the modified Hartley (1999) method of projective image rectification was modelled, and the details are as described as follows:

The aim of stereo image rectification is to convert the epipolar geometry that exists between a stereo pair into canonical form. This is achieved through an homography which maps the epipole to a point at infinity. Homography can be described as an invertible mapping of points and lines on the projective plane (Dubrofsky, 2009).

Mathematically, let the epipoles after rectification be represented as e'_{∞} and e''_{∞} .

Where;

$$e'_{\infty} = e''_{\infty} = [1 \quad 0 \quad 0]^T \tag{3.1}$$

Fundamental matrix of a rectified stereo pair has the form (3.2):

$$F_{\infty} = \begin{bmatrix} 0 & 0 & 0 \\ 0 & 0 & -1 \\ 0 & 1 & 0 \end{bmatrix} \quad (3.2)$$

Therefore, after rectification, the epipolar constraint is presented as (3.3):

$$\bar{m}''^T F_{\infty} \bar{m}' = 0 \quad (3.3)$$

Where \bar{m}' and \bar{m}'' are transformed corresponding pairs after rectification from their original values (m' and m''), and the homography used for the transformation are H' and H'' .

Therefore,

$$\bar{m}'' = H'' m'' \quad , \quad \bar{m}' = H' m' \quad (3.4)$$

Where H' and H'' can also be referred to as the rectifying homographies or matrices. Substituting equation (3.4) back into the epipolar constraint given in equation (3.3), equation (3.5) is obtained:

$$m''^T H''^T F_{\infty} H' m' = 0 \quad (3.5)$$

The problem with this (equation 3.5) is that the solution for H' and H'' are not unique, and this unideal solution can result in or introduce serious geometric distortions. Thus, in finding a unique solution for H' and H'' , attempt was made to investigate the algorithm developed by Hartley (1999) and to apply it to this model in view of preferring solution to the problem of automatic image registration.

Ideally, one of the homographies is expected to be closely similar to a rigid transformation (an isometry) within the neighbourhood of a selected point p_0 . Since the rigid transformation is basically defined by translation and rotation, the homography of one of the image pairs can be depicted as equation (3.6):

$$H'' = K R T \quad (3.6)$$

Where T and R are translation vector and rotational matrix respectively. The rotation matrix maps the epipole to a point $[1 \ 0 \ f]^T$ on the $x - axis$, and K is a transformation matrix that maps $[1 \ 0 \ f]^T$ to point $[1 \ 0 \ 0]^T$ at infinity along $x - axis$. Matrix K can be expressed as in equation (3.7):

$$K = \begin{bmatrix} 1 & 0 & 0 \\ 0 & 1 & 0 \\ -f & 0 & 1 \end{bmatrix} \quad (3.7)$$

Thus, H'' is basically dependent on two parameters, which are focal length (f) and the rotation angle(θ). If the translation vector (T) is ignored, then, H'' will be expressed as equation (3.8):

$$H'' = \begin{bmatrix} \cos \theta & \sin \theta & 0 \\ -\sin \theta & \cos \theta & 0 \\ -f \cos \theta & -f \sin \theta & 1 \end{bmatrix} \quad (3.8)$$

In order to match up the new epipolar lines, the next task is to find or derive the matrix H' which was then applied to the other image. In executing this task, the approach adopted by Hartley (1999) which minimizes the sum of squared distances as in equation (3.9) was used.

$$\sum_i d(H' m'_i, H'' m''_i)^2 \quad (3.9)$$

To solve for H' , it was subjected to a decomposition process which resulted in equation (3.10):

$$H' = H_A H_0 \quad (3.10)$$

where:

$$H_A = \begin{bmatrix} a & b & c \\ 0 & 1 & 0 \\ 0 & 0 & 1 \end{bmatrix}, \text{ which stands for affine transformation, and}$$

$$H_0 = H'' M$$

According to Hartley (1999), F matrix can be factorized as

$$F = S_e' M. \quad (3.11)$$

Where M has three parameters and it belongs to the non-singular matrices family and S_e is an asymmetric matrix, which was generated from vector e as shown in equation (3.12):

$$S_{e'} = \begin{bmatrix} 0 & -e_3' & e_2' \\ e_3' & 0 & -e_2' \\ -e_2' & e_1' & 0 \end{bmatrix} \quad (3.12)$$

It should be noted that $e' = [e_1' \ e_2' \ e_3']$ is the epipole of the first image. Thus, instead of directly minimizing $\sum_i d(H' m'_i, H'' m''_i)^2$, the following steps were taken:

- a. Firstly, the Matrix H'' was determined.
- b. The feature points on both image pairs were transformed as follows:

$$\bar{m}_i' = H_0 m_i' = H'' M m_i'' \quad (3.13a)$$

$$\bar{m}_i'' = H'' m_i'' \quad (3.13b)$$

- c. In order to find the matrix H_A using least squares method, $\sum_i d(H_A \bar{m}_i', \bar{m}_i'')^2$ was minimized.

$$\text{If } \bar{m}_i' = (\bar{x}_i', \bar{y}_i', 1) \text{ and } \bar{m}_i'' = (\bar{x}_i'', \bar{y}_i'', 1), \quad (3.14)$$

then:

$$\sum_i d(H_A \bar{m}_i', \bar{m}_i'')^2 = \sum_i (a\bar{x}_i' + b\bar{y}_i' + c - \bar{x}_i'')^2 + (\bar{y}_i' - \bar{y}_i'')^2 \quad (3.15)$$

Since $(\bar{y}_i' - \bar{y}_i'')^2$ is a constant, the minimization problem is simplified as (3.16):

$$\sum_i (a\bar{x}_i' + b\bar{y}_i' + c - \bar{x}_i'')^2 \quad (3.16)$$

which is a simple least-squares problem from which parameters a, b and c are determined.

- d. Matrix H' is then obtained by equation (3.17):

$$H' = H_A H_0 \quad (3.17)$$

3.2.1.2 One dimensional automatic scanning and correspondence search

Following the implementation of the above modified Hartley method of projective image rectification, the stereo image was transformed to ensure that the corresponding epipolar lines are

parallel to the x-axis of the image, thus, simplifying the search for conjugate points from $2D$ to $1D$ search space.

A series of correspondence were determined automatically using the computed photo-base obtained by finding the difference between the principal points of the rectified image. Using this parameter, the developed algorithm initiates the auto-scanning process from a specified position on the left image plus the photo-base, resulting in the corresponding position on the right image. A register was created for the registered photo coordinates which was stored in the computer memory in preparation for the next stage of the registration process (formulation of transformation homography) which is discussed in subsection 3.2.1.3.

3.2.1.3 Formulation of transformation homography

The formulation of transformation homography employs the use of RANSAC algorithm in determining the best fitting transformation matrix using the corresponding photo points detected in subsection 3.2.1.2. The choice of RANSAC is informed by its ability to effectively cope with large percentage of outliers or mismatches in the input data set. Also, RANSAC is highly efficient when compared to other sampling techniques because it only makes use of the required minimum number of input data set possible for the generation of candidate solutions, before proceeding to the enlargement of these data set with consistent data points in its estimation of model parameters (Ajayi, 2014; Fischler and Bolles, 1981).

The RANSAC algorithmic procedure can be highlighted as follows:

- a. The minimum number of points needed for the determination of the parameters of the model was randomly selected.
- b. A unique solution for the model parameters was derived and provided.
- c. The number of points that fits with a predefined tolerance ϵ from the entire points available was determined.

- d. In the event that the percentage inliers over the total matched points within the set is greater than the predefined threshold τ , all extracted inliers for the re-estimation of the model parameters were used and the process was truncated.
- e. When the percentage inliers over the total matched points within the set is not greater than the predefined threshold τ , steps (a) to (c) was iteratively executed over and over again but not exceeding N_i times.

Now, the number of iterations N_i was set to be high enough to ensure that the probability p (which is always often set to 0.99) is valid. This implies that a minimum of one of the random sample sets will be free from outliers.

In arriving at the value for N_i , \bar{a} was assumed to denote the probability that any selected data point is an inlier and $\bar{b} = 1 - \bar{a}$ represents the probability of observing an outlier. N_i iterations of the minimum number of points denoted by q are needed. Thus,

$$1 - p = \left(1 - \bar{a}^q\right)^{N_i} \quad (3.18)$$

Which can further be processed as presented in equation (3.19):

$$N_i = \frac{\log(1-p)}{\log(1-(1-\bar{b})^q)} \quad (3.19)$$

3.2.1.4 Image registration using the inverse of the formulated

Having successfully derived the transformation parameters or homography, the next and final stage is to determine the inverse of the derived homography. This inverse homography was then applied to each of the stereo pair in order to get a registered image without compromising or losing the original quality. This is the final stage of the developed epipolar correlation-based integrated image registration algorithm.

It should be noted that each of the three feature detection and extraction algorithms was used to first extract conjugate features on the overlapping image pairs before epipolar constraints as

highlighted in steps 1-4 were imposed on them. The extracted features were used as input parameters for the integrated epipolar correlation image registration module.

3.2.2 Estimation of fundamental matrix

Figure 3.8 presents the activity diagram of eight-point algorithm which was used for the fundamental matrix estimation. The eight-point algorithm is a linear estimation approach and as such, it computes the Fundamental Matrix (F) as a linear system of equations. The choice of 8-point algorithm is informed by its property of computational efficiency, implementation simplicity and high sensitivity to outliers or presence of noise and its sensitivity to scale and origin of coordinates. For the implementation of 8-point algorithm in the estimation of fundamental matrix, a minimum of eight (8) conjugate points are needed, and when more points are provided, a linear least-squares error is minimized across all points. Coefficient Matrix (A) was built from the input conjugate points by finding their Kronecker product (Langville and Stewart, 2004). After this stage, the singular value decomposition of Matrix (A) was obtained and the singular vector with the minimal singular value was selected which was finally used for the estimation of the fundamental matrix. The major advantage of the eight-point algorithm method is that it leads to a non-iterative computation method which is easy to implement using any linear algebra numerical package (Carlo, 2017). In order to produce a reliable result, the normalized eight-point algorithm requires that the inputs (point correspondences) must match precisely.

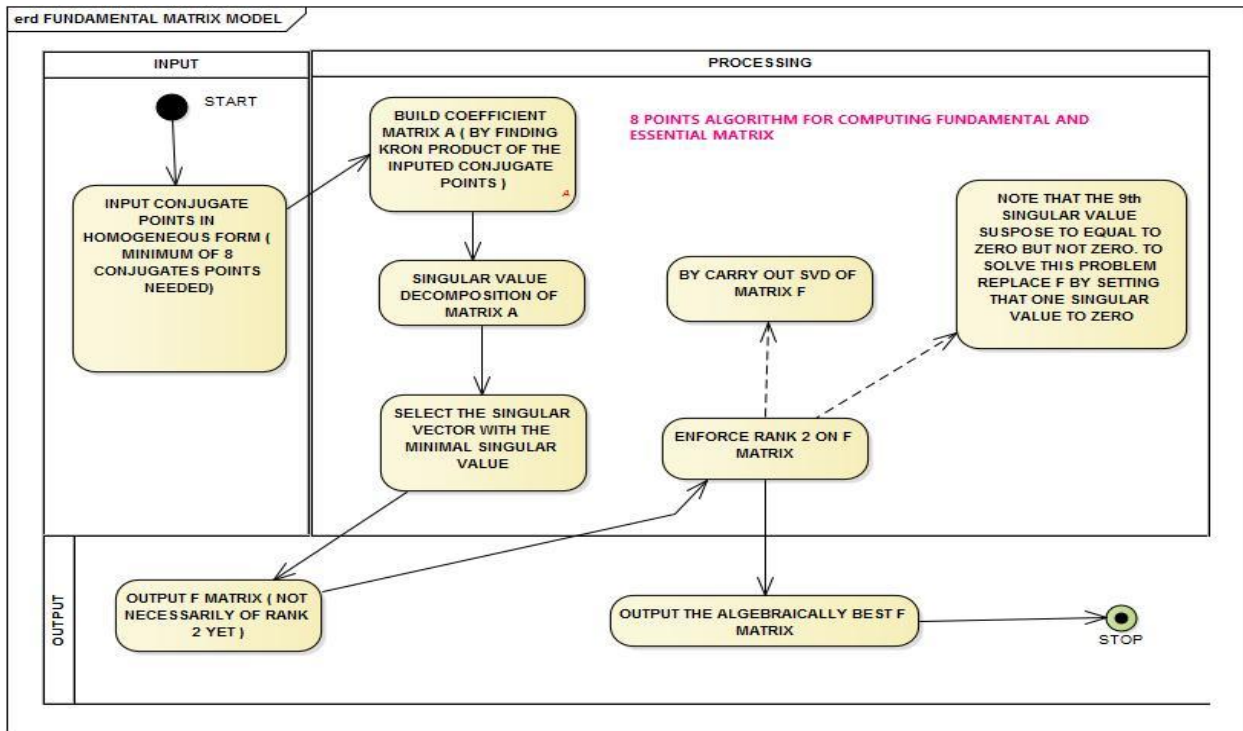


Figure 3.8. Eight (8) point algorithm activity diagram for the estimation of fundamental matrix

3.3 Validation of Model and Performance Evaluation

A digital semi-automatic stereo comparator was developed and embedded within the developed image registration scheme so as to ensure that spatial comparison can be carried out on the rectified images to see how robust the developed model is. The stereo comparator allows conjugate point measurements to be made directly on the rectified stereo pairs. It accurately measures xy coordinates of interest points in the image plane. These measurements were then used for the accuracy test of the model and to test its performance with processing time.

The accuracy check uses the coplanarity constraint to test for the reliability of the point correspondences measured directly on the digital stereo comparator. The test is based on the fact that for point correspondences, the signed distance (residual) w_i which can be described as the distance between the epipolar line in the right image and its conjugate point in the left image, should ideally be equal to zero (perfectly accurate which shows perfect correlation). This signed distance w_i can be mathematically expressed as shown in equation (3.20).

$$w_i = [x_i'' \quad y_i'' \quad 1]F^T \begin{bmatrix} x_i' \\ y_i' \\ 1 \end{bmatrix} = \text{vec}(\mathbf{x}''F^T\mathbf{x}') = (\mathbf{x}' \otimes \mathbf{x}'')^T \text{vec}(F^T) = (\mathbf{x}' \otimes \mathbf{x}'')^T \mathbf{f} \quad (3.20)$$

Where the operator \otimes is the Kronecker product.

Apart from the computed signed distances, the scheme's accuracy was also assessed by the estimation of Root Mean Square Error (RMSE) which is a frequently adopted measure of the difference between values predicted by a model and the values actually observed from the modelling. These individual differences are also known as residuals or errors, and the RMSE aggregates them into a single measure which is used to judge the predictive quality of the model. The RMSE was estimated using equation (3.21).

$$R = \sqrt{\frac{\sum_{i=1}^N w_i^2}{N}} \quad (3.21)$$

Where R is the RMSE, N is the total number of points measured directly on the digital stereo comparator and w_i is as defined in equation (3.20).

The cumulative signed distances of the automatically extracted corresponding feature points were estimated together with the signed distances of the conjugate points measured directly on the rectified image pairs using the digital stereo comparator and their results were compared. Also, the processing run time of each of the developed and implemented algorithms was estimated and compared.

3.4 Data Used for Model Experimentation

Two different image registration campaigns were adopted for the experimentation of the developed registration scheme using different overlapping image pairs. The first campaign seeks to evaluate the performance of the developed scheme with low resolution images while the second campaign was used to evaluate the performance of the developed scheme with high resolution images. The images used to test the performance level of the scheme in the first image registration

campaign were extracted on Wednesday, 30th August, 2017 from google earth real-time online image data repository. The image pairs are of the size 796 x 619 pixels and 834 x 621 pixels respectively, showing part of the built-up area of the Federal University of Technology, Minna, Niger State, Nigeria (Main Campus, Gidan Kwano). Also, an aerial survey flight mission was conducted on Tuesday, 7th November, 2017, using a DJI Phantom 4 (Quadcopter) Unmanned Aerial Vehicle (UAV) to acquire overlapping image pairs covering part of the same campus, which were used for the second image registration campaign. Figures 3.9a and 3.9b present the google earth image pairs used for the first image registration scheme's experimentation. While figure 3.9a shows the base image (master image), figure 3.9b shows the search image. The overlapping image pair covers some part of the School of Agriculture and Agricultural Technology (SAAT), the School of Engineering and Engineering Technology (SEET), University Convocation Square, School of Environmental Technology (SET), Electronic examination centre, University Senate building, University library, University auditorium, ICT building, and the School's post office. The images used for the second image registration campaign are presented in Figures 3.10a and 3.10b. The size of each of the image pair is 3000 x 4000 pixels and it covers part of the Entrepreneurship Centre, the University security department and other features within the University campus.



Figure 3.9a: Image data of part of FUTMinna, Main campus, Minna (Base image)



Figure 3.9b: Image data of part of FUTMinna, Main campus, Minna (Search image)



Figure 3.10a: UAV acquired image of part of FUTMinna, Main Campus (Base image)



Figure 3.10b: UAV acquired image of part of FUTMinna, Main Campus (Search image)

Also, in order to ascertain the robustness of the developed image registration scheme, coordinates of fifteen (15) ground control points (GCPs) distributed across the area covered by the overlapping

image pairs used for both image registration campaigns were acquired with the aid of a Etrex handheld global positioning system (GPS) receiver. These GCPs are points that are identified on the overlapping image pairs as well as on the ground. Table 3.1 shows the coordinates of the 15 GCPs used for the first image registration campaign while the coordinates of the GCPs used for the second registration campaign is presented in Table 3.2.

Table 3.1: GCPs used for the first image registration campaign

STATION ID	Eastings (m)	Northings (m)	Height (m)
FUTGK01	220363.000	1054669.000	241.000
FUTGK02	220394.000	1054704.000	241.000
FUTGK03	220405.000	1054869.000	244.000
FUTGK04	220528.000	1054702.000	240.000
FUTGK05	220497.000	1054856.000	245.000
FUTGK06	220514.000	1054940.000	245.000
FUTGK07	220434.000	1054942.000	246.000
FUTGK08	220427.000	1055042.000	243.000
FUTGK09	220381.000	1055012.000	246.000
FUTGK10	220368.000	1055190.000	243.000
FUTGK11	220217.000	1055123.000	249.000
FUTGK12	220203.000	1054920.000	256.000
FUTGK13	220179.000	1055017.000	254.000
FUTGK14	220144.000	1055077.000	251.000
FUTGK15	220324.000	1054911.000	242.000

Table 3.2: GCPs used for the second image registration campaign

STATION ID	Easting (m)	Northing (m)	Height (m)
FUTGK-D-01	220609.000	1055157.000	232.000
FUTGK-D-02	220627.000	1055189.000	234.000
FUTGK-D-03	220615.000	1055183.000	233.000
FUTGK-D-04	220609.000	1055187.000	233.000
FUTGK-D-05	220591.000	1055187.000	233.000
FUTGK-D-06	220635.000	1055206.000	232.000
FUTGK-D-07	220636.000	1055204.000	233.000
FUTGK-D-08	220635.000	1055207.000	232.000
FUTGK-D-09	220633.000	1055205.000	233.000
FUTGK-D-10	220633.000	1055207.000	233.000
FUTGK-D-11	220632.000	1055207.000	233.000
FUTGK-D-12	220632.000	1055212.000	233.000
FUTGK-D-13	220632.000	1055213.000	233.000
FUTGK-D-14	220684.000	1055179.000	233.000
FUTGK-D-15	220679.000	1055177.000	233.000

3.5 Model Packaging into Software Development

The developed algorithms were automated and compiled into an executable file as a stand-alone application for simplification of computational complexities and user-friendly processing using JAVA programming language. Details of the programming (coding) and the system (hardware and software) specifications are as described in subsequent subsections.

3.5.1 System specifications

The specification of the system used for the software development is subdivided into hardware and software specifications. The configuration of the hardware used which is the Laptop Personal Computer (PC) are as follows:

1. Processor: – Intel (R) Core (TM) i7-3537U CPU @ 2.00GHz 2.50GHz
2. Random Access Memory (RAM): – 4.00 Gigabyte (GB) (2.45 GB Usable)
3. Operating System type: - 64-bit Operating System, x64-based processor
4. Hard drive size: - One Terabyte (1 TB)

Using the above system configuration PC, the developed registration scheme successfully registered images extracted from google earth because of the small size of the images but could not perform at optimum level when it was experimented with UAV acquired images used for the second image registration campaign because of their larger image sizes. This therefore necessitated the need for PCs with higher specifications for optimal results when images of relatively large sizes are to be registered. For the second image registration campaign, a PC equipped with 8 GB installed RAM, and Intel (R) Core (TM) i7-7700HQ CPU @2.80GHz processor was used, though it was also tested with a 4 GB and 16 GB installed RAM with intel core i7 PC specification to ascertain the effect of the PC's installed RAM on the speed and accuracy of the developed image registration scheme.

The software tools used for this phase of the research work are as highlighted as follows:

1. Java version “1.8.0_111”: - Java (TM) SE Runtime Environment (build 1.8.0_111-b14); with Hotspot (TM) 64-Bit Server VM (build 25.111-b14, mixed mode). This actually is the Java Virtual Machine that was used.
2. IntelliJ IDEA 2016.1.3 which was used for developing a user-friendly graphical user interface.

3. BoofCV (v0.14.1).
4. 64 bit, Microsoft windows operating system

3.5.2 Data specifications

The software was designed to automatically register overlapping pairs of images of any size and any source (multisource), with at least 60% overlap. This is to ensure that the epipoles of the two image pairs do not fall inside any of the image. The program was designed to truncate itself or stop running when any of the epipoles is found inside the image.

CHAPTER FOUR

4.0 RESULTS AND DISCUSSION

4.1 Model Outlook

The Graphical User Interface (GUI) of the developed image registration scheme, packaged into a software tool is presented in Figures 4.1 and 4.2. The GUI shows the outlook of the software's interface which the user interacts with directly. It shows both the welcome page and the modules of the scheme. The GUI was designed entirely using codes in IntelliJ IDEA 2016.1.3 working environment. The coding method used in designing the GUI gives full control over the properties of each object used when compared to other simpler and easy ways of building a GUI.



Figure 4.1: Welcome page of the developed model

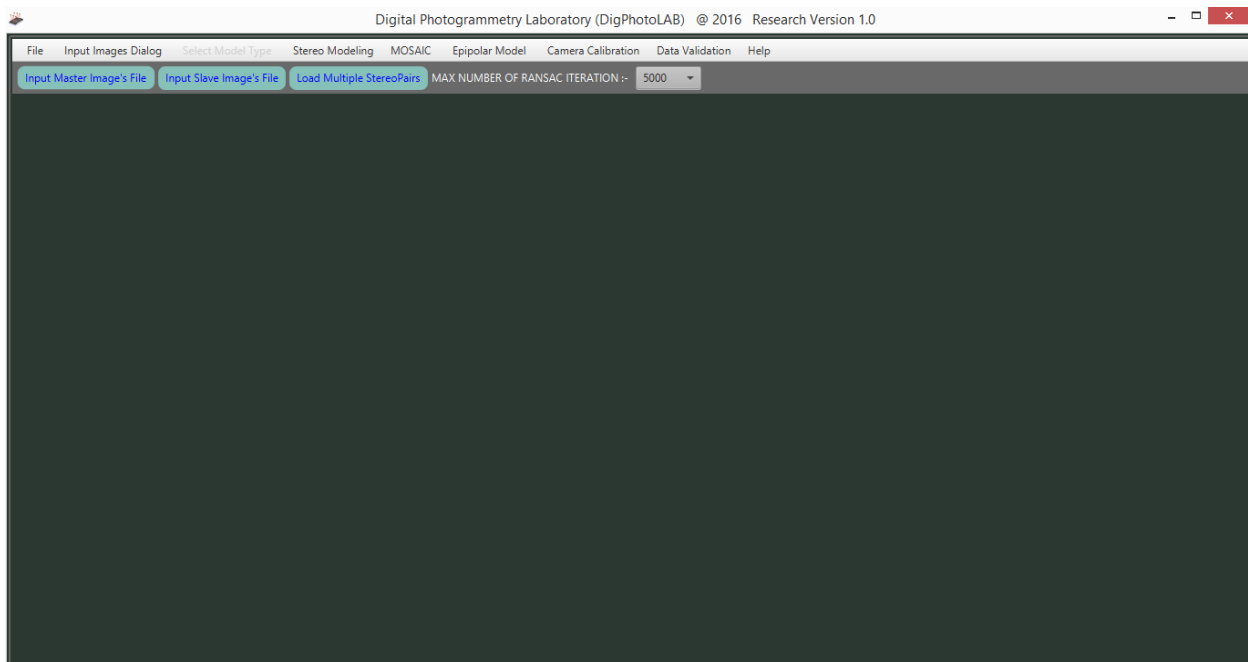


Figure 4.2: GUI of the developed model's working page showing the model's different modules

4.2 Automatic Image Registration Using Three Selected Feature Detection and Extraction Algorithms

The results of the mosaics generated from each of the three (3) implemented feature detection and extraction algorithms are presented in subsections 4.2.1, 4.2.2 and 4.2.3 using the stereopairs presented in Figures 3.9a and 3.9b. For these three methods, Sum of Absolute Difference metric described by the first equation in Table 2.4 was used for the feature match, projective transformation function described in equations (2.9) and (2.10) was used for the computation of the transformation matrix (T) and bilinear interpolation algorithm described in equations (2.1) – (2.5) of subsection 2.1.3 was used for the image resampling.

4.2.1 Automatic image registration using Modified Harris Corner Detector (MHCD) (first registration campaign)

Figure 4.3 shows the associated pairs extracted from the overlapping image pairs using the MHCD algorithmic procedure discussed in subsection 3.1.2 of chapter 3. The corresponding features include both the matched inliers and outliers. Figure 4.4 shows the matched inliers only which

was finally used for mosaic generation in the first image registration campaign having successfully excluded the outliers or mismatches using RANSAC algorithm described in subsection 3.2.2. Figure 4.5 shows the scheme's register of conjugate points which contains the image coordinates (in pixels) of all the automatically extracted conjugate points. A total of 456 conjugate points were automatically extracted using MHCD and their image coordinates were stored in the coordinate register and presented in Appendix A. The final mosaic generated from the image registration process is presented in Figures 4.6a and 4.6b. While Figure 4.6a shows the mosaic within the developed software environment, Figure 4.6b shows the generated mosaic which has been exported as an image.

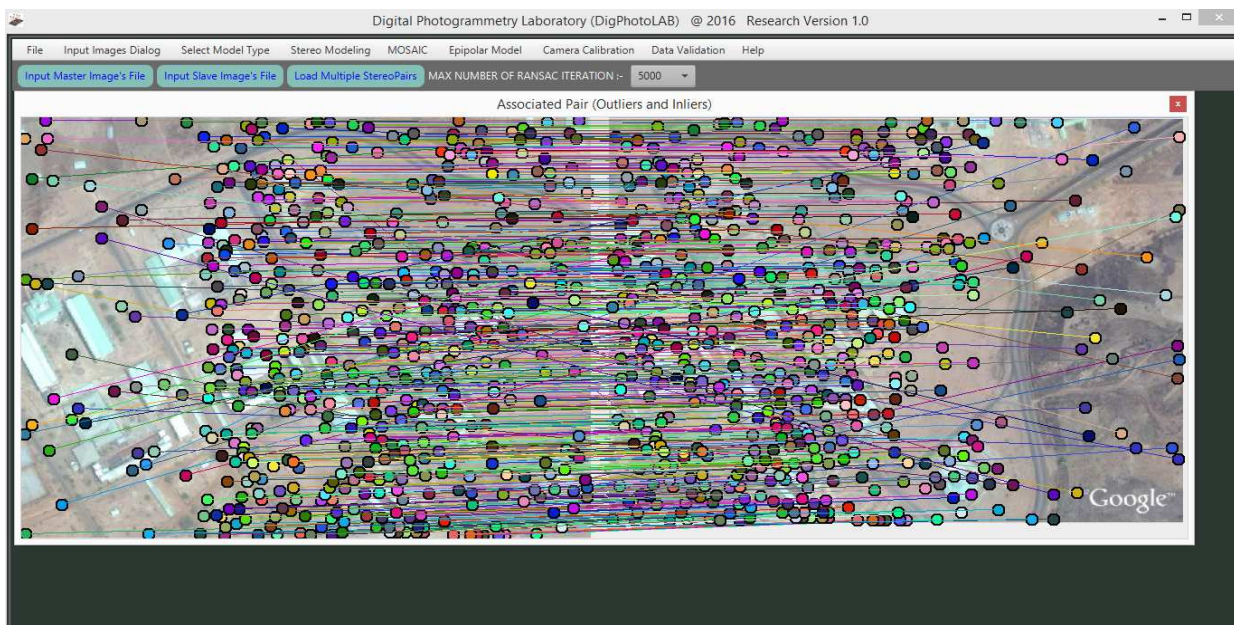


Figure 4.3: Associated image pairs containing the inliers and outliers (Using MHCD)

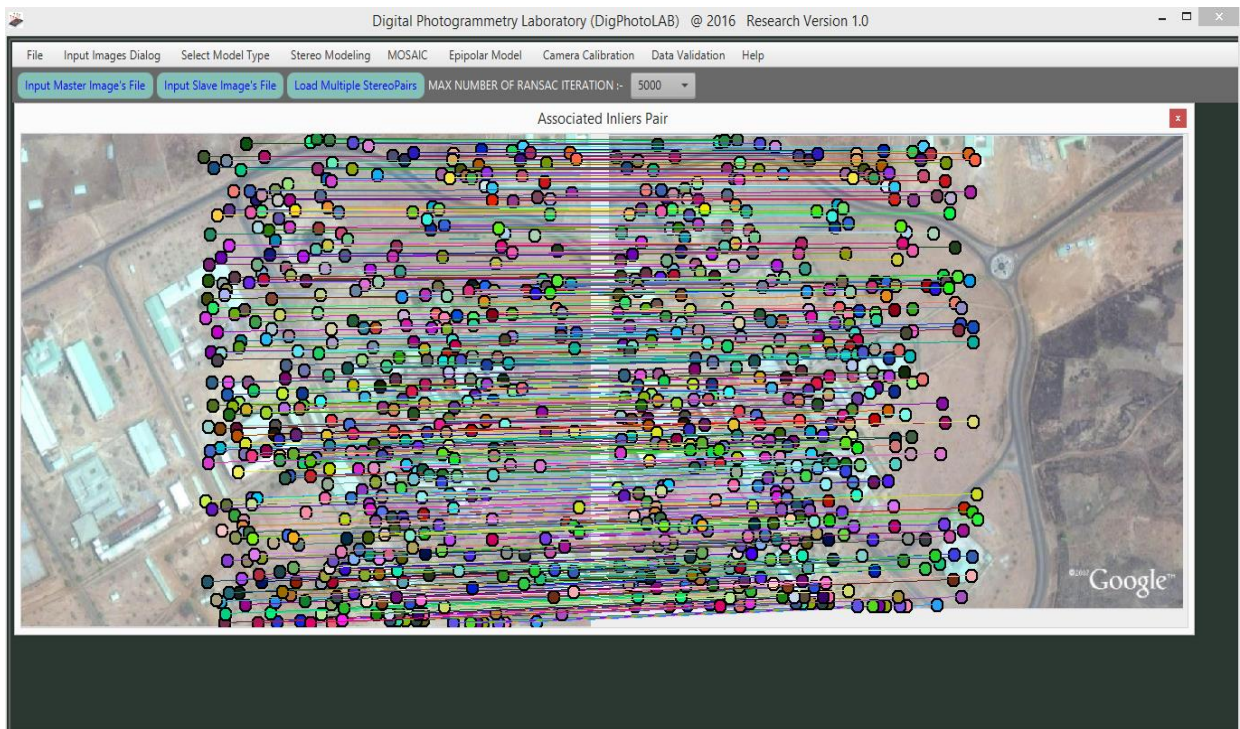


Figure 4.4: MHCD associated image pairs containing only the inliers (outliers excluded)

Point ...	PhotoA_x (pixels)	PhotoA_y (pixels)	PhotoB_x (pixels)	PhotoB_y (pixels)	TransPhotoB_x (pixels)	TransPhotoB_y (pixels)
pt 0	598.0	313.0	354.0	315.0	598.0094574542425	313.1106596459795
pt 1	719.0	612.0	476.0	614.0	720.106331979084	612.1587546860097
pt 2	403.0	9.0	159.0	10.0	402.9479491032773	8.160790630087003
pt 3	412.0	6.0	168.0	8.0	411.9485509009829	6.162915963781845
pt 4	430.0	7.0	186.0	7.0	429.9500270947397	5.165769295333544
pt 5	675.0	613.0	431.0	615.0	675.080491604651	613.1407983922192
pt 6	314.0	12.0	70.0	14.0	313.9452918195992	12.14683950746491
pt 7	463.0	11.0	219.0	13.0	462.9538116783436	11.16754953701766
pt 8	485.0	15.0	241.0	17.0	484.9569615827083	15.168850358028225
pt 9	700.0	16.0	456.0	17.0	700.0085126291743	15.198402134211584
pt 10	666.0	613.0	422.0	615.0	666.0755088791677	613.1371725223503
pt 11	645.0	613.0	401.0	615.0	645.0641622794097	613.1287122719682
pt 12	642.0	19.0	398.0	22.0	641.9911663941175	20.18869140368117
pt 13	685.0	21.0	441.0	23.0	685.0044124126772	21.194371423503647
pt 14	636.0	613.0	392.0	615.0	636.059419345882	613.1250864986517
pt 15	627.0	613.0	383.0	615.0	627.0547483480736	613.1214607543003

Figure 4.5: MHCD algorithm's conjugate points register

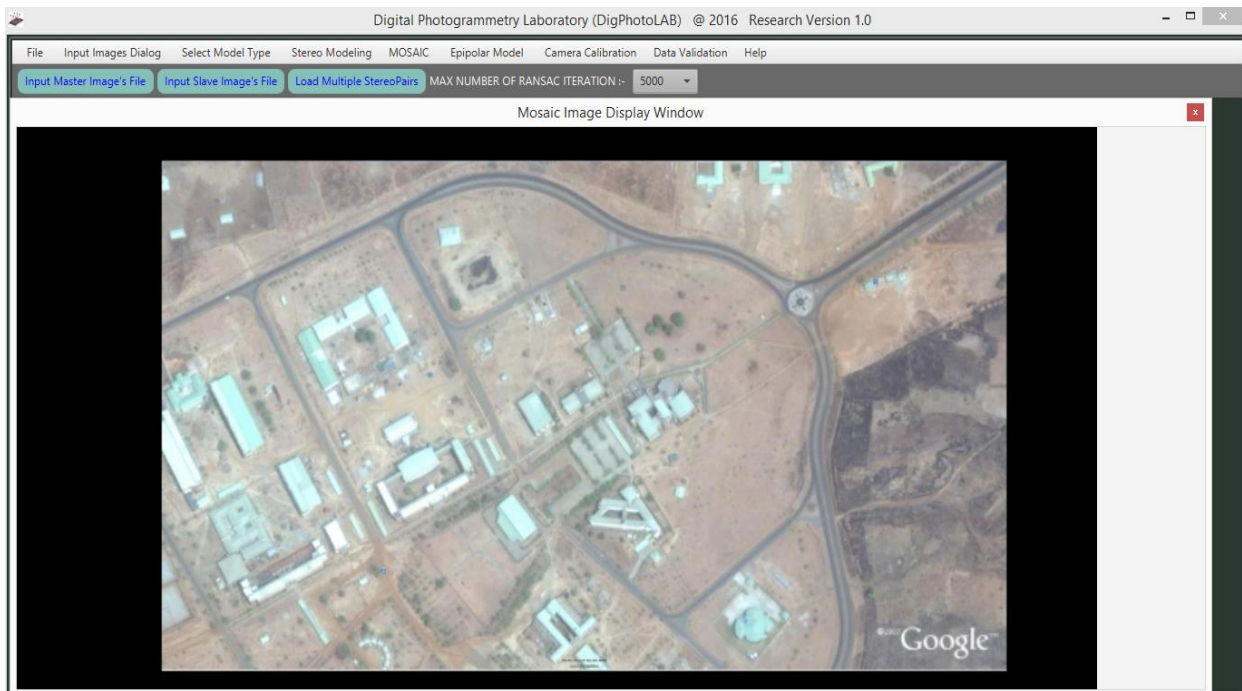


Figure 4.6a: Mosaic generated in the developed software environment using MHCD



Figure 4.6b: Mosaic generated using MHCD

The computed homography of the image registration is $T_{Harris} = \begin{bmatrix} 1.00 & 0.00 & -243.836 \\ -0.00 & 1.00 & 1.887 \\ 0.00 & 0.00 & 0.99 \end{bmatrix}$

The homography shows that the diagonal is approximately equal to 1 and the parameter vectors of the computed homography are: $a = 1.000$, $b = 0.000$, $t_x = -243.836$ and $t_y = 1.887$. Where t_x and t_y are the translation along the x and y axis respectively, $a = \cos \alpha$ and $b = \sin \alpha$ and α is the rotation angle. The parameter vectors show that the MHCD feature descriptor is indeed invariant to rotation since the rotation angle reported is equal to zero which shows that the algorithm does not vary under rotation.

4.2.2 Automatic image registration using Scale Invariant Feature Transform (SIFT) (first registration campaign)

The associated pairs which contains both inliers and outliers automatically extracted using SIFT algorithmic procedure discussed in subsection 3.1.2 of chapter 3 is shown in Figure 4.7 while the remaining matched points (inliers) after the exclusion of outliers using RANSAC algorithmic procedure discussed in subsection 3.2.1.3 is shown in Figure 4.8. These inliers were the final matched corresponding features used for the final image registration. The image coordinates (in pixels) of all the automatically extracted conjugate points were extracted and stored in the scheme's coordinate register as shown in Figure 4.9. A total of 1129 conjugate points were automatically extracted using the SIFT algorithm and their coordinates were stored in the software's coordinate register, which can also be saved or exported as a .txt file (notepad). Appendix B presents the photo coordinates automatically extracted using the SIFT algorithm for the image registration. Figure 4.10 shows the mosaic generated within the working environment of the developed software while Figure 4.10b shows the final mosaic when it has been exported from the software.

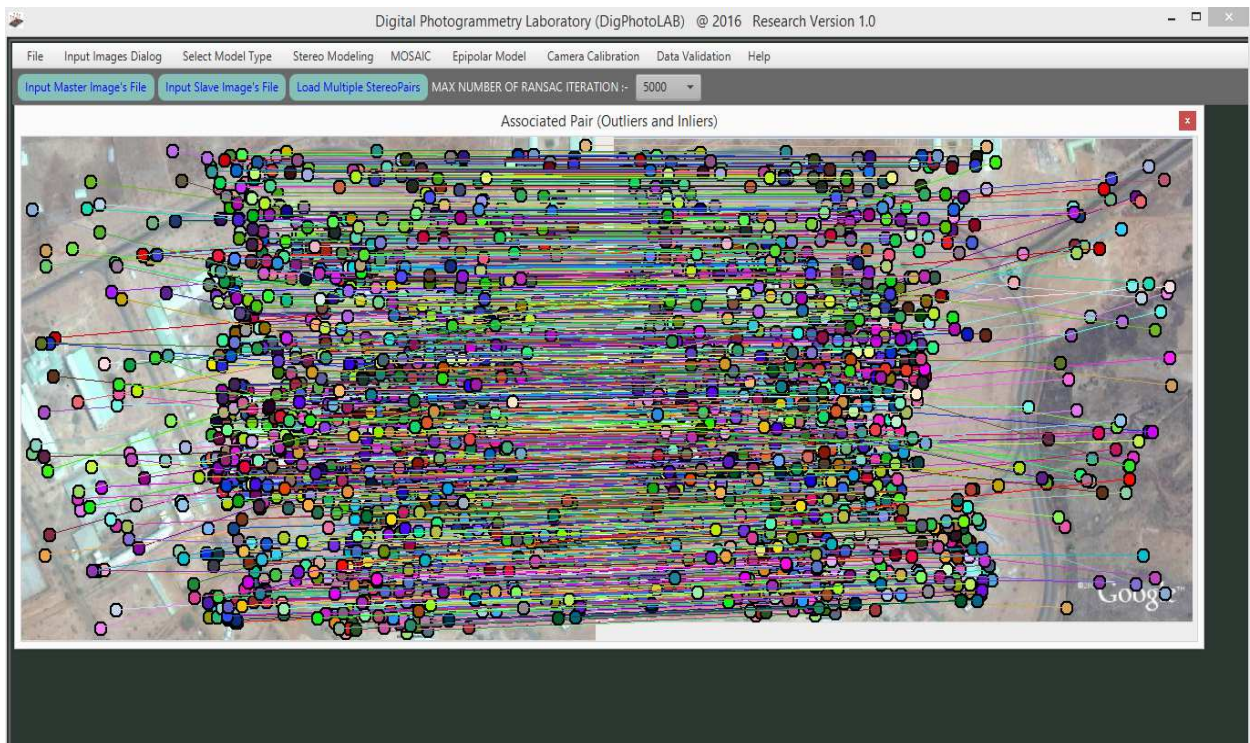


Figure 4.7: Associated image pairs containing the inliers and outliers (Using SIFT Model)

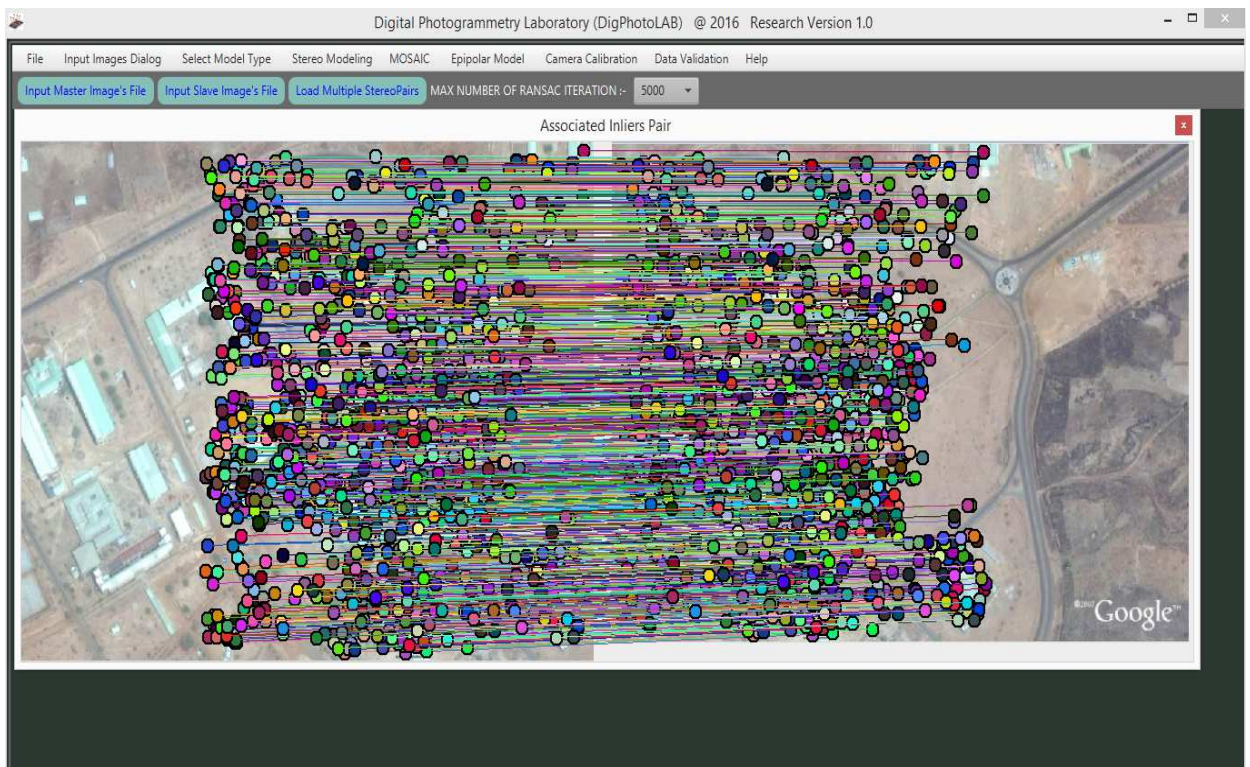


Figure 4.8: SIFT's associated image pairs containing only the inliers (outliers excluded)

Digital Photogrammetry Laboratory (DigPhotoLAB) @ 2016 Research Version 1.0

File Input Images Dialog Select Model Type Stereo Modeling MOSAIC Epipolar Model Camera Calibration Data Validation Help

List of Conjugate Points

Point ...	PhotoA_x (pixels)	PhotoA_y (pixels)	PhotoB_x (pixels)	PhotoB_y (pixels)	TransPhotoB_x (pixels)	TransPhotoB_y (pixels)
pt 0	403.51397705078125	149.75914001464844	159.41786193847656	151.90599060058594	403.35216680003344	149.8735043763582
pt 1	276.4941101074219	407.7198181152344	32.51270294189453	410.2607421875	276.5102020961244	408.2589499528352
pt 2	655.8392944335938	343.02288818359375	411.9065517578125	345.03399658203125	655.8795732109054	343.0467497675448
pt 3	510.185791015625	548.2872314453125	266.1556701660156	550.2666625976562	510.17278470662706	548.3063078738693
pt 4	599.8799438476562	358.30718994140625	355.9158630371094	360.3161926269531	599.8913705875259	358.32824378873113
pt 5	411.09210205078125	343.7821350097656	165.2572479248047	343.0359191894531	409.2323623148021	341.0329207714339
pt 6	311.2397155761719	219.0399932861328	67.1548233032266	221.04324340820312	311.1095222747903	219.01686946770226
pt 7	605.8655395507812	219.21600341796875	361.92498779296875	221.26242065429688	605.8700537159006	219.24962599892822
pt 8	267.365234375	573.8892822265625	23.74109649658203	575.3856811523438	267.77427553095043	573.4071904536142
pt 9	288.1858215332031	343.8004150390625	44.118106842041016	345.71185302734375	288.1010174652571	343.7016833894388
pt 10	363.3360900878906	348.24462890625	119.5528335571289	350.03387451171875	363.531709620621	348.0290871857309
pt 11	540.831298828125	430.329345703125	296.725554199219	432.5431213378906	540.7167861996303	430.56415532015745
pt 12	682.398193359375	255.19931030273438	438.2694396972656	257.271240234375	682.2237601685156	255.2687735773593
pt 13	462.2283935546875	454.15869140625	218.10787963867188	456.0904235839844	462.1055125627653	454.10958991069583
pt 14	420.3049621582031	377.1962585449219	176.20997619628906	379.14935302734375	420.1924042443236	377.1528012036496
pt 15	304.04736328125	259.1221618652344	60.042449051171875	261.061552734375	304.0061886008685	259.0704088786231

Figure 4.9: SIFT model's conjugate points register

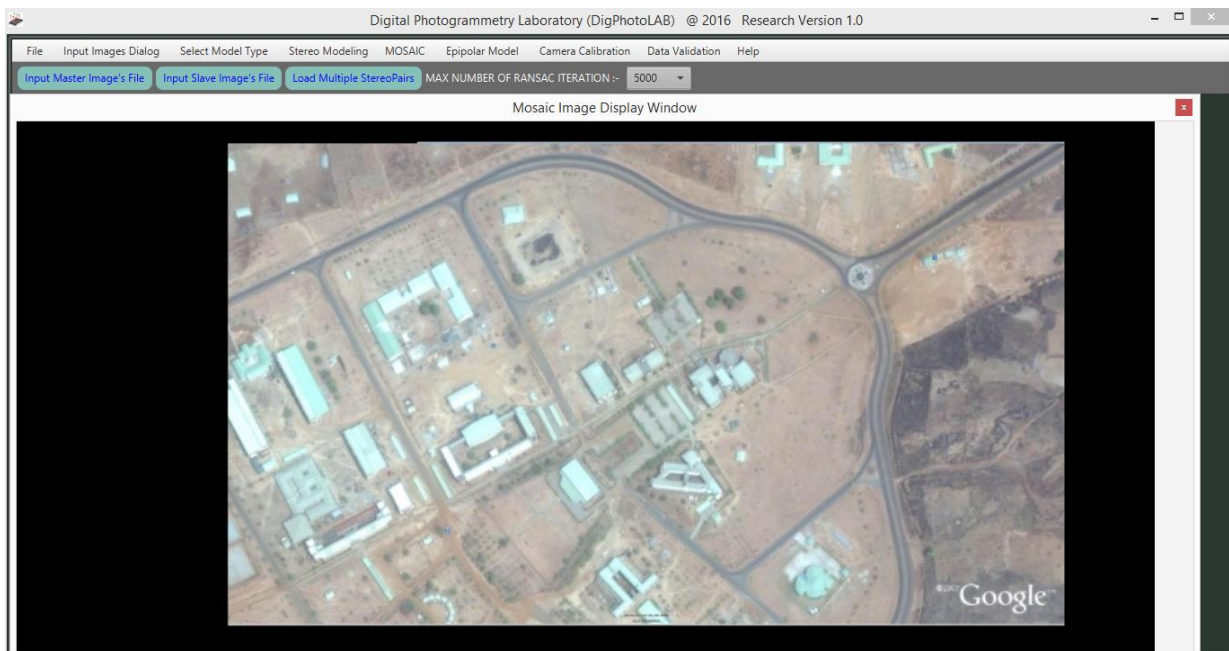


Figure 4.10a: Mosaic generated in the developed software environment using SIFT



Figure 4.10b: Mosaic generated using SIFT Model

The estimated homography of the image registration is $T_{SIFT} = \begin{bmatrix} 1.00 & 0.00 & -243.967 \\ -0.00 & 1.00 & 2.061 \\ 0.00 & 0.00 & 1.00 \end{bmatrix}$

From the estimated homography, it was observed that the diagonal of the matrix is constant (with value 1.00) and the parameter vectors of the computed homography are: $a = 1.000$, $b = 0.000$, $t_x = -243.967$ and $t_y = 2.061$. Where t_x and t_y are the translation along the x and y axis respectively. Also, $a = \cos \alpha$, $b = \sin \alpha$ and α is the rotation angle. The parameter vectors show that the SIFT is indeed invariant to rotation since the rotation angle reported is equal to zero which shows that the algorithm is stable and does not vary under rotation.

4.2.3 Automatic image registration using Speeded Up Robust Features (SURF) (first registration campaign)

Figure 4.11 shows the associated pairs which includes both the matched inliers and outliers automatically extracted using SURF feature descriptor as discussed in subsection 3.1.2 of chapter 3 while Figure 4.12 shows the matched inliers only, having successfully excluded the outliers or

mismatches using RANSAC algorithm discussed in subsection 3.2.1.3. These matched corresponding features adjudged to be inliers were the conjugate features used for the final image registration. The image coordinates (in pixels) of these corresponding or conjugate points were automatically extracted and stored in the model's coordinate register. A total of 665 conjugate points were automatically extracted and their image coordinates stored in the software's coordinate register which can also be saved or exported as a .txt file (notepad). The image coordinate of the automatically extracted conjugate points are presented in Appendix C. Figure 4.13 shows the scheme's register of conjugate points while the final mosaic generated from the image registration process is presented in Figures 4.14a and 4.14b. Figure 4.14a shows the mosaic within the developed software environment while Figure 4.14b shows the mosaic which has been exported as an image.

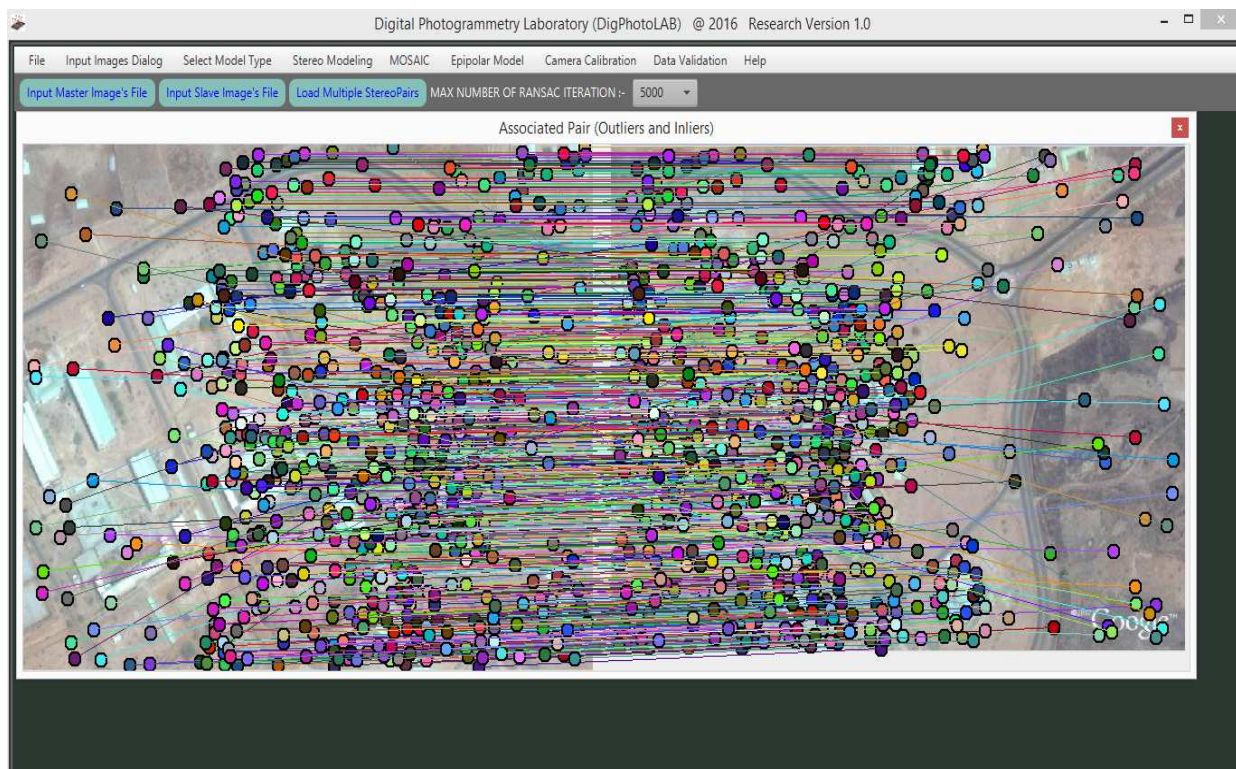


Figure 4.11: Associated image pairs containing the inliers and outliers (using SURF Model)

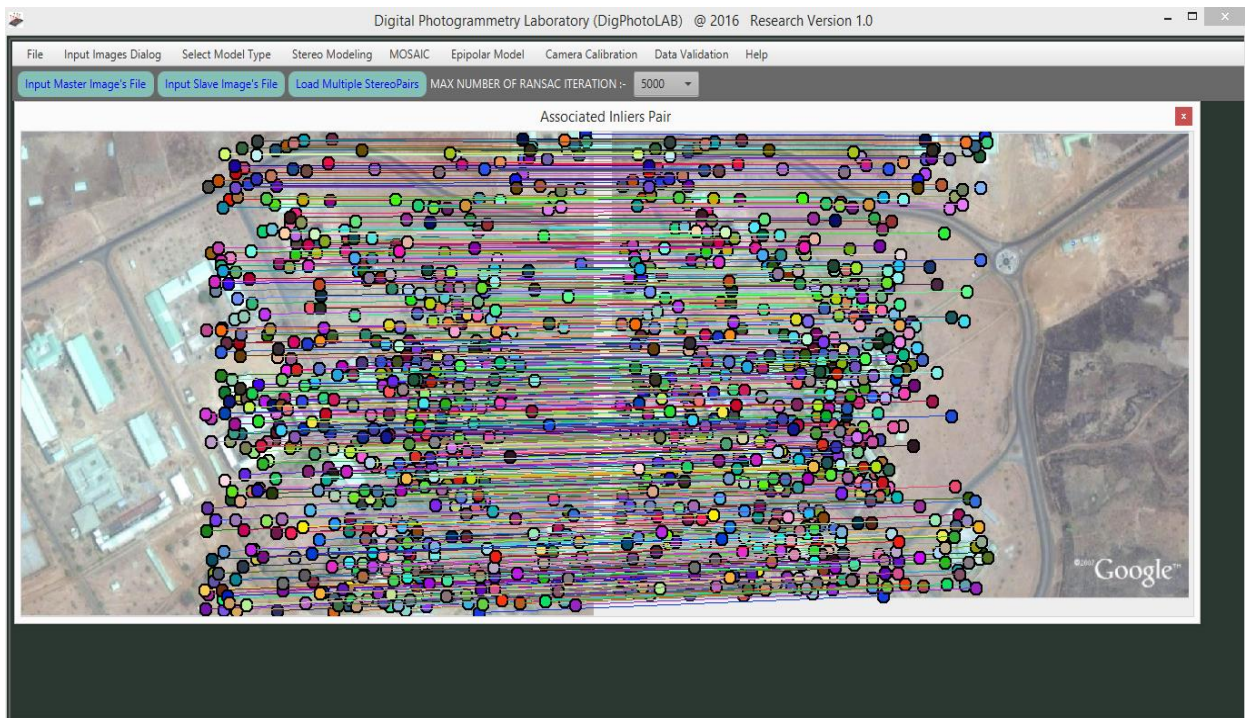


Figure 4.12: SURF's associated image pairs containing only the inliers (outliers excluded)

Point ...	PhotoA_x (pixels)	PhotoA_y (pixels)	PhotoB_x (pixels)	PhotoB_y (pixels)	TransPhotoB_x (pixels)	TransPhotoB_y (pixels)
pt 0	624.4442138671875	450.9883728027344	379.9394226074219	453.2109680175781	623.963345743418	451.22776188807086
pt 1	601.34765625	450.2864074707031	357.43798828125	452.3023986816406	601.4605411917964	450.3192481816289
pt 2	605.82080078125	227.30978393554688	361.85076904296875	229.34600830078125	605.9109688015106	227.35217802813594
pt 3	403.9377746582031	150.06365966796875	159.8754119873047	152.102783203125	403.89875311297595	150.09766794300347
pt 4	544.0921630859375	519.7969360351562	300.1141052246094	521.6776733398438	544.1248156017796	519.6828802487958
pt 5	599.4189453125	461.9275817871094	356.2367248535156	464.5085144042969	600.2572033050374	462.52392326505765
pt 6	778.09814453125	556.5419311523438	534.15673828125	558.5542602539062	778.1647664300127	556.5547248346205
pt 7	542.676513671875	297.3714904785156	298.6787109375	299.3683166503906	542.7168174557794	297.38668238445365
pt 8	354.50262451171875	359.9139709472656	110.4806137084961	361.7780456542969	354.49547076673156	359.8019117202259
pt 9	684.910339354688	285.34063720703125	440.8892822265625	287.232421875	684.955094161883	285.2462656558158
pt 10	280.8996887207031	610.200927734375	36.299285888671875	612.424072265625	280.3261565525413	610.3972135484998
pt 11	591.5140991210938	450.0112609863281	347.36383056640625	452.2478942871094	591.3857542741962	450.26473144446634
pt 12	392.4205017089844	379.1725769042969	148.38986206054688	381.1986999511719	392.4066565088745	379.22159932425507
pt 13	466.8443298339844	559.8118286132812	222.87890625	561.5166015625	466.88779102517987	559.5107320619096
pt 14	676.1605224609375	251.48284912109375	432.16302490234375	253.3787841796875	676.2343977540904	251.38749948061638
pt 15	697.8749389648438	34.844280168701172	453.91461181640625	36.74591827382578	698.0412907275826	34.68115403160794

Figure 4.13: SURF Model's conjugate points register



Figure 4.14a: Mosaic generated in the developed software environment using SURF model



Figure 4.14b: Mosaic generated using SURF Model

The estimated homography of the image registration is $T_{SURF} = \begin{bmatrix} 1.00 & 0.00 & -244.028 \\ -0.00 & 1.00 & 2.036 \\ 0.00 & 0.00 & 1.00 \end{bmatrix}$

From the estimated homography, it was observed that the diagonals of the matrix is constant (with values 1.00) and the parameter vectors of the computed homography are: $a = 1.000$, $b = 0.000$, $t_x = -244.028$ and $t_y = 2.036$. Where t_x and t_y are the translation along the x and y axis respectively. Also, $a = \cos \alpha$, $b = \sin \alpha$ and α is the rotation angle. The parameter vectors show that the SIFT algorithm is indeed invariant to rotation since the rotation angle reported is equal to zero which shows that the algorithm is stable and does not vary under rotation.

From the results of the three algorithms presented this subsection, it was discovered that the three feature descriptors proved to be indeed invariant to rotation as observed from the parameter vectors recorded in their estimated homography which shows a rotation angle that is equal to zero. This attests to the stability of the three algorithms. Moreover, it was discovered that that the SIFT algorithm proved to be more robust than the MHCD and the SURF algorithms in the automatic detection and extraction of point correspondences. It automatically extracted 1129 point correspondences which is approximately 2.5 times more than the point correspondences automatically extracted by the MHCD algorithm (456) and 1.70 times more than the point correspondences automatically extracted by the SURF algorithm (665). This observation also agreed with the findings of Vivek and Kanchan (2014) and Panchal *et al.*, (2013) which submitted that the SIFT model is very powerful in the automatic extraction of corresponding features.

4.3 Automatic Image Registration based on the Integrated Epipolar Correlation Algorithms

Each of the selected feature detection and extraction algorithms discussed in subsection 2.1.1 were integrated with epipolar correlation for the development of the integrated epipolar correlation image registration scheme. The integration takes input parameters from the selected feature descriptors before imposing epipolar constraints on them for the removal of outliers and the final registration of the overlapping image pairs by the implementation of the processes highlighted in

subsection 3.1.2 of chapter 3. This process was performed for the MHCD algorithm (integrated MHCD-epipolar correlation), the SURF (integrated SURF-epipolar correlation) and the SIFT (integrated SIFT-Epipolar correlation) algorithms.

4.3.1 Integrated MHCD-epipolar correlation image registration scheme (first registration campaign)

Figure 4.15 presents the matched inliers using the integrated MHCD-epipolar correlation which shows the associated pairs and the epipolar lines parallel to the x axis. This means that MHCD was first used to extract the corresponding features on the overlapping image pairs, before imposing epipolar constraints on extracted features for the exclusion of outliers. The mosaic generated through this process is shown in Figure 4.16. The computed fundamental matrix which encodes or encapsulates the intrinsic and extrinsic parameters that exists between the overlapping image pairs as at the time of image capture or scene exposure was computed during the process of stereo rectification using the eight-point algorithm method described in subsection 3.2.2 and it is given as:

$$F_{8pt(MHCD-Epipolar)} = \begin{bmatrix} 0.000 & 0.000 & 0.003 \\ -0.000 & -0.000 & -0.003 \\ -0.003 & 0.003 & 0.701 \end{bmatrix}$$

The determinant of the estimated fundamental matrix for the integrated MHCD-Epipolar correlation model is equal to zero ($\det(F) = 0$) which satisfies one of the basic important properties of an ideal fundamental matrix. This shows that the estimated fundamental matrix is accurate and by extension, the image registration process.

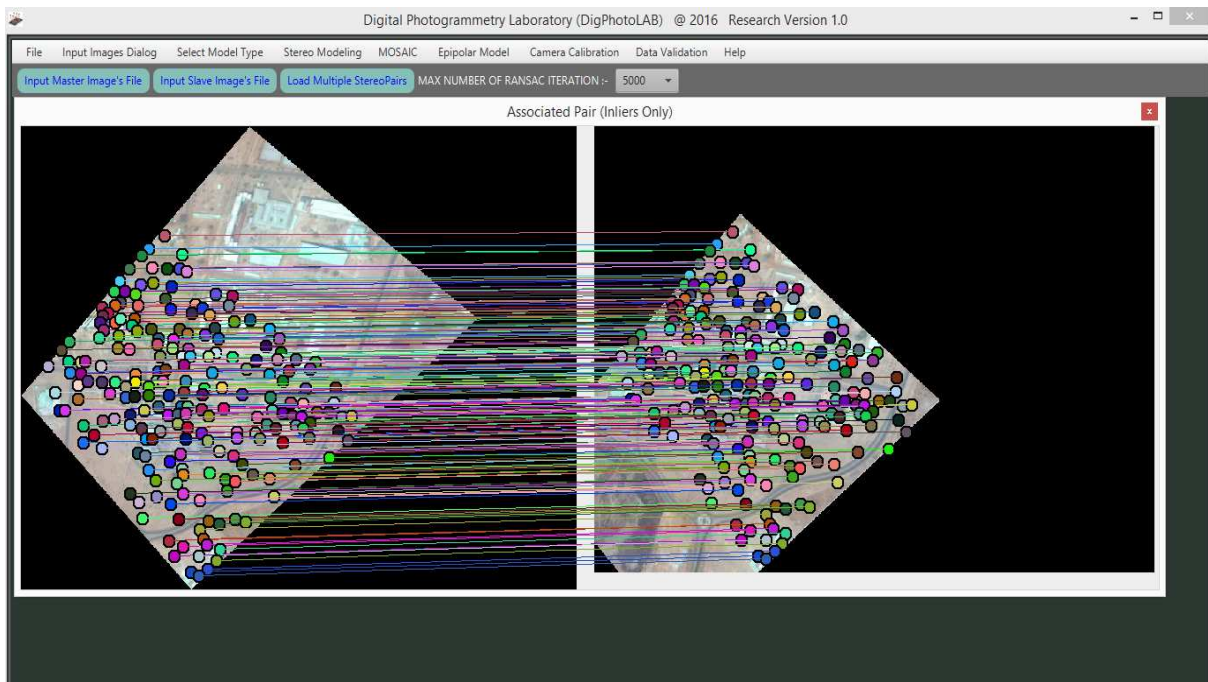


Figure 4.15: Integrated MHCD-Epipolar correlated inliers

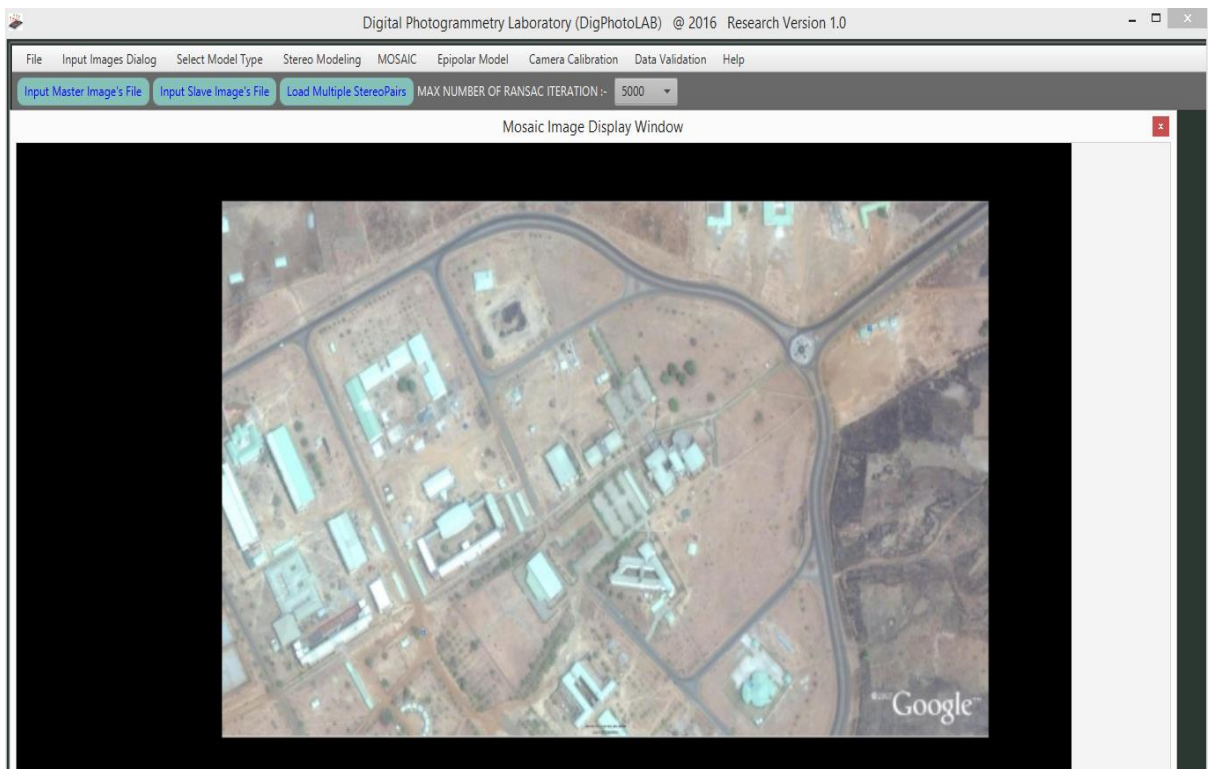


Figure 4.16: Mosaic generated using integrated MHCD-epipolar correlation registration model

The estimated homography of the integrated MHCD – epipolar correlation image registration algorithm is:

$$H_{MHCD-Epipolar} = \begin{bmatrix} 1.000 & 0.000 & -243.836 \\ -0.000 & 1.000 & 1.887 \\ 0.000 & 0.000 & 0.999 \end{bmatrix} \text{ which has the same parameter vectors as the}$$

estimated homography obtained when only MHCD was used as shown in subsection 4.2.1. This implies that the invariant to scale and rotation quality of MHCD has not been compromised even when it has been integrated with epipolar correlation.

4.3.2 Integrated SURF-epipolar correlation image registration scheme (first campaign)

The matched inliers obtained using the integrated SURF-epipolar correlation image registration model is presented in Figure 4.17 while the mosaic generated from the overlapping image pairs using the integrated algorithm is presented in Figure 4.18. The computed fundamental matrix using Eight (8) point algorithm discussed in subsection 3.2.3 is given as:

$$F_{8pt(SURF-Epipolar)} = \begin{bmatrix} 0.000 & 0.000 & 0.001 \\ 0.000 & 0.000 & -0.001 \\ -0.001 & 0.002 & 0.331 \end{bmatrix}$$

The determinant of the estimated fundamental matrix for the integrated SURF-epipolar correlation algorithm is also equal to zero (i.e. $\det(F) = 0$) which satisfies one of the important properties of an ideal fundamental matrix. This shows that the estimated fundamental matrix is accurate and by extension, the image registration process.

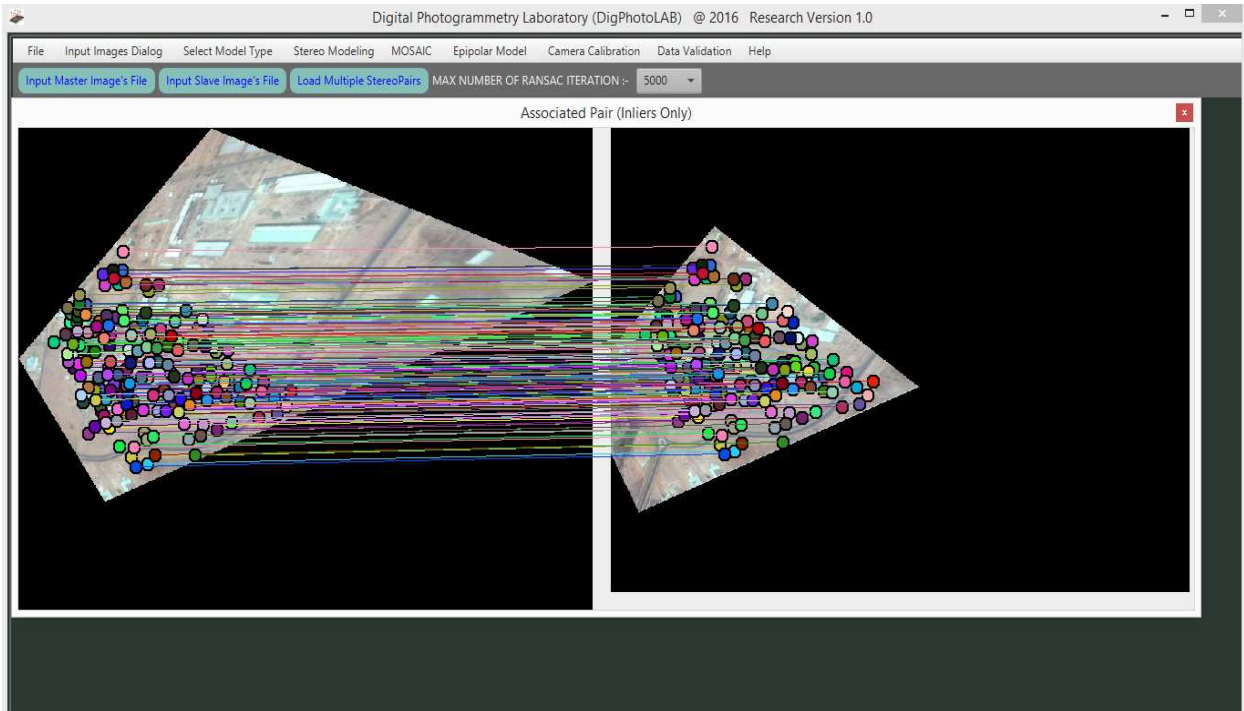


Figure 4.17: SURF-Epipolar correlated inliers

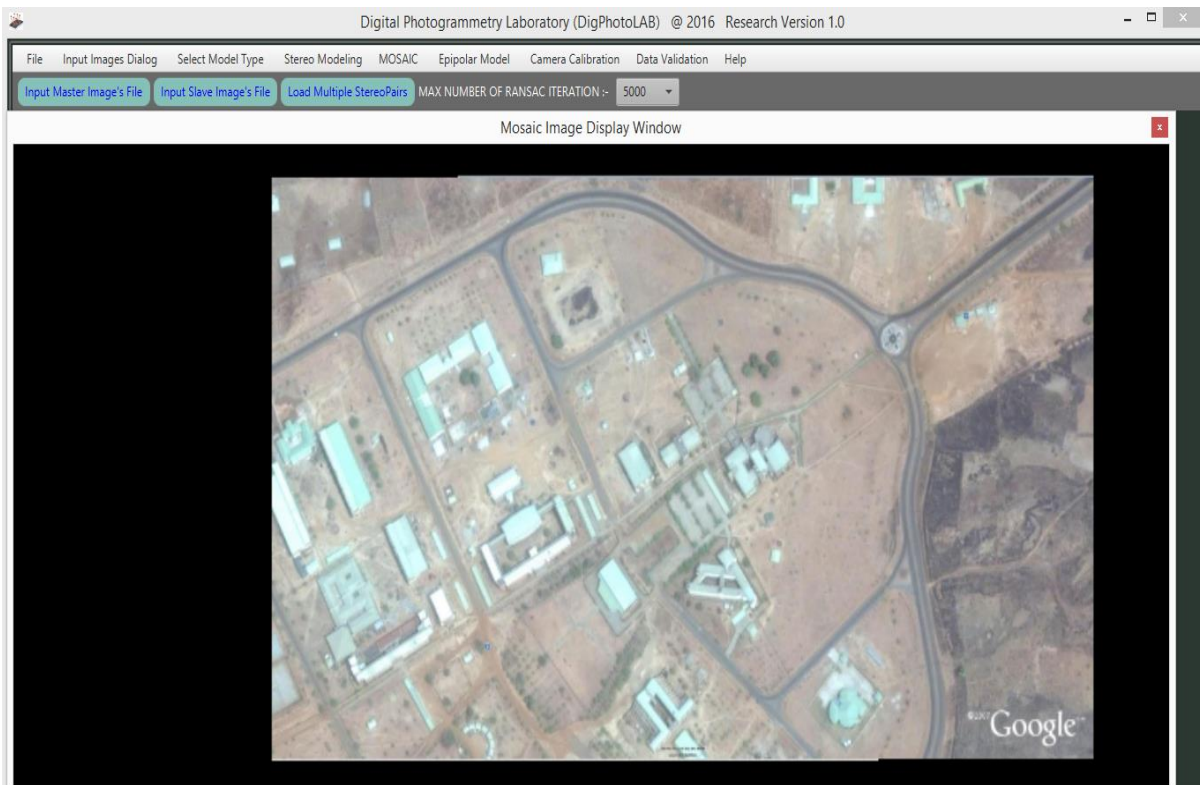


Figure 4.18: Mosaic generated using integrated SURF-epipolar correlation registration model

The estimated homography of the integrated SURF-epipolar correlation algorithm is:

$$H_{SURF-Epipolar} = \begin{bmatrix} 1.000 & -0.000 & -244.028 \\ 0.000 & 1.000 & 2.038 \\ 0.000 & -0.000 & 1.000 \end{bmatrix} \text{ which is also the same as the estimated homography}$$

obtained in the registration process where only SURF was used. This observation implies that the integration of SURF with epipolar correlation does not compromise SURF feature descriptor's primary qualities of been invariant under scale and rotation.

4.3.3 Integrated SIFT-epipolar correlation image registration scheme (first registration campaign)

The matched inliers obtained using the integrated SIFT-epipolar correlation image registration algorithm is presented in Figure 4.19 while the mosaic generated from the overlapping image pairs using the integrated algorithm is presented in Figure 4.20. The computed fundamental matrix using the Eight (8) point algorithm discussed in subsection 3.2.3 is given as:

$$F_{8pt(SIFT-Epipolar)} = \begin{bmatrix} 0.000 & 0.000 & 0.004 \\ 0.000 & 0.000 & -0.001 \\ -0.004 & 0.002 & 0.980 \end{bmatrix}$$

It can be observed from the estimated fundamental matrix for the integrated SIFT-epipolar correlation algorithm that the determinant of the matrix is also equal to zero (i. e. $\det(F) = 0$) which satisfies one of the basic and important properties of an ideal fundamental matrix. This shows that the estimated fundamental matrix is also accurate and by extension, the image registration process.

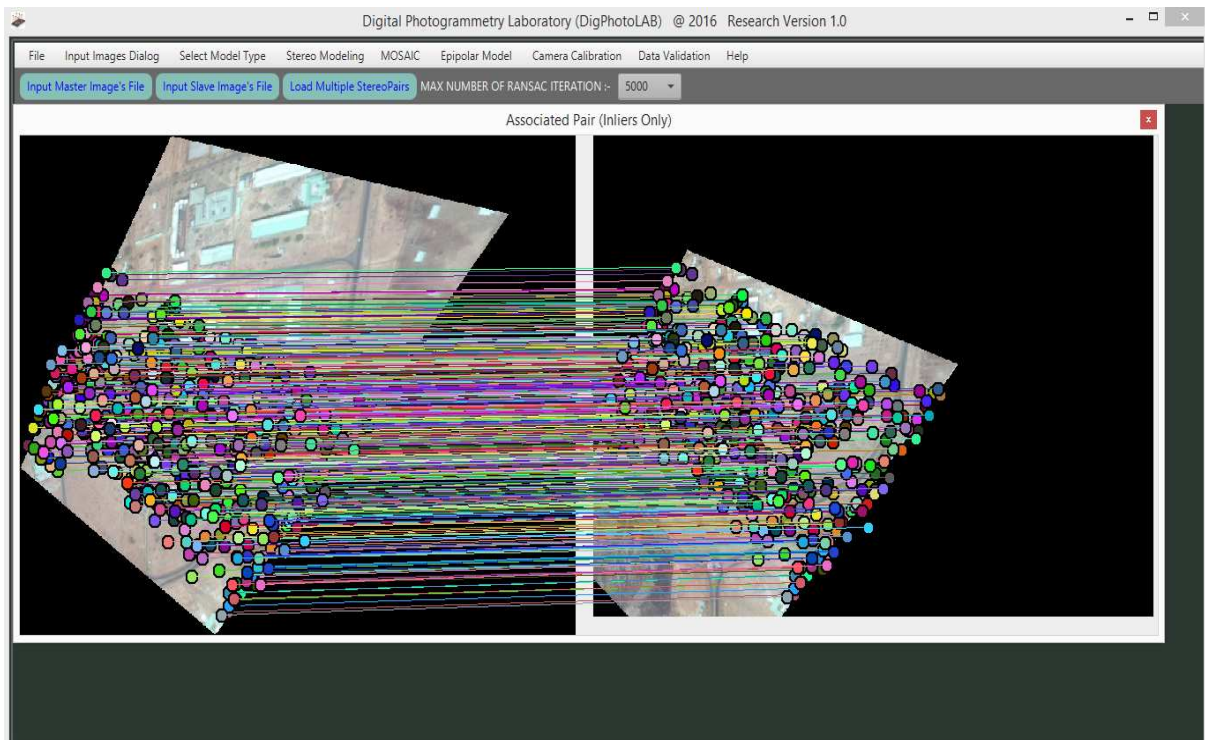


Figure 4.19: SIFT-epipolar correlated inliers



Figure 4.20: Mosaic generated using integrated SIFT-epipolar correlation registration model

The estimated homography using the integrated SIFT–epipolar correlation algorithm for the development of the automatic overlapping image registration scheme is:

$$H_{SIFT-Epipolar} = \begin{bmatrix} 1.000 & -0.000 & -243.967 \\ -0.000 & 1.000 & 2.061 \\ 0.000 & 0.000 & 1.000 \end{bmatrix}$$

Just like MHCD and SURF, the homography obtained from the registration process where the integrated SIFT–epipolar algorithm is the same as the homography obtained when only SIFT feature descriptor was used. This observation shows that SIFT’s primary qualities, part of which is been invariant to scale and rotation, is not compromised due to the integration.

4.4 Performance Evaluation of the Developed Schemes using the Integrated Algorithms

The performance evaluation of the developed registration scheme is sub-divided into two different approaches for the first image registration campaign. The first approach adopted the use of the automatically extracted point correspondences using the three selected feature descriptors implemented for the image registration scheme to determine a measure of accuracy by computing the resultant signed distances of each of the point correspondences. The second approach on the other hand adopted the use of the RMSE (equation 3.21) and the signed distances (equation 3.20) obtained from the conjugate points that were measured directly on the rectified image pairs using the developed stereo- comparator. Ideally, the signed distance of each of the established point correspondences should be equal to zero which connotes perfect correlation. Since this is near-impossible in practical applications, it is expected that the value of the obtained signed distance should be close to zero as much as possible. This implies that the closer the value of the signed distance or residual is to zero, the more accurate the image registration is and the farther away the signed distance is to zero, the less accurate the image registration is.

Also, the estimated run time for each of the developed algorithms was computed to see how fast their processing time is in the automatic registration of overlapping images. This also helps in ascertaining the performance of the algorithms with respect to speed.

4.4.1 Accuracy evaluation of the schemes using automatically extracted point correspondences (first registration campaign)

The signed distances of each of the point correspondences established automatically using MHCD, SIFT and SURF model were computed and their cumulative was estimated. For MHCD, a total of 456 point correspondences were automatically established and the signed distances or residuals of each of these key-points were computed. These residuals were summed so as to be able to get the total residual recorded in the process of registering the stereo pair using MHCD. The total signed distances obtained is 0.0457 pixels. A total of 1129 corresponding points were established using SIFT algorithm for the image registration and a computed signed of 0.0328 pixels was obtained while a computed signed distance of -0.0009 pixels was obtained from the 656 point correspondences which were automatically extracted using the SURF algorithm in the image registration process. A cumulative signed distance of 0.0000 pixels was obtained from the point correspondences extracted using each of the integrated MHCD-epipolar, SURF-epipolar and SIFT-epipolar correlation based algorithms. This means that the images were perfectly correlated and there is no mismatch at all when the integrated algorithms were used. The obtained result also shows that even though SIFT automatically extracted the highest number of point correspondences, the accuracy of SURF is the best of the three existing models implemented with an accuracy measure of -0.0009 pixels while SIFT also proved to be more accurate than MHCD which also extracted the lowest number of point correspondences. This is in tandem with the result obtained by Bolarinwa (2017). Though SURF proved to be more accurate than the MHCD and SIFT algorithm, the integrated epipolar correlation algorithms proved to be more accurate than

SURF algorithm as it gave the best correlation when compared to all the three feature descriptors implemented in this study for the first image registration campaign.

To further test the robustness of the developed model, attempt was made to measure point data directly on the selected three feature detection and extraction algorithm (MHCD, SURF, and SIFT) based image registration scheme and the three integrated epipolar correlation-based image registration scheme (MHCD-epipolar, SURF-epipolar, and SIFT-epipolar). Details of this analysis are presented in subsection 4.4.2.

4.4.2 Accuracy evaluation of the schemes using measured conjugate point data

The coordinates of the 15 GCPs presented in Table 3.1 were used for direct conjugate point measurements on the rectified images using the developed stereo comparator. For the registration model using the three-different feature detection and extraction algorithms (MHCD, SURF, and SIFT), and these three algorithms integrated with epipolar correlation independently (MHCD-epipolar, SURF-epipolar, and SIFT-epipolar), the coordinates of the GCPs were fed into the image registration scheme directly on the rectified image pair through the stereo comparator by identifying the GCPs on the image pairs. To do this, the stereo comparator module of the software was activated as shown in Figure 4.21. As soon as this is done, the rectified stereo pair pops up as shown in Figure 4.22. On the rectified stereo pair (base image), conjugate points were measured directly by double clicking on the point and inputting the Northing, Easting and Height coordinates of the GCP into the columns provided (Figure 4.23). Once the data is successfully entered, the stereo comparator automatically identifies and marks the conjugate points of the selected point on the other image pair (search image) as shown in Figure 4.24.

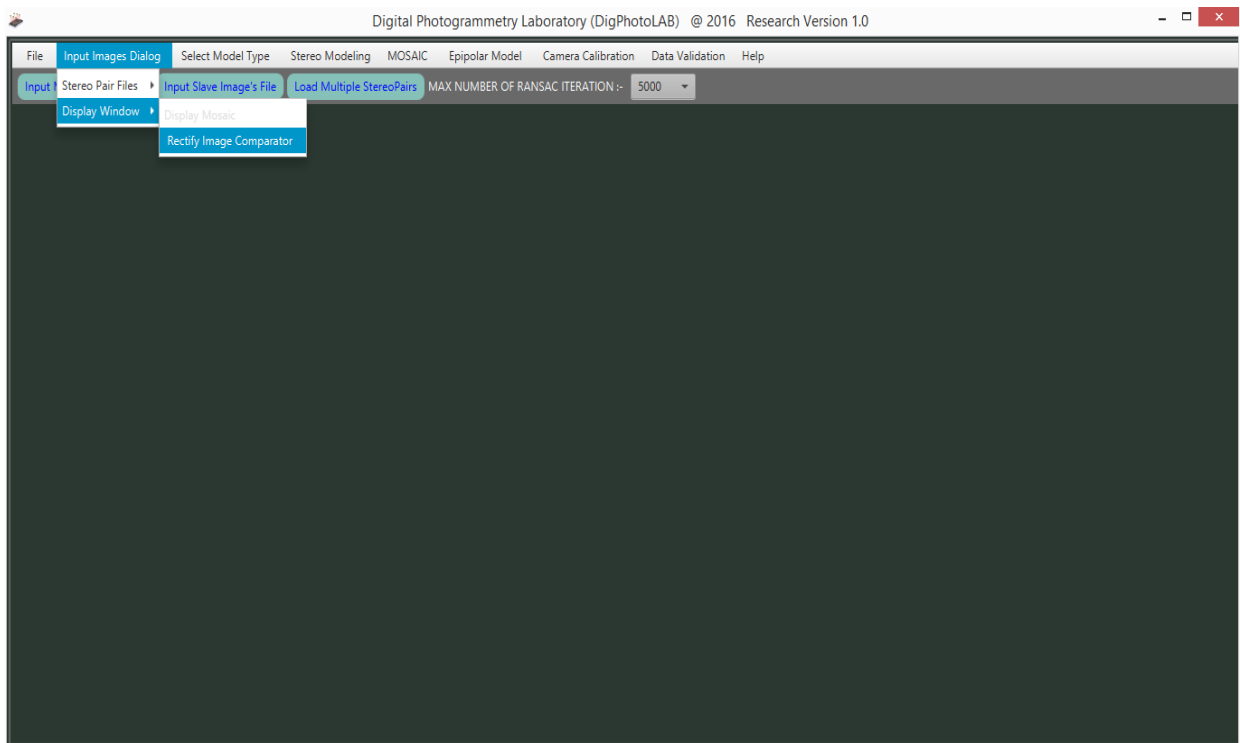


Figure 4.21: Engaging the stereo comparator

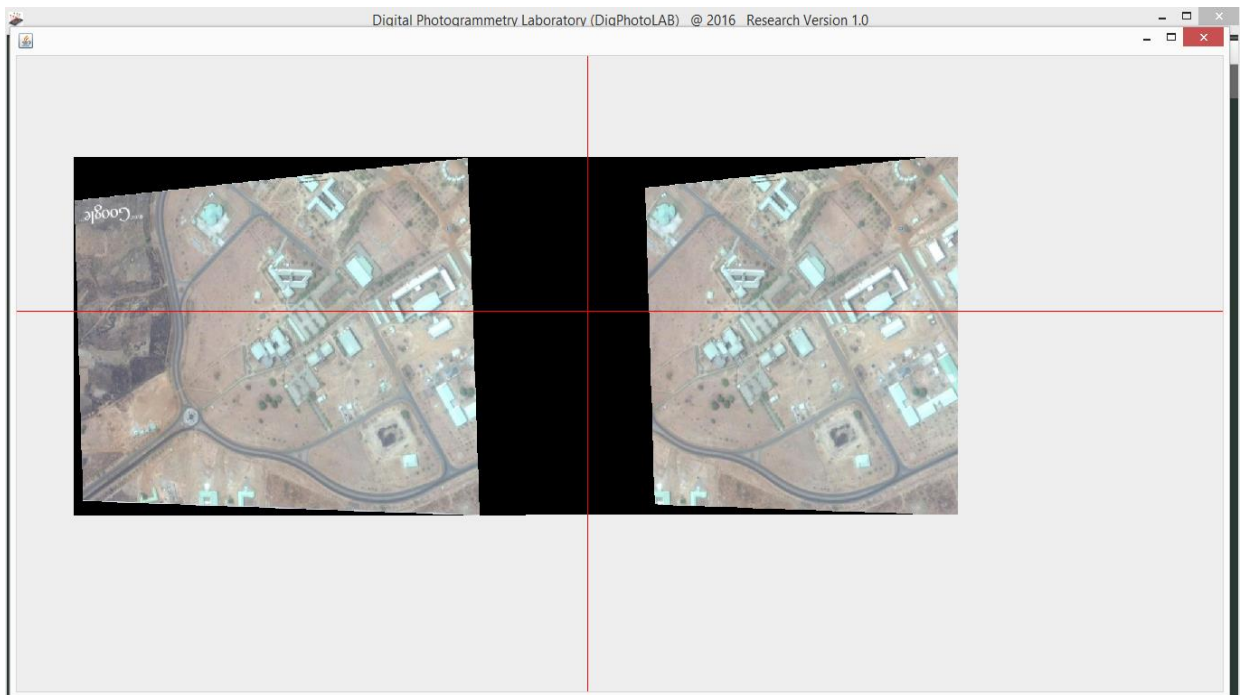


Figure 4.22: The rectified stereo pair

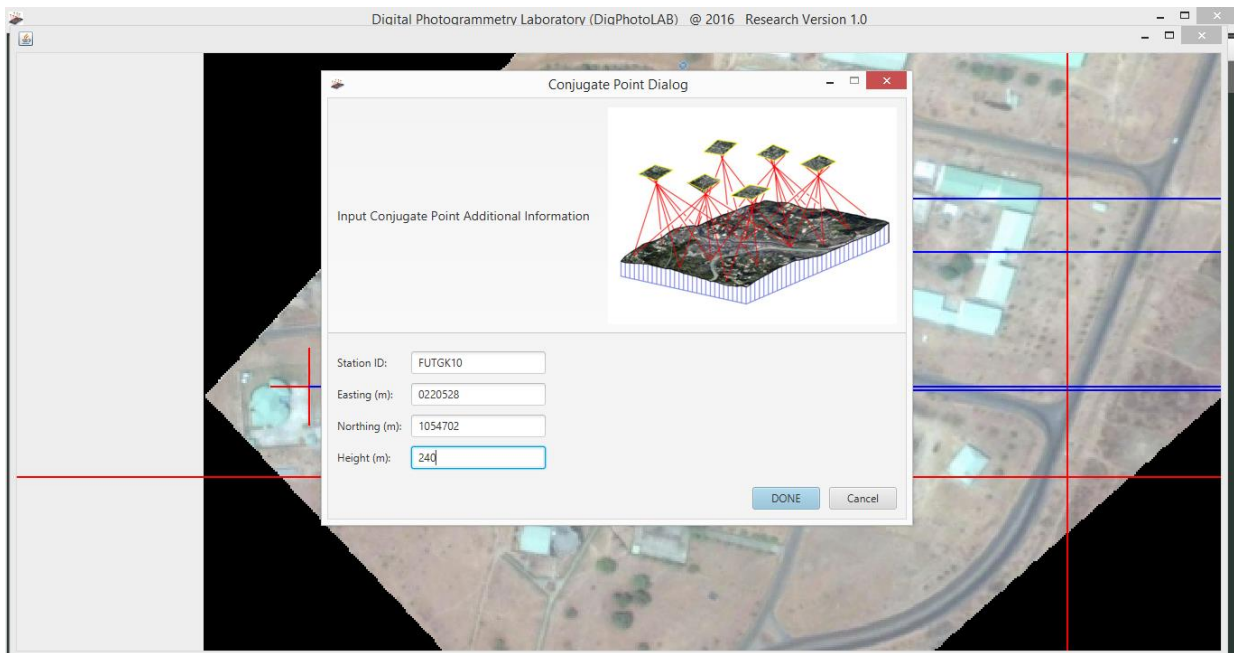


Figure 4.23: Coordinate input interface for keypoint measurement

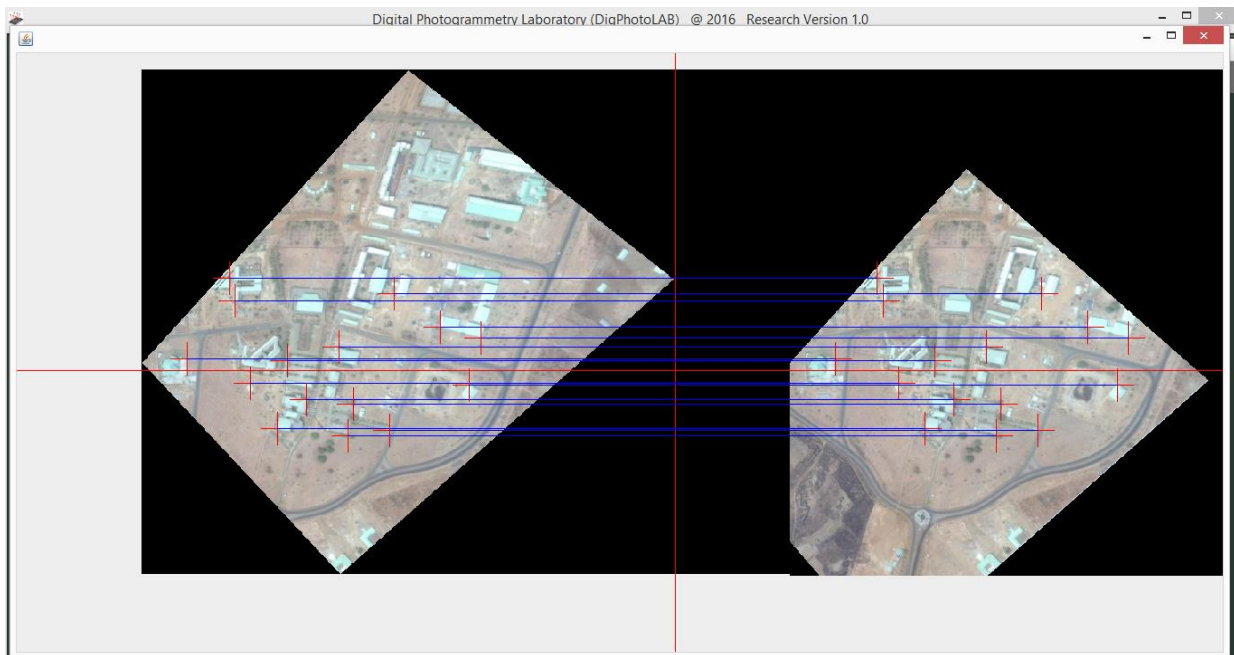


Figure 4.24: Measured conjugate points

Once all the points have been successfully measured, the software automatically generates a report which contains the image coordinates of each of the GCPs whose ground coordinates were entered into the comparator, computes the signed distances, and also computes the root mean square error.

This process was repeated for each of the three (3) feature detection and extraction algorithms used for the development of the image registration scheme and for the developed integrated epipolar correlation-based image registration schemes.

Table 4.1 presents the result obtained when the measurement was carried out on the rectified image using MHCD. A signed distance of 0.0000 pixels was computed and a root mean square of $6.6424709043813145 \times 10^{-14}$ was obtained which shows the value or degree of mismatch (Forkuo, 2008) when MHCD algorithm was adopted.

Table 4.1: Image locations of measured conjugate points and their signed distances (MHCD)

ID	Image location of conjugate points in Image A		Image location of conjugate points in Image B		Residuals
	x (Pixels)	y (Pixels)	x (Pixels)	y (Pixels)	Signed Distance (Pixels)
FUTGK01	326.135	325.812	82.166	327.861	0.000
FUTGK02	314.688	216.504	70.683	218.471	0.000
FUTGK03	280.135	149.717	36.075	151.602	0.000
FUTGK04	474.124	327.863	230.177	329.862	0.000
FUTGK05	526.639	599.599	282.622	601.422	0.000
FUTGK06	552.646	555.428	308.610	557.276	0.000
FUTGK07	564.883	384.318	320.880	386.275	0.000
FUTGK08	714.832	545.887	470.561	547.605	0.000
FUTGK09	652.870	406.136	408.771	408.038	0.000
FUTGK10	679.844	297.282	435.768	299.219	0.000
FUTGK11	594.855	299.049	350.857	301.009	0.000
FUTGK12	585.880	187.594	341.924	189.526	0.000
FUTGK13	535.137	225.283	291.189	227.237	0.000
FUTGK14	521.709	139.078	277.780	140.973	0.000
FUTGK15	356.931	100.207	112.932	102.032	0.000

The result obtained when SIFT algorithm was used for the image registration is presented in Table 4.2. Cumulative signed distance of 0.0000 pixels was obtained and a root mean square error of $1.0407069005343235 \times 10^{-13}$ was computed which shows the value or degree of mismatch when SIFT algorithm was adopted.

Table 4.2: Image locations of measured conjugate points and their signed distances (SIFT)

ID	Image location of conjugate points in Image A		Image location of conjugate points in Image B		Residuals
	x (Pixels)	y (Pixels)	x (Pixels)	y (Pixels)	Signed Distances (Pixels)
FUTGK01	526.183	597.188	282.138	599.086	0.000
FUTGK02	552.381	555.668	308.344	557.591	0.000
FUTGK03	563.213	380.676	319.225	382.679	0.000
FUTGK04	714.255	547.080	470.202	549.003	0.000
FUTGK05	653.132	404.135	409.137	406.126	0.000
FUTGK06	680.407	297.590	436.452	299.609	0.000
FUTGK07	592.279	296.984	348.318	299.007	0.000
FUTGK08	585.753	187.575	341.825	189.611	0.000
FUTGK09	535.371	224.975	291.425	227.011	0.000
FUTGK10	521.672	139.628	277.746	141.666	0.000
FUTGK11	355.137	101.630	111.185	103.674	0.000
FUTGK12	329.406	323.265	85.424	325.294	0.000
FUTGK13	315.479	218.308	71.507	220.355	0.000
FUTGK14	279.242	149.997	35.271	152.048	0.000
FUTGK15	477.815	333.152	233.837	335.172	0.000

The result obtained when SURF algorithm was used for the registration scheme is presented in Table 4.3. A cumulative signed distance of 0.0000 pixels was computed and a root mean square error of $1.257834901735638 \times 10^{-13}$ was obtained which shows the value or degree of mismatch using SURF algorithm.

Table 4.3: Image locations of measured conjugate points and their signed distances (SURF)

ID	Image location of conjugate points in Image A		Image location of conjugate points in Image B		Residuals
	x (Pixels)	y (Pixels)	x (Pixels)	y (Pixels)	Signed Distances (Pixels)
FUTGK01	527.229	598.630	283.186	600.526	0.000
FUTGK02	552.077	556.071	308.024	557.976	0.000
FUTGK03	567.007	377.581	322.973	379.567	0.000
FUTGK04	711.639	547.453	467.428	549.256	0.000
FUTGK05	656.823	403.772	412.712	405.712	0.000
FUTGK06	678.203	296.363	434.098	298.352	0.000
FUTGK07	592.408	299.387	348.372	301.392	0.000
FUTGK08	583.953	188.307	339.942	190.332	0.000
FUTGK09	535.541	224.778	291.545	226.801	0.000
FUTGK10	525.013	138.359	281.031	140.379	0.000
FUTGK11	354.622	103.174	110.624	105.155	0.000
FUTGK12	327.824	324.663	83.820	326.722	0.000
FUTGK13	316.812	216.881	72.799	218.910	0.000
FUTGK14	279.457	151.241	35.417	153.237	0.000
FUTGK15	478.106	330.847	234.114	332.870	0.000

For the integrated epipolar correlation algorithms, the results obtained from the integrated MHCD-epipolar, SURF-epipolar and SIFT-epipolar based image registration scheme's performance evaluation are presented in Tables 4.4, 4.5 and 4.6 respectively. The result shows the photo location of measured conjugate points on the base and search image pairs and they also show the signed distances between them. A cumulative signed distance of 0.0000 pixels was computed and a RMSE value of $6.645046828487534 \times 10^{-14}$ was obtained when the integrated MHCD-epipolar algorithm was used while a RMSE of $1.2591535854453049 \times 10^{-13}$ and a cumulative signed distance of 0.0000 was obtained when the integrated SURF-epipolar algorithm was used. The cumulative signed distance of 0.0000 was also obtained when the integrated SIFT-epipolar

algorithm was used but with a RMSE of $1.0413002255322562 \times 10^{-13}$ which shows the value or degree of mismatch from the integrated epipolar correlation-based image registration algorithms. Though all the six (6) methods gave the same signed distance value of 0.0000 which attests to their robustness, they gave different root mean square errors which shows the degree of accuracy obtainable from them.

Table 4.4: Image locations of measured conjugate points and their signed distances using MHCD-epipolar correlation algorithm

ID	Image location of conjugate points in Image A		Image location of conjugate points in Image B		Residuals
	x (Pixels)	y (Pixels)	x (Pixels)	y (Pixels)	Signed Distances (Pixels)
FUTGK01	524.215	599.485	280.200	601.311	0.000
FUTGK02	555.054	558.098	311.015	559.941	0.000
FUTGK03	566.112	378.252	322.110	380.211	0.000
FUTGK04	712.269	545.794	468.002	547.514	0.000
FUTGK05	652.851	403.648	408.753	405.552	0.000
FUTGK06	679.844	297.282	435.768	299.219	0.000
FUTGK07	591.322	297.887	347.327	299.847	0.000
FUTGK08	584.722	188.763	340.767	190.696	0.000
FUTGK09	534.012	224.162	290.065	226.115	0.000
FUTGK10	523.943	138.999	280.014	140.894	0.000
FUTGK11	353.755	101.400	109.754	103.225	0.000
FUTGK12	330.550	323.520	86.583	325.567	0.000
FUTGK13	315.795	215.386	71.790	217.352	0.000
FUTGK14	278.091	149.789	34.028	151.674	0.000
FUTGK15	477.453	331.381	233.504	333.380	0.000

Table 4.5: Image locations of measured conjugate points and their signed distances using SURF-epipolar correlation algorithm

ID	Image location of conjugate points in Image A		Image location of conjugate points in Image B		Residuals
	x (Pixels)	y	x (Pixels)	y	Signed Distances (Pixels)
		(Pixels)		(Pixels)	
FUTGK01	527.229	598.630	283.186	600.526	0.000
FUTGK02	552.077	556.071	308.024	557.976	0.000
FUTGK03	568.562	375.538	324.527	377.524	0.000
FUTGK04	711.639	547.453	467.428	549.256	0.000
FUTGK05	661.328	407.623	417.213	409.559	0.000
FUTGK06	680.411	297.951	436.303	299.940	0.000
FUTGK07	592.042	295.902	348.007	297.908	0.000
FUTGK08	585.694	189.476	341.682	191.501	0.000
FUTGK09	532.548	225.381	288.553	227.404	0.000
FUTGK10	522.222	139.090	278.242	141.110	0.000
FUTGK11	355.706	101.749	111.709	103.729	0.000
FUTGK12	328.886	325.940	84.882	327.999	0.000
FUTGK13	316.626	219.369	72.613	221.399	0.000
FUTGK14	279.457	151.241	35.417	153.237	0.000
FUTGK15	475.177	331.241	231.185	333.264	0.000

Table 4.6: Image locations of measured conjugate points and their signed distances using SIFT-epipolar correlation algorithm

ID	Image location of conjugate points in Image A		Image location of conjugate points in Image B		Residuals
	x (Pixels)	y (Pixels)	x (Pixels)	y (Pixels)	Signed Distances (Pixels)
FUTGK01	528.701	598.094	284.655	599.991	0.000
FUTGK02	554.901	556.519	310.863	558.441	0.000
FUTGK03	565.913	374.758	321.927	376.763	0.000
FUTGK04	713.114	545.146	469.062	547.070	0.000
FUTGK05	654.123	405.773	410.127	407.764	0.000
FUTGK06	678.935	298.528	434.980	300.547	0.000
FUTGK07	592.279	296.984	348.318	299.007	0.000
FUTGK08	585.753	187.575	341.825	189.611	0.000
FUTGK09	535.960	222.835	292.014	224.871	0.000
FUTGK10	521.672	139.628	277.746	141.666	0.000
FUTGK11	355.662	102.651	111.710	104.695	0.000
FUTGK12	327.306	326.311	83.325	328.340	0.000
FUTGK13	315.998	219.484	72.027	221.531	0.000
FUTGK14	278.779	148.938	34.809	150.990	0.000
FUTGK15	477.077	331.722	233.099	333.743	0.000

From the computed RMSE for each of the six (6) algorithms implemented in the developed automatic image registration scheme, the integrated epipolar correlation based image registration algorithms proved to be more accurate when compared to the conventional vector based SIFT, SURF and MHCD based image registration algorithms. However, the comparative analysis of the RMSE obtained from the implementation of SIFT, SURF and MHCD using measured conjugate point data shows that SIFT outperforms SURF and MHCD in terms of matching accuracy. This is followed by SURF while the most inaccurate result was obtained from MHCD algorithm. Also, the integrated MHCD-epipolar algorithm gave a more accurate result when compared to the integrated SURF-epipolar and SIFT-epipolar algorithms.

4.4.3 Performance evaluation of the schemes using processing run time

The processing run time (measured in milliseconds) used for the accurate registration of the stereo pairs by each of the algorithms was estimated and the result is presented in Table 4.7. From the estimated run time which defines the processing speed of the algorithms, it was discovered that SIFT algorithm expended the highest number of milliseconds for the automatic image registration (slowest) with 3350 milliseconds, while the fastest of the six algorithms is the integrated MHCD-epipolar correlation-based image registration algorithm which expended an estimated processing run time of 463 milliseconds. It was also observed that the integrated SURF-epipolar algorithm was 2.5 times faster than the conventional SURF algorithm while the integrated SIFT-epipolar algorithm was 2 times faster than the conventional SIFT algorithm. The integrated MHCD – epipolar correlation algorithm was however 4 times faster than the conventional MHCD algorithm. This shows that the image registration scheme that is based on the integrated epipolar correlation algorithms is faster than the automatic image registration scheme developed using the three (3) conventional vector-based feature detection and extraction algorithms.

Table 4.7: Estimated processing run time of each of the automatic registration algorithms

S/N	Model	Processing Run Time (Milli Seconds)
1	MHCD	1836
2	SIFT	3350
3	SURF	3015
4	MHCD-Epipolar	463
5	SURF-Epipolar	1153
6	SIFT-Epipolar	1630

In general, the developed integrated epipolar correlation-based image registration scheme proved to be more robust when compared to the automatic image registration scheme developed using the three conventional feature descriptors in terms of matching accuracy and processing speed. This is however an improvement to the algorithm developed by He *et al.* (2008) which integrated similarity constraint and epipolar constraint in developing a novel epipolar correlation algorithm because though the algorithm of He *et al.* (2008) proved to be more accurate than existing algorithms just like the integrated algorithms developed in this study, it expended more computation or processing time which implies that the algorithm's accuracy was improved at the expense of more processing time.

Also, though SIFT extracted the highest number of corresponding points which attests to its stability, it is very slow in processing or registering the images because it expended more processing run time when compared to the other implemented algorithms. This is also in agreement with the findings of Juan and Gwun (2009), and El-gayar *et al.* (2013).

4.5 Second Image Registration Campaign

This section describes the results obtained from the scheme's experimentation using UAV acquired overlapping image pairs which is the second image registration campaign of this study. The scheme's robustness was tested using accuracy and processing time (speed of the registration). The developed registration scheme was also experimented on PCs with different RAM configuration to examine the effect of PC configuration on the scheme's accuracy and speed using the overlapping image pairs presented in Figures 3.12a and 3.12b.

4.5.1 Automatic image registration using UAV acquired image pairs

For the second image registration campaign, the same methods adopted for the first image registration campaign described in subsections 4.2 and 4.3 was also used, except for the overlapping image pairs used for the experimentation. While the stereopairs presented in Figures

3.11a and 3.11b were used for the first image registration campaign, overlapping image pairs presented in Figures 3.12a and 3.12b were used for the second image registration campaign as earlier discussed in subsection 3.4 of chapter 3.

Figure 4.25 presents the matched features which contains both the inliers and outliers (associated pairs) of the overlapping image pairs using the MHCD algorithmic procedure described in subsection 2.1.1 of chapter 2, while Figure 4.26 shows the matched inliers only after the successful exclusion of the outliers using RANSAC algorithm described in subsection 3.2.2. The photo coordinates of the extracted conjugate points were stored in the scheme's coordinate register, an excerpt of which is presented in Figure 4.27. A total of 172 conjugate points were automatically extracted using the MHCD algorithm and their image coordinates (in pixels) are presented in Appendix D. Figure 4.28 presents the mosaic generated using the MHCD for the second registration campaign. The mosaic is presented within the developed software's working environment.

The computed homography for the image registration using the MHCD is presented as:

$$H_{MHCD} = \begin{bmatrix} 1.001 & -0.005 & -74.022 \\ -0.009 & 1.024 & 583.624 \\ 0.000 & 0.000 & 0.976 \end{bmatrix}$$

The parameter vectors of the computed homography using MHCD in the second image registration campaign are: $a = 1.001$, $b = -0.005$, $t_x = -74.002$ and $t_y = 583.624$. Where t_x and t_y are the translation along the x and y axis respectively. Also, $a = \cos \alpha$, $b = \sin \alpha$ and α is the rotation angle. The parameter vectors show that the MHCD algorithm is indeed invariant to rotation since the rotation angle reported is approximately equal to zero which shows that the algorithm is stable and does not vary under rotation when temporal image pairs acquired using a UAV are used.

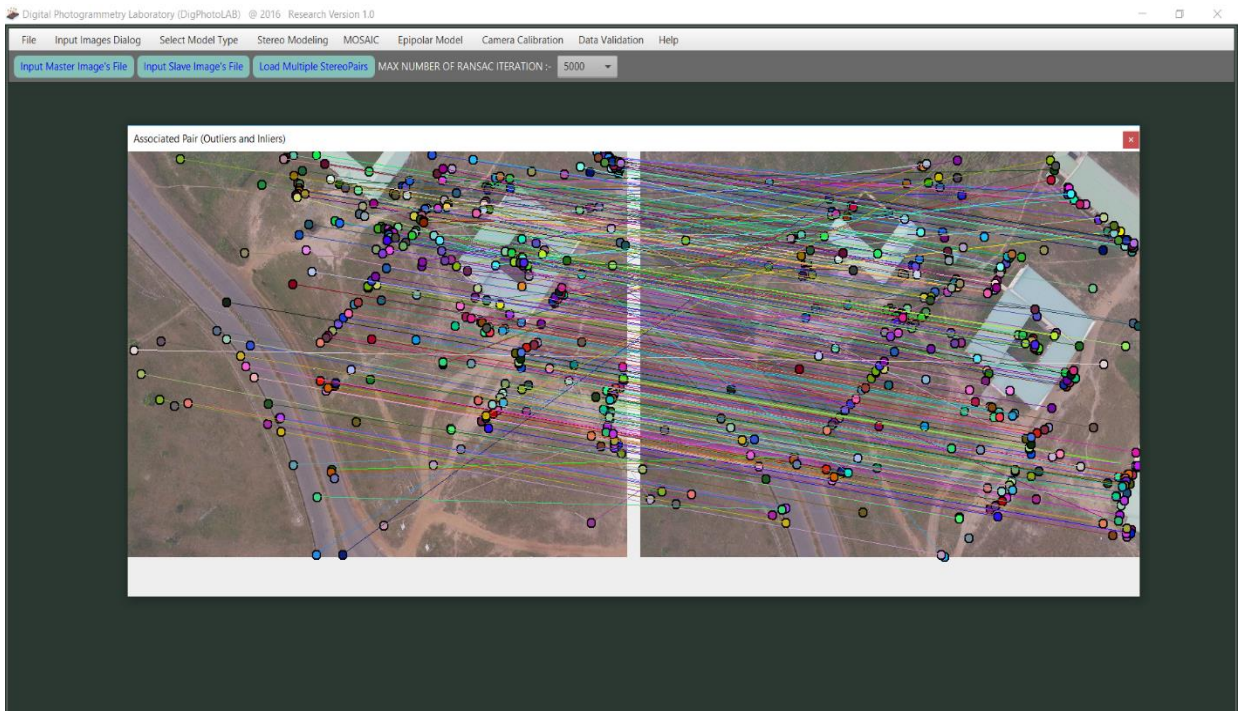


Figure 4.25: Associated image pairs using MHCD for the second registration campaign

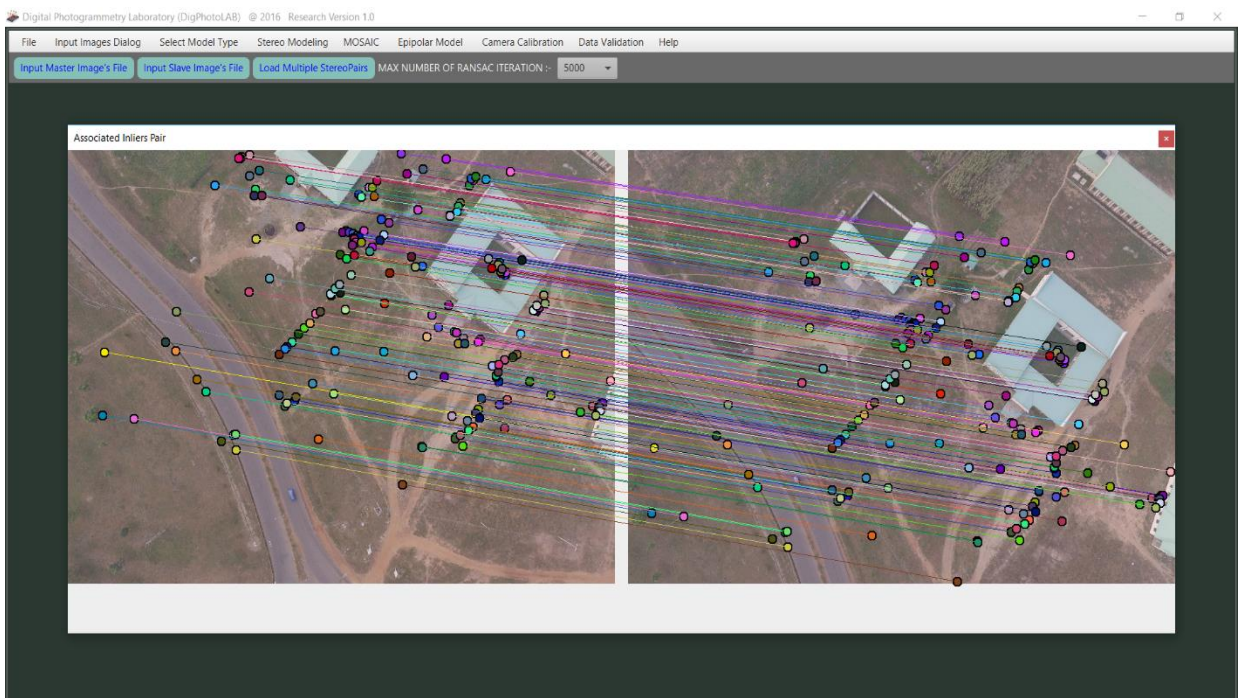


Figure 4.26: Matched inliers using MHCD for the second registration campaigns

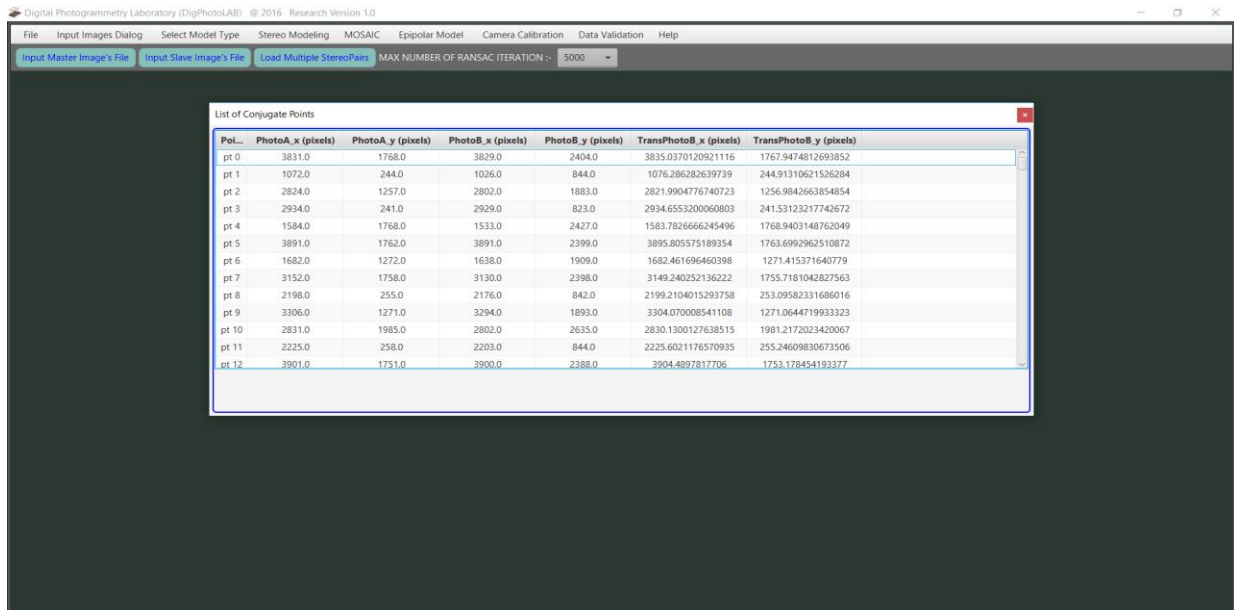


Figure 4.27: MHCD's conjugate point register for the second campaign

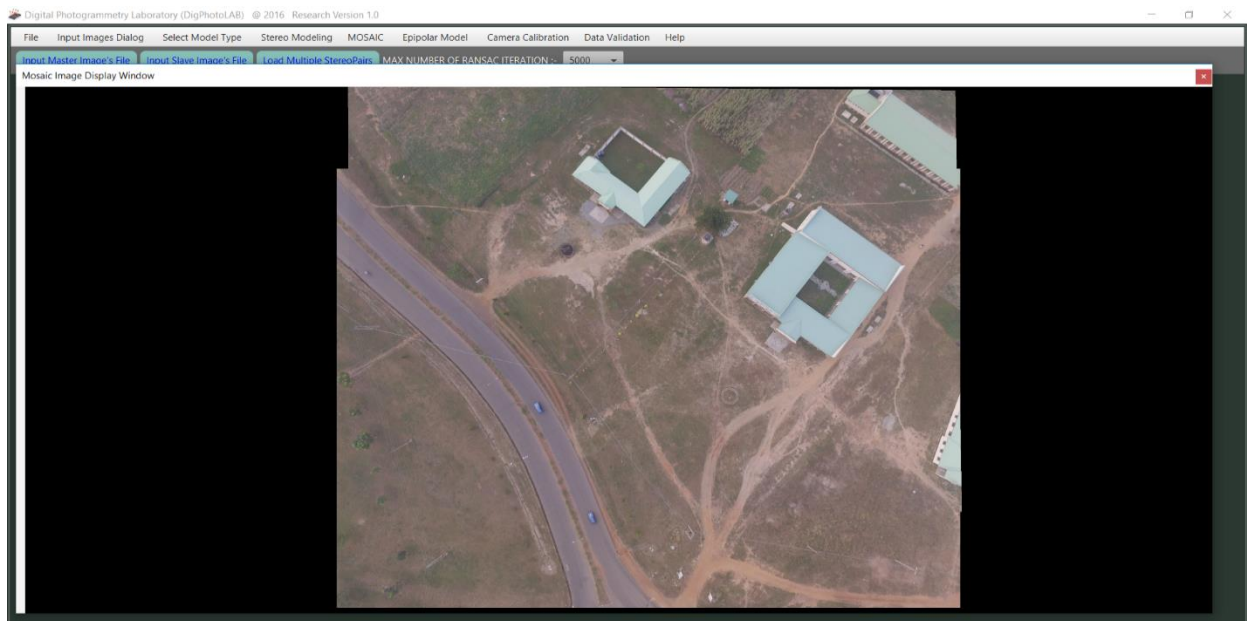


Figure 4.28: Mosaic generated using MHCD for the second registration campaign

The image showing the matched corresponding features which contains both inliers and outliers extracted using the algorithmic procedure of SURF described in subsection 2.1.1 of chapter 2 is presented in Figure 4.29 while the image showing the matched inliers after the successful exclusion of mis-matches using RANSAC algorithm described in subsection 3.2.2 is presented in Figure 4.30. A total of 671 corresponding points were automatically matched and extracted and their photo-coordinates presented in Appendix E. An extract of the coordinates is shown in the

image presented as Figure 4.31. The photo coordinates can also be exported as a .txt file for further processing or analysis outside the developed software's working environment. The final registered image using SURF descriptor is presented as Figure 4.32 and the computed homography for the registration is given as:

$$H_{SURF} = \begin{bmatrix} 1.001 & -0.006 & -78.035 \\ -0.005 & 1.019 & 575.158 \\ 0.000 & 0.000 & 0.970 \end{bmatrix}$$

From the estimated homography, it was observed that the diagonals of the matrix is constant (1) and the parameter vectors of the computed homography are: $a = 1.001$, $b = -0.006$, $t_x = -78.035$ and $t_y = 575.158$. Where t_x and t_y are the translation along the x and y axis respectively. Also, $a = \cos \alpha$, $b = \sin \alpha$ and α is the rotation angle. The parameter vectors show that SURF algorithm is indeed invariant to rotation since the rotation angle reported is approximately equal to zero which shows that the algorithm is stable and does not vary under rotation even when UAV acquired temporal image pairs are used.

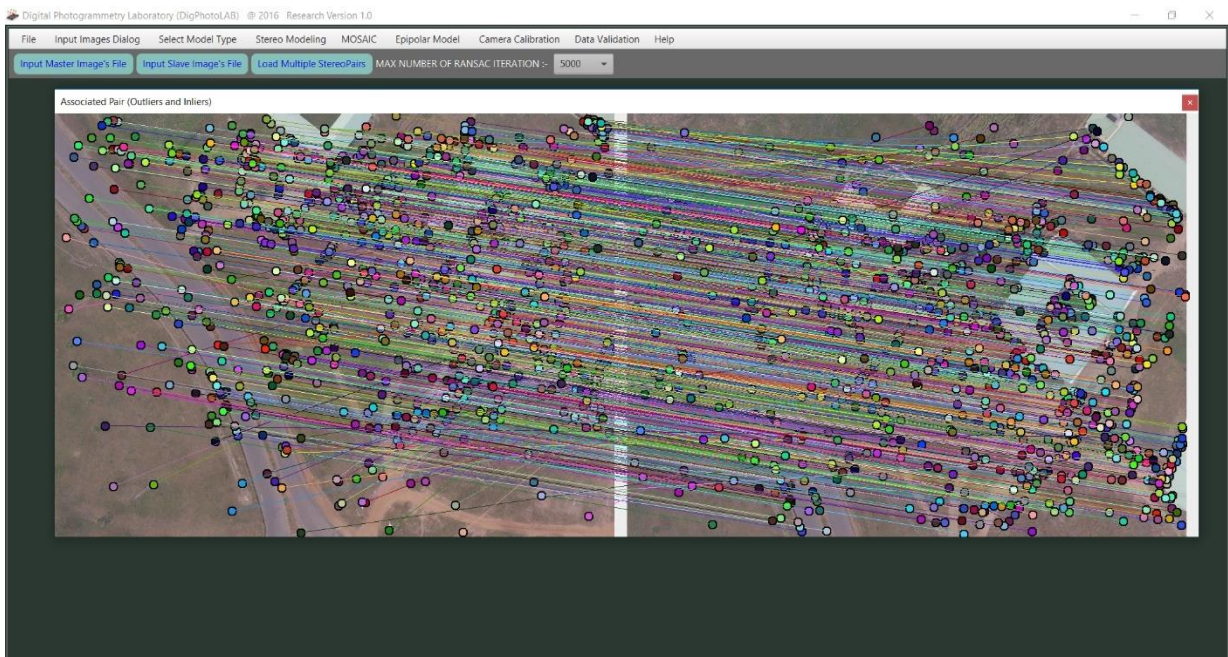


Figure 4.29: Associated image pairs using SURF for the second registration campaign

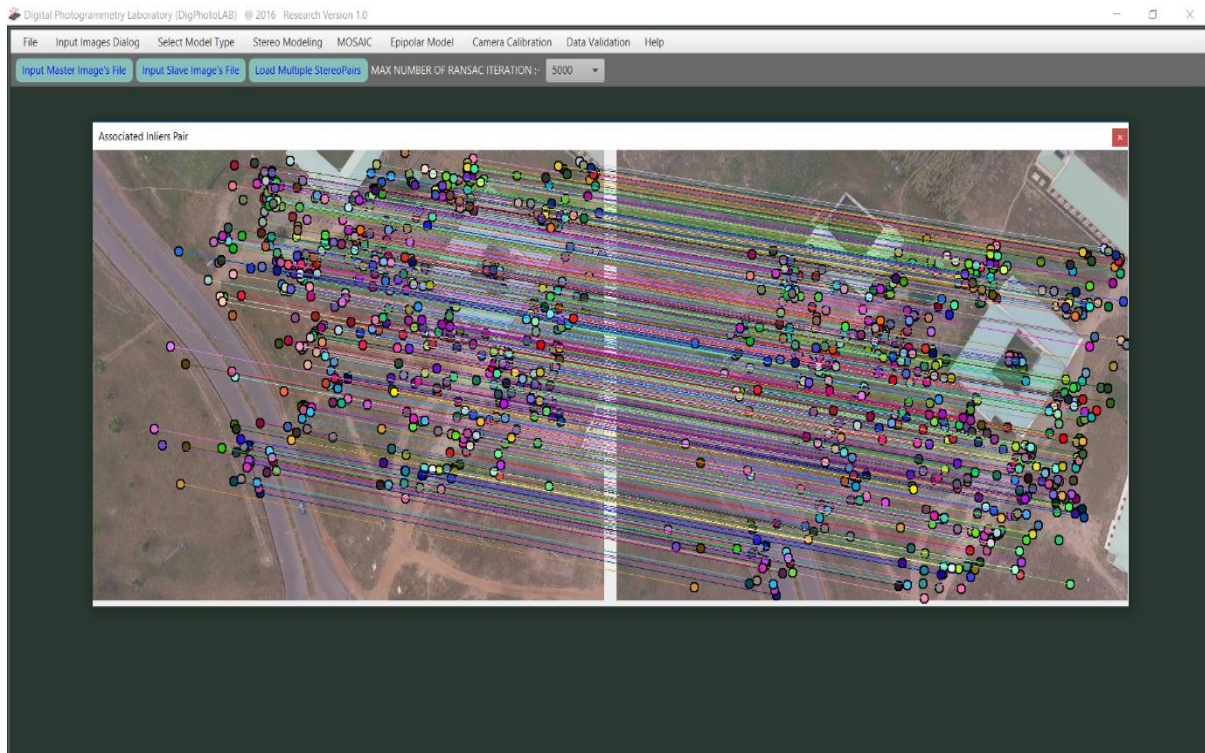


Figure 4.30: Matched inliers using SURF for the second registration campaign

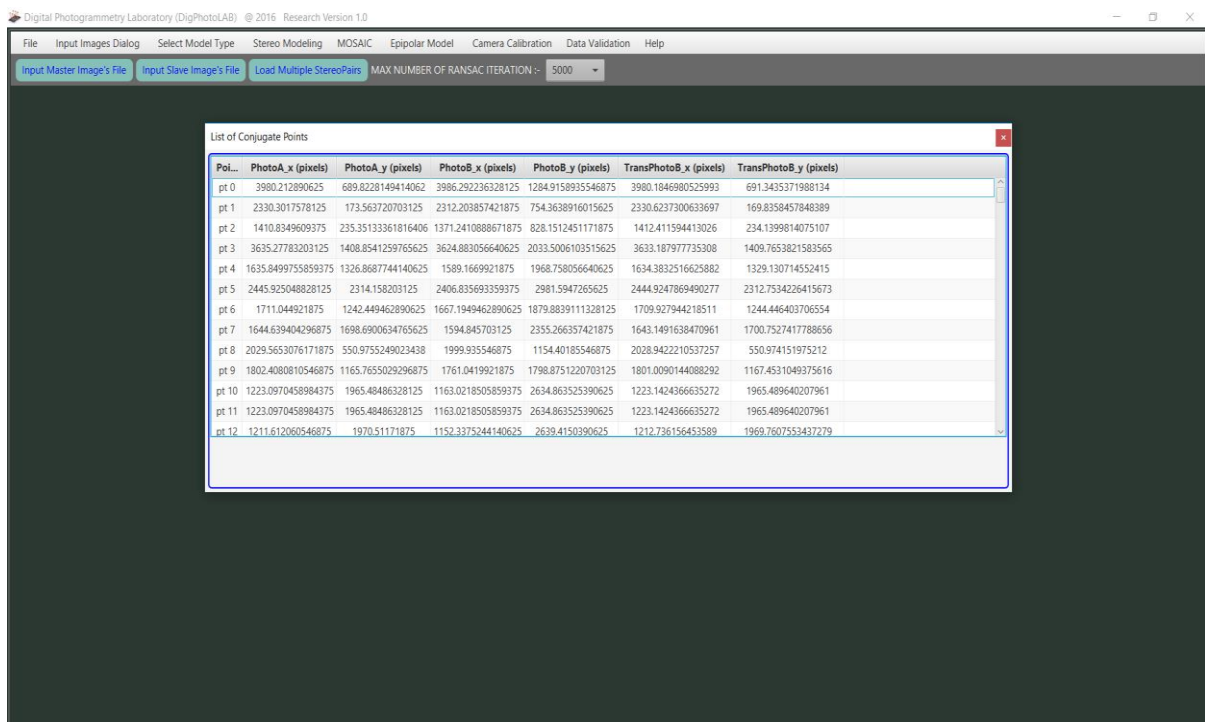


Figure 4.31: SURF's conjugate point register for the second campaign

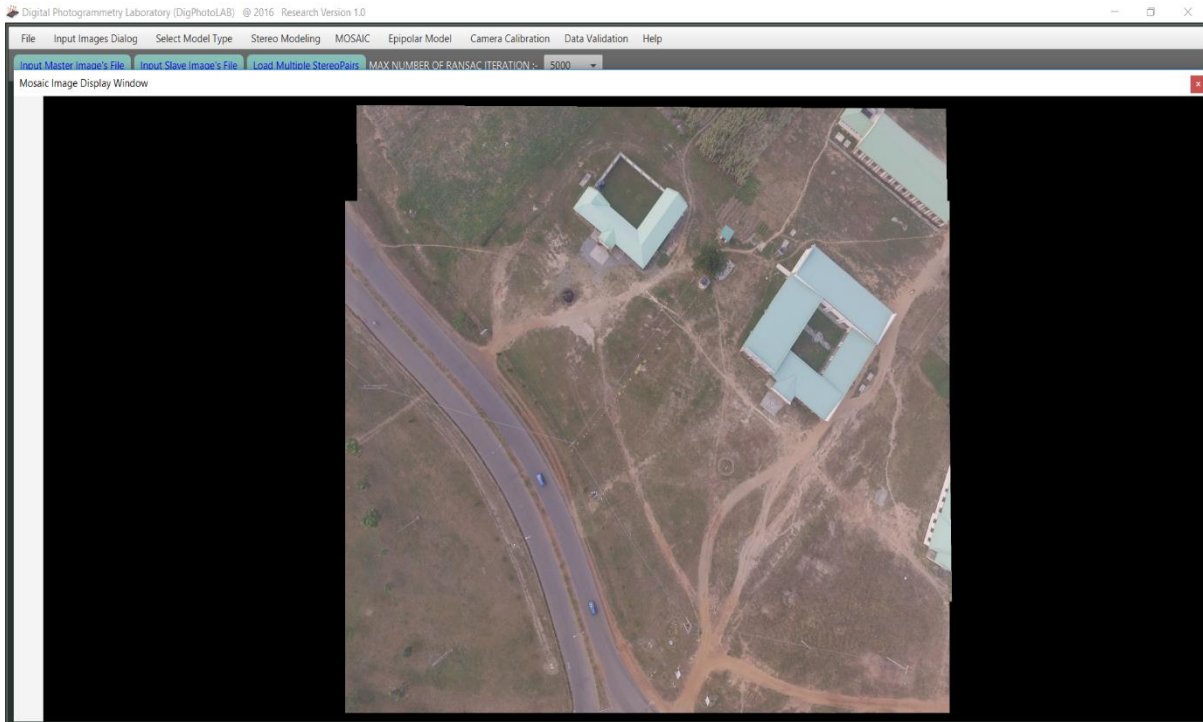


Figure 4.32: Mosaic generated using SURF for the second registration campaign

Using SIFT descriptor described in subsection 2.1.1 of chapter 2, a total of 1067 corresponding feature points were automatically extracted from the overlapping image pairs. Figure 4.33 presents the associated pairs (inliers and outliers inclusive) of the overlapping image pairs using the SIFT algorithm while Figure 4.34 shows the matched inliers only after successfully excluding the mismatches using RANSAC algorithm described in subsection 3.2.2. The photo coordinates (in pixels) of the extracted conjugate points are presented in Appendix F, and an excerpt of the register is shown as an image presented in Figure 4.35. The mosaic generated from the automatic image registration process using the SIFT feature descriptor is presented as Figure 4.36 and the computed homography for the registration is given as:

$$H_{SIFT} = \begin{bmatrix} 1.001 & -0.005 & -72.334 \\ -0.008 & 1.023 & 582.473 \\ 0.000 & 0.000 & 0.976 \end{bmatrix}$$

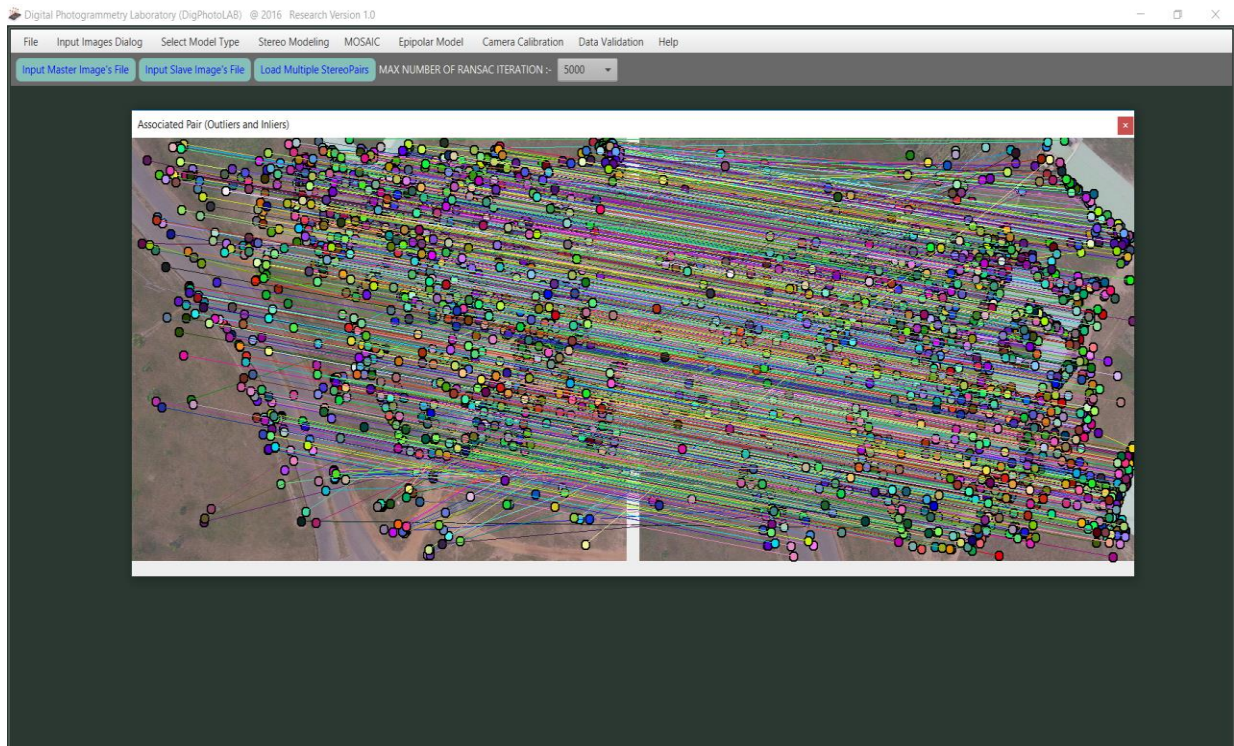


Figure 4.33: Associated image pairs using SIFT for the second registration campaign

From the estimated homography using the SIFT algorithm, it was observed that the diagonals of the matrix is approximately constant (1) and the parameter vectors of the computed homography are: $a=1.001$, $b=-0.005$, $t_x=-72.334$ and $t_y=582.473$. Where t_x and t_y are the translation along the x and y axis respectively, $a=\cos\alpha$, $b=\sin\alpha$ and α is the rotation angle. The parameter vectors show that the SIFT algorithm is indeed invariant to rotation since the rotation angle reported is approximately equal to zero which shows that the algorithm is stable and does not vary under rotation when UAV acquired temporal image pairs are used.

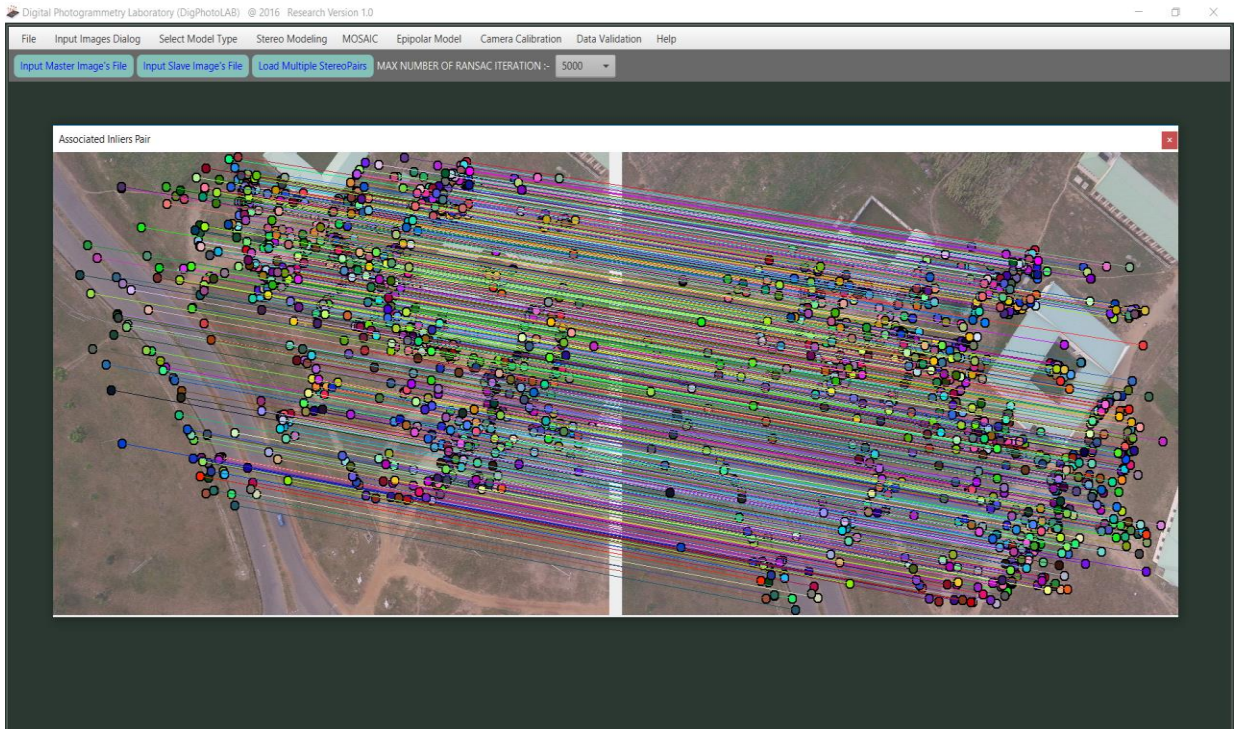


Figure 4.34: Matched inliers using SIFT for the second registration campaign

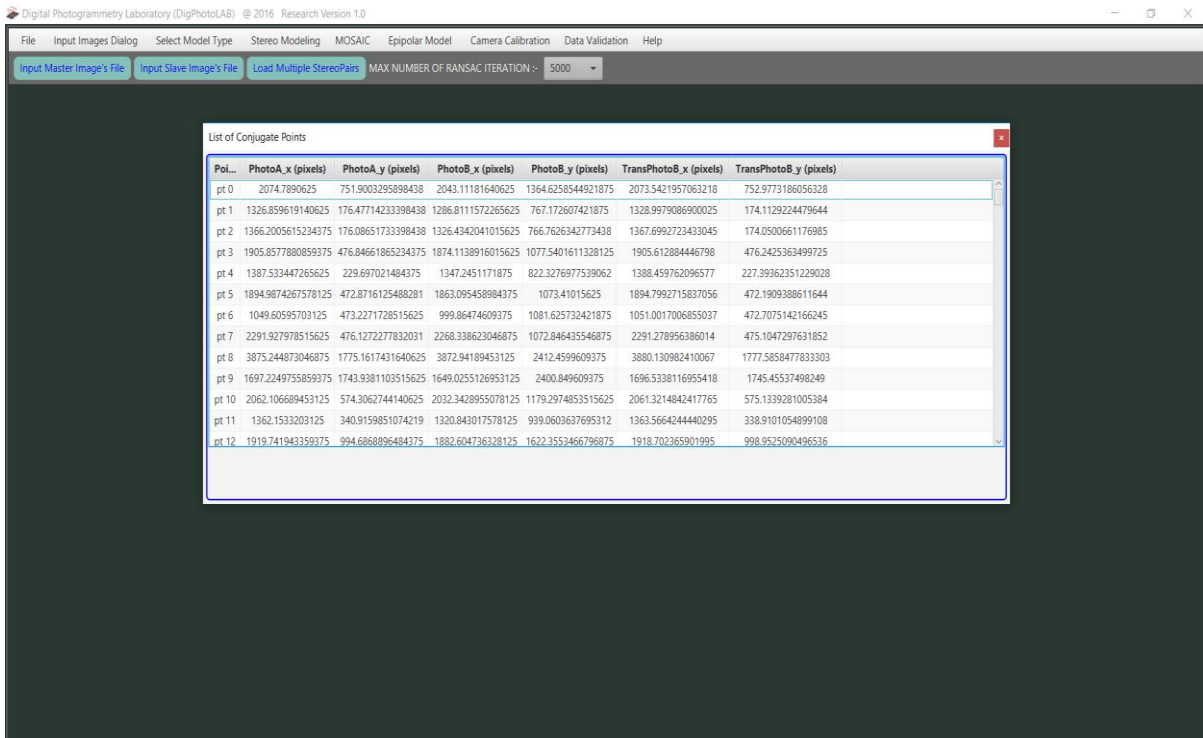


Figure 4.35: SIFT's conjugate point register for the second campaign

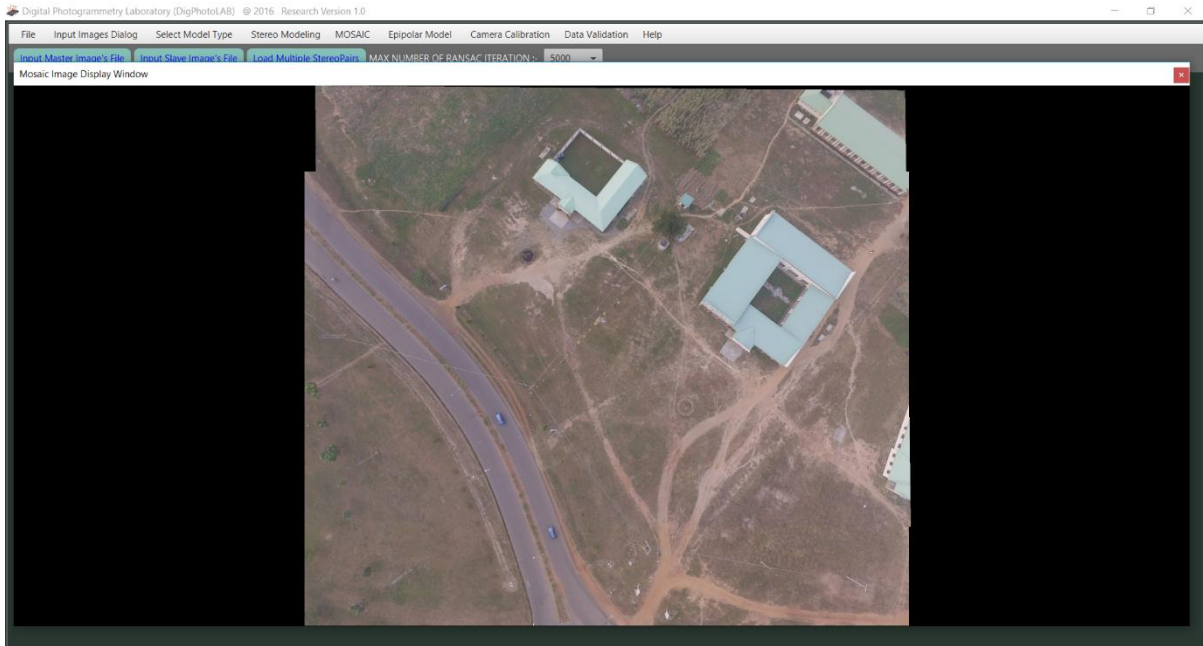


Figure 4.36: Mosaic generated using SIFT for the second registration campaign

From the results obtained and highlighted in Figures 5.1 – 5.12 and based on the homography estimated for each of the implemented feature descriptors, it was observed that each of the feature descriptors proved to be invariant to rotation even when they were experimented with UAV acquired images. However, it was also noted that the SIFT descriptor was very robust in the automatic detection and extraction of corresponding features when compared to the MHCD and SURF descriptors. The SIFT algorithm automatically extracted conjugate points that are 1.59 times more than the conjugate points automatically extracted by SURF algorithm and 6.2 times more than the corresponding features automatically extracted by MHCD. This observation is also in agreement with the results obtained from the first registration campaign as presented in subsection 4.3.3 and the results obtained by Panchal *et al.*, (2013) and Vivek and Kanchan (2014) which attests to the robustness of SIFT in the automatic extraction of corresponding features or key points.

4.5.2 Automatic image registration based on the integrated epipolar correlation algorithms (second image registration campaign)

For the second image registration campaign, each of the three-selected feature detection and extraction algorithms discussed in subsection 2.1.1 were employed first in the automatic detection and extraction of corresponding features before imposing epipolar constraints on them as discussed in subsection 3.2.2 for accurate pixel-to-pixel match which was finally used for the mosaic generation. The fundamental matrix was computed using the normalised eight-point algorithm for each of the three integrated models.

Figure 4.37 presents the correlated inliers obtained using the integrated MHCD-Epipolar correlation algorithm while the final mosaic generated through this process is presented in Figure 4.38. The resultant fundamental matrix is given as:

$$F_{MHCD-epipolar} = \begin{bmatrix} 0.000 & 0.000 & -0.001 \\ 0.000 & 0.000 & 0.000 \\ 0.001 & 0.000 & -0.042 \end{bmatrix}$$

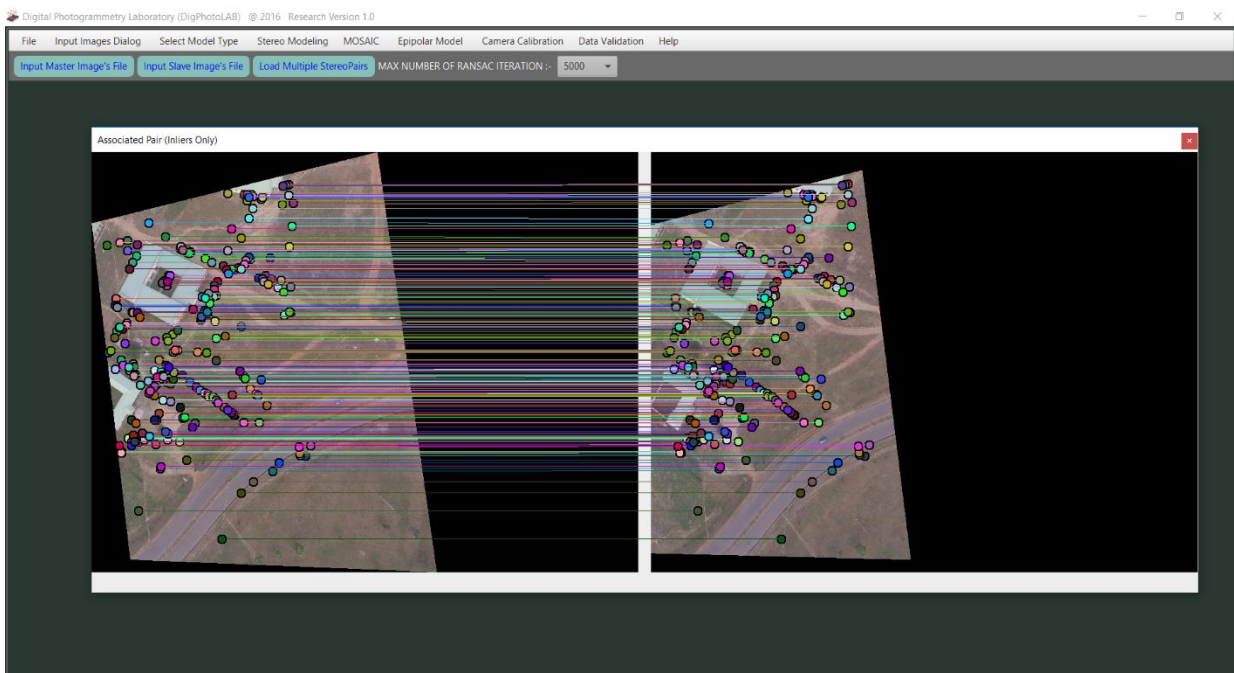


Figure 4.37: Integrated MHCD-Epipolar correlated inliers (second registration campaign)

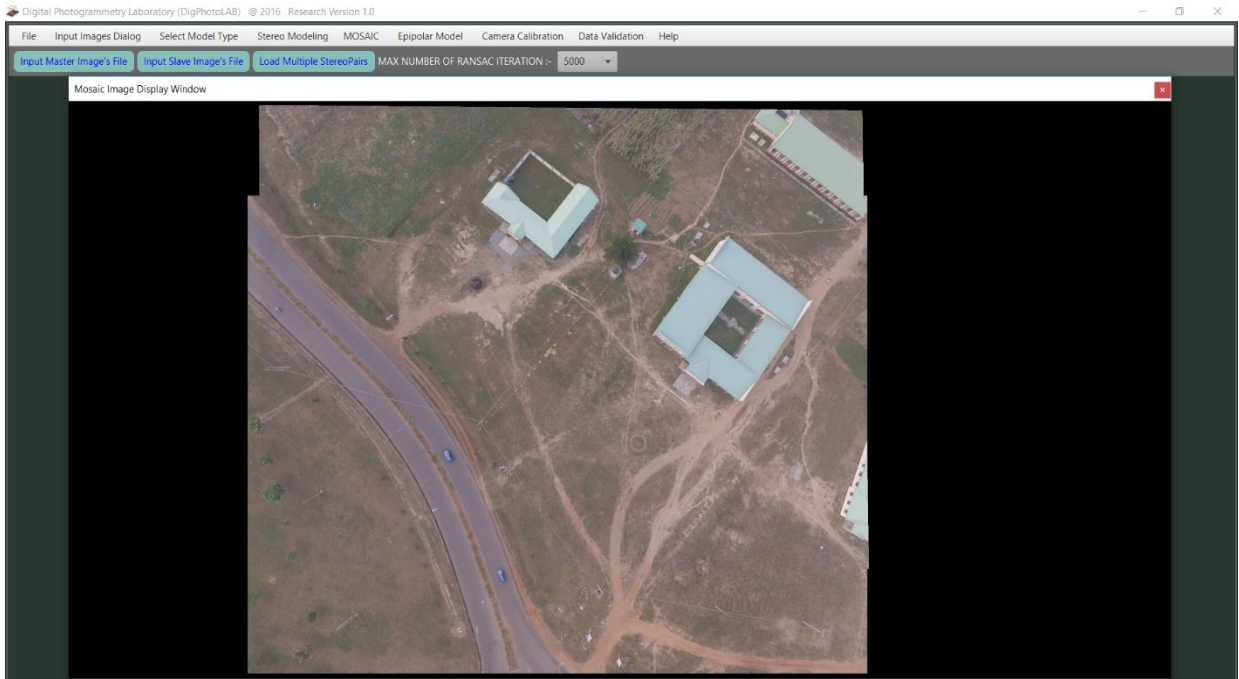


Figure 4.38: Mosaic generated using integrated MHCD-epipolar model (second registration campaign)

The determinant of the estimated fundamental matrix for the integrated MHCD-epipolar correlation algorithm using UAV acquired overlapping image pairs is equal to zero, i. e. $\det(F) = 0$ which satisfies one of the important properties of a fundamental matrix. This shows that the estimated fundamental matrix is accurate and by extension, the image registration process.

The correlated inliers obtained using the integrated SURF-epipolar correlation algorithm is presented in Figure 4.39 while the final registered image obtained using the SURF-epipolar correlation algorithm is presented in Figure 4.40. The resultant fundamental matrix is given as:

$$F_{SURF-epipolar} = \begin{bmatrix} 0.000 & 0.000 & -0.001 \\ 0.000 & 0.000 & 0.000 \\ 0.001 & 0.000 & -0.085 \end{bmatrix}$$

The determinant of the estimated fundamental matrix for the integrated SURF-epipolar correlation algorithm using UAV acquired stereopair is equal to zero ($\det(F) = 0$) which satisfies one of the

basic properties of a fundamental matrix. This shows that the estimated fundamental matrix is accurate and by extension, the image registration process.

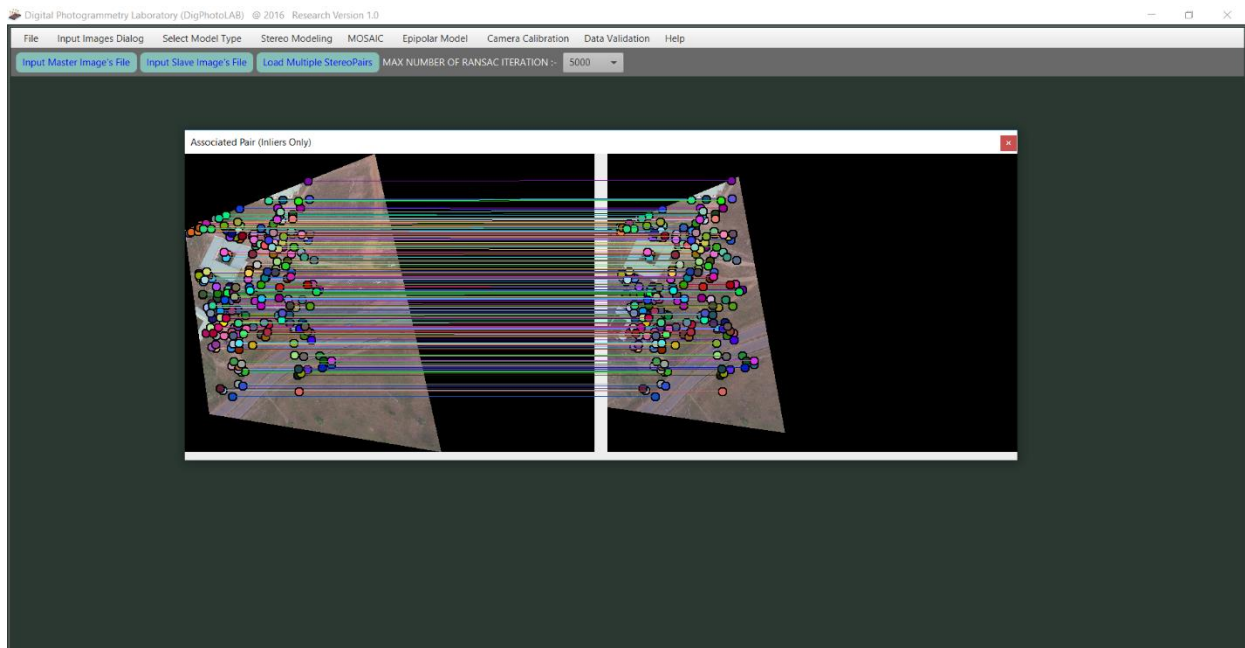


Figure 4.39: Integrated SURF-Epipolar correlated inliers (second registration campaign)

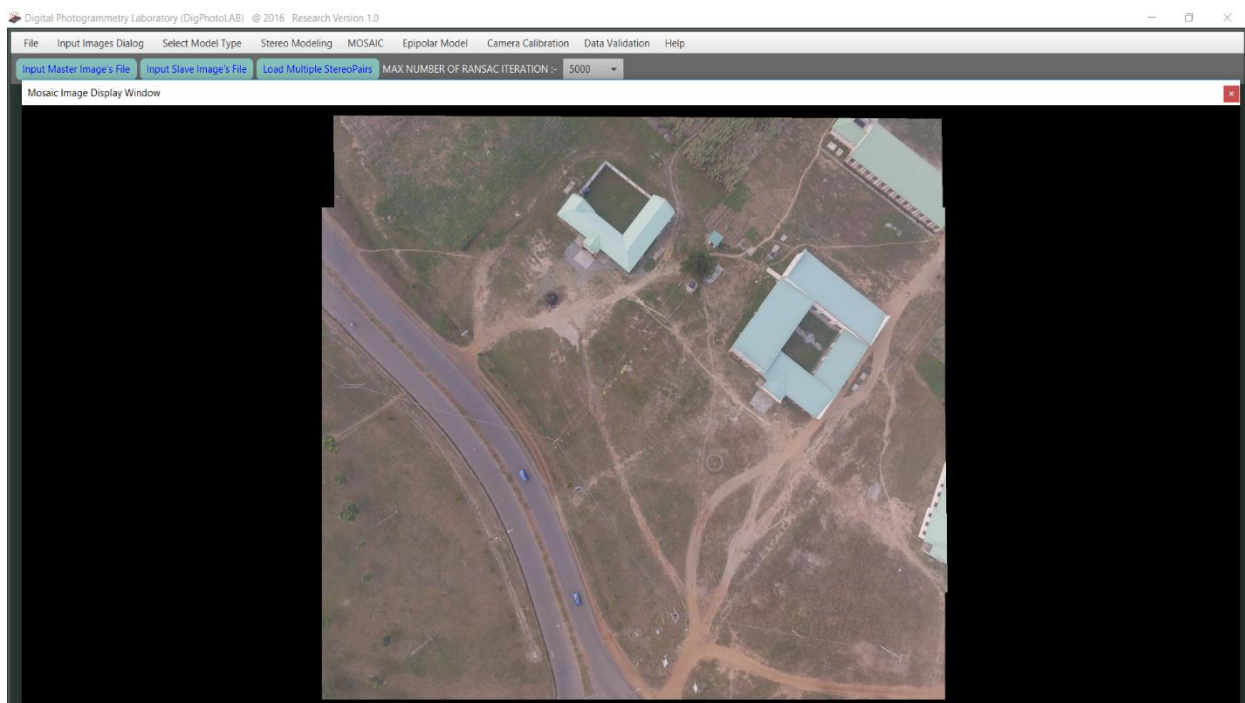


Figure 4.40: Mosaic generated using integrated SURF-epipolar model (second registration campaign)

A graphical representation of the correlated inliers obtained using the integrated SIFT-epipolar correlation algorithm is presented in Figure 4.41 while the final mosaic produced from the overlapping image pairs using the integrated algorithm is presented as Figure 4.42. The computed fundamental matrix which encapsulates the intrinsic projective geometry between the two image pairs is:

$$F_{SIFT-epipolar} = \begin{bmatrix} 0.000 & 0.000 & -0.001 \\ 0.000 & 0.000 & 0.000 \\ 0.001 & 0.000 & -0.184 \end{bmatrix}$$

The determinant of the estimated fundamental matrix for the integrated SIFT - epipolar correlation algorithm using overlapping image pairs acquired with the aid of a UAV is also equal to zero ($\det(F) = 0$) which satisfies one of the basic conditions of a fundamental matrix. This shows that the estimated fundamental matrix is accurate and by extension, the image registration process.

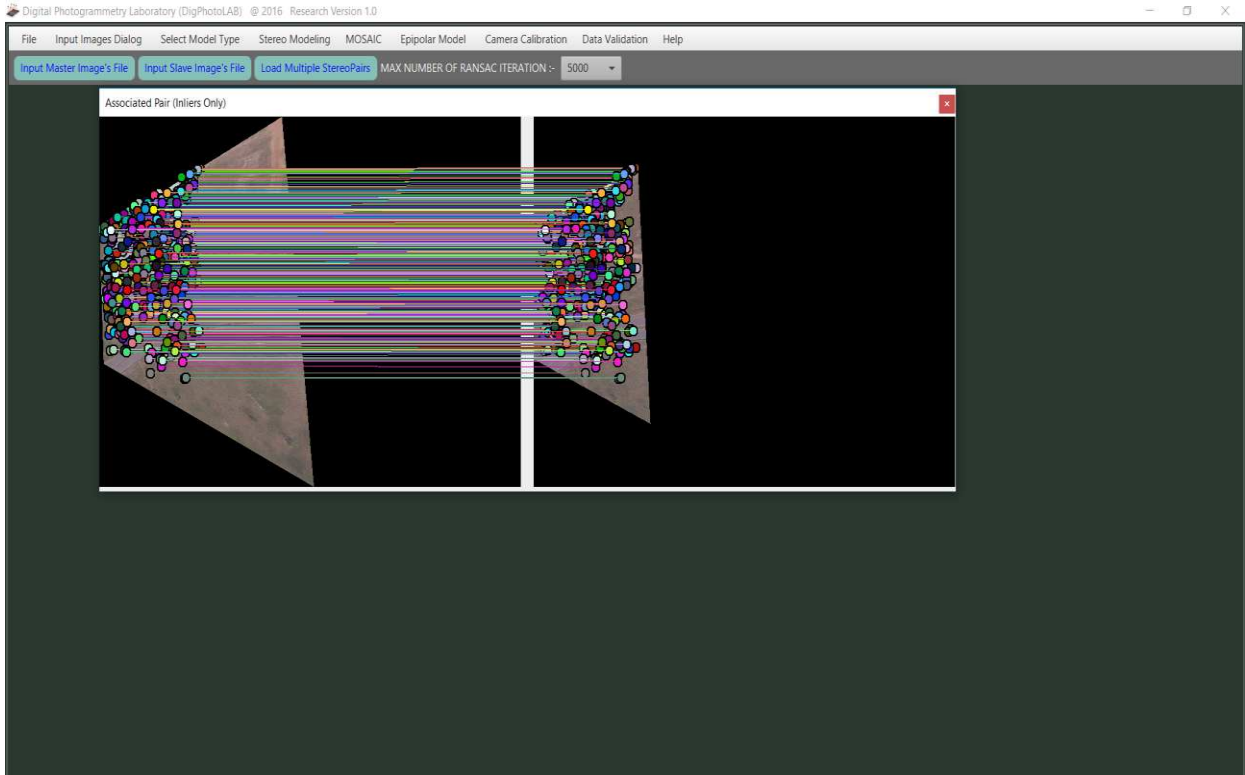


Figure 4.41: Integrated SIFT-Epipolar correlated inliers (second registration campaign)

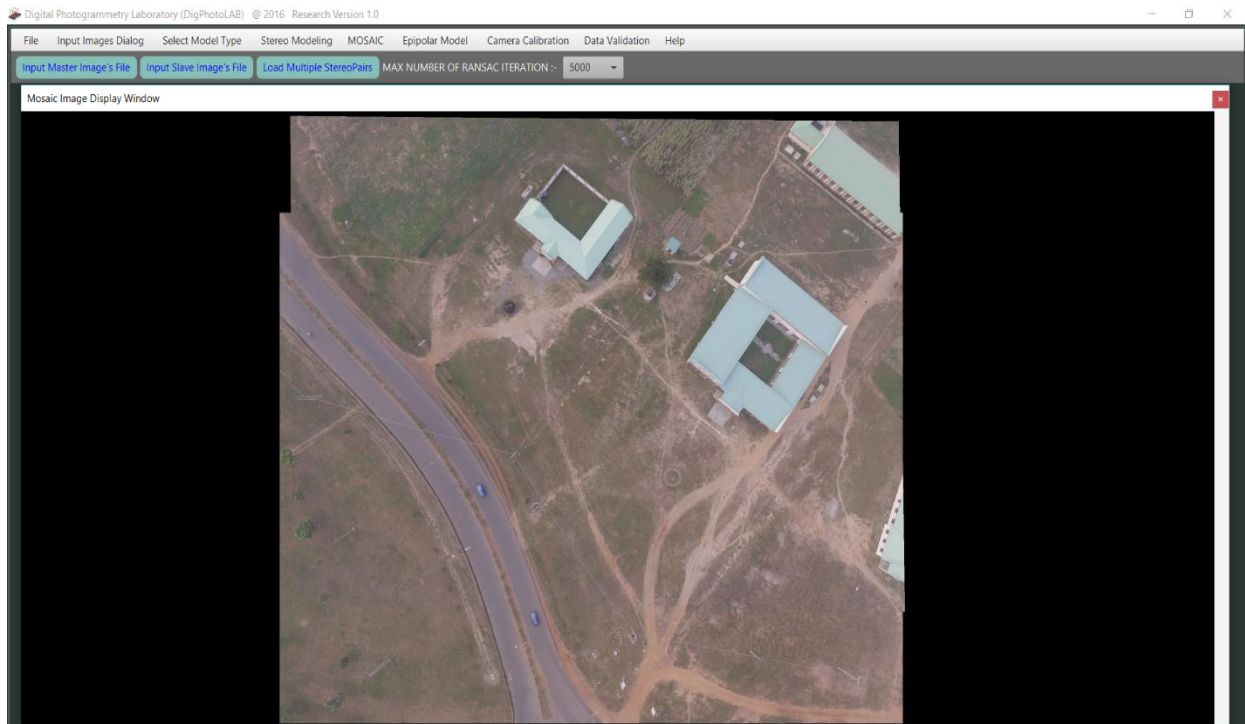


Figure 4.42: Mosaic generated using integrated SIFT-epipolar model (second registration campaign)

4.6 Performance evaluation of the developed scheme using UAV images

The two different approaches that were used for the evaluation of the first image registration campaign were also adopted for the second image registration campaign using UAV acquired overlapping image pairs. The first approach involves only the computation of the resultant signed distances of each of the automatically extracted point correspondences to evaluate the degree of mismatch using equation (3.68) while the RMSE (equation 3.69) and the cumulative signed distances obtained from the measured conjugate point data using the stereo-comparator were adopted as the second approach.

For the first approach, cumulative signed distance of 0.000 pixels, 0.000 pixels and 0.001 pixels were obtained from MHCD, SURF and SIFT algorithms respectively which shows perfect correlation for both MHCD and SURF, and near-perfect correlation for the SIFT descriptor. Perfect correlation was also recorded for the three integrated algorithms with each of them

recording a cumulative signed distance of 0.000 pixels which shows that no single mis-match was recorded during the correlation.

Based on the number of point correspondences automatically extracted, it was observed that the SIFT algorithm extracted the highest number of corresponding points with 1067 conjugate points while the SURF algorithm extracted 671 conjugate points which was followed by the MHCD which extracted 172 conjugate points. This shows that the SIFT algorithm proved to be more robust in the automatic extraction of corresponding features when compared to SURF and MHCD. This observation was also confirmed by the results obtained in the first image registration campaign (subsection 4.2.2) and by Bolarinwa (2017) and Panchal *et al.*, (2013).

For the second performance evaluation approach, the GCPs presented in Table 3.2 were used to automatically locate conjugate points on the image pairs using the developed stereo-comparator. The details of this process have been earlier discussed in subsection 4.4.2. Figure 4.43 presents the rectified stereopair while the GCP coordinate input interface for conjugate point measurement on the rectified stereopair is shown in Figure 4.44 and an image showing the measured conjugate points is presented in Figure 4.45. This process was repeated for the six implemented algorithms.

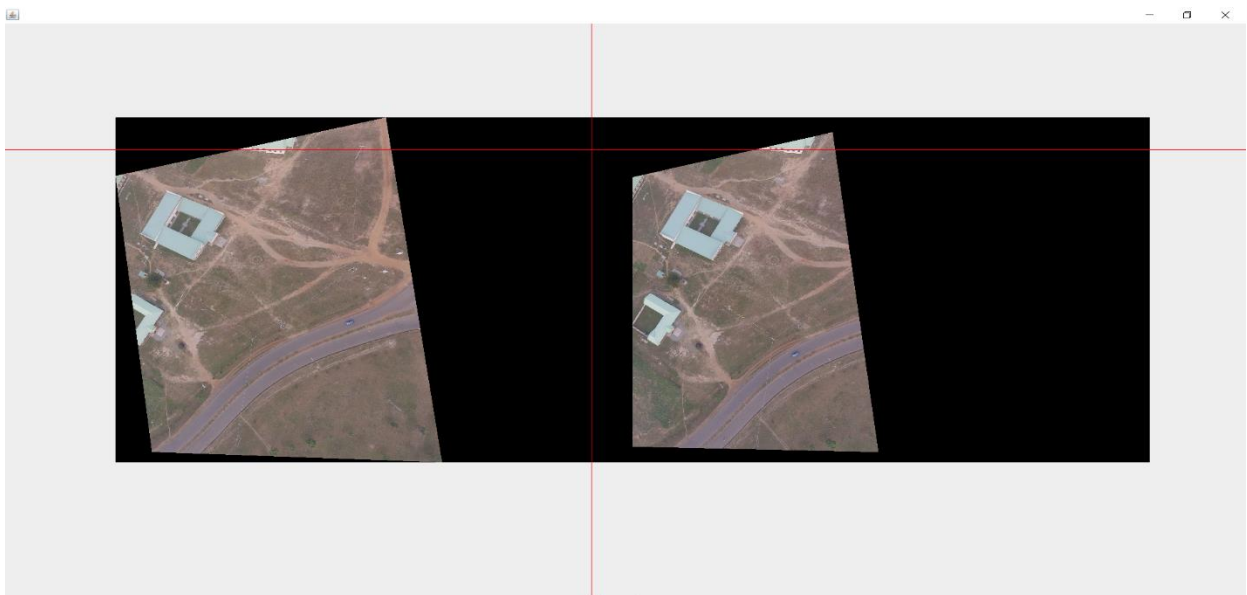


Figure 4.43: The rectified stereo pair (second registration campaign)

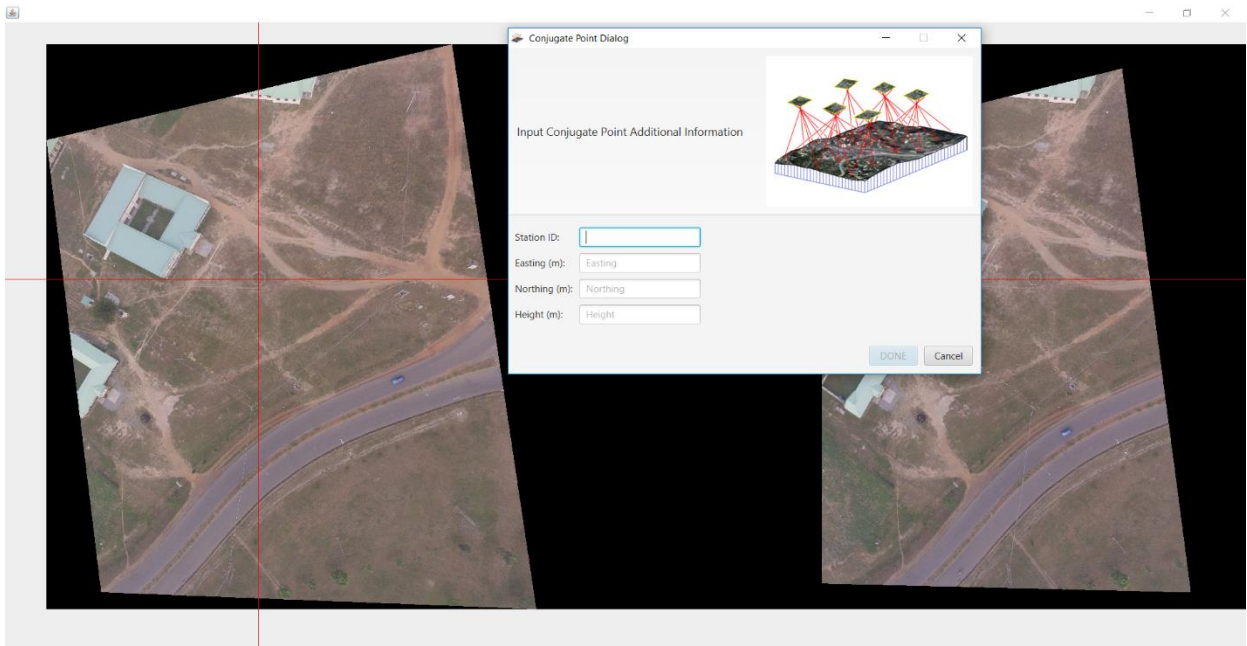


Figure 4.44: Conjugate point measuring interface (second registration campaign)

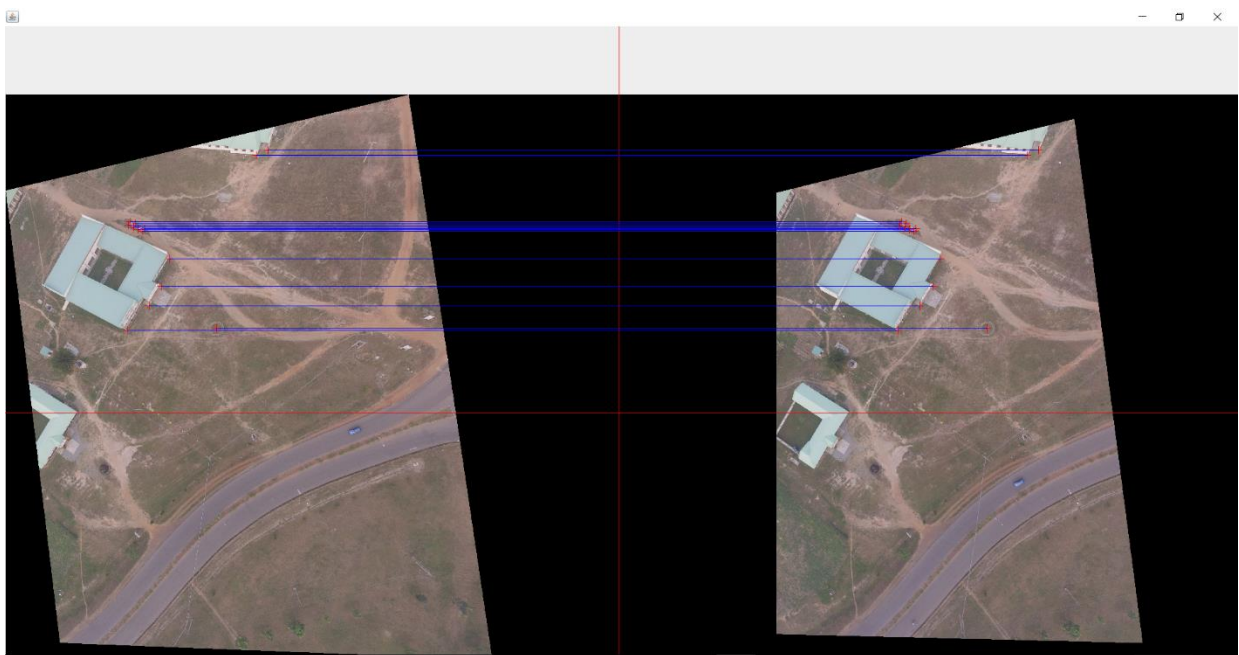


Figure 4.45: Measured conjugate points (second registration campaign)

The result obtained using MHCD algorithm is presented in Table 4.8. A signed distance of 0.000 was computed and a RMSE of $5.74974632623059 \times 10^{-14}$ was obtained.

Table 4.8: Photo coordinates of measured conjugate points using MHCD (second image registration campaign)

ID	Image location of conjugate points in Image A		Image location of conjugate points in Image B		Residuals
	x (Pixels)	y (Pixels)	x	y	Signed Distance
	(Pixels)	(Pixels)	(Pixels)	(Pixels)	(Pixels)
FUTGK-D-01	2517.248	1552.172	2486.885	2192.373	0.000
FUTGK-D-02	3141.448	1282.213	3127.368	1906.770	0.000
FUTGK-D-03	2935.104	1176.964	2913.999	1819.004	0.000
FUTGK-D-04	2815.871	1078.300	2796.549	1699.187	0.000
FUTGK-D-05	3416.458	1120.877	3410.274	1736.076	0.000
FUTGK-D-06	3396.152	1104.729	3389.353	1721.007	0.000
FUTGK-D-07	3420.877	1069.581	3415.013	1684.166	0.000
FUTGK-D-08	3443.985	1087.671	3438.445	1702.776	0.000
FUTGK-D-09	3470.109	1054.104	3465.519	1667.566	0.000
FUTGK-D-10	3451.931	1034.994	3446.799	1649.411	0.000
FUTGK-D-11	3473.838	999.086	3469.584	1611.812	0.000
FUTGK-D-12	3496.692	1018.857	3492.737	1632.171	0.000
FUTGK-D-13	3828.283	2081.920	3821.378	2731.689	0.000
FUTGK-D-14	3813.617	2000.083	3806.914	2647.940	0.000
FUTGK-D-15	3875.180	1818.211	3870.772	2462.143	0.000

Table 4.9 presents the photo coordinates of the measured conjugate points using SURF and their signed distances. A cumulative signed distance of 0.000 was observed and a RMSE of $1.153481152605981 \times 10^{-13}$ was obtained.

Table 4.9: Photo coordinates of measured conjugate points and their signed distances using SURF (second image registration campaign)

ID	Image location of conjugate points in Image A		Image location of conjugate points in Image B		Residuals
	x (Pixels)	y (Pixels)	x (Pixels)	y (Pixels)	Signed Distance (Pixels)
FUTGK-D-01	2517.161	1554.763	2487.033	2196.046	0.000
FUTGK-D-02	3139.986	1281.164	3124.857	1905.993	0.000
FUTGK-D-03	2926.008	1190.211	2905.228	1822.420	0.000
FUTGK-D-04	2782.964	1075.447	2763.109	1695.540	0.000
FUTGK-D-05	2609.824	879.176	2588.598	1493.103	0.000
FUTGK-D-06	3415.922	1121.928	3407.757	1738.040	0.000
FUTGK-D-07	3396.373	1104.191	3388.033	1719.793	0.000
FUTGK-D-08	3420.092	1069.979	3412.574	1684.036	0.000
FUTGK-D-09	3442.217	1086.367	3434.937	1700.858	0.000
FUTGK-D-10	3470.081	1052.479	3463.697	1665.400	0.000
FUTGK-D-11	3450.429	1034.387	3443.872	1646.784	0.000
FUTGK-D-12	3474.721	999.394	3468.328	1612.129	0.000
FUTGK-D-13	3493.780	1019.497	3487.521	1632.829	0.000
FUTGK-D-14	3827.696	2077.513	3817.169	2724.743	0.000
FUTGK-D-15	3804.463	1997.277	3794.421	2641.693	0.000

The photo coordinates of the measured conjugate points and their signed distances using the SIFT algorithm is presented in Table 4.10. A RMSE of $2.7426860557049027 \times 10^{-13}$ was observed and a cumulative signed distance of 0.0000 was obtained.

Table 4.10: Photo coordinates of measured conjugate points and their signed distances using SIFT (second image registration campaign)

ID	Image location of conjugate points in Image A		Image location of conjugate points in Image B		Residuals
	x (Pixels)	y (Pixels)	x (Pixels)	y (Pixels)	Signed Distance (Pixels)
FUTGK-D-01	2515.768	1554.831	2485.023	2196.245	0.000
FUTGK-D-02	3135.543	1281.555	3120.446	1906.336	0.000
FUTGK-D-03	2925.952	1189.691	2907.528	1813.009	0.000
FUTGK-D-04	2780.029	1074.980	2759.852	1695.320	0.000
FUTGK-D-05	2604.452	881.302	2582.768	1495.894	0.000
FUTGK-D-06	3414.916	1119.596	3407.474	1735.293	0.000
FUTGK-D-07	3394.461	1105.157	3386.751	1720.496	0.000
FUTGK-D-08	3420.435	1070.676	3413.659	1684.409	0.000
FUTGK-D-09	3445.664	1088.340	3439.223	1702.509	0.000
FUTGK-D-10	3448.713	1038.414	3442.898	1650.602	0.000
FUTGK-D-11	3472.279	1053.511	3466.793	1666.052	0.000
FUTGK-D-12	3473.939	999.646	3469.095	1610.063	0.000
FUTGK-D-13	3495.269	1020.655	3489.391	1634.594	0.000
FUTGK-D-14	3824.058	2081.935	3814.306	2730.720	0.000
FUTGK-D-15	3804.087	1997.551	3794.881	2643.308	0.000

For the integrated algorithms, Table 4.11 presents the photo coordinates of the measured conjugate points when an integrated MHCD-epipolar correlation algorithm was used for the image registration scheme. The result shows that a cumulative signed distance and a RMSE of 0.0000 and $5.645108717019096 \times 10^{-14}$ were obtained respectively.

Table 4.11: Coordinates of the conjugate points measured using MHCD-epipolar algorithm (second image registration campaign)

ID	Image location of conjugate points in Image A		Image location of conjugate points in Image B		Residuals
	x (Pixels)	y (Pixels)	x (Pixels)	y (Pixels)	Signed Distance (Pixels)
FUTGK-D-01	2518.115	1556.488	2487.724	2196.858	0.000
FUTGK-D-02	3134.136	1279.849	3119.919	1904.379	0.000
FUTGK-D-03	2921.869	1190.286	2902.554	1820.804	0.000
FUTGK-D-04	2779.811	1078.461	2759.966	1698.162	0.000
FUTGK-D-05	2605.839	879.724	2584.100	1494.572	0.000
FUTGK-D-06	3417.686	1122.545	3411.512	1737.801	0.000
FUTGK-D-07	3396.460	1103.245	3389.685	1719.458	0.000
FUTGK-D-08	3420.877	1069.581	3415.013	1684.166	0.000
FUTGK-D-09	3445.842	1086.370	3440.358	1701.402	0.000
FUTGK-D-10	3468.563	1053.917	3463.940	1667.386	0.000
FUTGK-D-11	3450.382	1034.806	3445.218	1649.230	0.000
FUTGK-D-12	3473.519	1000.594	3469.241	1613.385	0.000
FUTGK-D-13	3497.336	1015.849	3493.427	1629.032	0.000
FUTGK-D-14	3828.947	2079.347	3822.086	2729.003	0.000
FUTGK-D-15	3809.943	1996.953	3803.190	2644.714	0.000

When the integrated SURF-epipolar correlation algorithm was used for the automatic image registration, a cumulative signed distance and RMSE of 0.0000 and $1.1544770733452483 \times 10^{-13}$ were recorded and the photo coordinates of the measure conjugate points are presented in Table 4.12.

Table 4.12: Coordinates of the conjugate points measured using SURF-epipolar algorithm (second image registration campaign)

ID	Image location of conjugate points in Image A		Image location of conjugate points in Image B		Residuals
	x (Pixels)	y (Pixels)	x (Pixels)	y (Pixels)	Signed Distance (Pixels)
	FUTGK-D-01	2518.542	1556.528	2488.423	2197.867
FUTGK-D-02	3138.160	1280.901	3123.000	1905.738	0.000
FUTGK-D-03	2924.641	1188.227	2903.356	1822.163	0.000
FUTGK-D-04	2781.097	1075.179	2761.208	1695.278	0.000
FUTGK-D-05	2606.699	884.517	2585.354	1498.683	0.000
FUTGK-D-06	3418.421	1120.424	3410.320	1736.454	0.000
FUTGK-D-07	3394.488	1103.920	3386.115	1719.529	0.000
FUTGK-D-08	3422.612	1068.449	3415.158	1682.423	0.000
FUTGK-D-09	3444.739	1084.845	3437.522	1699.254	0.000
FUTGK-D-10	3473.245	1054.837	3466.894	1667.821	0.000
FUTGK-D-11	3449.793	1036.208	3443.204	1648.682	0.000
FUTGK-D-12	3474.075	1001.235	3467.650	1614.047	0.000
FUTGK-D-13	3495.692	1019.771	3489.465	1633.097	0.000
FUTGK-D-14	3830.693	2082.159	3820.168	2729.536	0.000
FUTGK-D-15	3806.119	1997.516	3796.104	2641.924	0.000

The photo coordinates of the conjugate points measured on the rectified image when the integrated SIFT-epipolar correlation algorithm was used is presented in Table 4.13. While a cumulative signed distance of 0.000 was recorded, a RMSE value of $2.744940097552583 \times 10^{-13}$ was obtained.

Table 4.13: Coordinates of the conjugate points measured using SIFT-epipolar algorithm (second image registration campaign)

ID	Image location of conjugate points in Image A		Image location of conjugate points in Image B		Residuals
	x	y	x	y	Signed Distance (Pixels)
	(Pixels)	(Pixels)	(Pixels)	(Pixels)	
FUTGK-D-01	2518.646	1552.924	2487.980	2194.236	0.000
FUTGK-D-02	3132.805	1281.433	3117.652	1906.236	0.000
FUTGK-D-03	2925.233	1192.217	2906.767	1815.641	0.000
FUTGK-D-04	2782.286	1077.799	2762.125	1698.225	0.000
FUTGK-D-05	2610.529	881.574	2588.967	1496.115	0.000
FUTGK-D-06	3417.792	1119.725	3410.410	1735.398	0.000
FUTGK-D-07	3394.461	1105.157	3386.751	1720.496	0.000
FUTGK-D-08	3422.228	1073.523	3415.459	1687.348	0.000
FUTGK-D-09	3441.631	1090.902	3435.076	1705.211	0.000
FUTGK-D-10	3469.348	1053.380	3463.802	1665.945	0.000
FUTGK-D-11	3447.561	1041.180	3441.691	1653.487	0.000
FUTGK-D-12	3473.939	999.646	3469.095	1610.063	0.000
FUTGK-D-13	3496.464	1017.856	3490.641	1631.679	0.000
FUTGK-D-14	3827.224	2080.602	3817.553	2729.306	0.000
FUTGK-D-15	3811.789	1999.457	3802.723	2645.212	0.000

The summary of the cumulative signed distances and the root mean square errors obtained from the automatic image registration using UAV data for the six implemented models is presented in Table 4.14.

Table 4.14: Summary of the obtained RMSE and signed distances using the six algorithms

S/N	Algorithm	Signed distances	RMSE	No Matched Points
1	MHCD	0.0000	$5.74974632623059 \times 10^{-14}$	172
2	SIFT	0.0010	$1.153481152605981 \times 10^{-13}$	1067
3	SURF	0.0000	$2.7426860557049027 \times 10^{-13}$	671
4	MHCD-Epipolar	0.0000	$5.845108717019096 \times 10^{-14}$	N/A
5	SIFT-Epipolar	0.0000	$1.1544770733452483 \times 10^{-13}$	N/A
6	SURF-Epipolar	0.0000	$2.744940097552583 \times 10^{-13}$	N/A

From the summarized result presented in Table 4.14, it can be observed that the integrated MHCD-epipolar correlation algorithm produced the most accurate registration of the overlapping image pairs when compared to the five remaining algorithms. This is closely followed by the conventional MHCD. Also, it could be observed that integrated SURF-epipolar algorithm and SIFT-epipolar algorithm both outperformed the conventional SURF and SIFT algorithms in terms of matching accuracy.

4.6.1 Performance evaluation of the algorithms using processing time (second registration campaign)

The summary of the time taken by each of the six algorithms to successfully register the same overlapping image pairs is presented in Table 4.15. The result shows that the integrated MHCD-epipolar algorithm is not just the most accurate of the six algorithms, it is also the fastest. With an estimated processing time of 1770 milli seconds, the integrated MHCD-epipolar algorithm proved to be 3.76 times faster than the conventional MHCD which expended 6649 milli seconds for the image registration process. Just as observed with the accuracy, the integrated SIFT-epipolar algorithm and SURF-epipolar algorithm both proved to be faster than the conventional SIFT and SURF algorithms respectively. While the integrated SURF-Epipolar algorithm expended an

approximate processing run time of 7055 milli seconds, the conventional SURF algorithm executed the same task using 13109 milli seconds which implies that the integrated SURF-epipolar algorithm is 1.86 times faster than the conventional SURF algorithm. Also, with an approximate processing run time of 5923 milli seconds, the integrated SIFT-epipolar algorithm proved to be 1.80 times faster than the conventional SIFT algorithm. This observation is also the same with the results obtained in the first image registration campaign as presented in Section 4.4, and an improvement to the model developed by He *et al.* (2008).

Table 4.15: Estimated processing run time for each of the algorithms (second registration campaign)

S/N	Algorithm	Processing Run Time (Milli Seconds)
1	MHCD	6649
2	SIFT	10646
3	SURF	13109
4	MHCD-Epipolar	1770
5	SIFT-Epipolar	5923
6	SURF-Epipolar	7055

4.7 Performance evaluation of the algorithms using PCs of different RAM configuration

Since the results presented for the second image registration campaign were obtained using an 8 GB installed RAM PC, both 4GB PCs and 16GB installed RAM PCs were also used to evaluate the effect of the specification of the PCs on the obtainable accuracy and the processing run time.

Table 4.16 presents the result obtained from the scheme's evaluation using a 4GB installed RAM PC while the result obtained when a 16GB installed RAM PC was used is presented in Table 4.17.

It was observed that only negligible differences were recorded in the RMSE of each of the algorithms using a 4GB, 8GB and 16GB installed RAM PCs while significant differences were recorded in their estimated processing run time. Specifically, it was noticed that when compared

to the 8 GB installed RAM PC, the registration scheme was 1.34 times faster when a 16 GB installed RAM PC was used while it was also 3.12 times faster when compared to the result obtained when a 4GB installed RAM was used. When an 8GB installed RAM PC was used, the registration scheme was also 2.5 times faster when compared to the result obtained when a 4GB installed RAM PC was used. Generally, it was observed that the registration scheme performed optimally in terms of the estimated processing run time when it was experimented on PCs with high installed RAM.

Table 4.16: Accuracy and estimated processing run time using a 4GB installed RAM PC

S/N	Algorithm	RMSE	Processing Time (Milli Seconds)
1	MHCD	$5.637152351124787 \times 10^{-14}$	13084
2	SURF	$1.1537498353680958 \times 10^{-13}$	22971
3	SIFT	$2.7430314817352836 \times 10^{-13}$	29048
4	MHCD-Epipolar	$5.7201649084955135 \times 10^{-14}$	3282
5	SURF-Epipolar	$1.153603107575023 \times 10^{-13}$	19397
6	SIFT-Epipolar	$2.7449575802239245 \times 10^{-13}$	18506

Table 4.17: Accuracy and estimated processing run time using a 16GB installed RAM PC

S/N	Algorithm	RMSE	Processing Time (Milli Seconds)
1	MHCD	$5.63304808639551406 \times 10^{-14}$	4628
2	SURF	$1.1530573443150327 \times 10^{-13}$	10257
3	SIFT	$2.7436532587981856 \times 10^{-13}$	8866
4	MHCD-Epipolar	$5.7284285292329594 \times 10^{-14}$	1102
5	SURF-Epipolar	$1.1542988306504167 \times 10^{-13}$	5594
6	SIFT-Epipolar	$2.741389046510796 \times 10^{-13}$	4704

The results presented in Tables 4.16 and 4.17 also shows the same trend with the results earlier presented for the first and second image registration campaigns with the integrated MHCD-epipolar correlation algorithm, outperforming all the other algorithms in terms of accuracy and speed when the 4 GB, 8GB and 16GB installed RAM PCs were used. For the conventional vector-based feature descriptors, the MHCD outperformed both SIFT and SURF descriptors in terms of accuracy and speed, while the SIFT descriptor also gave higher accuracy when compared to SURF which agrees with the findings of Krishna and Varghese (2015).

CHAPTER FIVE

5.0 CONCLUSION AND RECOMMENDATIONS

5.1 Conclusions

From the findings of this study, the following subsections present the conclusions that were drawn from each of the objectives of this study as highlighted in subsection 1.3 of Chapter One. The conclusions also reflect the answers to each of the research questions that were posed in subsection 1.2 of Chapter One and the actualization of each of the research objectives.

5.1.1 Effect of feature descriptors on the developed image registration scheme

The following are the conclusions drawn from the obtained results and findings of this research with respect to the first objective and the first research question:

The SIFT algorithm proved to be more robust when compared with SURF algorithm and MHCD in terms of automatic extraction of corresponding features because it automatically extracted more corresponding points in the two image registration campaigns. It automatically extracted point correspondences which is approximately 2.5 times more than the point correspondences automatically extracted by the MHCD and 1.70 times more than the point correspondences automatically extracted by the SURF algorithm for the first image registration campaign using google earth acquired images. For the second registration campaign using UAV acquired image pairs, it automatically extracted conjugate points that are 1.59 times more than the conjugate points automatically extracted by SURF algorithm and 6.2 times more than the corresponding features automatically extracted by MHCD.

In terms of measured conjugate points, the MHCD proved to be more robust than the other two feature detection and extraction algorithms because it gave a root mean square error that is lower than the results obtained from SURF and SIFT algorithms.

The SIFT algorithm also proved to be the slowest of all the three (3) existing feature detection and extraction algorithms implemented in this study. It expended more processing run time for the automatic image registration in both registration campaigns which was also the same even when PCs of different RAM specifications were used. This shows that the SIFT descriptor is very slow in the automatic extraction of point correspondences, irrespective of the specifications of the PC used.

5.1.2 Effect of the developed integrated algorithms on the automatic image registration scheme

The conclusions drawn from the findings of this research with respect to the second objective and research question are as follows:

The integrated epipolar correlation algorithms optimized the developed automatic image registration scheme by improving the overall speed and accuracy of the scheme. The algorithms performed better in terms of matching accuracy and processing time when compared to the accuracy and speed of the other three existing feature detection and extraction algorithms implemented in this research (MHCD, SIFT and SURF).

The RMSE obtained from the integrated epipolar correlation-based image registration scheme shows that the three integrated epipolar algorithms are more accurate than the conventional MHCD, SIFT and SURF algorithms respectively, while the integrated MHCD-epipolar algorithm gave the most accurate registration. This implies that the integrated MHCD-epipolar algorithm is more accurate than the other five implemented algorithms.

In terms of speed of the developed scheme using the novel integrated algorithms, the integrated SURF-epipolar algorithm and the SIFT-epipolar algorithm is 2.5 times and 2 times faster than the conventional SURF and SIFT algorithm respectively, while the integrated MHCD – epipolar algorithm is 4 times faster than the conventional MHCD algorithm for the first registration

campaign using google earth images. For the second image registration campaign using UAV acquired images, the integrated MHCD-epipolar algorithm is 3.76 times faster than the conventional MHCD, while the integrated SURF-Epipolar algorithm and the SIFT-epipolar algorithm are 1.86 times and 1.80 times faster than the conventional SURF and SIFT algorithms.

5.1.3 Performance evaluation of the developed image registration scheme

The conclusions drawn from the inferences made from the obtained results and findings of this study with respect to the third objective and research question are highlighted as follows:

The speed of the developed automatic image registration scheme was faster in the first registration campaign when compared with the second registration campaign, which implies that the size of the image pairs has considerable effect on the speed of the developed registration scheme. The integrated MHCD-epipolar algorithm is not just faster and more accurate than the conventional MHCD algorithm, it also performed better in terms of speed and accuracy when compared with the other algorithms implemented for the development of the automatic image registration scheme.

The specification of the PCs used have considerable effect on the speed of the algorithms while only negligible effect is noticed on the accuracy of each of the algorithms. This implies that the accuracy of the developed image registration scheme remains constant irrespective of the specification of the PCs used, but when PCs with high installed RAM specifications are used, the algorithms are much faster which shows that the speed of the registration scheme increases with increase in the installed RAM specifications of the PCs. Finally, the specification of the PCs used have no effect on the number of feature correspondences automatically extracted by the developed image registration scheme.

5.2 Recommendations

This study has investigated the robustness of three feature detection and extraction algorithms in the development of an automatic image registration scheme. It has also integrated both geometric constraints (using the extracted point correspondences from the three feature extraction models) and epipolar constraints (epipolar correlation algorithm) in the development of a novel integrated scheme for the automatic registration of overlapping images which has proved to be very robust with respect to processing time and matching accuracy. The following are the recommendations that are drawn from the findings of this study:

1. It is recommended that the SIFT algorithm be adopted for an image registration paradigm when the robustness of the extracted corresponding features is the primary interest of the image registration task.
2. The developed image registration scheme based on the integrated MHCD – epipolar algorithm is recommended as the ideal tool for automatic registration of overlapping images when the dual advantages of speed and accuracy are desired.

Based on the findings of this research, further research efforts can focus on the following:

1. Investigation of the impact of the presence of noise in the stereo pairs on the overall image registration accuracy.
2. Application of image pre-processing techniques on the overlapping image pairs before their registration for a more accurate registration output.
3. Extension of the developed integrated image registration scheme for optimal and seamless registration of multiple stereopairs at a time.
4. Improving the developed co-registration scheme to perform optimally with multimodal stereopairs with less than 60% overlap.

5.3 Contributions to Knowledge

The following are the major contributions of this research to the existing body of knowledge:

1. A novel integrated automatic image registration algorithm based on epipolar correlation has been developed which proved to be more robust (with respect to speed and accuracy) than the automatic image registration algorithm that is based on selected conventional feature descriptors. The novel registration algorithm integrates both the geometric and epipolar constraints which makes it more robust in terms of accuracy and speed (processing time).
2. An automatic image registration software which contains a stereo comparator for direct point data measurement and accuracy assessment has also been developed. The software is also equipped with a module for automatic camera calibration which automatically generate the intrinsic and extrinsic parameters of a camera. The developed registration scheme will be of particular interest to the military, cartographers, radiologists, digital photogrammetrists and remote sensing experts as a tool for educational, training and industrial applications.

REFERENCES

- Adrien, B., & Peter, S. (2004). Non-linear estimation of the fundamental matrix with minimal parameters. *IEEE Transactions on Pattern Analysis and Machine Intelligence*, 26(4), 1-7.
- Ajayi, O. G. (2014). A MATLAB Program for the automatic registration of overlapping images. Unpublished MSc thesis submitted to the Department of Surveying and Geoinformatics, Faculty of Engineering, University of Lagos, Nigeria.
- Ajayi, O.G., Odumosu, J.O., Okorochoa, C.V., Nzelibe, I.C., Ahmadu, H.A., & Bawa, S. (2014). Semi-automatic generation of mosaic from overlapping images using MATLAB. *International Journal of Engineering and Advanced Technology Studies*, 2(4), 1-15.
- Alam, F., Rahman, S. U. R., Tairan, N., Shah, H., Abohashrh, M. S., & Abbas, S. (2019). An Automatic Medical Image Registration Approach Based on Common Sub-regions of Interest. *Journal of Medical Imaging and Health Informatics*, 9(2), 251-260, doi: 10.1166/jmihi.2019.2601
- Alexander, E., & Summers, E. (2003). Fast registration algorithm using a variational principle for mutual information, *Proceedings of SPIE International Society Optical Engineering*, 5032, 1053–1063.
- Al-Manasir, K., & Fraser, C. S. (2006). Automatic registration of terrestrial laser scanner data via imagery. *ISPRS Commission V Symposium 'Image Engineering and Vision Metrology*, XXXVI, 5, Dresda, September 25-27.
- Alpert, N. M., Berdichevsky, D., Cervin, Z., Morris, E.D., & Fischman, A.J. (1996). Improved methods for image registration. *NeuroImage*, 3, 10-18.
- Al-Ruzouq, R. (2004). Semi-Automatic registration of multisource satellite imagery with varying geometric resolutions. Unpublished PhD thesis submitted to the Geomatics Engineering Department, Faculty of Graduate Studies, Calgary, Alberta.
- Anand, R., & James, S. D. (1998). Matching point features using mutual information. *Proceedings of Biomedical Image Analysis Workshop*, 172-181.
- Andronache, A., Siebenthal. M., Székely, G., & Cattin, P. (2008). Non-rigid registration of multi-modal images using both mutual information and cross-correlation. *Medical Image Analysis*. 12(1), 3-15.
- Anil, K. P., Rohit, R., & Yamini, C. (2014). Image registration and its various forms: a survey. *International Journal of Science, Engineering and Technology Research (IJSETR)*, 3(4), 1122-1128.
- Anuta, P. E. (1969). Regulation of multispectral video imagery. *Society of Photo-optical Instrumentation Engineers' Journal*, 7, 168-175.
- Anuta, P. E. (1970). Spatial registration of multispectral and multi-temporal digital imagery using fast fourier transformation. *IEEE Transactions on Geoscience Electronics*, 8(4), 353-368.
- Apicella, A., Kippenhan, J. S., & Nagel, J. H. (1989). Fast multi-modality image matching. *Medical imaging III: Image Processing, Proceedings*, 1092, 252-263.

- Apicella, A., Nagel, J. H., & Dura, R. (1988). Fast multimodality image matching. *Proceedings of the Annual International Conference of IEEE Engineering in Medicine and Biology Society*, 10, 414-415.
- Appledorn, C. R. (1996). A new approach to the interpolation of sampled data. *IEEE Transactions on Medical Imaging*, 15, 369–376.
- Armagam, E., Nuno, G., & Rafael, G. (2013). Fast topology estimation for image mosaicing using adaptive information thresholding. *Robotics and Autonomous Systems*. 61, 125-136.
- Armangue, X., Pages, J., Salvi, J., & Batlle, J. (2001). Comparative survey on fundamental matrix estimation. *Proceedings of International Conference on Image Processing*, 2, 209-212.
- Arun, P.V., & Katiyar, S. K. (2013). An Investigation towards wavelet based optimization of Automatic Image Registration Techniques. *Computer Vision and Pattern Recognition*, 1-11 Retrieved from <https://arxiv.org/ftp/arxiv/papers/1303/1303.6927.pdf>
- Ashburner, J. (2007). A fast diffeomorphic image registration algorithm. *Neuroimage*, 38, 95-113.
- Atiquzzaman, M. (1992). Multiresolution hough transform-An efficient method of detecting pattern or images. *IEEE transactions in pattern analysis and machine intelligence*, 14(11), 1090-1095.
- Ayman, F. H., Young, R., & Morgan, M. (2003). Automatic matching and three dimensional reconstruction of free form linear features from stereo images. *Photogrammetric Engineering & Remote Sensing*, 69(2), 189-197.
- Banerjee, S., Mukherjee, D.P., & Majumdar, D.D. (1995). Point landmarks for registration of CT and NMR images, *Pattern Recognition Letters*, 16, 1033–1042.
- Barbara, Z., & Flusser, J. (2003). Image registration methods: A survey. *Image and vision Computing*, 21, 977-1000.
- Barnea, D. J., & Silverman, H. F. (1992). a class of algorithms for fast digital image registration. *IEEE Transaction in Computation*, 21(2), 179-186.
- Barrodale, I., Skea, D., Berkley, M., Kuwahara, R., & Poeckert, R. (1993). Warping digital images using thin plate splines, *Pattern Recognition*, 26, 375–376.
- Barrow, H.G., Tenenbaum, J.M., Bolles, R.C., & Wolf, H.C. (1977). Parametric correspondence and chamfer matching: Two new techniques for image matching. *Proceedings of the Fifth International Joint Conference on Artificial Intelligence*, 659–663.
- Bay, H., Ess, A., Tuytelaars, T., & Van, G. L. (2008). Speeded Up Robust Features (SURF). *Computer Vision and Image Understanding*, 110(3), 346-359.
- Bay, H., Tuytelaars, T., & Van Gool, L. (2006). SURF: Speeded Up Robust Features. In A. Leonardis, H. Bischof, and A. Pinz (Eds.), *Proceedings of the Ninth European Conference on Computer Vision* (pp. 404-417), Part I, LNCS 3951. Berlin, Germany: Springer-Verlag Berlin Heidelberg.

- Ben, G., Darko, Z., Nikos, K., Nikos, P., & Nassir, N. (2009). Linear image registration through MRF optimization. Retrieved on 18/03/2018 from <http://www.campar.in.tum.de/pub/glocker2009sibi/glocker2009isbi.pdf>.
- Bhattacharya, D., & Sinha, S. (1997). Invariance of stereo images via theory of complex moments, *Pattern Recognition*, 30, 1373–1386.
- Bhavani, S.Y. (2005). Self-calibration based on robust point matching and fundamental matrix estimation, ECSE 6650 Computer Vision Final Project.
- Bing, W., & Xiaoli, W. (2013). Video serial images registration based on FBM algorithm. *Research Journal of Applied Sciences, Engineering and Technology* 5(17), 4274 – 4278.
- Bolarinwa, O. O. (2017). Development of a semi-automated digital stereo comparator. Unpublished MSc thesis submitted to the Department of Surveying and Geoinformatics, University of Lagos, Akoka-Lagos.
- Bracewell, R.N. (1965). *The Fourier transform and its applications*, New York, NY: McGraw-Hill.
- Brivio, P.A., Ventura, A.D., Rampini, A., & Schettini, R. (1992). Automatic selection of control points from shadow structures, *International Journal of Remote Sensing*, 13, 1853–1860.
- Bro-Nielsen, M., & Gramkow, C. (1996). Fast fluid registration of medical images, *In Proceedings Visualization in Biomedical Computing*, Hamburg, Germany, 267–276.
- Brown, L. G. (1992). A survey of image registration technique. *ACM Computing Surveys*, 24(4), 325-376.
- Brown, M., & Lowe, D. G. (2007). Automatic panoramic image stitching using invariant features. *International Journal of Computer Vision*, 74(1), 59–73.
- Bruce, D. L., & Takeo, K. (1981). An alternate image registration technique with an application to stereo vision. *Proceedings of image understanding workshop*, 121-130.
- Burr, D. J. (1981). A dynamic model registration. *Computer Vision Graphics and Image Processing*, 15, 102-112.
- Cain, S.C., Hayat, M. M., & Armstrong, E. E. (2001). Projection-based image registration in the presence of fixed-pattern noise. *IEEE Transactions on Image Processing*, 10, 1860–1872.
- Calvin, J. M., Gotsman, C. J., & Zheng, C. (2019). Global optimization for image registration. AIP Conference Proceedings, 2070, doi: <https://doi.org/10.1063/1.5089975>
- Canny, J. (1986). A computational approach to edge detection. *IEEE Transactions on Pattern Analysis and Machine Intelligence*, 8, 679–698.
- Carlo, T. (2017). The eight-point algorithm. Study notes Retrieved on 13/01/2018 from <https://www2.cs.duke.edu/fall17/notes>.

- Castillo, C. D., & Jacobs, D. W. (2009). Using stereo matching with general epipolar geometry for 2D face recognition across pose. *IEEE Transactions on Pattern Analysis and Machine Intelligence*, 31(12), 2298-2304.
- Chen-Yu, L., Ashish T., & Mohan, M. T (2013). A novel approach for driver eye gaze estimation using epipolar geometry. *UCSD ECE 285 Technical Report*. Winter 2013.
- Chung-Hsien, T., & Yu-Ching, L., (2017). An accelerated image matching technique for UAV orthoimage registration. *ISPRS Journal of Photogrammetry and Remote Sensing*, 128, 130–145.
- Cideciyan, A. V., Jacobson, S. G., Kemp, C. M., Knightton, R. W., & Magel, J. H. (1992). Registration of high resolution images of the retina. *Proceedings of SPIE Medical Imaging VI: Image Processing*, 1652, 310–322.
- Coello, C. A. C. (1998). A comprehensive survey of evolutionary-based multi objective optimization techniques. *Knowledge and Information Systems*, 1, 269–308.
- Collignon, A., Maes, F., Delaere, D., Vandermeulen, D., Suetens, P., & Marchal, G. (1995). Automated multimodality image registration using information theory. *Information Processing in Medical Imaging*, 3, 263–274.
- Crum, W. R., Hartkens, T., & Hill, D. L. G. (2004). Non-rigid image registration: theory and practice. *The British Journal of Radiology*, 77, 140-153.
- Dai, Y. H. (2003). A family of hybrid conjugate gradient methods for unconstrained optimization, *Mathematics of Computation*, 72(243), 1317–1328.
- Dalley, G., & Flynn, P. (2002). Pair-wise range image registration: a study in outlier classification. *Computer Vision and Image Understanding*, 87, 104-112, doi:10.1006/cviu.2002.0986.
- Daniel, F. (2013). *Robust image registration for improved clinical efficiency using local structure analysis and model-based processing*. Linköping University, Sweden: LiU-Tryck Press.
- Daoping, Z., & Ke, C. (2018). A novel diffeomorphic model for image registration and its algorithm. *Journal of Mathematical Imaging and Vision*, 60, 1261–1283, <https://doi.org/10.1007/s10851-018-0811-3>
- Dare, P., & Dowman, I. (2000). A new approach to automatic feature-based registration of SAR and SPOT images. *International Archives of Photogrammetry and Remote Sensing*, XXXIII, Part B, 125-130.
- Darko, Z., Ben, G., Oliver, K., Martin, G., Nikos, K., Ali, K., Nikos, P., & Nassir, N. (2010). Linear intensity-based image registration by Markov random fields and discrete optimization. *Medical Image Analysis*, 14, 550-562.
- David, M. M., Nathan, S. N., & Jacqueline, L. M. (1999). Efficient algorithms for robust feature matching. *Pattern Recognition*. 32, 17-38.
- David, M. M., Nathan, S. N., Christine, D. P., Ruth, S., & Angela, Y. W. (2014). On least trimmed squares estimator. *Algorithmica*, 69, 148-183, doi: 10.1007/s00453-012-9721-8.

- De-Castro, E., & Morandi, C. (1987). Registration of translated and rotated images using finite Fourier transforms. *IEEE Transactions on Pattern Analysis and Machine Intelligence*, 9, 700-703.
- De-Castro, E., Cristini, G., Martelli, A., Morandi, C., & Vascotto M. (1987). Compensation of random eye motion in television ophthalmoscopy: Preliminary results. *IEEE Transactions on Medical Imaging*, 6, 74-81.
- Diaa, E. M. N., & Hany H. A. (2007). A Neural network system for matching dental radiographs. *The Journal of the Pattern Recognition Society*, 65-79.
- Diana, E. B. O. (2005). Using epipolar geometry in stereo image analysis. Unpublished MSc thesis submitted to the International Centre of Theoretical Physics, Scuola Internazionale Superiore di Studi Avanzatic, Trieste, Italy.
- Diego, S. (2006). Optimization based image registration. ELEC 503- Term Project, August 11.
- Dilipsinh, B., Mahasweta, J., & Vikram, A. (2014). A study of features extraction techniques for image mosaicing. *International Journal of Innovative Research in Computer and Communication Engineering*, 2(3), 3432-3437.
- Domke, J., & Aloimonos, Y. (2006a). A probabilistic framework for correspondence and egomotion, *Proceedings of the Workshop on Dynamical Vision*, 232-242.
- Domke, J., & Aloimonos, Y. (2006b). A probabilistic notion of correspondence and the epipolar constraint, *Proceedings of Third International Symposium on 3D Data Processing, Visualization, and Transmission*, 41-48.
- Dowman, I. J. (1998). Automating image registration and absolute orientation solutions and problems. *Photogrammetric Record*, 16(91), 5-18.
- Dubrofsky, E. (2009). Homography estimation. Unpublished MSc thesis submitted to the faculty of graduate studies (computer science), the University of British Columbia (Vancouver).
- Ehab, S., & Murad, Q. (2017). Recent advances in features extraction and description algorithms: a comprehensive survey. *18th International Conference on Industrial Technology (ICIT)*, Toronto, Canada.
- Eldad, H., & Modersitzki, J. (2006). Intensity gradient based registration and fusion of multi-modal images. In R. Larsen, M. Nielsen, and J. Sporring (Eds.), *Medical Image Computing and Computer – Assisted Intervention* (pp. 726-733). Berlin, Germany: Springer-Verlag Berlin Heidelberg.
- El-gayar, M. M., Soliman, H., & Meky, N. (2013). A comparative study of image low level feature extraction algorithms. *Egyptian Informatics Journal*, 14(2), 175-181.
- Feng, C. L., & Hung, Y. S. (2003). A robust method for estimating the fundamental matrix. *Proc. VIIth Digital Image Computing: Techniques and Applications*, 633-642.
- Feng, Y., Lawrence, J., Cheng, K., Montgomery, D., Forrest, L., McLaren D. B., McLaughlin S, Argyle D. J., & Nailon W. H. (2016). Image registration in veterinary radiation oncology:

- indications, implications, and future advances. *Veterinary Radiology and Ultrasound*, 57(2), 113-123, doi: 10.1111/vru.12342.
- Fereshteh, S. B., Ahmadrza, B., Reihaneh, R., Zeyun, Y., & Roshan, M. D. (2018). Multi-modal medical image registration with full or partial data: a manifold learning approach. *Journal of Imaging*, 5(5), doi:10.3390/jimaging5010005
- Fischer, B., & Modersikzi, J. (2006). Image fusion and registration – a variational approach. *Computational science and high performance computing II*, 91, 193-203. Retrieved from <http://www.math.uni-luebeck.de/SAFIR>.
- Fischler, M. & Bolles, R. C. (1981). Random sample consensus: a paradigm for model fitting with applications to image analysis and automated cartography. *Communications of the ACM*, 24(6), 381–395.
- Fitzpatrick, J. M., & West, J. B. (1998). A blinded evaluation and comparison of image registration methods. empirical evaluation techniques in computer vision. In Kevin. W, Bowyer and P. Jonathan Phillips (Eds.), *Institute of Electrical and Electronics Engineer*, Los Alamitos, ICA: Society Press.
- Fitzpatrick, J. M., Pickens III, D. R., Grefenstette, J. J., Price, R. P., & James, A. E. Jr. (1987). Technique for automatic motion correction in digital subtraction angiography. *Optical Engineering*, 26, 1085- 1093.
- Flusser, J. (1994). A moment-based approach to registration of images with affine geometric distortion. *IEEE Transaction on Geoscience and Remote Sensing*, 32(1), 382– 387.
- Fonseca, L. M. G., & Manjunath, B. S. (1996). Registration techniques for multi sensor remotely sensed imagery. *Photogrammetric Engineering and Remote Sensing*, 56(2), 1049–1056.
- Forkuo, E.K. (2008). Digital terrain modeling in a GIS environment. *The International archives of the Photogrammetric, Remote Sensing and Spatial Information Sciences*, XXXVII (B2). Beijing 2008.
- Frederick, M., Collignon, A., Vandermeulen, D., Marchal, G., & Suetens, P. (1997). Multimodality image registration by maximization of mutual information. *IEEE Transaction on Medical Imaging*, 16(2), 187-198.
- Frederik, M., Vandermeulen D., & Suetuns, P., (2003). Medical image registration using mutual information. *Proceedings of the Institute of Electrical and Electronics Engineers' Conference*, 91(10), 1699-1722.
- Fusiello, A., Trucco, E., & Verri, A. (2000). A compact algorithm for rectification of stereo pairs. *Machine Vision and Applications*, 12(1), 16-22.
- Gang, H., & Yun, Z. (2005). The image registration techniques for high resolution remote sensing image in hilly area. *Proceedings of ISPRS WG VIII/1, Joint Symposia URBAN – URS 2005*, XXXVI-8/W27, 14-16th March, 2005, Tempe, AZ, USA.
- George, W., & Siavash, Z. (2000). Robust image registration using log-polar transform. *Proceedings of IEEE International Conference on Image Processing*, September 2000.

- Gerlot, P., & Bizais, Y. (1987). Image registration: a review and a strategy for medical applications. In C. N. de Graaf and M. A. Viergever (Eds.), *Information processing in Medical Imaging* (pp. 81-89), New York, NY: Plenum Press.
- Gerlot, P., & Bizais, Y. (1992). Registration of multimodality medical images using a region overlap criterion. *Graphical Models and Image Processing*, 54, 396-406.
- Goshtasby, A. (1988). Registration of images with geometric distortions. *IEEE Transactions on Geoscience and Remote Sensing*, 26, 60-64.
- Goshtasby, A., Lawrence, S., Studholme, C., & Terzopoulos, D. (2003). Non-rigid image registration: Guest editor's Introduction. *Computer Vision and Image Understanding*, 89, 109 -113.
- Gruen, A.W. (1985). Adaptive Least Square Correlation: A powerful image matching techniques. *South African Journal of Photogrammetry, Remote Sensing and Cartography*, 14(3), 175-187.
- Guoyan, Z. (2010). Effective incorporating spatial information in a mutual information based 3D-2D registration of a CT volume to X-ray images. *Computerized Medical Imaging and Graphics*, 34, 553-562.
- Haber, E., & Modersitzki, J. (2006). Intensity gradient based registration and fusion of multi-modal images. *Medical image computing and computer-assisted intervention*, 46,292-299.
- Harris, C., & Stephens, M. (1988). A combined corner and edge detector. *Proceedings of the 4th Alvey Vision Conference*, 147-151.
- Hartley, R., & Zisserman, A. (2000). *Multiple view geometry in computer vision*. Cambridge, Massachusetts: Cambridge University Press.
- Hartley, R. (1999). Theory and practice of projective rectification. *International Journal of Computer Vision*, 35, 115-127.
- Hartley, R. I. (1992). Estimation of relative camera positions for uncalibrated cameras. *Proceeding of Second European Conference on Computer Vision, Lecture Notes in Computer Science*, 588, 579-587.
- Hartley, R. I. (1997). In defense of the eight-point algorithm. *IEEE Transactions on Pattern Analysis and Machine Intelligence*, 19 (6), 580-593.
- Hassaballah, M., Abdelmgeid, A. A., & Alshazly, H. A. (2016). Image features detection, description and matching. In A.I. Awad & M. Hassaballah (Eds.), *Image Feature Detectors and Descriptors, Studies in Computational Intelligence 630* (pp. 11-45). Switzerland: Springer International Publishing.
- Hassan, R., Zahra, K., & Collins, D.L. (2014). Self-similarity weighted mutual information: A new nonrigid image registration metric. *Medical Image Analysis*, 18, 343-358.
- He, M., Dai, Y., & Zhang, J. (2008). Image registration by integrating similarity and epipolar constraints. *Industrial Electronic and Applications. ICIEA 2008, 3rd IEEE Conference*, 3-5, 1870-1874, Singapore, doi: 10.1109/ICIEA.2008.4582844.

- Hector, F. G. G., Jose, L. M., & Johan, V. H. (2008). Image registration based on kernel-predictability. *Computer Vision and Image Understanding*, 112, 160-172.
- Herbin, M., Venot, A., Devaux, J. Y., Walter, E., Lebruchec, J. F., Dubertret, L., & Roucayrol, J. C. (1989). Automated registration of dissimilar images: Application to medical imagery. *Comput. Vision Graphics Image Processing*, 47, 77-88.
- Hiba, A. M. (2016). The image registration techniques for medical imaging (MRI-CT), *American Journal of Biomedical Engineering*, 6(2), 53-58, doi: 10.5923/j.ajbe.20160602.02.
- Hipwell, J. H., Vavourakis, V., Han, L., Mertzaniidou, T., Eiben, B., & Hawkes D. J. (2016). A review of biomechanically informed breast image registration. *Physics in Medicine and Biology*, 61(2), R1-R31, doi: 10.1088/0031-9155/61/2/R1.
- HO-Ming, C., Albert, C. S C., Simon, C. H. Y., Alexander N., & William M. W. (2003). Multi-modal image registration by minimizing Kullback – Leibler distance between expected and observed joint class histogram. In T. Dohi and R. Kikinis (Eds.), *Medical Image Computing and Computer – Assisted Intervention*, LNCS 2489, (pp. 525-532). Berlin, Germany: Springer-Verlag Berlin Heidelberg.
- Huzefa, F. N. (2005). Entropic graphs for image registration. Unpublished PhD thesis submitted to the Department of Biomedical Engineering, University of Michigan, United States of America.
- Jacqueline, L., Nathan, S. N., & Roger, D. E. (2012). *Image registration for remote sensing*. Cambridge, United Kingdom: Cambridge University Press.
- Jan, S., Tomas, K., Jan, F., & Libor, P. (2010). FGPA based speeded up robust features. The Gerstner Laboratory for Intelligent Decision Making and Control, Department of Cybernetics, Faculty of Electrical Engineering, Czech Technical University, Prague.
- Jawed, K., Morris, J., Khan, T., & Gimelfarb, G. (2009). Real time rectification for stereo correspondence. *International Conference on Computational Science and Engineering*, 2, 277-284.
- Jégou, H., Perronnin, F., Douze, M., Sánchez, J., Pérez, P., & Schmid, C. (2012). Aggregating local descriptors into a compact code. *IEEE Transaction on Pattern Analysis and Machine Intelligence*, 34(9), 1704–1716.
- Jing-Fu, H., Shang-Houg, L., & Chia-Ming, C. (2007). Robust fundamental matrix estimation with accurate outlier detection. *Journal of Information Science and Engineering*, 23, 1213 - 1225.
- Jinxiang, C., & Song, D. M. (1998). Robust epipolar geometry estimation using genetic algorithm. *Pattern Recognition Letters*, 19, 829 - 838.
- Joachim, B., Horst, B., Andreas, K., & Konrad, K. (2004). Robust and fully automated image registration using invariant features. *Proceedings of the ISPRS Congress, Commission VII, XXXV-B7*, July 12-23, Instabul, Turkey.
- Joseph, L., Susan, S., Young, R., & Gutierrez, O. (2011). *An iterative image registration technique using a scale-space model*. Department of Computer Science and Engineering, Texa A & M University, Technical report tamu – cs – tr – 2011 – 12 – 1.

- Juan, D. G. A. (2013). Multichannel image information similarity measures: application to colposcopy image registration. Unpublished PhD thesis submitted to Department of Cybernetics, Faculty of electrical Engineering, Czech Technical University in Prague.
- Juan, L., & Gwun, O. (2009). A comparison of SIFT, PCA-SIFT, and SURF. *International Journal of Image Processing*, 3(4): 143-152.
- Junck, L., Moen, J. G., Hutchins, G. D., Brown, M. B., & Kuhl, D. E. (1990). Correlation methods for the centering, rotation and alignment of functional brain images. *Journal of Nuclear Medicine*, 31, 1220-1226.
- Jurgen, A. D. (2011). *Robust estimation using least trimmed squares*. Institute for Economic Modelling, Oxford Martin School, Economics Dept., University of Oxford, UK.
- Kai, L., Yongsheng, Z., Zhenchao, Z., & Guangling, L. (2019). A coarse-to-fine registration strategy for multi-sensor images with large resolution differences. *Remote Sensing*, 11 (470), doi:10.3390/rs11040470
- Kanade, K., Jansa, J., & Kager, H. (1997). *Photogrammetry- advanced methods and applications*, Allemagne, Ferd. Dummlers Verlag, ISBN 3-427-78684-6.
- Kang, Z. (2008). Epipolar image generation and corresponding point matching from coaxial vehicle-based image. Delft, Netherland: Faculty of Aerospace Engineering Delft University of Technology, *ASPRS 2008 Annual Conference Portland, Oregon*.
- Kazhdan, M., Thomas, F., & Szymon, R. (2003). rotation invariant spherical harmonic representation of 3D shape descriptors. *Eurographics Symposium on Geometry Processing*. Edited by Kobbelt, L., Schröder, P., and Hoppe, H.
- Kerner, S., Kaufman, I., & Raizman, Y. (2016). Role of tie-points distribution in aerial photography. *The International Archives of the Photogrammetry, Remote Sensing and Spatial Information Science, the European Calibration and Orientation Workshop, EuroCOW, 10-12, Lausanne, Switzerland, XL(3/W4)*, 41-44.
- Kiefer, J., & Wolfowitz, J. (1952). Stochastic estimation of the maximum of a regression function, *Annals of Mathematical Statistics*, 23(3), 462–466.
- Klein, S. (2008). *Optimisation methods for medical image registration*. Utrecht University, the Netherlands: Uitgeverij BOX Press.
- Klein, S., Josien, P. W. P., Marius, S., & Max, A. V. (2009). Adaptive stochastic gradient descent optimisation for image registration. *International Journal of Computer Vision*, 81, 227-239.
- Kleissl, J. (2013). *Solar energy forecasting and resource assessment*, Cambridge, MA: Academic Press.
- Krishna, S., & Varghese, A. (2015). Feature based automatic multiview image registration. *International Journal of Computer Science and Software Engineering*, 4(11), 308-314.
- Kuijper, A. (2004). Mutual information aspects of scale space images. *Pattern Recognition*, 37, 2361–2373. Retrieved from <http://www.elsevier.com/locate/ymvis>.

- Langville, A. N., & Stewart, W. J. (2004). The kronecker product and stochastic automata networks. *Journal of Computational and Applied Mathematics*, 167(2), 429-447, doi:10.1016/j.cam.2003.10.101.
- Lehmann, T. M., Go'nnner, C., & Addendum K. (2001). B-spline interpolation in medical image processing, *IEEE Transaction on Medical Imaging*, 20, 660–665.
- Lesse, J. A., Novak, G. S., & Clark, B. B. (1971). An automatic technique for obtaining cloud motion from geosynchronous satellite data using cross correlation. *Methods of Application and Analysis*, 10, 110-132.
- Letser, H., & Arrige, S.R. (1999). A survey of hierarchical nonlinear medical image registration. *Pattern Recognition*, 129-149.
- Li, H., Manjunath, B. S., & Mitra, S. K. (1995). A contour based approach to multisensor image registration, *IEEE Trans. Image Processing*, 4, 320–334.
- Li, Y., Wang, S., Tian, Q., & Ding, X. (2015). A survey of recent advances in visual feature detection. *Neurocomputing*, 149, 736–751.
- Lin, H., Chuan, L., Dong, Z., & Simiao, F. (2011). The mutual information based correlation analysis between fault types and monitor data. *Procedia Engineering*, 15, 5268-5273.
- Lin, Q & Labuz, J. F. (2013). Fracture of sandstone characterized by digital image correlation. *International Journal of Rock Mechanics and Mining Sciences*, 60, 235-245, doi: 10.1016/j.ijrmms.2012.12.043.
- Lisa, T., & Ghassan, H. (2003). Medical image registration: a review. *Computer Methods in Biomechanics and Biomedical Engineering*, 17(2), 73-93, doi: 10.1080/10255842.2012.670855.
- Liu, A., Pizer, S., Eberly, D., Morse, B., Rosenman, J., Chaney, E., Bullitt, E., & Carrasco, V. (1994). Volume registration using the 3D core. In Robb, R. A. (Eds.), *Visualization in Biomedical Computing* (pp. 217-226), Vol. 2359, Bellingham, WA: SPIE Press.
- Lowe, D. G. (1999). Object recognition from local scale-invariant features. *Proceedings of the International Conference on Computer Vision*, 1150-1157.
- Lowe, D. G. (2004). Distinctive image features from scale invariant key points. *International Journal of Computer Vision*, 60(2), 91-110.
- Lu, Y., Gao, K., Zhang, T., & Xu, T. (2018). A novel image registration approach via combining local features and geometric invariants. *PLoS ONE* 13(1). Retrieved on 17/02/2018 from <https://doi.org/10.1371/journal.pone.0190383>.
- Ludovico, C. (2011). Algorithms for on-line image registration from Multiple views. Unpublished PhD thesis submitted to Department of Information Technology, University of Bologna, Italy. Cycle XXIII – ING – INF/05.
- Luong, V. N. D. (2009). Review and enhancement optimization methods in image registration. Unpublished MEng thesis submitted to the Department of Computing, Imperial College London.

- Maes, F., Collignon, A., Vandermeulen, D., Marchal, G., & Suetens, P. (1996). Multi-modality image registration by maximization of mutual information. In *Mathematical Methods in Biomedical Image Analysis* (14–22), Los Alamitos, CA: IEEE Computer Society Press.
- Maintz, J. B. A., van den Elsen, P. A., & Viergever, M. A. (1998). Comparison of edge-based and ridge-based registration of CT and MR brain images. *Medical Image Analysis*, 1, 151–161.
- Makela, T., Clarysse, P., Sipila, O., Pauna, N., Phan, Q. C., & Katila, T. (2002). A Review Cardiac Image Registration Methods. *IEEE Transactions on Medical Imaging*, 21(9), 1011-1021.
- Mallon, J., & Whelan, P. F. (2005). Projective rectification from the fundamental matrix. *Image and Vision Computing*, 23(7), 643–650.
- Mandava, V. R., Fitzpatrick, J.M., & Pickens III, D. R. (1989). Adaptive search space scaling in digital image registration. *IEEE Transaction on Medical Imaging*, 8, 251-262.
- Marco, Z. (2006). *Computational Methods for Automatic Image Registration*. A dissertation submitted in partial fulfilment of the requirement for the degree doctor of philosophy in Electrical and Computer Engineering, University of California.
- Marnak, S., Yashwant, H., Shuvra, S. B., & Raj, S. (2006). Reconfigurable image registration on FPGA Platforms. *Proceedings of the IEEE Biomedical Circuits and Systems Conference*, November 2006.
- Mason, G. O., & Wong, K. W. (1992). Image alignment by line triples. *Photogrammetric Engineering and Remote Sensing*, 58, 1329-1334.
- Matas, J., Chum, O., Urban, M., & Pajdla, T. (2004). Robust wide-baseline stereo from maximally stable extremal regions. *Image and Vision Computing*, 22(10):761-767.
- Md-Mashiur, R., & Zadidul, K. A. (2015). Comparative analysis of image registration using pixel, wavelet and translation method. *Electrical and Electronic Engineering*, 5(2), 23-33.
- Medha, V. W., Pradeep, M. P., & Hemant, K. A. (2002). Image registration techniques an overview. *International Journal of Signal Processing, Image Processing and Pattern Recognition*, 2(3), 11-27.
- Meyer, C. R., Boes, J. L., Kim, B., Bland, P. H., Zasadny, K. R., Kison, P. V., Koral, K. F., Frey, K. A., & Wahl, R. L. (2007). Demonstration of accuracy and clinical versatility of mutual Information for automatic multimodality image fusion using alpine and thin-plate spline warped geometric deformations. *Medical Image Analysis*, 1(2), 195-206.
- Mian, A. S., Bennamoun, M., & Owens, R. A. (2004). From unordered range images to 3D models. a fully automatic multiviews correspondence algorithm. *Proceedings of the Theory and Practice of Computer Graphics*, 0-7695-2137-1/04.
- Michael, I., & Shmuel, P. (1991). Improving resolution by image registration. *CVGIP: Graphical models and image processing*, 53(3), 231-239.
- Mohammad, R. K., & Somayeh, A. (2011). Analytical classification of multimodal image registration based on medical application. *International Journal of Advances in Engineering and Technology*, 1(4), 138-147.

- Moshfeghi, M. (1991). Elastic matching of multimodality medical images. *Graphical Models and Image Processing*, 53, 271-282.
- Mosienko, N. J. (1973). Experiences with the epipolar image correlation technique. Unpublished MEng thesis submitted to the Department of Surveying Engineering, University of New Brunswick, Canada.
- Mubarak, S. (1997). *Fundamentals of computer vision*. Orlando: Computer Science Department, University of Central Florida, 1-133.
- Nahla, I. J., & Monica, M. (2008). Application of fuzzy neural network for image tumor description. *World Academy of Science, Engineering and Technology*, 44, 18-31.
- Nathan, D. C., Noble, J. A., & David, J. H. (2009). A demon's algorithm for image registration with locally adaptive regularization. In G. Z. Yang (Eds.), *Medical Image Computing and Computer – Assisted Intervention, Part I, LNCS 5761* (pp. 574 – 581). Berlin, Germany: Springer – Verlag Berlin Heidelberg.
- Nemir, A., Wan, A., & Wan, K. A. (2012). MRI monomodal feature-based registration based on the efficiency of multiresolution representation and mutual information. *American Journal of Biomedical Engineering*, 2(3), 98-104, doi: 10.5923/j.ajbe.20120203.02.
- Nick, M., & Heinz, R. (1996). An image matching scheme using a hybrid feature and area based approach. *International Archives of Photogrammetry and Remote Sensing*, XXXI (B3), 703-709.
- Nister, D. (2003). Pre-emptive RANSAC for live structure and motion estimation. *Proceedings of IEEE International Conference on Computer Vision*, 199-206.
- Nixon, M. S., & Aguado, A. S. (2008). *Feature extraction and image processing*. Oxford, OX: Elsevier Press.
- Nzelibe, I. U. (2014). A MATLAB program for conjugate point search on a pair of overlapping photographs using epipolar correlation. Unpublished MSc thesis submitted to the Department of Surveying and Geoinformatics, University of Lagos, Akoka-Lagos.
- Olaleye, J. B. (2010). Mapping from images by vector photogrammetry, Unpublished Series in Geoinformatics, Lecture Note 10-1, Dept. of Surveying and Geoinformatics, University of Lagos.
- Olaleye, J. B., Ajayi O. G., Omogunloye, O. G., Odumosu, J. O., & Okorochoa C. V. (2015). Automatic registration of simultaneously overlapping images. *NED University Journal of Research - Applied Sciences*, XII (4), 53-66.
- Panchal, P. M., Panchal, S. R., & Shah, S. K. (2013). A comparison of SIFT and SURF. *International Journal of Innovative Research in Computer and Communication Engineering*, 1(2), 323-327.
- Peli, E., Augliere, R. A., & Timberlake, G. T. (1987). Feature based registration of retinal images. *IEEE Transactions on Medical Imaging*, 6, 272-278.

- Pellejero, O. A., Sagues, C., & Guerrero, J. J. (2004). Automatic computation of the fundamental matrix from matched lines. *Current Topics in Artificial Intelligence*, LNSC-LNAI 3040, 197-206.
- Peter, J. K., & Semhill, P. (2003). Image registration for MRI. *Modern Signal Processing MSRI publications*, 46, 1-14.
- Peter, Z., Murray, E. A., & Jiankang, S. (2008). Nonlinear registration using variational principle for mutual information. *Pattern Recognition*, 41, 2493–2502.
- Pluim, J.P.W., Maintz, J.B.A., & Viergever, M.A. (2000). Interpolation artefacts in mutual information based image registration. *Computer Vision and Image Understanding*, 77, 211-232, doi:10.1006/cviu.1999.0816.
- Pluim, J.P.W., Maintz, J.B.A., & Viergever, M.A. (2001). Mutual information matching in multiresolution contexts. *Image and Vision Computing*, 19, 45–52.
- Potuckova, M. (2004). Image matching and its applications in photogrammetry. Unpublished PhD thesis submitted to the Faculty of Civil Engineering, Technical University in Prague, Czech Republic.
- Prachya, C. (1999). High performance automatic image registration for remote sensing. Unpublished PhD thesis submitted to the George Mason University, Fairfax, Virginia.
- Pratt, W. K. (1974). Correlation techniques for image registration. *IEEE Transactions on Aerospace Electronic systems*, 10(3), 353-358.
- Press, W. H., Teukolsky, S. A., Vetterling, W. T., & Flannery, B. P. (1992). *Numerical Recipes in C*, (2nd ed.). Cambridge: Cambridge University Press.
- Rania, H., Zhou, W., & Magdy, S. (2009). Multi-sensor image registration based on local phase coherence. *IEEE International Conference on Image processing*, Cairo, Egypt.
- Rittavee, M., Yuan, F. Z., & Robert, L. E. (2009). Image registration using adaptive polar transform. *IEEE Transaction on Image Processing*, 18(10), 2340-2354, doi: 10.1109/TIP.2009.2025010.
- Robbins, H., & Monro S. (1951). A stochastic approximation method, *Annals of Mathematical Statistics*, 22(3), 400-407.
- Rousseeuw, P. J., & van Driessen, K. (2006). Computing LTS regression for large data sets. *Data mining and Knowledge Discovery*, 12, 29-45.
- Scharstein, D., & Szeliski, R. (2002). A taxonomy and evaluation of dense two-frame stereo correspondence algorithms, *International Journal of Computer Vision*, 47(1/2/3), 7-42.
- Schenk, T., Li, J., & Toth, C. (1991). Toward an autonomous system for orienting digital stereo pairs. *Photogrammetric Engineering and Remote Sensing*, 57, 1057–1064.
- Shih-Ming, J. (2012). Technique of image registration in digital image processing – A review. *International Journal of Information Technology and Knowledge Management*, 5(2), 239 – 243.

- Shuto, L., Jinglin, P., James, T., & Kwok, J. Z. (2006). Multimodal registration using Discrete Wavelet Frame Transform. *The 18th International Conference on Pattern recognition*, 3, 880
- Sindhu, M. G. (2014). Classification of image registration techniques and algorithms in digital image processing- a research survey. *International Journal of Computer Trends and Technology*, 15(2), 78-82.
- Sombir, S. B., Bhumika, G., & Pirvez, R. (2014). Image registration concepts and techniques: a review. *International Journal of Engineering Research and Applications*, 4(4), 30-35.
- Stefan, P., Stefanos, Z., Christian, L., & Daniel, R. (2014). A robust similarity measure for non rigid image registration with outliers. *Biomedical Imaging (ISBI), IEEE 11th International Symposium*, 568-571, doi: 10.1109/ISBI.2014.6867934.
- Steiner, D., & Kirby, M. E. (1977). Geometrical referencing of LANDSAT images by affine transformation and overlaying of map data. *Photogrammetria*, 33, 54-75.
- Strutz, T. (2016). *Data Fitting and Uncertainty* (2nd ed.). Berlin, Germany: Springer Vieweg Verlag.
- The´venaz, P., & Unser, M. (1997). Spline pyramids for intermodal image registration using mutual information. *Proceedings Wavelet- Applications in signal and image processing (of SPIE) V*, 3169, 236-247.
- The´venaz, P., Blu, T., & Unser, M. (2003). *Image interpolation and resampling*, Handbook of Medical Image Processing. New York, NY: Academic Press.
- Thitipon, C., Guoliang, F., & Stephen, R. F. (2006). Hybrid retinal image registration. *IEEE Transactions on Information Technology in Biomedicine Journal*, 10(1), 129-142.
- Ting, X. L., & Heng, H. C. (2016). Medical image registration based on an improved ant colony optimization Algorithm. *International Journal of Pharmacy, Medicine and Biological Sciences*, 5(1), 17-22.
- Torr, P. H. S., & Zisserman, A. (1997). Performance characterization of fundamental matrix estimation under image degradation. *Machine Vision and Applications*, 9, 321-333.
- Tseng, Y H, Tzen, J. J, Tang, K. P., & Lin, S. H (1997). Image to image registration by matching area features using fourier descriptor and neural networks. *Photogrammetric Engineering and Remote Sensing*, 63(8), 975-983.
- Tuytelaars, T., & Mikolajczyk, K. (2007). Local invariant feature detectors: a survey. *Foundation and Trends in Computer Graphics and Vision*, 3(3), 177–280, doi: 10.1561/0600000017.
- Tuytelaars, T. (2006). *Local Invariant Features: What? Why? When? How?* ECCV Tutorial Delivered on May 7th, 2006. Retrieved from Kuleuven Website: <http://homes.esat.kuleuven.be/~tuytelaa/ECCV06tutorial.html>
- van den Elsen, P. A. (1994). Retrospective fusion of CT and MR brain images using mathematical operators. In *Association for the Advancement of Artificial Intelligence (AAAI) Symposium on Medical Applications of Computer Vision*, 30–33. Stanford University, Stanford, CA.

- van den Elsen, P. A., Maintz, J. B. A., Pol, E. J. D., & Viergever, M. A. (1995). Automatic registration of CT and MR brain images using correlation of geometrical features. *IEEE Transactions in Medical Images*, 14, 384–398.
- Van, W. P., & Stein M. (1977). A LANDSAT digital image rectification system. *IEEE Transactions on Geosciences and Electronics*, 15, 130-137.
- Venot, A., & Leclerc, V. (1984). Automated correction of patient motion and gray values prior to subtraction in digitized angiography. *IEEE Transactions on Medical Imaging*, 3, 179-186.
- Venot, A., Devaux, J. Y., Herbin, M., Lebruchec, J. F., Dubertret, L., Raulo, Y., & Roucayrol, J. C. (1988). An automated system for the registration and comparison of photographic images in medicine. *IEEE Transactions on Medical Imaging*, 7, 298-303.
- Venot, A., Liehn, J. C., Lebruchec, J. F., & Roucayrol, J. C. (1986). Automated comparison of scintigraphic images. *Journal of Nuclear Medicine*, 27, 1337-1342.
- Viola, P., & Wells III, W. M. (1995). Alignment by maximization of mutual information. *In Proceedings of IEEE International Conference on Computer Vision*, Los Alamitos, CA, 16-23.
- Vivek, K. G., & Kanchan, C. (2014). An analytical study of SIFT and SURF in image registration. *International Journal of Engineering and Innovative Technology*, 3(9), 130-134.
- Wachowiak, M., & Peters, T. (2006). High-performance medical image registration using new optimization techniques. *IEEE Transactions on Information Technology in Biomedicine*, 10(2), 344-353.
- Walia, E., & Suneja, A. (2010). A conceptual study on image matching techniques. *Global Journal of Computer Science and Technology*, 10(12), 83-88.
- Wan, R., & Li, M. (2003). An overview of medical image registration. *Proceedings of the Fifth International Conference on Computational Intelligence and Multimedia Applications*, 385-390.
- Wells III, W.M., Viola, P., Astumi, H., Nakajima, S., & Kikinis, R., (1996). Multi-modal volume registration by maximization of mutual information. *Medical Image Analysis*, 1(1), 35-51.
- Whitehead, A., & Roth, G. (2004). Estimating intrinsic camera parameters from the fundamental matrix using an evolutionary approach. *EURASIP Journal on Applied Signal Processing*, 8, 1113–1124.
- Wong, R. Y. (1977). Sensor transformations. *IEEE Transactions on Systems, Man, and Cybernetics*, 7, 836-841.
- Woods, R. P. (2009). Within-modality registration using intensity-based cost functions. In I. N. Bankman (Eds.), *Handbook of Medical Image Processing and Analysis* (pp. 605-611). Burlington, VT: Academic Press.
- Xiang, H., (2014). *Non-rigid image registration problem using fluid dynamics and mutual information*, New York, NY: University School of Medicine Press.

- Xiaofeng, F. (2011). Automatic registration of multimodal airborne imagery. Unpublished dissertation submitted in partial fulfillment of the requirements for the degree of Doctor of Philosophy (PhD) in the Chaster F. Carlson center for Imaging Science, Rochester Institute of Technology, United Kingdom.
- Xiaolong, D., & Siamak, K. (1999). A feature based image registration algorithm using improved chain-code representation combined with invariant moments. *IEEE Transactions on Geoscience and Remote Sensing*, 37(5), 2351-2362.
- Xiaoman, L., Guoman, H., Lei, P., & Zheng, Z. (2008). Study on airborne SAR image matching using epipolar geometry. *The International Archives of the Photogrammetry, Remote Sensing and Spatial Information Sciences*, XXXVIII(B1), 399-402.
- Xu, Z., & Li, Z. (2000). Least median of squares matching for automated detection of surface deformations. *International Archives of Photogrammetry and Remote Sensing*, XXXVII(B3), 1000-1007.
- Yanagisawa, M., Shigemitsu, S., & Akatsuka T. (1984). Registration of locally distorted images by multi window pattern matching and displacement interpolation: The proposal of an algorithm and its application to digital subtraction angiography. *In Proceedings of the 7th International Conference on Pattern recognition*, 1288-1291.
- Yeqing, L, Chen, C., Fei, Y., & Junzhou, H. (2015). Deep sparse representation for robust image registration. *The IEEE Conference on Computer Vision and Pattern Recognition (CVPR)*, 4894-4901.
- Yoshinori, D., Toshiyuki, H., Henry, J., & Tomoyuki, N. (2002). A method for creating mosaic images using voronoi diagrams. *European Association of Computer Graphics (Eurographics) Conference*, 1-8. Retrieved from http://nis-ei.eng.hokudai.ac.jp/~doba/papers/egshort02_mosaic.pdf
- Yu, J. J. H., Hung, B.N., & Liou, C. L. (1989). Fast algorithm for digital retinal image alignment. *Proceedings of the Annual International Conference of IEEE Engineering in Medicine and Biology Society*, 11, 374-375.
- Zhang, P. F., Li, X. Y., & Ma, L. (2014). Grid computing based on game optimization theory for networks scheduling. *Journal of Network and Computer Applications*, 9(5), 1295-1300.
- Zhengyou, Z. (1998). Determining the epipolar geometry and its uncertainty: a review. *International Journal of Computer Vision*, 27(2), 161-198.
- Zhiyong, G., Bin, G., & Jiarui, L. (2008). Monomodal image registration using mutual information-based methods. *Image and Vision Computing*, 26, 164-173, doi:10.1016/j.imavis.2006.08.002.
- Zhou, F., Zhou, C., & Zheng, Q. (2015). Method for fundamental matrix estimation combined with feature lines. *Neurocomputing*, 160, 300-307.
- Zichun, Z., G., Yiqi, C., Yin, Y., Jing, W., Xun, J., & Weihua, M. (2016). 3D-2D deformable image registration using feature based nonuniform meshes. *BioMed Research International*, 1-19, doi: 10.1155/2016/4382854.

APPENDIX A

Table A1: Image coordinates of associated image pairs automatically obtained using Modified Harris Corner Detector algorithm on google earth image pairs.

ID	Image location of conjugate points in Image A		Image location of conjugate points in Image B		Residuals
	x (Pixels)	y (Pixels)	x (Pixels)	y (Pixels)	Signed Distance (Pixels)
Pt 1	598.000	313.000	354.000	315.000	-0.0001
Pt 2	719.000	612.000	476.000	614.000	0.0034
Pt 3	403.000	9.000	159.000	10.000	0.0020
Pt 4	412.000	6.000	168.000	8.000	-0.0010
Pt 5	430.000	7.000	186.000	7.000	0.0049
Pt 6	675.000	613.000	431.000	615.000	-0.0003
Pt 7	314.000	12.000	70.000	14.000	-0.0008
Pt 8	463.000	11.000	219.000	13.000	-0.0010
Pt 9	485.000	15.000	241.000	17.000	-0.0010
Pt 10	700.000	16.000	456.000	17.000	0.0025
Pt 11	666.000	613.000	422.000	615.000	-0.0003
Pt 12	645.000	613.000	401.000	615.000	-0.0004
Pt 13	642.000	19.000	398.000	22.000	-0.0041
Pt 14	685.000	21.000	441.000	23.000	-0.0008
Pt 15	636.000	613.000	392.000	615.000	-0.0004
Pt 16	627.000	613.000	383.000	615.000	-0.0004
Pt 17	603.000	613.000	360.000	615.000	0.0031
Pt 18	254.000	28.000	10.000	30.000	-0.0005
Pt 19	339.000	28.000	95.000	29.000	0.0021
Pt 20	519.000	27.000	275.000	28.000	0.0021
Pt 21	603.000	25.000	359.000	26.000	0.0023
Pt 22	711.000	23.000	467.000	25.000	-0.0007
Pt 23	766.000	24.000	522.000	26.000	-0.0005
Pt 24	434.000	613.000	190.000	615.000	-0.0005
Pt 25	390.000	611.000	146.000	613.000	-0.0005
Pt 26	357.000	612.000	114.000	614.000	0.0031
Pt 27	286.000	33.000	42.000	35.000	-0.0006
Pt 28	330.000	613.000	87.000	615.000	0.0032
Pt 29	535.000	32.000	291.000	33.000	0.0022
Pt 30	283.000	613.000	38.000	615.000	-0.0038
Pt 31	602.000	32.000	359.000	34.000	0.0020
Pt 32	697.000	32.000	452.000	34.000	-0.0036
Pt 33	775.000	31.000	531.000	33.000	-0.0004
Pt 34	434.000	36.000	190.000	38.000	-0.0009

ID	Image location of conjugate points in Image A		Image location of conjugate points in Image B		Residuals
	x (Pixels)	y (Pixels)	x (Pixels)	y (Pixels)	Signed Dist (Pixels)
Pt 35	639.000	39.000	396.000	41.000	0.0021
Pt 36	733.000	36.000	489.000	38.000	-0.0006
Pt 37	269.000	42.000	25.000	44.000	-0.0005
Pt 38	306.000	45.000	64.000	46.000	0.0080
Pt 39	414.000	43.000	171.000	45.000	0.0020
Pt 40	462.000	44.000	218.000	46.000	-0.0009
Pt 41	613.000	45.000	370.000	47.000	0.0021
Pt 42	562.000	609.000	318.000	611.000	-0.0005
Pt 43	552.000	609.000	309.000	611.000	0.0030
Pt 44	497.000	51.000	253.000	52.000	0.0022
Pt 45	536.000	610.000	292.000	612.000	-0.0005
Pt 46	621.000	52.000	377.000	53.000	0.0024
Pt 47	650.000	49.000	406.000	51.000	-0.0007
Pt 48	525.000	610.000	281.000	611.000	0.0026
Pt 49	515.000	609.000	271.000	611.000	-0.0005
Pt 50	448.000	610.000	204.000	612.000	-0.0005
Pt 51	426.000	56.000	182.000	58.000	-0.0008
Pt 52	755.000	602.000	511.000	603.000	0.0034
Pt 53	628.000	55.000	384.000	57.000	-0.0007
Pt 54	699.000	53.000	456.000	54.000	0.0056
Pt 55	663.000	601.000	419.000	603.000	-0.0003
Pt 56	562.000	602.000	318.000	604.000	-0.0005
Pt 57	372.000	62.000	128.000	64.000	-0.0007
Pt 58	433.000	59.000	189.000	60.000	0.0022
Pt 59	554.000	602.000	310.000	604.000	-0.0005
Pt 60	527.000	601.000	283.000	603.000	-0.0005
Pt 61	513.000	602.000	269.000	604.000	-0.0005
Pt 62	496.000	602.000	252.000	604.000	-0.0005
Pt 63	354.000	70.000	110.000	72.000	-0.0006
Pt 64	647.000	65.000	403.000	67.000	-0.0007
Pt 65	658.000	67.000	414.000	69.000	-0.0006
Pt 66	419.000	602.000	175.000	605.000	-0.0034
Pt 67	348.000	601.000	104.000	603.000	-0.0003
Pt 68	285.000	602.000	41.000	604.000	-0.0002
Pt 69	591.000	593.000	347.000	595.000	-0.0004
Pt 70	769.000	74.000	525.000	75.000	0.0031
Pt 71	328.000	82.000	84.000	84.000	-0.0005
Pt 72	336.000	77.000	93.000	78.000	0.0053
Pt 73	418.000	78.000	172.000	80.000	-0.0066
Pt 74	450.000	594.000	206.000	596.000	-0.0005

ID	Image location of conjugate points in Image A		Image location of conjugate points in Image B		Residuals
	x (Pixels)	y (Pixels)	x (Pixels)	y (Pixels)	Signed Dist (Pixels)
Pt 75	739.000	82.000	496.000	83.000	0.0059
Pt 76	358.000	83.000	114.000	85.000	-0.0006
Pt 77	374.000	83.000	129.000	86.000	-0.0065
Pt 78	542.000	588.000	298.000	590.000	-0.0004
Pt 79	504.000	588.000	260.000	590.000	-0.0005
Pt 80	433.000	589.000	189.000	591.000	-0.0004
Pt 81	657.000	83.000	415.000	85.000	0.0053
Pt 82	686.000	84.000	442.000	86.000	-0.0005
Pt 83	354.000	587.000	111.000	589.000	0.0032
Pt 84	313.000	590.000	69.000	592.000	-0.0002
Pt 85	427.000	91.000	183.000	93.000	-0.0007
Pt 86	278.000	587.000	34.000	588.000	0.0027
Pt 87	574.000	91.000	331.000	93.000	0.0023
Pt 88	583.000	94.000	339.000	96.000	-0.0007
Pt 89	558.000	584.000	314.000	585.000	0.0027
Pt 90	482.000	585.000	238.000	587.000	-0.0005
Pt 91	290.000	95.000	46.000	98.000	-0.0032
Pt 92	440.000	581.000	196.000	583.000	-0.0004
Pt 93	335.000	97.000	91.000	98.000	0.0024
Pt 94	382.000	96.000	138.000	98.000	-0.0006
Pt 95	443.000	98.000	199.000	100.000	-0.0007
Pt 96	396.000	586.000	151.000	588.000	-0.0039
Pt 97	272.000	584.000	28.000	586.000	-0.0001
Pt 98	546.000	98.000	301.000	100.000	-0.0036
Pt 99	739.000	100.000	494.000	103.000	-0.0066
Pt 100	273.000	102.000	30.000	104.000	0.0027
Pt 101	360.000	105.000	116.000	106.000	0.0024
Pt 102	743.000	580.000	500.000	581.000	0.0069
Pt 103	330.000	117.000	88.000	123.000	-0.0060
Pt 104	374.000	117.000	130.000	118.000	0.0024
Pt 105	415.000	118.000	171.000	120.000	-0.0006
Pt 106	524.000	580.000	280.000	582.000	-0.0004
Pt 107	464.000	576.000	220.000	578.000	-0.0004
Pt 108	376.000	578.000	132.000	580.000	-0.0003
Pt 109	591.000	114.000	347.000	116.000	-0.0006
Pt 110	304.000	576.000	59.000	578.000	-0.0037
Pt 111	345.000	121.000	101.000	123.000	-0.0004
Pt 112	572.000	119.000	328.000	122.000	-0.0037
Pt 113	263.000	126.000	18.000	128.000	-0.0031
Pt 114	447.000	125.000	203.000	126.000	0.0024

ID	Image location of conjugate points in Image A		Image location of conjugate points in Image B		Residuals
	x (Pixels)	y (Pixels)	x (Pixels)	y (Pixels)	Signed Dist (Pixels)
Pt 115	675.000	125.000	431.000	128.000	-0.0036
Pt 116	290.000	575.000	46.000	576.000	0.0027
Pt 117	354.000	133.000	110.000	135.000	-0.0004
Pt 118	456.000	132.000	211.000	134.000	-0.0035
Pt 119	771.000	574.000	526.000	576.000	-0.0034
Pt 120	630.000	569.000	386.000	570.000	0.0029
Pt 121	290.000	139.000	46.000	141.000	-0.0002
Pt 122	427.000	139.000	183.000	142.000	-0.0035
Pt 123	523.000	141.000	279.000	143.000	-0.0005
Pt 124	670.000	141.000	426.000	143.000	-0.0003
Pt 125	411.000	145.000	167.000	146.000	0.0025
Pt 126	364.000	574.000	120.000	575.000	0.0026
Pt 127	748.000	146.000	503.000	148.000	-0.0031
Pt 128	347.000	151.000	104.000	153.000	0.0027
Pt 129	393.000	153.000	149.000	155.000	-0.0004
Pt 130	452.000	152.000	208.000	154.000	-0.0005
Pt 131	519.000	153.000	275.000	156.000	-0.0036
Pt 132	588.000	154.000	344.000	155.000	0.0027
Pt 133	685.000	149.000	441.000	152.000	-0.0035
Pt 134	278.000	155.000	34.000	157.000	-0.0001
Pt 135	262.000	163.000	17.000	165.000	-0.0031
Pt 136	419.000	563.000	175.000	565.000	-0.0004
Pt 137	662.000	162.000	418.000	164.000	-0.0003
Pt 138	370.000	168.000	126.000	170.000	-0.0003
Pt 139	424.000	169.000	180.000	171.000	-0.0004
Pt 140	487.000	170.000	243.000	172.000	-0.0004
Pt 141	724.000	558.000	480.000	560.000	0.0000
Pt 142	336.000	174.000	92.000	176.000	-0.0002
Pt 143	376.000	177.000	132.000	179.000	-0.0003
Pt 144	529.000	173.000	285.000	175.000	-0.0004
Pt 145	533.000	561.000	288.000	565.000	-0.0101
Pt 146	261.000	184.000	17.000	186.000	0.0000
Pt 147	297.000	180.000	53.000	182.000	-0.0001
Pt 148	338.000	183.000	94.000	184.000	0.0027
Pt 149	397.000	184.000	153.000	186.000	-0.0003
Pt 150	728.000	183.000	485.000	185.000	0.0030
Pt 151	281.000	188.000	38.000	190.000	0.0030
Pt 152	318.000	186.000	74.000	187.000	0.0027
Pt 153	480.000	189.000	236.000	191.000	-0.0004
Pt 154	498.000	185.000	254.000	187.000	-0.0004

ID	Image location of conjugate points in Image A		Image location of conjugate points in Image B		Residuals
	x (Pixels)	y (Pixels)	x (Pixels)	y (Pixels)	Signed Dist (Pixels)
Pt 155	630.000	190.000	386.000	192.000	-0.0003
Pt 156	434.000	562.000	190.000	564.000	-0.0004
Pt 157	767.000	188.000	524.000	191.000	-0.0002
Pt 158	383.000	561.000	139.000	563.000	-0.0003
Pt 159	336.000	562.000	92.000	564.000	-0.0002
Pt 160	308.000	558.000	64.000	560.000	-0.0001
Pt 161	286.000	195.000	42.000	197.000	0.0000
Pt 162	582.000	191.000	338.000	192.000	0.0028
Pt 163	647.000	192.000	402.000	194.000	-0.0033
Pt 164	660.000	196.000	416.000	198.000	-0.0002
Pt 165	706.000	196.000	461.000	198.000	-0.0031
Pt 166	733.000	191.000	489.000	193.000	0.0000
Pt 167	284.000	202.000	41.000	204.000	0.0031
Pt 168	259.000	561.000	15.000	563.000	0.0000
Pt 169	417.000	201.000	173.000	203.000	-0.0003
Pt 170	467.000	197.000	223.000	199.000	-0.0004
Pt 171	564.000	201.000	320.000	203.000	-0.0003
Pt 172	625.000	197.000	382.000	199.000	0.0028
Pt 173	718.000	200.000	474.000	202.000	0.0000
Pt 174	738.000	199.000	493.000	200.000	0.0003
Pt 175	259.000	206.000	14.000	209.000	-0.0058
Pt 176	349.000	207.000	105.000	209.000	-0.0002
Pt 177	531.000	204.000	287.000	206.000	-0.0004
Pt 178	594.000	203.000	350.000	206.000	-0.0035
Pt 179	646.000	210.000	402.000	211.000	0.0030
Pt 180	267.000	218.000	23.000	220.000	0.0001
Pt 181	312.000	220.000	69.000	222.000	0.0030
Pt 182	673.000	554.000	428.000	556.000	-0.0036
Pt 183	747.000	219.000	503.000	220.000	0.0035
Pt 184	297.000	225.000	53.000	228.000	-0.0029
Pt 185	414.000	224.000	171.000	226.000	0.0028
Pt 186	579.000	225.000	334.000	226.000	-0.0002
Pt 187	685.000	226.000	441.000	228.000	-0.0001
Pt 188	569.000	553.000	325.000	555.000	-0.0003
Pt 189	755.000	224.000	512.000	226.000	0.0033
Pt 190	257.000	231.000	13.000	233.000	0.0001
Pt 191	361.000	227.000	118.000	229.000	0.0029
Pt 192	534.000	228.000	290.000	229.000	0.0028
Pt 193	591.000	231.000	347.000	234.000	-0.0034
Pt 194	608.000	228.000	363.000	230.000	-0.0033

ID	Image location of conjugate points in Image A		Image location of conjugate points in Image B		Residuals
	x (Pixels)	y (Pixels)	x (Pixels)	y (Pixels)	Signed Dist (Pixels)
Pt 195	631.000	231.000	387.000	233.000	-0.0002
Pt 196	658.000	227.000	415.000	229.000	0.0030
Pt 197	326.000	236.000	82.000	238.000	-0.0001
Pt 198	499.000	552.000	255.000	554.000	-0.0004
Pt 199	463.000	234.000	219.000	236.000	-0.0003
Pt 200	479.000	553.000	234.000	555.000	-0.0038
Pt 201	424.000	554.000	181.000	555.000	0.0061
Pt 202	331.000	553.000	87.000	554.000	0.0027
Pt 203	495.000	243.000	251.000	243.000	0.0059
Pt 204	538.000	239.000	293.000	239.000	0.0028
Pt 205	573.000	243.000	328.000	246.000	-0.0065
Pt 206	631.000	240.000	388.000	242.000	0.0030
Pt 207	274.000	248.000	30.000	250.000	0.0001
Pt 208	349.000	245.000	105.000	246.000	0.0028
Pt 209	594.000	245.000	349.000	247.000	-0.0033
Pt 210	754.000	246.000	510.000	247.000	0.0035
Pt 211	775.000	250.000	529.000	252.000	-0.0060
Pt 212	771.000	549.000	527.000	551.000	0.0002
Pt 213	373.000	253.000	129.000	255.000	-0.0001
Pt 214	745.000	546.000	501.000	548.000	0.0001
Pt 215	685.000	255.000	441.000	257.000	0.0000
Pt 216	753.000	253.000	508.000	255.000	-0.0029
Pt 217	717.000	548.000	474.000	550.000	0.0035
Pt 218	611.000	547.000	367.000	550.000	-0.0035
Pt 219	306.000	260.000	62.000	262.000	0.0000
Pt 220	342.000	257.000	98.000	260.000	-0.0030
Pt 221	434.000	262.000	191.000	264.000	0.0029
Pt 222	548.000	261.000	304.000	263.000	-0.0002
Pt 223	602.000	258.000	357.000	260.000	-0.0033
Pt 224	675.000	258.000	431.000	260.000	0.0000
Pt 225	304.000	267.000	61.000	270.000	0.0003
Pt 226	491.000	267.000	247.000	269.000	-0.0002
Pt 227	606.000	266.000	361.000	268.000	-0.0033
Pt 228	525.000	548.000	281.000	550.000	-0.0004
Pt 229	451.000	545.000	207.000	547.000	-0.0003
Pt 230	265.000	274.000	21.000	275.000	0.0030
Pt 231	386.000	272.000	142.000	273.000	0.0028
Pt 232	563.000	270.000	319.000	272.000	-0.0002
Pt 233	361.000	549.000	117.000	551.000	-0.0002
Pt 234	278.000	275.000	34.000	277.000	0.0001

ID	Image location of conjugate points in Image A		Image location of conjugate points in Image B		Residuals
	x (Pixels)	y (Pixels)	x (Pixels)	y (Pixels)	Signed Dist (Pixels)
Pt 235	528.000	280.000	284.000	283.000	-0.0033
Pt 236	594.000	276.000	350.000	278.000	-0.0002
Pt 237	630.000	279.000	385.000	281.000	-0.0033
Pt 238	665.000	280.000	421.000	282.000	0.0000
Pt 239	273.000	283.000	30.000	285.000	0.0033
Pt 240	475.000	283.000	231.000	285.000	-0.0002
Pt 241	566.000	284.000	322.000	286.000	-0.0002
Pt 242	589.000	285.000	344.000	288.000	-0.0065
Pt 243	603.000	285.000	359.000	287.000	-0.0001
Pt 244	613.000	283.000	369.000	285.000	-0.0001
Pt 245	369.000	290.000	125.000	292.000	-0.0001
Pt 246	510.000	291.000	266.000	293.000	-0.0002
Pt 247	650.000	290.000	406.000	292.000	0.0000
Pt 248	680.000	288.000	437.000	290.000	0.0032
Pt 249	395.000	296.000	151.000	298.000	-0.0001
Pt 250	455.000	294.000	211.000	296.000	-0.0002
Pt 251	430.000	544.000	186.000	546.000	-0.0003
Pt 252	379.000	544.000	134.000	546.000	-0.0037
Pt 253	429.000	302.000	184.000	304.000	-0.0033
Pt 254	597.000	299.000	353.000	301.000	-0.0001
Pt 255	368.000	306.000	124.000	307.000	0.0029
Pt 256	522.000	308.000	279.000	309.000	0.0061
Pt 257	627.000	308.000	383.000	310.000	-0.0001
Pt 258	673.000	309.000	429.000	311.000	0.0000
Pt 259	500.000	533.000	256.000	535.000	-0.0003
Pt 260	289.000	312.000	45.000	315.000	-0.0027
Pt 261	316.000	311.000	72.000	313.000	0.0001
Pt 262	463.000	315.000	219.000	317.000	-0.0002
Pt 263	501.000	316.000	257.000	318.000	-0.0002
Pt 264	564.000	314.000	320.000	316.000	-0.0002
Pt 265	435.000	535.000	191.000	537.000	-0.0003
Pt 266	642.000	313.000	397.000	316.000	-0.0065
Pt 267	650.000	314.000	406.000	316.000	0.0000
Pt 268	315.000	535.000	72.000	537.000	0.0034
Pt 269	288.000	535.000	44.000	537.000	0.0000
Pt 270	324.000	321.000	80.000	323.000	0.0000
Pt 271	686.000	321.000	441.000	324.000	-0.0064
Pt 272	699.000	319.000	455.000	320.000	0.0034
Pt 273	287.000	326.000	42.000	328.000	-0.0031
Pt 274	365.000	325.000	121.000	326.000	0.0029

ID	Image location of conjugate points in Image A		Image location of conjugate points in Image B		Residuals
	x (Pixels)	y (Pixels)	x (Pixels)	y (Pixels)	Signed Dist (Pixels)
Pt 275	392.000	325.000	149.000	327.000	0.0031
Pt 276	545.000	323.000	301.000	325.000	-0.0002
Pt 277	634.000	328.000	390.000	330.000	0.0000
Pt 278	480.000	330.000	236.000	332.000	-0.0002
Pt 279	533.000	333.000	289.000	334.000	0.0029
Pt 280	659.000	334.000	415.000	336.000	0.0000
Pt 281	267.000	340.000	23.000	343.000	-0.0026
Pt 282	304.000	337.000	61.000	339.000	0.0033
Pt 283	394.000	340.000	150.000	342.000	-0.0001
Pt 284	417.000	335.000	174.000	337.000	0.0031
Pt 285	563.000	338.000	319.000	339.000	0.0030
Pt 286	623.000	336.000	379.000	337.000	0.0032
Pt 287	295.000	342.000	51.000	344.000	0.0001
Pt 288	314.000	345.000	70.000	347.000	0.0001
Pt 289	367.000	344.000	123.000	346.000	0.0000
Pt 290	388.000	344.000	144.000	346.000	-0.0001
Pt 291	505.000	343.000	261.000	345.000	-0.0002
Pt 292	520.000	346.000	275.000	348.000	-0.0034
Pt 293	605.000	343.000	361.000	345.000	-0.0001
Pt 294	290.000	352.000	46.000	354.000	0.0002
Pt 295	342.000	349.000	98.000	351.000	0.0000
Pt 296	547.000	351.000	303.000	353.000	-0.0001
Pt 297	727.000	349.000	484.000	351.000	0.0035
Pt 298	703.000	527.000	459.000	529.000	0.0000
Pt 299	626.000	527.000	383.000	528.000	0.0065
Pt 300	597.000	357.000	353.000	359.000	-0.0001
Pt 301	531.000	531.000	287.000	532.000	0.0028
Pt 302	433.000	360.000	189.000	362.000	-0.0001
Pt 303	649.000	359.000	405.000	361.000	0.0000
Pt 304	261.000	367.000	17.000	369.000	0.0003
Pt 305	277.000	370.000	32.000	372.000	-0.0031
Pt 306	300.000	369.000	56.000	371.000	0.0001
Pt 307	354.000	366.000	110.000	368.000	0.0000
Pt 308	458.000	365.000	213.000	367.000	-0.0034
Pt 309	584.000	365.000	340.000	367.000	-0.0001
Pt 310	675.000	365.000	430.000	366.000	0.0001
Pt 311	513.000	528.000	269.000	529.000	0.0028
Pt 312	353.000	376.000	109.000	378.000	0.0000
Pt 313	463.000	376.000	219.000	378.000	-0.0002
Pt 314	520.000	373.000	276.000	374.000	0.0029

ID	Image location of conjugate points in Image A		Image location of conjugate points in Image B		Residuals
	x (Pixels)	y (Pixels)	x (Pixels)	y (Pixels)	Signed Dist. (Pixels)
Pt 315	567.000	375.000	323.000	377.000	-0.0001
Pt 316	593.000	375.000	349.000	377.000	-0.0001
Pt 317	629.000	372.000	385.000	373.000	0.0032
Pt 318	732.000	374.000	488.000	376.000	0.0002
Pt 319	773.000	373.000	529.000	375.000	0.0004
Pt 320	301.000	378.000	57.000	380.000	0.0001
Pt 321	383.000	377.000	139.000	379.000	-0.0001
Pt 322	426.000	378.000	181.000	379.000	-0.0004
Pt 323	486.000	528.000	243.000	529.000	0.0062
Pt 324	360.000	383.000	116.000	386.000	-0.0029
Pt 325	536.000	385.000	292.000	388.000	-0.0033
Pt 326	277.000	393.000	32.000	395.000	-0.0031
Pt 327	313.000	389.000	69.000	390.000	0.0030
Pt 328	430.000	391.000	186.000	393.000	-0.0001
Pt 329	492.000	390.000	248.000	391.000	0.0029
Pt 330	554.000	392.000	310.000	394.000	-0.0001
Pt 331	597.000	391.000	353.000	393.000	-0.0001
Pt 332	682.000	393.000	439.000	395.000	0.0034
Pt 333	263.000	397.000	18.000	399.000	-0.0031
Pt 334	342.000	397.000	98.000	399.000	0.0000
Pt 335	461.000	399.000	216.000	401.000	-0.0034
Pt 336	477.000	398.000	233.000	400.000	-0.0002
Pt 337	511.000	400.000	267.000	401.000	0.0029
Pt 338	660.000	395.000	416.000	397.000	0.0000
Pt 339	464.000	532.000	220.000	534.000	-0.0003
Pt 340	335.000	531.000	91.000	534.000	-0.0030
Pt 341	312.000	401.000	68.000	403.000	0.0001
Pt 342	321.000	404.000	78.000	406.000	0.0034
Pt 343	361.000	403.000	117.000	405.000	0.0000
Pt 344	379.000	401.000	135.000	402.000	0.0029
Pt 345	411.000	406.000	166.000	408.000	-0.0034
Pt 346	503.000	404.000	260.000	406.000	0.0031
Pt 347	588.000	401.000	343.000	403.000	-0.0034
Pt 348	660.000	404.000	416.000	406.000	0.0000
Pt 349	325.000	528.000	81.000	530.000	-0.0001
Pt 350	361.000	409.000	117.000	412.000	-0.0029
Pt 351	393.000	412.000	149.000	414.000	-0.0001
Pt 352	403.000	410.000	159.000	412.000	-0.0001
Pt 353	605.000	407.000	361.000	409.000	-0.0001
Pt 354	261.000	413.000	17.000	416.000	-0.0026

ID	Image location of conjugate points in Image A		Image location of conjugate points in Image B		Residuals
	x (Pixels)	y (Pixels)	x (Pixels)	y (Pixels)	Signed Dist. (Pixels)
Pt 355	537.000	415.000	293.000	417.000	-0.0002
Pt 356	683.000	415.000	438.000	417.000	-0.0032
Pt 357	302.000	424.000	58.000	426.000	0.0001
Pt 358	430.000	420.000	186.000	422.000	-0.0001
Pt 359	471.000	420.000	226.000	422.000	-0.0035
Pt 360	492.000	419.000	248.000	421.000	-0.0002
Pt 361	553.000	424.000	309.000	426.000	-0.0002
Pt 362	560.000	421.000	317.000	423.000	0.0032
Pt 363	375.000	429.000	132.000	431.000	0.0033
Pt 364	404.000	429.000	161.000	430.000	0.0062
Pt 365	569.000	427.000	325.000	429.000	-0.0001
Pt 366	588.000	428.000	344.000	430.000	-0.0001
Pt 367	608.000	429.000	364.000	431.000	-0.0001
Pt 368	368.000	432.000	124.000	435.000	-0.0030
Pt 369	494.000	436.000	249.000	438.000	-0.0035
Pt 370	516.000	432.000	272.000	433.000	0.0029
Pt 371	547.000	433.000	303.000	435.000	-0.0002
Pt 372	587.000	436.000	344.000	439.000	0.0000
Pt 373	738.000	524.000	494.000	525.000	0.0035
Pt 374	428.000	439.000	184.000	440.000	0.0028
Pt 375	678.000	525.000	434.000	527.000	-0.0001
Pt 376	587.000	522.000	341.000	522.000	-0.0008
Pt 377	564.000	526.000	319.000	529.000	-0.0069
Pt 378	475.000	447.000	231.000	449.000	-0.0002
Pt 379	530.000	444.000	286.000	446.000	-0.0002
Pt 380	472.000	521.000	227.000	524.000	-0.0068
Pt 381	447.000	523.000	202.000	525.000	-0.0037
Pt 382	503.000	454.000	259.000	456.000	-0.0002
Pt 383	598.000	452.000	354.000	454.000	-0.0001
Pt 384	628.000	453.000	384.000	454.000	0.0031
Pt 385	649.000	451.000	405.000	453.000	0.0000
Pt 386	758.000	517.000	514.000	517.000	0.0069
Pt 387	257.000	460.000	13.000	461.000	0.0030
Pt 388	322.000	457.000	78.000	459.000	0.0000
Pt 389	329.000	457.000	86.000	458.000	0.0062
Pt 390	424.000	457.000	181.000	458.000	0.0062
Pt 391	460.000	457.000	216.000	459.000	-0.0002
Pt 392	559.000	455.000	315.000	457.000	-0.0002
Pt 393	546.000	519.000	302.000	521.000	-0.0003
Pt 394	387.000	515.000	143.000	517.000	-0.0002

ID	Image location of conjugate points in Image A		Image location of conjugate points in Image B		Residuals
	x (Pixels)	y (Pixels)	x (Pixels)	y (Pixels)	Signed Dist. (Pixels)
Pt 395	286.000	466.000	43.000	468.000	0.0035
Pt 396	321.000	464.000	76.000	466.000	-0.0034
Pt 397	486.000	464.000	242.000	467.000	-0.0033
Pt 398	266.000	470.000	22.000	472.000	0.0002
Pt 399	487.000	471.000	243.000	473.000	-0.0002
Pt 400	603.000	469.000	359.000	471.000	-0.0001
Pt 401	598.000	509.000	355.000	511.000	0.0032
Pt 402	352.000	512.000	108.000	513.000	0.0028
Pt 403	298.000	478.000	54.000	480.000	0.0001
Pt 404	397.000	474.000	154.000	477.000	0.0003
Pt 405	503.000	474.000	258.000	475.000	-0.0005
Pt 406	562.000	477.000	319.000	479.000	0.0032
Pt 407	451.000	483.000	208.000	485.000	0.0032
Pt 408	517.000	481.000	273.000	484.000	-0.0033
Pt 409	532.000	481.000	288.000	483.000	-0.0002
Pt 410	658.000	483.000	413.000	485.000	-0.0034
Pt 411	310.000	485.000	67.000	487.000	0.0034
Pt 412	494.000	486.000	250.000	489.000	-0.0033
Pt 413	535.000	489.000	291.000	491.000	-0.0002
Pt 414	761.000	488.000	516.000	488.000	0.0036
Pt 415	309.000	492.000	66.000	494.000	0.0034
Pt 416	521.000	496.000	277.000	498.000	-0.0003
Pt 417	583.000	491.000	338.000	493.000	-0.0036
Pt 418	771.000	492.000	527.000	493.000	0.0037
Pt 419	280.000	497.000	36.000	499.000	0.0001
Pt 420	310.000	500.000	65.000	502.000	-0.0034
Pt 421	318.000	499.000	74.000	501.000	0.0000
Pt 422	507.000	502.000	263.000	503.000	0.0028
Pt 423	563.000	501.000	320.000	504.000	0.0000
Pt 424	779.000	499.000	535.000	502.000	-0.0031
Pt 425	299.000	506.000	55.000	508.000	0.0000
Pt 426	323.000	507.000	80.000	510.000	0.0005
Pt 427	372.000	503.000	128.000	505.000	-0.0002
Pt 428	379.000	506.000	135.000	510.000	-0.0061
Pt 429	454.000	507.000	211.000	509.000	0.0032
Pt 430	484.000	506.000	239.000	508.000	-0.0037
Pt 431	542.000	504.000	298.000	505.000	0.0029
Pt 432	657.000	508.000	414.000	511.000	0.0001
Pt 433	732.000	507.000	487.000	509.000	-0.0033
Pt 434	296.000	72.000	53.000	73.000	0.0053

ID	Image location of conjugate points in Image A		Image location of conjugate points in Image B		Residuals
	x (Pixels)	y (Pixels)	x (Pixels)	y (Pixels)	Signed Dist. (Pixels)
Pt 435	721.000	79.000	476.000	81.000	-0.0034
Pt 436	731.000	60.000	488.000	61.000	0.0058
Pt 437	667.000	118.000	423.000	120.000	-0.0004
Pt 438	659.000	428.000	416.000	430.000	0.0033
Pt 439	717.000	127.000	471.000	129.000	-0.0062
Pt 440	587.000	50.000	343.000	52.000	-0.0008
Pt 441	702.000	564.000	459.000	567.000	0.0001
Pt 442	548.000	23.000	303.000	25.000	-0.0039
Pt 443	329.000	164.000	84.000	165.000	-0.0004
Pt 444	749.000	184.000	506.000	186.000	0.0031
Pt 445	319.000	71.000	75.000	73.000	-0.0005
Pt 446	478.000	243.000	234.000	244.000	0.0028
Pt 447	773.000	269.000	529.000	271.000	0.0003
Pt 448	415.000	275.000	171.000	277.000	-0.0002
Pt 449	779.000	468.000	534.000	470.000	-0.0030
Pt 450	266.000	312.000	22.000	314.000	0.0002
Pt 451	433.000	244.000	189.000	246.000	-0.0002
Pt 452	404.000	613.000	161.000	615.000	0.0031
Pt 453	320.000	98.000	76.000	100.000	-0.0004
Pt 454	566.000	107.000	324.000	107.000	0.0116
Pt 455	598.000	55.000	354.000	57.000	-0.0008
Pt 456	725.000	416.000	481.000	417.000	0.0035
				SUM:	0.0457

APPENDIX B

Table B1: Image coordinates of associated image pairs automatically extracted using Scale Invariant Feature Transform algorithm on google earth image pairs

ID	Image location of conjugate points in Image A		Image location of conjugate points in Image B		Residuals
	x (Pixels)	y (Pixels)	x (Pixels)	y (Pixels)	Signed Dist (Pixels)
Pt 1	403.514	149.759	159.418	151.906	-0.0009
Pt 2	276.494	407.720	32.513	410.261	-0.0010
Pt 3	655.839	343.023	411.907	345.034	0.0002
Pt 4	510.186	548.287	266.156	550.267	-0.0001
Pt 5	599.880	358.307	355.916	360.316	0.0001
Pt 6	411.092	343.782	165.257	343.036	-0.0029
Pt 7	311.240	219.040	67.155	221.043	-0.0004
Pt 8	605.866	219.216	361.925	221.262	-0.0001
Pt 9	267.365	573.889	23.741	575.386	0.0031
Pt 10	288.186	343.800	44.118	345.712	-0.0002
Pt 11	363.336	348.245	119.553	350.034	0.0016
Pt 12	540.831	430.329	296.726	432.543	-0.0012
Pt 13	682.398	255.199	438.269	257.271	-0.0011
Pt 14	462.228	454.159	218.108	456.090	-0.0005
Pt 15	420.305	377.196	176.210	379.149	-0.0004
Pt 16	304.047	259.122	60.042	261.092	0.0000
Pt 17	557.303	365.252	313.489	367.164	0.0012
Pt 18	341.289	259.285	97.196	261.310	-0.0005
Pt 19	781.025	10.929	537.003	12.690	0.0001
Pt 20	743.348	522.740	499.309	524.646	0.0001
Pt 21	430.793	260.672	186.786	262.693	-0.0002
Pt 22	392.505	152.939	148.484	154.894	-0.0001
Pt 23	256.060	510.547	12.091	512.558	0.0000
Pt 24	400.887	341.242	157.004	343.329	0.0004
Pt 25	365.402	340.578	121.601	342.350	0.0015
Pt 26	319.745	220.486	75.828	222.469	0.0004
Pt 27	322.885	408.470	78.912	410.661	-0.0003
Pt 28	517.826	152.338	273.931	154.251	0.0005
Pt 29	587.587	153.350	343.681	155.254	0.0005
Pt 30	737.438	574.608	493.438	576.703	-0.0003
Pt 31	545.159	347.998	301.199	349.992	0.0002
Pt 32	330.018	455.102	86.082	457.061	0.0004
Pt 33	392.338	379.547	148.262	381.520	-0.0004
Pt 34	262.843	155.727	18.895	157.693	0.0003
Pt 35	611.175	338.552	366.739	340.397	-0.0019

ID	Image location of conjugate points in Image A		Image location of conjugate points in Image B		Residuals
	x (Pixels)	y (Pixels)	x (Pixels)	y (Pixels)	Signed Dist (Pixels)
Pt 36	358.871	376.229	114.911	378.110	0.0004
Pt 37	589.357	443.809	345.670	445.722	0.0020
Pt 38	296.966	367.546	52.898	369.587	-0.0005
Pt 39	372.348	404.722	128.183	406.790	-0.0011
Pt 40	585.875	459.718	341.926	461.635	0.0005
Pt 41	417.169	339.038	173.117	340.996	-0.0002
Pt 42	454.334	579.421	210.328	581.474	-0.0002
Pt 43	493.557	266.804	249.502	268.677	0.0000
Pt 44	634.810	127.094	390.745	129.115	-0.0007
Pt 45	467.033	578.049	223.125	580.085	0.0004
Pt 46	311.749	339.208	67.800	341.193	0.0003
Pt 47	284.996	268.151	40.950	270.276	-0.0005
Pt 48	449.983	124.972	206.102	126.992	0.0003
Pt 49	595.744	429.492	351.931	431.404	0.0013
Pt 50	537.596	267.919	293.559	269.942	-0.0004
Pt 51	680.799	335.171	436.777	337.145	-0.0002
Pt 52	533.585	607.662	289.508	609.582	-0.0003
Pt 53	561.696	335.126	317.809	337.044	0.0007
Pt 54	631.639	453.125	387.680	455.130	0.0002
Pt 55	584.031	427.964	340.009	430.116	-0.0006
Pt 56	491.716	533.079	247.835	535.120	0.0006
Pt 57	350.226	440.983	106.247	442.925	0.0002
Pt 58	616.293	463.030	372.334	465.067	0.0001
Pt 59	270.356	581.925	26.204	583.955	-0.0011
Pt 60	624.864	450.690	380.871	452.750	-0.0002
Pt 61	266.554	563.958	22.708	565.865	0.0009
Pt 62	564.941	271.459	320.997	273.398	0.0003
Pt 63	610.633	247.149	366.603	249.147	-0.0003
Pt 64	538.694	201.697	294.798	203.645	0.0005
Pt 65	265.590	163.278	21.645	165.199	0.0004
Pt 66	614.789	451.211	370.677	453.258	-0.0008
Pt 67	562.622	605.278	318.507	607.348	-0.0009
Pt 68	262.772	366.297	18.681	368.209	-0.0003
Pt 69	282.003	333.295	37.906	335.311	-0.0006
Pt 70	520.351	495.249	276.453	497.384	0.0002
Pt 71	515.388	527.502	271.204	529.391	-0.0008
Pt 72	570.490	384.308	326.575	385.808	0.0019
Pt 73	473.630	550.684	229.901	552.480	0.0021
Pt 74	286.951	203.129	42.872	205.094	-0.0003

ID	Image location of conjugate points in Image A		Image location of conjugate points in Image B		Residuals
	x (Pixels)	y (Pixels)	x (Pixels)	y (Pixels)	Signed Dist (Pixels)
Pt 75	510.746	581.953	264.846	582.239	-0.0067
Pt 76	636.184	273.786	392.135	275.783	-0.0004
Pt 77	659.826	275.849	415.874	277.927	-0.0002
Pt 78	310.646	227.101	66.677	229.064	0.0002
Pt 79	524.442	523.362	280.652	525.530	0.0007
Pt 80	541.872	501.867	297.893	503.845	0.0002
Pt 81	614.313	402.003	370.188	403.982	-0.0007
Pt 82	640.258	201.299	396.336	203.494	-0.0005
Pt 83	299.216	375.386	55.204	377.378	-0.0001
Pt 84	415.387	225.922	171.339	228.000	-0.0005
Pt 85	485.805	526.405	241.770	528.615	-0.0008
Pt 86	478.052	167.313	234.077	169.304	0.0000
Pt 87	553.347	325.185	309.117	327.123	-0.0011
Pt 88	265.172	278.943	21.234	280.822	0.0005
Pt 89	545.733	451.758	301.751	453.691	0.0003
Pt 90	500.937	324.839	257.106	326.858	0.0007
Pt 91	278.722	585.422	34.712	587.414	-0.0002
Pt 92	300.710	428.900	56.657	430.897	-0.0003
Pt 93	697.865	34.952	453.917	36.875	-0.0001
Pt 94	592.978	244.964	348.997	247.004	-0.0002
Pt 95	605.970	227.218	361.989	229.232	-0.0002
Pt 96	286.949	327.097	43.049	329.174	0.0003
Pt 97	304.726	386.109	60.809	388.008	0.0006
Pt 98	614.416	279.352	370.317	281.239	-0.0003
Pt 99	619.846	601.350	375.881	603.284	0.0005
Pt 100	334.632	402.224	90.659	404.193	0.0002
Pt 101	629.917	278.698	385.882	280.665	-0.0002
Pt 102	523.450	562.732	279.592	565.089	-0.0002
Pt 103	533.339	561.538	289.166	563.570	-0.0011
Pt 104	738.095	528.337	494.069	530.422	-0.0004
Pt 105	548.764	600.784	304.203	602.359	-0.0022
Pt 106	429.136	385.085	185.033	386.975	-0.0003
Pt 107	607.178	470.054	363.210	472.014	0.0003
Pt 108	643.793	470.524	399.704	472.458	-0.0003
Pt 109	433.552	587.310	189.654	589.347	0.0005
Pt 110	326.325	545.933	82.443	547.867	0.0007
Pt 111	586.231	408.787	342.151	410.760	-0.0004
Pt 112	583.031	194.998	339.060	196.963	0.0000
Pt 113	566.023	283.545	321.933	285.458	-0.0003

ID	Image location of conjugate points in Image A		Image location of conjugate points in Image B		Residuals
	x (Pixels)	y (Pixels)	x (Pixels)	y (Pixels)	Signed Dist (Pixels)
Pt 114	529.356	229.579	285.239	231.472	-0.0004
Pt 115	553.786	423.019	309.792	425.095	-0.0002
Pt 116	684.924	285.460	440.983	287.434	0.0002
Pt 117	284.426	450.717	40.360	452.731	-0.0005
Pt 118	495.104	540.707	251.144	542.802	0.0000
Pt 119	580.215	421.380	335.596	423.639	-0.0042
Pt 120	360.576	388.239	116.479	390.239	-0.0006
Pt 121	379.152	543.393	135.036	545.358	-0.0007
Pt 122	658.793	317.934	414.838	319.893	0.0002
Pt 123	259.719	589.845	15.579	591.852	-0.0010
Pt 124	742.291	549.942	498.285	551.667	0.0010
Pt 125	559.036	318.356	315.093	320.509	-0.0002
Pt 126	552.494	389.233	308.504	391.073	0.0005
Pt 127	610.423	388.595	366.478	390.746	-0.0002
Pt 128	381.436	398.868	137.448	400.858	0.0001
Pt 129	291.572	315.845	47.522	317.859	-0.0003
Pt 130	664.462	388.427	420.635	390.560	0.0004
Pt 131	341.314	397.071	97.282	399.006	-0.0001
Pt 132	297.036	178.935	53.139	181.090	0.0001
Pt 133	554.413	568.810	310.519	570.979	0.0001
Pt 134	458.476	294.096	214.617	296.069	0.0007
Pt 135	475.580	177.550	231.628	179.660	-0.0002
Pt 136	612.233	238.320	368.170	240.390	-0.0007
Pt 137	568.936	313.655	325.038	315.784	0.0000
Pt 138	341.012	350.982	96.988	352.996	-0.0002
Pt 139	532.374	600.037	288.342	601.967	0.0000
Pt 140	549.793	591.081	305.826	592.964	0.0005
Pt 141	513.284	291.938	269.402	293.910	0.0006
Pt 142	549.144	293.509	305.138	295.485	-0.0001
Pt 143	628.257	372.097	384.200	374.169	-0.0006
Pt 144	271.891	398.779	27.843	400.747	-0.0002
Pt 145	263.743	398.289	19.865	399.982	0.0012
Pt 146	348.335	349.447	104.205	351.516	-0.0009
Pt 147	256.290	398.536	12.027	400.176	-0.0008
Pt 148	680.287	291.786	436.310	293.753	0.0001
Pt 149	336.004	423.560	91.570	425.428	-0.0021
Pt 150	431.389	437.063	187.404	439.118	-0.0001
Pt 151	595.994	351.903	352.015	353.971	-0.0002
Pt 152	285.570	592.294	41.589	594.311	-0.0001

ID	Image location of conjugate points in Image A		Image location of conjugate points in Image B		Residuals
	x (Pixels)	y (Pixels)	x (Pixels)	y (Pixels)	Signed Dist (Pixels)
Pt 153	619.991	295.743	375.886	297.592	-0.0002
Pt 154	576.248	593.105	332.179	594.775	0.0006
Pt 155	756.983	514.969	513.028	516.977	0.0003
Pt 156	582.253	180.871	338.194	182.913	-0.0006
Pt 157	611.038	396.323	366.981	398.439	-0.0007
Pt 158	495.058	565.229	250.814	567.035	-0.0010
Pt 159	304.746	370.323	60.669	372.262	-0.0003
Pt 160	601.326	450.417	357.334	452.445	-0.0001
Pt 161	598.388	299.569	354.271	301.594	-0.0008
Pt 162	676.120	307.264	432.271	309.205	0.0008
Pt 163	562.957	307.624	317.542	309.294	-0.0063
Pt 164	499.472	308.208	255.594	310.178	0.0006
Pt 165	535.869	301.593	291.794	303.757	-0.0009
Pt 166	572.241	350.271	328.189	352.310	-0.0005
Pt 167	279.903	414.714	35.651	416.407	-0.0008
Pt 168	487.111	540.293	243.531	542.652	0.0015
Pt 169	434.226	595.567	190.368	597.406	0.0012
Pt 170	265.911	415.792	21.942	417.731	0.0002
Pt 171	601.642	423.618	357.669	425.625	0.0001
Pt 172	515.195	553.874	271.360	555.931	0.0008
Pt 173	350.656	394.323	106.530	396.199	-0.0004
Pt 174	560.957	424.760	316.854	426.743	-0.0005
Pt 175	540.515	540.377	296.594	542.324	0.0006
Pt 176	262.275	394.726	18.349	396.958	-0.0001
Pt 177	354.148	69.455	110.025	71.494	-0.0007
Pt 178	514.087	306.230	270.082	308.110	0.0002
Pt 179	269.332	393.949	25.475	395.925	0.0008
Pt 180	400.918	223.882	157.071	225.964	0.0005
Pt 181	288.771	393.794	44.746	395.841	-0.0003
Pt 182	780.261	63.834	536.447	65.686	0.0007
Pt 183	448.623	608.236	204.469	610.287	-0.0011
Pt 184	299.039	383.442	55.071	385.499	0.0000
Pt 185	479.895	269.247	235.892	271.171	0.0001
Pt 186	693.110	303.000	449.017	304.875	-0.0002
Pt 187	751.038	510.843	507.029	512.810	0.0001
Pt 188	766.599	577.099	522.759	579.219	0.0006
Pt 189	457.339	597.304	213.188	599.334	-0.0010
Pt 190	277.525	185.014	33.506	186.796	0.0003
Pt 191	757.657	578.974	513.695	580.882	0.0006

ID	Image location of conjugate points in Image A		Image location of conjugate points in Image B		Residuals
	x (Pixels)	y (Pixels)	x (Pixels)	y (Pixels)	Signed Dist (Pixels)
Pt 192	508.001	307.297	264.167	309.239	0.0009
Pt 193	585.883	415.280	341.950	417.194	0.0006
Pt 194	729.505	513.029	485.605	515.015	0.0007
Pt 195	524.171	597.337	280.212	599.420	0.0000
Pt 196	539.663	565.615	296.150	567.185	0.0041
Pt 197	521.990	146.374	277.961	147.797	0.0013
Pt 198	587.852	394.379	343.962	396.159	0.0012
Pt 199	509.956	532.083	265.914	534.147	-0.0004
Pt 200	274.932	570.198	30.890	571.932	0.0001
Pt 201	492.620	429.111	248.646	430.992	0.0004
Pt 202	419.872	215.139	175.917	217.046	0.0004
Pt 203	559.160	593.762	315.237	595.648	0.0008
Pt 204	481.167	453.956	237.214	455.737	0.0008
Pt 205	528.787	591.781	284.900	593.766	0.0007
Pt 206	580.582	382.968	336.525	385.058	-0.0006
Pt 207	422.249	165.229	176.916	165.897	-0.0029
Pt 208	430.151	164.354	186.127	166.249	0.0000
Pt 209	353.686	23.134	109.600	25.148	-0.0005
Pt 210	311.844	261.408	67.854	263.419	0.0000
Pt 211	652.028	293.553	407.885	295.420	-0.0004
Pt 212	541.445	438.899	297.226	440.677	-0.0006
Pt 213	539.744	239.279	295.598	240.912	0.0002
Pt 214	314.362	312.760	70.383	314.753	0.0001
Pt 215	640.984	359.101	397.047	361.091	0.0003
Pt 216	590.588	450.829	346.659	452.837	0.0003
Pt 217	739.489	83.373	495.813	85.159	0.0016
Pt 218	542.584	212.943	298.520	215.006	-0.0007
Pt 219	450.516	292.876	206.511	294.954	-0.0003
Pt 220	288.242	86.665	44.108	88.445	-0.0002
Pt 221	454.426	603.820	210.497	605.863	0.0003
Pt 222	357.742	84.977	113.750	86.935	0.0000
Pt 223	590.265	191.113	346.240	193.338	-0.0010
Pt 224	343.555	252.104	99.310	253.883	-0.0008
Pt 225	601.400	274.559	357.408	276.733	-0.0007
Pt 226	471.741	415.628	227.859	417.489	0.0010
Pt 227	782.146	551.969	538.133	553.848	0.0004
Pt 228	718.080	556.294	474.117	558.300	0.0003
Pt 229	637.685	475.603	393.477	477.139	0.0003
Pt 230	784.733	544.366	540.738	546.481	-0.0003

ID	Image location of conjugate points in Image A		Image location of conjugate points in Image B		Residuals
	x (Pixels)	y (Pixels)	x (Pixels)	y (Pixels)	Signed Dist (Pixels)
Pt 231	602.846	30.925	358.946	32.886	0.0001
Pt 232	427.157	398.776	183.124	400.610	0.0002
Pt 233	468.142	175.878	224.099	177.875	-0.0003
Pt 234	632.544	265.918	388.668	267.917	0.0004
Pt 235	718.025	200.927	473.830	202.875	-0.0010
Pt 236	598.666	502.978	354.137	505.742	-0.0054
Pt 237	361.650	403.376	117.706	405.472	0.0000
Pt 238	271.564	589.113	27.792	591.068	0.0013
Pt 239	594.188	200.412	350.371	202.237	0.0012
Pt 240	772.539	581.732	528.473	584.253	-0.0022
Pt 241	568.177	536.718	324.119	538.522	0.0002
Pt 242	299.317	34.920	55.364	36.915	0.0001
Pt 243	587.571	327.414	342.855	328.271	-0.0003
Pt 244	631.123	421.432	387.214	423.372	0.0007
Pt 245	334.140	95.921	90.002	97.922	-0.0007
Pt 246	367.160	18.673	123.647	20.832	0.0014
Pt 247	765.566	24.101	521.572	26.071	-0.0005
Pt 248	468.081	278.946	224.051	281.080	-0.0006
Pt 249	531.757	173.827	287.689	175.742	-0.0003
Pt 250	284.023	385.916	40.077	387.975	0.0001
Pt 251	269.144	195.372	25.019	197.218	-0.0003
Pt 252	262.047	36.698	17.967	38.620	-0.0002
Pt 253	652.266	283.747	408.319	285.682	0.0003
Pt 254	595.410	337.871	351.603	340.462	-0.0009
Pt 255	607.907	414.384	363.995	416.405	0.0004
Pt 256	643.078	193.234	399.304	195.340	0.0004
Pt 257	365.740	245.289	121.744	247.542	-0.0006
Pt 258	297.793	570.967	53.706	572.931	-0.0006
Pt 259	476.769	322.583	232.774	324.771	-0.0005
Pt 260	686.438	262.194	442.314	264.277	-0.0011
Pt 261	561.537	387.367	317.547	389.293	0.0002
Pt 262	417.071	354.875	174.037	358.712	0.0005
Pt 263	409.889	153.549	166.660	155.198	0.0042
Pt 264	736.076	561.928	492.200	563.940	0.0008
Pt 265	578.034	558.528	334.172	560.341	0.0014
Pt 266	471.209	423.198	227.347	425.241	0.0006
Pt 267	298.763	595.843	54.775	597.873	-0.0001
Pt 268	256.587	26.265	12.474	28.264	-0.0005
Pt 269	422.443	121.192	178.313	122.962	-0.0002

ID	Image location of conjugate points in Image A		Image location of conjugate points in Image B		Residuals
	x (Pixels)	y (Pixels)	x (Pixels)	y (Pixels)	Signed Dist (Pixels)
Pt 270	616.779	233.240	372.809	235.230	0.0000
Pt 271	583.318	375.778	339.500	377.600	0.0014
Pt 272	380.852	102.370	137.084	104.196	0.0013
Pt 273	612.327	479.824	368.496	481.769	0.0011
Pt 274	542.447	228.723	298.271	230.793	-0.0012
Pt 275	462.961	604.163	218.795	606.192	-0.0011
Pt 276	556.344	542.026	312.463	544.065	0.0006
Pt 277	658.154	411.486	414.108	413.395	0.0000
Pt 278	575.190	90.252	331.323	92.650	-0.0010
Pt 279	288.892	23.884	44.972	25.802	0.0004
Pt 280	352.806	338.034	108.008	340.804	-0.0059
Pt 281	471.450	337.255	227.509	339.400	-0.0001
Pt 282	531.691	386.208	287.802	388.257	0.0004
Pt 283	277.109	578.063	33.156	580.080	0.0001
Pt 284	704.612	31.513	460.869	33.243	0.0014
Pt 285	273.913	369.516	30.025	371.483	0.0006
Pt 286	359.066	410.357	115.455	412.639	0.0014
Pt 287	382.507	142.432	138.583	144.463	0.0002
Pt 288	339.226	570.105	95.125	572.217	-0.0010
Pt 289	597.617	378.240	353.515	380.159	-0.0004
Pt 290	373.269	254.047	129.152	256.152	-0.0009
Pt 291	534.217	416.255	290.039	418.117	-0.0006
Pt 292	656.805	448.415	413.113	450.649	0.0009
Pt 293	634.758	438.384	390.751	440.419	-0.0002
Pt 294	522.671	425.641	278.737	427.693	0.0002
Pt 295	329.073	560.315	84.918	562.168	-0.0007
Pt 296	463.231	403.328	219.096	405.323	-0.0008
Pt 297	536.219	524.610	292.387	526.701	0.0007
Pt 298	475.089	519.156	230.993	521.170	-0.0006
Pt 299	761.271	524.792	516.851	526.571	-0.0016
Pt 300	549.575	511.211	305.757	513.394	0.0005
Pt 301	454.183	508.517	210.278	510.517	0.0005
Pt 302	735.090	505.718	491.175	507.694	0.0006
Pt 303	305.547	505.742	61.419	508.027	-0.0014
Pt 304	492.076	17.139	248.082	19.163	-0.0004
Pt 305	721.973	502.961	478.116	504.710	0.0017
Pt 306	727.414	497.097	483.427	499.070	0.0002
Pt 307	736.536	492.999	492.189	494.800	-0.0013
Pt 308	456.182	495.343	212.414	497.107	0.0019

ID	Image location of conjugate points in Image A		Image location of conjugate points in Image B		Residuals
	x (Pixels)	y (Pixels)	x (Pixels)	y (Pixels)	Signed Dist (Pixels)
Pt 309	542.172	528.194	297.915	530.186	-0.0015
Pt 310	564.528	526.628	320.310	528.793	-0.0018
Pt 311	759.938	484.882	515.939	486.959	-0.0003
Pt 312	687.243	22.513	443.153	24.469	-0.0008
Pt 313	631.213	481.643	387.038	483.229	0.0003
Pt 314	603.539	478.679	359.350	480.879	-0.0017
Pt 315	257.924	480.359	13.965	482.350	0.0002
Pt 316	493.531	474.325	249.716	476.624	0.0002
Pt 317	473.859	472.786	230.116	474.733	0.0016
Pt 318	699.821	25.206	455.274	27.070	-0.0024
Pt 319	484.963	467.218	240.992	469.254	0.0000
Pt 320	627.728	461.229	383.568	463.242	-0.0010
Pt 321	493.471	459.627	249.354	461.790	-0.0011
Pt 322	331.270	33.037	87.328	34.914	0.0004
Pt 323	653.867	459.309	410.059	461.861	-0.0008
Pt 324	470.505	458.844	226.771	460.844	0.0015
Pt 325	525.936	532.602	281.816	534.408	-0.0002
Pt 326	559.404	454.822	315.642	457.083	0.0005
Pt 327	446.052	454.122	202.197	456.186	0.0006
Pt 328	611.973	453.102	367.984	455.086	0.0001
Pt 329	462.019	451.967	218.091	454.017	0.0002
Pt 330	632.037	450.201	388.066	452.255	0.0000
Pt 331	285.077	448.466	40.898	447.909	0.0040
Pt 332	335.417	447.478	91.691	449.356	0.0017
Pt 333	592.832	442.394	348.905	444.511	0.0000
Pt 334	530.969	444.108	286.936	445.998	0.0001
Pt 335	578.045	439.768	334.542	442.157	0.0015
Pt 336	308.968	438.515	64.905	440.563	-0.0005
Pt 337	279.146	435.574	34.197	435.673	-0.0015
Pt 338	476.238	431.656	231.276	433.313	-0.0044
Pt 339	570.180	428.585	326.145	430.542	-0.0001
Pt 340	427.948	427.479	183.916	429.739	-0.0009
Pt 341	383.998	427.289	139.975	429.491	-0.0006
Pt 342	309.993	426.563	65.903	428.674	-0.0008
Pt 343	614.928	424.893	370.958	426.907	0.0001
Pt 344	525.021	425.708	281.033	427.711	0.0000
Pt 345	294.032	421.458	50.208	423.511	0.0008
Pt 346	502.067	601.742	258.087	603.805	-0.0001
Pt 347	440.063	603.455	195.850	605.411	-0.0013

ID	Image location of conjugate points in Image A		Image location of conjugate points in Image B		Residuals
	x (Pixels)	y (Pixels)	x (Pixels)	y (Pixels)	Signed Dist (Pixels)
Pt 348	581.276	418.084	337.268	420.022	0.0001
Pt 349	435.292	419.158	191.200	421.085	-0.0004
Pt 350	326.565	417.775	82.644	419.705	0.0005
Pt 351	268.124	416.186	24.119	418.152	0.0000
Pt 352	540.820	413.135	296.192	415.677	-0.0050
Pt 353	426.766	411.965	182.806	413.946	0.0002
Pt 354	310.180	56.311	66.590	57.910	0.0025
Pt 355	335.162	413.201	91.226	415.213	0.0003
Pt 356	411.644	409.274	167.475	411.736	-0.0021
Pt 357	275.981	409.982	32.028	411.806	0.0006
Pt 358	456.306	407.121	212.256	409.122	-0.0003
Pt 359	437.098	403.854	193.165	405.772	0.0005
Pt 360	312.037	399.739	68.001	401.730	-0.0002
Pt 361	284.022	401.694	40.140	403.681	0.0006
Pt 362	273.721	62.566	29.458	64.908	-0.0018
Pt 363	452.529	538.266	208.371	540.631	-0.0019
Pt 364	567.985	394.898	323.782	396.685	-0.0005
Pt 365	466.243	395.547	222.220	397.535	-0.0001
Pt 366	370.803	393.940	126.369	396.295	-0.0032
Pt 367	487.171	538.416	243.575	539.195	0.0056
Pt 368	280.004	394.657	36.045	396.728	0.0000
Pt 369	777.297	539.058	533.388	541.023	0.0007
Pt 370	384.746	385.946	140.729	387.954	-0.0001
Pt 371	295.642	386.835	51.768	388.913	0.0005
Pt 372	353.069	383.597	109.051	385.548	0.0000
Pt 373	491.875	381.344	247.857	383.250	0.0001
Pt 374	335.203	542.836	91.224	544.981	-0.0003
Pt 375	412.163	380.771	168.095	382.802	-0.0005
Pt 376	464.076	542.403	220.139	544.066	0.0012
Pt 377	566.685	375.909	322.821	377.995	0.0004
Pt 378	370.547	372.173	126.506	374.111	-0.0001
Pt 379	307.224	370.577	63.230	372.622	-0.0001
Pt 380	388.558	368.411	144.483	369.565	0.0016
Pt 381	594.928	366.023	350.889	367.982	-0.0002
Pt 382	583.336	364.760	339.270	366.646	-0.0001
Pt 383	372.782	364.267	131.587	367.487	0.0119
Pt 384	530.448	360.914	286.675	363.391	-0.0002
Pt 385	428.967	357.380	184.960	359.416	-0.0002
Pt 386	296.324	595.794	52.311	597.537	0.0003

ID	Image location of conjugate points in Image A		Image location of conjugate points in Image B		Residuals
	x (Pixels)	y (Pixels)	x (Pixels)	y (Pixels)	Signed Dist (Pixels)
Pt 387	513.081	353.116	269.164	354.938	0.0009
Pt 388	380.888	354.070	136.901	356.045	0.0001
Pt 389	368.852	353.543	124.826	355.574	-0.0002
Pt 390	340.180	353.194	96.099	355.216	-0.0005
Pt 391	648.472	350.134	404.437	352.094	-0.0002
Pt 392	502.255	349.120	258.458	351.075	0.0011
Pt 393	408.842	351.140	164.807	353.104	-0.0001
Pt 394	318.313	350.968	74.186	352.928	-0.0006
Pt 395	664.681	87.949	420.866	89.871	0.0006
Pt 396	351.585	93.346	107.381	95.429	-0.0012
Pt 397	374.964	342.990	131.004	344.834	0.0005
Pt 398	419.834	339.666	175.836	341.559	0.0002
Pt 399	608.490	338.738	364.415	340.792	-0.0006
Pt 400	591.422	593.180	347.847	595.199	0.0025
Pt 401	571.613	339.293	327.580	341.297	-0.0003
Pt 402	408.231	337.325	164.227	339.536	-0.0006
Pt 403	319.093	333.931	75.026	335.836	-0.0002
Pt 404	590.521	98.078	346.808	100.216	0.0005
Pt 405	510.924	331.101	266.278	333.778	-0.0053
Pt 406	275.172	100.759	31.246	102.702	0.0004
Pt 407	530.301	329.415	286.503	331.260	0.0014
Pt 408	470.051	327.907	228.337	331.701	0.0070
Pt 409	652.923	325.671	408.889	327.488	0.0003
Pt 410	606.740	325.917	362.704	327.802	0.0001
Pt 411	381.120	103.758	137.059	105.777	-0.0004
Pt 412	638.782	323.770	394.719	325.802	-0.0005
Pt 413	479.650	324.220	235.577	326.285	-0.0006
Pt 414	476.904	319.299	232.844	321.466	-0.0008
Pt 415	454.535	549.661	210.525	551.764	-0.0004
Pt 416	629.050	317.355	385.037	319.502	-0.0007
Pt 417	514.179	316.038	269.875	318.035	-0.0016
Pt 418	555.004	550.853	310.960	552.733	0.0001
Pt 419	490.509	313.386	246.385	314.735	0.0011
Pt 420	433.771	313.011	189.843	314.934	0.0005
Pt 421	285.628	589.435	41.565	591.394	-0.0005
Pt 422	459.165	310.968	215.136	312.992	-0.0003
Pt 423	402.185	113.794	158.178	115.725	0.0000
Pt 424	595.178	309.487	351.434	311.644	0.0007
Pt 425	640.285	303.929	397.313	306.707	0.0026

ID	Image location of conjugate points in Image A		Image location of conjugate points in Image B		Residuals
	x (Pixels)	y (Pixels)	x (Pixels)	y (Pixels)	Signed Dist (Pixels)
Pt 426	576.547	305.431	332.434	307.568	-0.0011
Pt 427	367.194	305.145	123.174	307.204	-0.0003
Pt 428	307.547	305.791	63.503	307.956	-0.0006
Pt 429	545.357	302.171	301.395	304.109	0.0003
Pt 430	600.591	300.081	356.547	302.123	-0.0005
Pt 431	634.751	294.658	390.358	296.209	-0.0007
Pt 432	491.225	294.714	247.726	297.717	-0.0003
Pt 433	461.090	294.846	217.067	296.884	-0.0003
Pt 434	538.349	289.642	294.323	291.923	-0.0010
Pt 435	373.286	289.303	129.312	291.269	0.0002
Pt 436	577.828	286.122	333.909	288.176	0.0001
Pt 437	424.252	121.695	180.303	123.936	-0.0005
Pt 438	422.884	585.722	178.875	587.630	0.0001
Pt 439	363.761	585.938	120.006	588.285	0.0006
Pt 440	663.655	285.328	419.642	287.303	-0.0002
Pt 441	640.986	284.600	396.899	287.329	-0.0029
Pt 442	509.317	284.326	265.339	286.387	-0.0002
Pt 443	485.281	285.167	241.290	287.213	-0.0002
Pt 444	316.035	522.872	71.915	524.896	-0.0008
Pt 445	273.700	267.969	29.714	270.065	-0.0001
Pt 446	381.040	130.910	137.660	133.136	0.0021
Pt 447	539.095	265.281	295.032	267.395	-0.0008
Pt 448	673.101	264.178	428.957	266.112	-0.0007
Pt 449	336.668	555.713	92.696	557.503	0.0005
Pt 450	629.326	558.304	385.397	560.343	0.0003
Pt 451	479.053	260.094	235.124	262.080	0.0003
Pt 452	475.964	560.240	231.964	562.424	-0.0005
Pt 453	400.918	135.602	156.854	137.515	-0.0002
Pt 454	523.317	560.518	279.647	562.699	0.0014
Pt 455	633.315	250.181	389.370	252.181	0.0001
Pt 456	547.570	559.237	303.579	561.180	0.0002
Pt 457	346.931	252.321	103.582	254.624	0.0025
Pt 458	278.916	249.930	34.923	251.762	0.0003
Pt 459	410.634	139.522	166.907	141.481	0.0012
Pt 460	453.004	140.287	208.950	142.479	-0.0009
Pt 461	571.893	242.329	328.014	244.491	-0.0001
Pt 462	296.491	239.554	52.396	241.788	-0.0010
Pt 463	273.770	146.926	29.719	148.896	-0.0002
Pt 464	359.123	146.106	115.291	148.452	-0.0001

ID	Image location of conjugate points in Image A		Image location of conjugate points in Image B		Residuals
	x (Pixels)	y (Pixels)	x (Pixels)	y (Pixels)	Signed Dist (Pixels)
Pt 465	544.421	228.726	300.304	231.075	-0.0017
Pt 466	533.052	229.344	289.000	231.332	-0.0004
Pt 467	308.969	230.038	65.161	231.808	0.0014
Pt 468	581.346	224.658	337.435	226.732	0.0000
Pt 469	562.326	564.804	318.402	566.909	0.0001
Pt 470	774.725	565.050	530.705	566.889	0.0005
Pt 471	257.707	568.225	13.703	570.150	0.0000
Pt 472	309.202	218.348	65.198	220.319	0.0000
Pt 473	450.975	152.298	207.003	154.286	0.0000
Pt 474	619.610	204.431	375.588	206.252	0.0002
Pt 475	271.652	202.976	27.695	205.034	0.0001
Pt 476	582.925	196.889	338.924	198.922	-0.0003
Pt 477	533.348	570.718	289.429	572.704	0.0005
Pt 478	592.635	192.427	349.060	194.611	0.0012
Pt 479	549.290	578.995	305.303	580.783	0.0007
Pt 480	294.647	189.430	51.263	191.715	0.0023
Pt 481	268.114	163.788	24.068	165.808	-0.0003
Pt 482	490.484	184.455	246.345	186.648	-0.0013
Pt 483	259.068	181.681	15.053	183.798	-0.0003
Pt 484	286.917	177.987	42.911	179.976	0.0000
Pt 485	324.079	397.785	80.292	399.647	0.0014
Pt 486	329.669	48.107	86.021	50.256	0.0010
Pt 487	476.452	249.046	233.008	250.789	0.0033
Pt 488	635.223	435.640	391.310	437.618	0.0005
Pt 489	485.577	336.029	241.528	338.098	-0.0005
Pt 490	293.765	72.182	49.789	73.995	0.0004
Pt 491	712.555	511.036	467.907	513.284	-0.0046
Pt 492	534.812	284.291	290.724	286.440	-0.0010
Pt 493	272.245	511.694	27.943	513.696	-0.0019
Pt 494	499.698	289.670	255.690	292.010	-0.0011
Pt 495	596.053	24.827	352.103	27.135	-0.0012
Pt 496	530.038	195.943	285.808	197.929	-0.0012
Pt 497	422.313	314.359	178.678	316.734	0.0009
Pt 498	523.309	163.179	278.946	162.545	0.0056
Pt 499	771.651	490.896	527.453	492.845	-0.0009
Pt 500	639.198	553.590	394.814	555.140	-0.0008
Pt 501	297.233	197.183	53.144	198.915	0.0001
Pt 502	320.401	40.264	76.166	42.180	-0.0009
Pt 503	382.178	120.525	138.001	122.636	-0.0012

ID	Image location of conjugate points in Image A		Image location of conjugate points in Image B		Residuals
	x (Pixels)	y (Pixels)	x (Pixels)	y (Pixels)	Signed Dist (Pixels)
Pt 504	440.125	175.197	197.758	175.867	0.0108
Pt 505	562.841	549.255	318.307	552.344	-0.0064
Pt 506	655.955	371.975	411.770	373.879	-0.0007
Pt 507	417.714	427.898	173.527	429.764	-0.0007
Pt 508	294.288	251.752	50.396	253.782	0.0004
Pt 509	670.244	116.225	426.897	118.285	0.0023
Pt 510	504.678	471.133	260.568	473.399	-0.0014
Pt 511	361.113	571.054	116.939	573.173	-0.0014
Pt 512	468.912	305.829	224.191	306.789	-0.0010
Pt 513	282.724	350.897	38.900	352.846	0.0010
Pt 514	486.443	361.086	242.045	363.177	-0.0024
Pt 515	463.979	330.859	218.876	331.281	-0.0016
Pt 516	321.551	51.991	76.275	54.404	-0.0063
Pt 517	574.143	102.522	330.073	104.265	0.0001
Pt 518	746.990	496.626	502.967	498.741	-0.0005
Pt 519	632.971	55.489	388.719	57.729	-0.0023
Pt 520	473.892	536.838	229.806	538.955	-0.0008
Pt 521	451.969	537.745	207.903	539.797	-0.0006
Pt 522	322.367	533.557	78.420	535.583	0.0002
Pt 523	305.333	22.343	61.320	24.316	-0.0001
Pt 524	463.025	527.211	218.833	529.482	-0.0019
Pt 525	687.613	22.825	443.674	24.859	-0.0004
Pt 526	709.803	21.826	465.772	23.873	-0.0009
Pt 527	774.331	522.355	530.043	524.275	-0.0013
Pt 528	525.612	28.235	281.157	30.384	-0.0026
Pt 529	594.659	24.495	350.726	26.462	-0.0001
Pt 530	720.119	533.922	477.509	534.785	0.0122
Pt 531	538.876	599.239	294.870	601.244	-0.0001
Pt 532	617.317	517.266	373.374	520.061	-0.0022
Pt 533	581.833	517.246	337.562	519.184	-0.0014
Pt 534	535.980	33.979	294.715	37.297	0.0071
Pt 535	738.116	534.982	493.973	536.992	-0.0008
Pt 536	677.416	32.503	433.338	34.683	-0.0015
Pt 537	551.329	510.724	307.254	512.534	0.0001
Pt 538	346.593	40.546	98.727	44.459	-0.0204
Pt 539	735.564	506.302	491.523	508.256	-0.0001
Pt 540	307.180	507.975	65.653	511.462	0.0111
Pt 541	262.848	42.362	18.675	44.285	-0.0006
Pt 542	500.500	540.202	256.414	542.184	-0.0005

ID	Image location of conjugate points in Image A		Image location of conjugate points in Image B		Residuals
	x (Pixels)	y (Pixels)	x (Pixels)	y (Pixels)	Signed Dist (Pixels)
Pt 543	611.572	42.658	367.631	44.556	0.0001
Pt 544	321.157	51.761	77.199	54.037	-0.0005
Pt 545	737.947	493.065	493.662	494.827	-0.0008
Pt 546	725.403	495.314	481.440	497.351	0.0001
Pt 547	456.067	495.588	212.255	497.486	0.0013
Pt 548	299.800	494.926	55.631	496.900	-0.0010
Pt 549	619.423	487.181	375.369	489.229	-0.0005
Pt 550	631.834	482.231	387.887	484.101	0.0007
Pt 551	303.674	61.780	59.660	63.601	0.0002
Pt 552	686.750	60.599	442.386	62.631	-0.0022
Pt 553	592.504	468.766	348.624	470.743	0.0007
Pt 554	473.495	472.749	229.563	474.678	0.0005
Pt 555	436.077	461.821	192.047	463.744	0.0000
Pt 556	297.255	593.140	53.283	595.621	-0.0010
Pt 557	283.377	72.057	39.203	73.987	-0.0007
Pt 558	638.713	460.910	392.571	464.241	-0.0163
Pt 559	493.934	458.968	250.520	461.037	0.0031
Pt 560	609.538	453.726	365.359	455.712	-0.0010
Pt 561	299.388	81.759	55.566	83.708	0.0008
Pt 562	585.135	453.990	341.223	455.994	0.0005
Pt 563	559.980	452.274	316.068	454.450	0.0000
Pt 564	644.328	447.211	400.336	449.006	0.0007
Pt 565	425.049	446.520	181.061	448.527	0.0000
Pt 566	390.670	87.093	145.420	88.939	-0.0052
Pt 567	575.006	438.487	331.317	440.542	0.0015
Pt 568	552.437	437.409	308.462	439.404	0.0001
Pt 569	573.969	93.598	329.943	95.735	-0.0008
Pt 570	607.873	431.665	363.870	433.646	0.0000
Pt 571	399.923	433.221	155.998	435.113	0.0006
Pt 572	276.245	100.613	32.231	102.483	0.0002
Pt 573	628.479	546.436	384.027	548.319	-0.0023
Pt 574	514.780	590.150	270.743	592.155	-0.0003
Pt 575	499.346	588.223	255.189	590.211	-0.0009
Pt 576	733.757	99.516	489.759	101.670	-0.0010
Pt 577	312.277	426.374	68.254	428.376	-0.0002
Pt 578	283.709	427.954	39.688	430.219	-0.0007
Pt 579	628.220	423.733	384.221	425.816	-0.0003
Pt 580	285.448	588.382	41.408	590.401	-0.0004
Pt 581	608.804	419.357	364.664	421.370	-0.0008

ID	Image location of conjugate points in Image A		Image location of conjugate points in Image B		Residuals
	x (Pixels)	y (Pixels)	x (Pixels)	y (Pixels)	Signed Dist (Pixels)
Pt 582	502.274	422.558	258.320	424.280	0.0010
Pt 583	488.731	419.936	244.711	422.031	-0.0004
Pt 584	395.925	419.078	151.749	421.211	-0.0013
Pt 585	724.610	550.746	480.563	552.613	0.0002
Pt 586	657.538	582.242	413.649	584.262	0.0006
Pt 587	579.107	416.871	335.005	418.827	-0.0005
Pt 588	387.042	118.014	142.965	119.863	-0.0001
Pt 589	516.583	416.963	271.606	419.141	-0.0059
Pt 590	330.731	416.007	86.662	417.965	-0.0003
Pt 591	304.921	415.125	60.994	417.124	0.0004
Pt 592	670.592	117.854	426.772	119.765	0.0007
Pt 593	269.598	417.835	25.492	420.006	-0.0010
Pt 594	638.501	581.545	393.773	583.721	-0.0049
Pt 595	475.968	586.195	231.930	588.247	-0.0004
Pt 596	635.265	408.801	391.407	410.600	0.0014
Pt 597	619.713	409.691	375.710	411.690	-0.0001
Pt 598	348.527	123.714	104.147	125.737	-0.0018
Pt 599	445.843	584.192	201.825	586.204	-0.0002
Pt 600	421.050	585.779	177.001	587.828	-0.0005
Pt 601	596.122	402.453	352.073	404.454	-0.0003
Pt 602	527.625	405.977	283.579	408.192	-0.0009
Pt 603	433.317	403.520	189.404	405.484	0.0005
Pt 604	272.401	405.857	28.379	407.808	-0.0001
Pt 605	661.571	400.825	417.522	402.784	-0.0002
Pt 606	541.582	397.373	297.612	399.221	0.0006
Pt 607	309.440	555.374	65.427	557.282	0.0000
Pt 608	361.726	400.074	117.658	402.108	-0.0005
Pt 609	294.205	396.471	50.277	398.453	0.0004
Pt 610	281.888	395.617	37.908	397.632	0.0000
Pt 611	463.549	133.667	219.495	135.735	-0.0006
Pt 612	724.394	132.400	480.328	134.295	-0.0004
Pt 613	606.983	390.048	362.940	392.038	-0.0003
Pt 614	337.571	556.267	93.597	558.192	0.0002
Pt 615	475.464	389.344	231.452	391.436	-0.0003
Pt 616	332.350	142.070	88.330	144.315	-0.0007
Pt 617	371.528	393.278	127.678	395.320	0.0007
Pt 618	421.891	139.320	177.849	141.407	-0.0005
Pt 619	526.192	386.026	282.331	388.114	0.0005
Pt 620	272.673	145.332	28.635	147.370	-0.0003

ID	Image location of conjugate points in Image A		Image location of conjugate points in Image B		Residuals
	x (Pixels)	y (Pixels)	x (Pixels)	y (Pixels)	Signed Dist (Pixels)
Pt 621	773.399	576.158	529.347	578.113	-0.0001
Pt 622	383.279	387.266	139.306	389.242	0.0002
Pt 623	621.642	381.724	377.543	383.720	-0.0006
Pt 624	519.505	378.022	275.548	379.983	0.0003
Pt 625	321.846	153.316	77.906	156.022	-0.0013
Pt 626	486.489	553.339	242.476	555.350	-0.0001
Pt 627	655.895	373.475	411.657	375.530	-0.0015
Pt 628	552.842	376.456	309.530	379.132	0.0016
Pt 629	352.165	159.883	108.065	162.215	-0.0013
Pt 630	380.043	157.779	135.876	160.011	-0.0014
Pt 631	536.164	553.882	292.280	555.639	0.0014
Pt 632	378.862	374.760	134.832	376.663	0.0000
Pt 633	404.024	370.000	160.068	371.822	0.0006
Pt 634	487.790	161.568	243.842	163.569	0.0001
Pt 635	364.742	365.121	120.692	367.121	-0.0003
Pt 636	650.194	361.541	406.410	363.293	0.0019
Pt 637	627.253	359.863	382.045	362.110	-0.0072
Pt 638	569.723	364.057	325.693	365.974	0.0000
Pt 639	542.291	360.142	298.440	362.207	0.0005
Pt 640	373.509	173.534	129.513	175.415	0.0002
Pt 641	455.409	178.366	211.563	180.331	0.0007
Pt 642	512.027	355.584	268.014	357.420	0.0003
Pt 643	397.794	357.940	153.791	359.880	0.0001
Pt 644	382.688	353.054	138.681	355.210	-0.0004
Pt 645	286.419	576.802	42.519	578.862	0.0003
Pt 646	591.130	350.554	344.310	350.097	-0.0073
Pt 647	459.978	350.016	215.921	352.094	-0.0006
Pt 648	437.141	347.381	191.497	347.984	-0.0051
Pt 649	318.463	350.384	74.379	352.400	-0.0005
Pt 650	281.927	351.498	37.958	353.460	0.0002
Pt 651	270.216	348.111	26.070	349.812	-0.0002
Pt 652	656.101	190.120	412.268	192.035	0.0008
Pt 653	608.999	341.110	364.948	343.114	-0.0004
Pt 654	558.600	346.324	315.598	349.208	0.0025
Pt 655	630.643	193.242	386.652	195.362	-0.0006
Pt 656	528.766	344.429	284.776	346.506	-0.0002
Pt 657	389.733	344.606	145.757	346.538	0.0002
Pt 658	350.273	344.758	106.305	346.770	0.0001
Pt 659	313.367	199.779	69.669	201.656	0.0016

ID	Image location of conjugate points in Image A		Image location of conjugate points in Image B		Residuals
	x (Pixels)	y (Pixels)	x (Pixels)	y (Pixels)	Signed Dist (Pixels)
Pt 660	516.469	340.891	272.454	342.669	0.0005
Pt 661	495.818	336.564	251.975	338.616	0.0006
Pt 662	483.670	338.203	239.692	340.196	0.0001
Pt 663	466.446	337.830	222.473	339.739	0.0003
Pt 664	606.666	198.983	362.642	200.836	0.0001
Pt 665	714.112	201.203	470.845	202.738	0.0048
Pt 666	279.980	337.620	35.944	339.503	0.0000
Pt 667	738.220	569.645	494.197	571.777	-0.0005
Pt 668	620.618	204.451	376.602	206.297	0.0002
Pt 669	644.250	204.951	400.133	206.882	-0.0006
Pt 670	544.634	329.762	300.660	331.779	0.0000
Pt 671	531.189	329.313	287.286	331.305	0.0004
Pt 672	460.243	329.338	213.136	326.997	-0.0048
Pt 673	341.298	333.385	96.566	335.092	-0.0032
Pt 674	588.081	211.332	344.090	213.025	0.0008
Pt 675	293.732	333.185	49.743	335.094	0.0002
Pt 676	606.913	326.126	362.921	328.111	0.0000
Pt 677	424.515	327.295	180.350	328.910	0.0001
Pt 678	567.611	219.170	323.683	221.260	-0.0001
Pt 679	634.897	215.224	390.097	216.862	-0.0029
Pt 680	639.646	322.502	395.551	324.754	-0.0014
Pt 681	516.573	317.478	272.610	319.480	0.0001
Pt 682	534.185	569.906	290.180	571.914	-0.0001
Pt 683	491.894	317.827	247.902	319.786	0.0001
Pt 684	504.024	557.639	259.974	559.572	-0.0001
Pt 685	523.695	557.618	279.761	559.545	0.0006
Pt 686	686.008	226.472	441.976	228.477	-0.0004
Pt 687	688.887	311.492	444.847	313.481	-0.0003
Pt 688	654.402	314.554	410.389	316.566	-0.0002
Pt 689	616.181	316.308	372.175	318.393	-0.0004
Pt 690	549.660	316.318	305.664	318.470	-0.0005
Pt 691	434.183	312.390	190.343	314.199	0.0012
Pt 692	361.245	316.387	117.003	318.643	-0.0019
Pt 693	573.736	557.641	329.699	559.583	0.0000
Pt 694	629.983	559.604	386.016	561.626	0.0002
Pt 695	533.381	229.997	289.380	232.007	-0.0002
Pt 696	547.976	229.700	303.722	231.834	-0.0018
Pt 697	713.562	560.319	469.668	562.042	0.0016
Pt 698	322.095	570.291	78.031	572.045	0.0000

ID	Image location of conjugate points in Image A		Image location of conjugate points in Image B		Residuals
	x (Pixels)	y (Pixels)	x (Pixels)	y (Pixels)	Signed Dist (Pixels)
Pt 699	641.313	305.967	397.250	307.986	-0.0005
Pt 700	633.302	234.851	389.261	236.691	0.0001
Pt 701	303.816	305.599	60.513	307.663	0.0034
Pt 702	296.750	240.775	52.843	242.882	0.0002
Pt 703	626.168	304.435	382.139	306.409	-0.0002
Pt 704	545.711	303.227	301.755	305.237	0.0001
Pt 705	556.799	241.502	312.972	243.645	0.0003
Pt 706	570.266	242.299	326.298	244.459	-0.0005
Pt 707	622.153	244.640	378.159	246.643	-0.0002
Pt 708	650.140	240.050	405.891	242.082	-0.0015
Pt 709	635.136	294.652	391.125	296.613	-0.0001
Pt 710	563.940	295.868	320.350	297.865	0.0020
Pt 711	477.514	246.588	233.647	248.737	0.0001
Pt 712	753.431	249.495	509.497	251.611	-0.0004
Pt 713	726.480	567.447	482.708	569.327	0.0018
Pt 714	591.426	290.691	347.465	292.711	0.0000
Pt 715	294.447	252.552	50.443	254.593	-0.0001
Pt 716	676.906	281.461	432.911	283.377	0.0001
Pt 717	602.298	253.945	358.287	255.984	-0.0003
Pt 718	633.340	251.887	389.383	253.876	0.0001
Pt 719	277.351	281.443	33.328	283.459	-0.0002
Pt 720	579.601	259.341	335.707	261.242	0.0007
Pt 721	271.789	564.450	27.709	566.442	-0.0006
Pt 722	379.501	264.240	135.427	266.001	0.0001
Pt 723	538.029	264.862	293.987	266.913	-0.0005
Pt 724	624.076	534.085	380.065	536.194	-0.0004
Pt 725	642.738	272.822	398.622	274.853	-0.0008
Pt 726	522.477	274.338	278.379	276.203	-0.0002
Pt 727	679.841	552.034	436.224	553.817	0.0030
Pt 728	462.083	469.407	218.463	471.462	0.0020
Pt 729	565.798	257.380	321.958	259.457	0.0004
Pt 730	338.883	151.825	96.274	157.147	-0.0010
Pt 731	293.669	480.595	49.413	482.764	-0.0019
Pt 732	334.454	125.819	91.934	132.593	-0.0039
Pt 733	315.763	521.966	71.792	523.899	0.0002
Pt 734	265.532	526.458	21.581	529.292	-0.0014
Pt 735	277.659	311.892	33.781	313.806	0.0008
Pt 736	687.369	516.317	443.217	518.250	-0.0006
Pt 737	515.304	513.053	271.831	514.832	0.0037

ID	Image location of conjugate points in Image A		Image location of conjugate points in Image B		Residuals
	x (Pixels)	y (Pixels)	x (Pixels)	y (Pixels)	Signed Dist (Pixels)
Pt 738	416.465	299.646	172.521	303.396	-0.0041
Pt 739	326.115	132.606	82.029	134.304	0.0002
Pt 740	346.205	168.070	102.014	170.156	-0.0011
Pt 741	386.685	302.390	142.746	304.357	0.0003
Pt 742	379.916	304.309	135.604	306.050	-0.0010
Pt 743	698.688	234.899	453.816	237.145	-0.0053
Pt 744	416.346	425.485	172.302	427.643	-0.0007
Pt 745	397.871	38.318	154.272	40.277	0.0016
Pt 746	747.708	74.371	503.771	76.302	0.0000
Pt 747	615.898	558.892	371.837	560.693	0.0003
Pt 748	354.024	264.612	110.023	266.422	0.0004
Pt 749	385.647	314.731	141.621	316.495	0.0004
Pt 750	583.845	106.113	339.561	108.109	-0.0016
Pt 751	432.136	99.824	188.193	101.715	0.0003
Pt 752	419.765	248.856	175.448	251.764	-0.0039
Pt 753	466.848	41.599	223.426	43.658	0.0020
Pt 754	424.187	540.703	180.226	542.602	0.0004
Pt 755	554.671	45.720	310.582	47.875	-0.0012
Pt 756	504.578	443.848	260.758	446.225	-0.0001
Pt 757	511.788	182.255	267.668	184.508	-0.0014
Pt 758	488.144	47.428	244.366	49.439	0.0006
Pt 759	494.092	49.932	249.940	51.739	-0.0004
Pt 760	313.740	546.497	69.572	548.887	-0.0019
Pt 761	651.552	433.921	407.569	436.236	-0.0010
Pt 762	524.998	485.879	280.980	487.939	-0.0003
Pt 763	622.104	258.472	378.239	260.432	0.0006
Pt 764	302.232	117.076	58.151	119.035	-0.0003
Pt 765	388.339	439.939	143.900	441.922	-0.0024
Pt 766	664.049	255.521	421.300	254.916	0.0145
Pt 767	527.666	194.159	283.559	196.246	-0.0009
Pt 768	584.254	240.284	340.289	242.418	-0.0004
Pt 769	580.428	61.310	336.655	63.389	0.0003
Pt 770	612.308	24.372	368.556	25.953	0.0018
Pt 771	494.696	588.423	250.725	590.451	0.0001
Pt 772	281.284	27.881	37.400	29.806	0.0005
Pt 773	475.607	569.092	231.192	570.926	-0.0021
Pt 774	326.115	30.433	82.019	32.441	-0.0005
Pt 775	536.139	548.431	292.163	550.433	0.0001
Pt 776	457.633	527.052	213.280	529.136	-0.0023

ID	Image location of conjugate points in Image A		Image location of conjugate points in Image B		Residuals
	x (Pixels)	y (Pixels)	x (Pixels)	y (Pixels)	Signed Dist (Pixels)
Pt 777	480.017	521.616	236.032	523.704	-0.0002
Pt 778	463.985	508.491	220.033	510.671	-0.0002
Pt 779	482.082	489.393	239.224	490.269	0.0095
Pt 780	274.204	56.121	29.954	58.125	-0.0011
Pt 781	613.405	468.282	369.517	470.305	0.0005
Pt 782	511.746	470.294	267.552	472.292	-0.0011
Pt 783	477.950	461.187	233.972	463.096	0.0003
Pt 784	595.949	444.961	352.300	447.109	0.0015
Pt 785	622.520	442.038	378.720	443.997	0.0012
Pt 786	557.023	437.121	313.032	439.119	0.0000
Pt 787	318.759	426.627	74.623	428.700	-0.0009
Pt 788	568.096	416.197	324.090	418.188	0.0000
Pt 789	548.118	414.936	304.149	416.806	0.0005
Pt 790	443.970	418.301	199.974	420.284	0.0000
Pt 791	306.382	410.537	62.396	412.476	0.0002
Pt 792	462.560	405.425	218.551	407.280	0.0003
Pt 793	429.272	403.057	186.047	404.967	0.0044
Pt 794	346.215	404.134	102.208	406.143	-0.0001
Pt 795	557.000	397.145	313.140	399.012	0.0011
Pt 796	328.435	397.511	84.387	399.557	-0.0004
Pt 797	403.078	376.219	159.060	378.228	-0.0002
Pt 798	285.214	359.510	41.052	361.277	-0.0004
Pt 799	577.438	336.593	333.378	338.653	-0.0006
Pt 800	623.369	322.071	379.345	324.010	0.0000
Pt 801	568.868	319.614	324.983	321.723	0.0002
Pt 802	311.891	321.623	67.950	323.580	0.0004
Pt 803	484.780	315.897	243.109	321.588	0.0019
Pt 804	664.209	294.888	420.210	296.947	-0.0003
Pt 805	609.534	298.252	364.581	301.478	-0.0088
Pt 806	523.087	294.029	279.105	296.032	0.0000
Pt 807	471.560	294.917	227.587	297.094	-0.0004
Pt 808	549.193	277.252	305.191	279.340	-0.0004
Pt 809	525.846	272.752	281.975	274.663	0.0008
Pt 810	432.436	121.202	188.429	123.255	-0.0003
Pt 811	289.862	268.955	47.861	273.458	0.0048
Pt 812	309.772	237.045	65.656	239.100	-0.0007
Pt 813	365.719	127.699	121.675	129.617	-0.0001
Pt 814	302.514	216.045	58.539	218.065	0.0000
Pt 815	324.022	210.330	79.895	212.312	-0.0006

ID	Image location of conjugate points in Image A		Image location of conjugate points in Image B		Residuals
	x (Pixels)	y (Pixels)	x (Pixels)	y (Pixels)	Signed Dist (Pixels)
Pt 816	554.815	206.857	310.221	209.037	-0.0035
Pt 817	642.224	180.520	398.088	182.675	-0.0014
Pt 818	281.414	177.466	37.550	179.413	0.0007
Pt 819	413.977	162.704	169.817	164.736	-0.0009
Pt 820	275.793	164.738	31.765	166.816	-0.0003
Pt 821	766.818	589.876	522.738	591.829	-0.0002
Pt 822	741.280	146.473	497.622	148.366	0.0015
Pt 823	743.140	590.030	499.236	592.024	0.0007
Pt 824	293.940	154.501	50.074	156.473	0.0006
Pt 825	317.574	152.151	73.516	154.413	-0.0009
Pt 826	409.369	590.807	165.184	592.682	-0.0009
Pt 827	550.218	581.792	306.344	583.744	0.0009
Pt 828	453.116	160.222	208.974	162.568	-0.0017
Pt 829	475.193	160.125	231.264	161.917	0.0007
Pt 830	527.321	158.500	283.318	160.530	-0.0003
Pt 831	566.520	573.709	322.810	575.615	0.0020
Pt 832	532.116	27.768	288.000	29.824	-0.0010
Pt 833	435.362	172.004	191.367	173.652	0.0008
Pt 834	454.794	183.735	210.762	185.673	-0.0001
Pt 835	732.190	30.647	488.168	32.554	-0.0004
Pt 836	681.909	555.168	439.519	555.656	0.0147
Pt 837	764.925	33.745	520.884	35.745	-0.0008
Pt 838	505.744	37.847	261.689	39.774	-0.0004
Pt 839	460.465	550.261	216.117	552.484	-0.0027
Pt 840	554.014	39.778	310.039	41.903	-0.0006
Pt 841	367.590	200.327	123.628	202.373	0.0000
Pt 842	557.378	537.870	313.228	539.859	-0.0009
Pt 843	444.275	537.892	200.328	539.654	0.0009
Pt 844	415.639	209.603	171.793	211.590	0.0007
Pt 845	730.690	37.201	486.710	39.194	-0.0005
Pt 846	393.381	525.762	149.084	527.792	-0.0019
Pt 847	667.618	216.767	423.778	218.480	0.0015
Pt 848	695.318	126.655	451.907	128.457	0.0029
Pt 849	619.800	222.373	375.885	224.249	0.0006
Pt 850	648.183	224.629	404.144	226.603	-0.0003
Pt 851	717.227	511.285	473.412	513.146	0.0016
Pt 852	328.481	234.583	84.536	236.839	-0.0003
Pt 853	537.185	500.954	293.189	502.929	0.0001
Pt 854	339.767	499.035	95.909	501.111	0.0006

ID	Image location of conjugate points in Image A		Image location of conjugate points in Image B		Residuals
	x (Pixels)	y (Pixels)	x (Pixels)	y (Pixels)	Signed Dist (Pixels)
Pt 855	526.740	47.478	286.405	51.865	0.0082
Pt 856	767.101	486.596	523.218	488.554	0.0008
Pt 857	527.730	249.946	283.778	251.736	0.0007
Pt 858	421.328	253.049	177.185	255.129	-0.0010
Pt 859	657.370	256.206	413.198	258.219	-0.0011
Pt 860	671.360	122.180	427.500	124.380	-0.0004
Pt 861	334.151	258.636	89.869	260.942	-0.0021
Pt 862	304.696	469.486	62.180	470.737	0.0098
Pt 863	379.205	270.941	134.932	272.327	0.0000
Pt 864	395.953	274.424	152.053	275.792	0.0019
Pt 865	301.517	124.860	57.400	126.402	0.0004
Pt 866	457.276	279.214	213.468	281.273	0.0007
Pt 867	369.351	455.727	125.482	457.472	0.0013
Pt 868	730.598	116.420	486.249	118.426	-0.0020
Pt 869	573.460	445.840	329.578	447.876	0.0005
Pt 870	569.257	116.888	324.502	119.084	-0.0042
Pt 871	355.638	288.910	111.529	291.453	-0.0018
Pt 872	333.928	115.669	89.876	117.088	0.0009
Pt 873	343.928	59.567	100.008	61.652	0.0000
Pt 874	540.810	295.064	296.706	297.069	-0.0006
Pt 875	397.249	437.640	153.530	439.701	0.0014
Pt 876	763.741	109.662	519.853	111.653	0.0000
Pt 877	691.187	294.650	447.208	296.620	0.0000
Pt 878	721.449	112.541	477.037	114.687	-0.0028
Pt 879	502.161	302.021	258.103	303.948	-0.0002
Pt 880	396.234	109.961	152.145	112.071	-0.0008
Pt 881	340.248	427.901	96.183	429.927	-0.0005
Pt 882	559.818	68.508	318.023	71.903	0.0049
Pt 883	506.734	421.271	262.723	423.106	0.0004
Pt 884	676.819	414.611	432.939	416.628	0.0005
Pt 885	316.002	73.863	73.872	71.830	0.0164
Pt 886	431.511	328.537	187.557	330.512	0.0002
Pt 887	523.733	406.491	279.726	408.408	0.0002
Pt 888	388.772	402.913	144.852	404.913	0.0004
Pt 889	640.187	77.154	395.727	78.852	-0.0014
Pt 890	647.573	341.876	403.488	343.799	-0.0003
Pt 891	648.164	389.372	404.165	391.397	-0.0001
Pt 892	550.685	85.038	306.556	87.486	-0.0022
Pt 893	600.480	373.941	356.441	375.903	-0.0002

ID	Image location of conjugate points in Image A		Image location of conjugate points in Image B		Residuals
	x (Pixels)	y (Pixels)	x (Pixels)	y (Pixels)	Signed Dist (Pixels)
Pt 894	510.196	361.341	266.435	363.455	0.0009
Pt 895	585.944	83.449	342.099	85.381	0.0005
Pt 896	619.384	558.488	375.455	560.422	0.0006
Pt 897	416.142	268.658	172.038	270.489	-0.0002
Pt 898	323.530	439.086	81.425	440.006	0.0127
Pt 899	497.360	151.217	253.423	153.181	0.0002
Pt 900	304.704	575.214	60.546	577.296	-0.0012
Pt 901	664.690	349.063	420.526	350.736	0.0001
Pt 902	382.436	28.846	138.914	30.328	0.0030
Pt 903	670.724	176.519	426.630	178.829	-0.0018
Pt 904	301.755	100.844	57.765	102.939	-0.0002
Pt 905	342.844	95.675	98.775	98.478	-0.0022
Pt 906	565.236	179.393	321.409	181.263	0.0010
Pt 907	723.148	72.265	477.706	72.924	-0.0020
Pt 908	608.169	191.617	364.206	193.233	0.0011
Pt 909	649.078	414.814	405.378	416.840	0.0015
Pt 910	450.714	101.091	206.849	103.224	0.0000
Pt 911	485.416	134.516	242.123	136.297	0.0036
Pt 912	657.627	105.186	413.572	106.230	0.0025
Pt 913	319.051	132.210	74.558	133.209	-0.0002
Pt 914	478.018	370.743	234.018	372.671	0.0001
Pt 915	322.756	44.340	78.637	46.224	-0.0004
Pt 916	704.112	223.847	460.115	225.780	0.0000
Pt 917	440.017	61.144	195.866	63.276	-0.0012
Pt 918	705.496	496.465	461.647	498.242	0.0016
Pt 919	363.233	491.810	119.677	493.667	0.0028
Pt 920	488.891	51.811	244.684	53.786	-0.0011
Pt 921	572.157	373.915	328.083	375.932	-0.0005
Pt 922	655.483	482.424	411.153	484.004	-0.0005
Pt 923	528.369	459.852	284.636	461.744	0.0018
Pt 924	738.465	467.584	494.049	469.540	-0.0022
Pt 925	610.421	272.065	366.866	274.065	0.0020
Pt 926	693.411	207.683	449.690	209.695	0.0010
Pt 927	593.780	271.821	350.578	273.524	0.0047
Pt 928	682.280	142.419	439.014	144.527	0.0026
Pt 929	580.218	277.853	336.199	280.036	-0.0008
Pt 930	424.944	479.696	181.603	482.558	0.0016
Pt 931	670.259	383.661	426.227	385.681	-0.0003
Pt 932	705.021	176.852	461.042	178.839	-0.0002

ID	Image location of conjugate points in Image A		Image location of conjugate points in Image B		Residuals
	x (Pixels)	y (Pixels)	x (Pixels)	y (Pixels)	Signed Dist (Pixels)
Pt 933	733.741	242.758	490.427	244.547	0.0038
Pt 934	341.828	194.895	97.885	197.124	-0.0003
Pt 935	439.636	193.888	195.980	195.784	0.0018
Pt 936	278.601	320.095	34.523	322.164	-0.0006
Pt 937	431.557	197.513	187.777	199.639	0.0006
Pt 938	469.288	200.187	225.453	202.355	0.0002
Pt 939	636.936	102.026	391.501	103.860	-0.0061
Pt 940	585.742	124.513	340.325	127.679	-0.0101
Pt 941	494.242	362.116	252.662	362.670	0.0166
Pt 942	533.772	109.580	289.805	111.764	-0.0006
Pt 943	515.820	219.802	271.548	221.904	-0.0017
Pt 944	700.568	264.364	458.538	268.349	0.0027
Pt 945	451.921	220.364	207.834	222.309	-0.0004
Pt 946	412.027	522.948	167.715	523.976	0.0005
Pt 947	372.150	43.547	127.909	45.491	-0.0010
Pt 948	332.942	518.159	88.709	520.240	-0.0016
Pt 949	513.392	203.765	269.522	205.890	0.0001
Pt 950	762.887	448.666	518.751	450.351	0.0004
Pt 951	672.393	494.590	428.343	496.597	-0.0003
Pt 952	660.340	473.798	416.185	476.439	-0.0030
Pt 953	507.984	488.167	263.844	490.152	-0.0008
Pt 954	549.957	484.084	306.109	485.956	0.0012
Pt 955	541.625	129.320	297.608	131.403	-0.0006
Pt 956	691.850	388.905	448.119	390.755	0.0019
Pt 957	452.157	245.398	208.118	247.304	0.0000
Pt 958	297.892	41.301	52.324	43.321	-0.0066
Pt 959	459.196	41.209	216.252	44.980	-0.0005
Pt 960	396.567	46.201	152.443	46.598	0.0031
Pt 961	577.073	51.536	334.617	54.897	0.0020
Pt 962	643.911	50.092	399.556	51.706	-0.0007
Pt 963	541.741	60.151	298.737	64.021	-0.0015
Pt 964	606.689	64.796	365.920	67.117	0.0123
Pt 965	319.312	74.989	75.992	76.607	0.0036
Pt 966	337.046	81.435	92.663	83.534	-0.0020
Pt 967	565.074	74.192	319.906	76.373	-0.0059
Pt 968	636.696	79.466	394.529	83.295	0.0016
Pt 969	367.193	91.082	123.527	92.904	0.0017
Pt 970	734.077	91.456	489.533	92.400	0.0009
Pt 971	299.842	101.911	57.246	104.367	0.0051

ID	Image location of conjugate points in Image A		Image location of conjugate points in Image B		Residuals
	x (Pixels)	y (Pixels)	x (Pixels)	y (Pixels)	Signed Dist (Pixels)
Pt 972	456.828	99.968	213.493	102.161	0.0022
Pt 973	499.610	100.012	254.913	101.426	-0.0017
Pt 974	688.202	101.378	445.757	103.875	0.0046
Pt 975	434.220	116.837	190.147	119.156	-0.0013
Pt 976	529.997	108.821	284.251	111.200	-0.0090
Pt 977	463.107	122.671	219.337	124.420	0.0015
Pt 978	585.112	128.973	340.523	131.338	-0.0040
Pt 979	484.046	131.836	240.396	133.967	0.0010
Pt 980	608.053	141.404	365.004	143.869	0.0025
Pt 981	295.341	149.355	52.366	151.523	0.0043
Pt 982	443.463	142.115	199.170	144.309	-0.0020
Pt 983	640.368	148.878	396.159	150.741	-0.0008
Pt 984	458.743	159.247	214.663	161.035	0.0000
Pt 985	531.256	160.098	285.581	163.436	-0.0117
Pt 986	335.201	167.891	90.805	169.336	-0.0007
Pt 987	393.509	173.332	149.893	175.787	0.0006
Pt 988	412.227	167.726	169.876	169.165	0.0088
Pt 989	470.522	166.171	227.059	167.570	0.0039
Pt 990	564.853	169.329	320.693	171.497	-0.0015
Pt 991	675.264	176.842	432.082	178.969	0.0030
Pt 992	452.806	188.297	208.315	190.695	-0.0034
Pt 993	608.308	183.498	364.276	186.086	-0.0022
Pt 994	413.468	199.182	170.416	199.519	0.0084
Pt 995	325.694	207.351	81.298	209.137	-0.0015
Pt 996	336.369	234.875	92.548	236.209	0.0023
Pt 997	407.604	230.175	164.061	231.793	0.0030
Pt 998	442.558	236.157	200.158	240.537	0.0016
Pt 999	656.557	229.955	412.368	229.717	0.0062
Pt 1000	366.625	246.716	122.891	248.252	0.0023
Pt 1001	543.471	254.544	300.318	255.987	0.0056
Pt 1002	421.535	270.859	177.384	272.533	0.0000
Pt 1003	527.555	272.101	284.183	274.883	0.0008
Pt 1004	454.291	278.465	211.104	280.316	0.0043
Pt 1005	686.657	283.250	441.920	283.465	0.0022
Pt 1006	472.538	297.059	228.840	299.277	0.0009
Pt 1007	497.199	290.709	252.866	292.603	-0.0015
Pt 1008	664.645	295.484	420.878	297.330	0.0015
Pt 1009	294.764	304.047	49.409	307.802	-0.0104
Pt 1010	410.967	307.251	166.949	308.589	0.0015

ID	Image location of conjugate points in Image A		Image location of conjugate points in Image B		Residuals
	x (Pixels)	y (Pixels)	x (Pixels)	y (Pixels)	Signed Dist (Pixels)
Pt 1011	353.487	316.271	109.328	318.704	-0.0018
Pt 1012	439.899	311.017	195.549	312.730	-0.0011
Pt 1013	483.848	316.075	240.364	318.957	0.0002
Pt 1014	306.900	327.164	63.608	329.112	0.0037
Pt 1015	452.160	332.041	207.198	333.814	-0.0044
Pt 1016	358.013	342.896	113.932	344.450	0.0005
Pt 1017	655.757	338.689	411.888	340.162	0.0023
Pt 1018	420.476	356.263	175.690	357.872	-0.0032
Pt 1019	319.483	373.361	74.668	375.698	-0.0051
Pt 1020	356.945	381.341	112.100	383.382	-0.0046
Pt 1021	369.448	372.093	125.424	373.998	0.0001
Pt 1022	620.441	371.396	375.780	373.654	-0.0044
Pt 1023	673.252	381.309	429.865	383.579	0.0023
Pt 1024	308.554	404.580	64.338	406.855	-0.0018
Pt 1025	347.269	405.017	103.849	405.522	0.0064
Pt 1026	578.647	395.272	334.222	397.459	-0.0029
Pt 1027	546.476	415.589	303.006	417.384	0.0034
Pt 1028	679.231	416.174	438.352	416.017	0.0242
Pt 1029	324.582	425.770	79.672	428.014	-0.0056
Pt 1030	371.757	420.810	125.875	425.388	-0.0162
Pt 1031	444.387	421.740	200.416	423.686	0.0003
Pt 1032	483.855	426.235	239.339	428.009	-0.0023
Pt 1033	399.352	440.416	154.502	442.531	-0.0050
Pt 1034	527.642	436.010	283.682	437.953	0.0004
Pt 1035	299.857	446.275	55.556	448.615	-0.0024
Pt 1036	755.499	447.173	513.644	449.796	0.0096
Pt 1037	410.288	460.915	166.732	463.079	0.0020
Pt 1038	477.630	465.559	232.682	467.941	-0.0064
Pt 1039	551.584	461.023	307.901	462.536	0.0032
Pt 1040	737.041	463.887	494.154	463.547	0.0146
Pt 1041	512.832	469.210	269.051	471.427	0.0006
Pt 1042	531.807	480.947	288.077	483.092	0.0011
Pt 1043	656.989	487.152	412.487	490.335	-0.0067
Pt 1044	725.026	488.931	479.377	491.079	-0.0099
Pt 1045	748.625	487.828	504.098	490.020	-0.0037
Pt 1046	701.299	493.164	456.340	495.138	-0.0054
Pt 1047	502.329	508.511	257.259	511.228	-0.0082
Pt 1048	575.419	525.815	332.551	528.343	0.0050
Pt 1049	351.601	536.970	107.389	539.266	-0.0020

ID	Image location of conjugate points in Image A		Image location of conjugate points in Image B		Residuals
	x (Pixels)	y (Pixels)	x (Pixels)	y (Pixels)	Signed Dist (Pixels)
Pt 1050	453.374	527.277	210.319	526.799	0.0119
Pt 1051	649.035	530.925	404.827	532.332	0.0007
Pt 1052	674.688	531.950	428.987	535.675	-0.0157
Pt 1053	409.550	541.736	165.564	543.297	0.0011
Pt 1054	536.802	545.882	292.753	547.768	0.0000
Pt 1055	433.844	560.381	188.420	562.814	-0.0096
Pt 1056	584.057	557.404	339.988	560.069	-0.0024
Pt 1057	656.047	557.136	412.967	558.965	0.0061
Pt 1058	685.219	559.151	441.652	561.183	0.0025
Pt 1059	472.207	571.567	227.783	573.036	-0.0012
Pt 1060	628.527	568.184	384.476	570.377	-0.0009
Pt 1061	758.480	568.129	513.309	570.740	-0.0091
Pt 1062	363.361	579.306	119.535	581.334	0.0009
Pt 1063	695.577	577.724	452.522	580.181	0.0042
Pt 1064	463.380	48.395	223.654	51.764	0.0140
Pt 1065	691.693	70.783	447.259	72.657	-0.0019
Pt 1066	546.370	93.868	302.298	96.238	-0.0017
Pt 1067	320.111	97.112	76.873	100.015	0.0013
Pt 1068	431.479	104.158	186.896	105.924	-0.0021
Pt 1069	608.110	98.609	367.180	99.389	0.0168
Pt 1070	467.323	110.737	223.486	113.426	-0.0013
Pt 1071	556.428	123.743	312.475	125.936	-0.0006
Pt 1072	405.727	134.186	161.813	136.499	-0.0005
Pt 1073	363.485	146.861	119.054	148.881	-0.0021
Pt 1074	469.339	156.651	224.912	158.507	-0.0017
Pt 1075	636.535	163.424	392.654	164.829	0.0022
Pt 1076	526.444	171.450	282.522	174.065	-0.0016
Pt 1077	610.476	171.266	367.178	173.081	0.0035
Pt 1078	691.894	173.849	446.741	178.618	-0.0151
Pt 1079	641.296	198.605	397.671	200.275	0.0026
Pt 1080	509.843	247.647	265.064	250.006	-0.0049
Pt 1081	326.983	259.668	83.070	261.273	0.0012
Pt 1082	355.247	274.717	111.078	276.352	-0.0001
Pt 1083	497.474	277.024	254.035	280.781	-0.0021
Pt 1084	584.870	283.661	341.247	284.878	0.0041
Pt 1085	414.790	295.942	170.858	298.761	-0.0017
Pt 1086	582.743	296.561	338.960	299.143	-0.0008
Pt 1087	620.772	304.654	377.177	306.906	0.0011
Pt 1088	342.827	329.801	98.001	331.906	-0.0045

ID	Image location of conjugate points in Image A		Image location of conjugate points in Image B		Residuals
	x (Pixels)	y (Pixels)	x (Pixels)	y (Pixels)	Signed Dist (Pixels)
Pt 1089	384.811	324.907	140.609	326.530	-0.0002
Pt 1090	544.214	324.193	299.976	326.686	-0.0027
Pt 1091	679.818	325.471	435.476	327.963	-0.0035
Pt 1092	572.242	336.713	328.555	338.516	0.0021
Pt 1093	371.126	348.276	128.101	350.875	0.0037
Pt 1094	545.529	355.322	301.306	357.181	-0.0008
Pt 1095	459.970	366.655	216.229	369.426	-0.0007
Pt 1096	548.440	400.691	302.933	402.590	-0.0079
Pt 1097	414.675	408.459	170.463	410.694	-0.0018
Pt 1098	481.612	411.563	237.501	413.333	0.0000
Pt 1099	451.490	434.829	207.096	436.637	-0.0017
Pt 1100	329.187	452.788	85.775	453.783	0.0054
Pt 1101	396.883	452.103	152.909	453.990	0.0004
Pt 1102	611.949	448.791	368.764	451.810	0.0013
Pt 1103	575.279	473.804	331.863	477.421	-0.0016
Pt 1104	432.742	500.457	187.706	502.972	-0.0073
Pt 1105	686.880	494.556	443.903	495.828	0.0083
Pt 1106	558.778	519.447	313.522	519.915	-0.0028
Pt 1107	711.711	520.507	466.499	523.011	-0.0088
Pt 1108	404.562	533.212	160.905	534.605	0.0034
Pt 1109	535.950	531.156	290.856	532.658	-0.0050
Pt 1110	491.598	544.484	248.319	546.674	0.0037
Pt 1111	330.968	560.714	87.867	562.918	0.0048
Pt 1112	474.271	144.472	231.868	144.934	0.0111
Pt 1113	596.476	231.381	352.722	232.748	0.0029
Pt 1114	500.620	273.821	256.518	275.160	0.0012
Pt 1115	402.345	289.178	159.400	289.221	0.0099
Pt 1116	629.135	304.131	384.401	306.231	-0.0042
Pt 1117	560.998	350.707	319.156	350.524	0.0176
Pt 1118	407.220	412.947	164.658	413.772	0.0106
Pt 1119	451.426	435.491	207.309	436.774	0.0012
Pt 1120	590.000	430.847	344.709	432.077	-0.0048
Pt 1121	465.346	489.546	225.242	492.548	0.0195
Pt 1122	574.179	483.855	329.792	484.286	0.0025
Pt 1123	383.828	533.960	139.308	535.869	-0.0029
Pt 1124	492.485	542.997	248.104	544.608	-0.0012
Pt 1125	632.924	89.688	386.410	90.503	-0.0075
Pt 1126	497.095	129.240	255.530	133.144	0.0054
Pt 1127	594.733	158.538	351.381	160.579	0.0026

ID	Image location of conjugate points in Image A		Image location of conjugate points in Image B		Residuals
	x (Pixels)	y (Pixels)	x (Pixels)	y (Pixels)	Signed Dist (Pixels)
Pt 1128	494.143	203.322	248.747	205.646	-0.0076
Pt 1129	388.832	497.458	145.953	500.400	0.0041
SUM:					0.0328

APPENDIX C

Table C1: Image coordinates of associated image pairs automatically obtained using Speeded Up Robust Feature algorithm on google earth image pairs.

ID	Image location of conjugate points in Image A		Image location of conjugate points in Image B		Residuals
	x (Pixels)	y (Pixels)	x (Pixels)	y (Pixels)	Signed Dist (Pixels)
Pt 1	624.444	450.988	379.939	453.211	-0.0022
Pt 2	601.348	450.286	357.438	452.302	0.0002
Pt 3	605.821	227.310	361.851	229.346	0.0001
Pt 4	403.938	150.064	159.875	152.103	-0.0002
Pt 5	544.092	519.797	300.114	521.678	0.0004
Pt 6	599.419	461.928	356.237	464.509	0.0007
Pt 7	778.098	556.542	534.157	558.554	0.0003
Pt 8	542.677	297.371	298.679	299.368	0.0001
Pt 9	354.503	359.914	110.481	361.778	0.0004
Pt 10	684.910	285.341	440.889	287.232	0.0006
Pt 11	280.900	610.201	36.299	612.424	-0.0024
Pt 12	591.514	450.011	347.364	452.248	-0.0012
Pt 13	392.421	379.173	148.390	381.199	-0.0001
Pt 14	466.844	559.812	222.879	561.517	0.0008
Pt 15	676.161	251.483	432.163	253.379	0.0006
Pt 16	697.875	34.844	453.915	36.746	0.0007
Pt 17	697.875	34.844	453.915	36.746	0.0007
Pt 18	430.921	260.604	186.894	262.668	-0.0002
Pt 19	745.451	507.109	501.530	509.155	0.0002
Pt 20	480.661	596.965	236.866	598.989	0.0005
Pt 21	480.661	596.965	236.866	598.989	0.0005
Pt 22	601.403	414.281	357.403	416.391	-0.0003
Pt 23	433.937	613.768	189.994	615.764	0.0001
Pt 24	320.857	459.430	76.812	461.367	0.0002
Pt 25	783.995	3.441	539.730	5.618	-0.0005
Pt 26	635.877	614.175	391.910	616.095	0.0002
Pt 27	640.797	285.421	396.836	287.352	0.0005
Pt 28	566.064	283.670	322.078	285.634	0.0002
Pt 29	356.050	612.660	112.237	614.614	0.0008
Pt 30	431.168	8.947	187.096	11.249	-0.0010
Pt 31	298.996	612.525	54.932	614.528	-0.0001
Pt 32	610.573	245.951	366.545	247.867	0.0003
Pt 33	593.467	244.924	349.478	246.888	0.0002
Pt 34	381.233	399.245	137.262	401.204	0.0003

ID	Image location of conjugate points in Image A		Image location of conjugate points in Image B		Residuals
	x (Pixels)	y (Pixels)	x (Pixels)	y (Pixels)	Signed Dist (Pixels)
Pt 35	367.809	18.361	123.994	20.468	-0.0001
Pt 36	676.818	307.238	433.015	309.299	0.0005
Pt 37	353.556	23.738	109.572	25.706	0.0000
Pt 38	634.676	127.071	390.654	129.149	-0.0001
Pt 39	634.676	127.071	390.654	129.149	-0.0001
Pt 40	372.817	404.182	128.774	406.217	-0.0001
Pt 41	478.352	167.515	234.257	169.452	0.0000
Pt 42	667.934	313.758	423.870	315.706	0.0002
Pt 43	486.043	526.449	241.754	528.561	-0.0013
Pt 44	467.667	177.275	223.619	179.267	-0.0001
Pt 45	267.172	563.908	23.283	565.894	0.0006
Pt 46	588.404	394.475	344.402	396.488	0.0000
Pt 47	562.835	605.263	318.832	607.345	-0.0004
Pt 48	512.130	605.731	268.255	607.733	0.0003
Pt 49	453.649	604.367	209.553	606.398	-0.0005
Pt 50	367.891	304.966	123.449	307.015	-0.0011
Pt 51	585.809	408.248	341.678	410.253	-0.0003
Pt 52	585.809	408.248	341.678	410.253	-0.0003
Pt 53	465.473	395.684	221.533	397.612	0.0004
Pt 54	308.963	45.742	64.826	47.894	-0.0006
Pt 55	373.241	116.532	129.184	118.599	-0.0003
Pt 56	373.241	116.532	129.184	118.599	-0.0003
Pt 57	322.612	408.697	77.861	410.577	-0.0017
Pt 58	612.032	238.688	367.965	240.618	0.0002
Pt 59	612.032	238.688	367.965	240.618	0.0002
Pt 60	351.286	393.838	107.145	395.727	0.0000
Pt 61	256.942	510.308	12.941	512.282	0.0003
Pt 62	256.942	510.308	12.941	512.282	0.0003
Pt 63	289.937	395.120	45.945	397.066	0.0003
Pt 64	774.804	565.019	530.730	566.866	0.0004
Pt 65	407.077	319.812	163.061	321.822	0.0000
Pt 66	343.431	420.024	99.361	422.026	-0.0001
Pt 67	280.076	596.514	35.592	598.450	-0.0014
Pt 68	576.429	593.088	332.362	594.942	0.0001
Pt 69	550.165	591.518	306.127	593.506	-0.0002
Pt 70	259.901	590.993	15.865	592.383	0.0013
Pt 71	552.788	422.795	308.810	424.863	-0.0001
Pt 72	664.288	388.610	420.216	390.590	0.0000
Pt 73	553.987	325.276	309.936	327.234	0.0001

ID	Image location of conjugate points in Image A		Image location of conjugate points in Image B		Residuals
	x (Pixels)	y (Pixels)	x (Pixels)	y (Pixels)	Signed Dist (Pixels)
Pt 74	335.900	424.030	91.918	426.015	0.0002
Pt 75	433.850	587.513	190.084	589.542	0.0007
Pt 76	490.112	185.601	245.967	187.647	-0.0004
Pt 77	551.521	388.993	307.600	390.957	0.0004
Pt 78	524.851	424.134	280.151	426.792	-0.0039
Pt 79	549.392	579.044	305.328	581.021	-0.0003
Pt 80	739.361	83.755	495.575	85.619	0.0012
Pt 81	288.032	86.893	44.035	88.751	0.0003
Pt 82	426.679	428.917	182.672	431.001	-0.0002
Pt 83	535.724	301.537	291.716	303.623	-0.0002
Pt 84	492.421	427.789	248.441	429.696	0.0003
Pt 85	492.421	427.789	248.441	429.696	0.0003
Pt 86	636.538	85.050	392.624	87.029	0.0004
Pt 87	743.663	580.452	499.570	582.435	-0.0003
Pt 88	644.161	470.804	400.201	472.780	0.0002
Pt 89	644.161	470.804	400.201	472.780	0.0002
Pt 90	462.926	233.894	218.977	235.899	0.0001
Pt 91	462.926	233.894	218.977	235.899	0.0001
Pt 92	462.926	233.894	218.977	235.899	0.0001
Pt 93	462.926	233.894	218.977	235.899	0.0001
Pt 94	455.212	580.948	211.171	582.955	-0.0002
Pt 95	557.213	288.029	313.308	290.134	0.0000
Pt 96	282.003	332.603	37.617	334.469	-0.0005
Pt 97	540.965	432.307	296.892	434.690	-0.0013
Pt 98	352.288	92.879	108.215	94.751	0.0001
Pt 99	632.193	450.923	388.185	452.838	0.0003
Pt 100	254.269	585.744	11.054	587.378	0.0037
Pt 101	266.828	573.768	22.914	575.713	0.0006
Pt 102	278.525	585.753	34.527	587.790	0.0001
Pt 103	647.204	298.112	403.219	300.088	0.0003
Pt 104	647.204	298.112	403.219	300.088	0.0003
Pt 105	579.243	384.891	336.174	386.441	0.0040
Pt 106	680.763	335.278	436.757	337.290	0.0001
Pt 107	310.054	437.574	66.337	439.879	0.0004
Pt 108	632.974	437.090	389.041	439.065	0.0003
Pt 109	553.447	568.663	309.484	570.689	-0.0001
Pt 110	432.925	437.727	188.626	439.483	-0.0002
Pt 111	341.364	259.563	97.339	261.607	-0.0001
Pt 112	429.054	385.196	184.962	387.044	0.0002

ID	Image location of conjugate points in Image A		Image location of conjugate points in Image B		Residuals
	x (Pixels)	y (Pixels)	x (Pixels)	y (Pixels)	Signed Dist (Pixels)
Pt 113	478.699	259.728	234.809	261.670	0.0004
Pt 114	453.087	136.357	209.186	138.556	-0.0003
Pt 115	716.634	557.076	472.658	559.083	0.0001
Pt 116	304.870	386.219	60.887	388.286	0.0001
Pt 117	410.842	139.364	166.773	141.289	0.0000
Pt 118	599.507	422.845	355.595	424.859	0.0003
Pt 119	556.592	556.063	312.578	558.155	-0.0004
Pt 120	285.851	592.733	41.848	594.573	0.0005
Pt 121	508.969	297.141	265.023	299.198	0.0000
Pt 122	303.982	340.878	59.970	342.934	0.0000
Pt 123	521.713	144.863	277.690	146.823	0.0001
Pt 124	365.608	339.734	121.587	341.861	-0.0002
Pt 125	614.310	279.168	370.229	281.087	0.0002
Pt 126	545.783	451.349	301.939	452.954	0.0016
Pt 127	289.256	343.829	45.244	345.733	0.0004
Pt 128	289.256	343.829	45.244	345.733	0.0004
Pt 129	338.018	344.311	93.958	346.349	-0.0001
Pt 130	434.173	595.821	190.223	597.753	0.0003
Pt 131	612.958	400.048	368.852	402.118	-0.0004
Pt 132	769.392	548.862	525.396	550.947	-0.0002
Pt 133	330.543	455.858	86.595	457.807	0.0004
Pt 134	354.198	69.404	110.105	71.324	-0.0001
Pt 135	379.050	543.821	135.033	545.865	-0.0001
Pt 136	379.050	543.821	135.033	545.865	-0.0001
Pt 137	326.137	545.231	82.147	547.159	0.0003
Pt 138	342.149	396.500	98.106	398.425	0.0002
Pt 139	263.205	395.975	19.177	398.028	0.0001
Pt 140	605.682	218.282	361.804	220.311	0.0003
Pt 141	457.675	597.987	213.586	600.047	-0.0006
Pt 142	655.712	343.081	411.756	345.084	0.0003
Pt 143	585.874	459.549	341.873	461.519	0.0001
Pt 144	295.504	384.695	51.593	386.724	0.0004
Pt 145	754.548	599.913	510.689	601.924	0.0004
Pt 146	475.919	177.039	231.865	179.046	-0.0001
Pt 147	569.847	383.622	326.679	385.135	0.0038
Pt 148	539.960	539.533	295.987	541.603	-0.0002
Pt 149	353.764	383.392	109.707	385.312	0.0001
Pt 150	544.893	347.293	300.920	349.283	0.0001
Pt 151	632.782	266.848	388.792	268.846	0.0002

ID	Image location of conjugate points in Image A		Image location of conjugate points in Image B		Residuals
	x (Pixels)	y (Pixels)	x (Pixels)	y (Pixels)	Signed Dist (Pixels)
Pt 152	535.745	535.146	291.770	537.125	0.0001
Pt 153	434.527	536.492	190.459	538.378	0.0000
Pt 154	434.527	536.492	190.459	538.378	0.0000
Pt 155	582.621	375.035	338.597	377.110	-0.0002
Pt 156	316.372	188.114	72.131	189.797	0.0002
Pt 157	480.316	188.573	236.360	190.557	0.0001
Pt 158	499.164	186.590	255.110	188.513	0.0001
Pt 159	348.832	349.280	104.453	351.642	-0.0017
Pt 160	696.963	53.718	452.927	55.844	-0.0002
Pt 161	572.923	351.036	328.917	353.083	-0.0001
Pt 162	572.923	351.036	328.917	353.083	-0.0001
Pt 163	619.904	349.247	375.926	351.121	0.0006
Pt 164	523.180	160.923	279.068	162.993	-0.0004
Pt 165	302.570	269.953	58.519	271.968	0.0000
Pt 166	638.392	352.153	394.449	354.173	0.0002
Pt 167	638.392	352.153	394.449	354.173	0.0002
Pt 168	392.731	153.067	148.677	155.062	-0.0001
Pt 169	392.731	153.067	148.677	155.062	-0.0001
Pt 170	269.088	202.923	25.384	204.954	0.0007
Pt 171	263.083	366.241	19.078	368.100	0.0005
Pt 172	601.121	357.440	357.129	359.442	0.0001
Pt 173	286.957	193.490	43.218	195.590	0.0004
Pt 174	541.199	214.723	297.645	216.349	0.0021
Pt 175	524.839	523.028	280.792	524.997	-0.0001
Pt 176	361.222	349.377	117.317	351.361	0.0004
Pt 177	567.237	376.383	323.217	378.411	-0.0001
Pt 178	567.237	376.383	323.217	378.411	-0.0001
Pt 179	540.071	375.949	296.102	378.053	-0.0002
Pt 180	312.161	339.871	68.189	341.898	0.0002
Pt 181	312.161	339.871	68.189	341.898	0.0002
Pt 182	518.324	153.076	274.238	155.042	0.0000
Pt 183	587.485	153.090	343.517	155.097	0.0001
Pt 184	587.485	153.090	343.517	155.097	0.0001
Pt 185	400.894	223.829	157.004	225.950	0.0000
Pt 186	400.894	223.829	157.004	225.950	0.0000
Pt 187	609.055	338.332	364.656	341.410	-0.0043
Pt 188	415.309	225.796	171.295	227.779	0.0000
Pt 189	757.482	515.293	513.533	516.917	0.0017
Pt 190	255.926	361.105	11.866	363.024	0.0003

ID	Image location of conjugate points in Image A		Image location of conjugate points in Image B		Residuals
	x (Pixels)	y (Pixels)	x (Pixels)	y (Pixels)	Signed Dist (Pixels)
Pt 191	603.840	478.532	359.630	480.345	-0.0001
Pt 192	596.149	327.934	352.091	329.977	-0.0002
Pt 193	564.790	271.177	320.744	273.242	-0.0002
Pt 194	653.874	325.645	409.983	327.625	0.0005
Pt 195	393.003	324.271	148.989	326.340	-0.0001
Pt 196	559.640	318.814	315.670	321.024	-0.0005
Pt 197	586.650	312.656	342.650	314.660	0.0001
Pt 198	263.112	155.356	19.181	157.445	0.0001
Pt 199	775.213	29.732	531.197	31.867	0.0000
Pt 200	344.936	252.170	100.950	254.213	0.0000
Pt 201	344.936	252.170	100.950	254.213	0.0000
Pt 202	481.787	505.325	237.800	507.483	-0.0004
Pt 203	507.126	307.074	263.697	310.229	-0.0017
Pt 204	557.683	364.951	313.652	366.946	0.0000
Pt 205	628.236	372.015	384.165	374.027	-0.0001
Pt 206	628.236	372.015	384.165	374.027	-0.0001
Pt 207	445.871	299.576	201.467	300.560	0.0016
Pt 208	758.064	21.833	514.006	23.954	-0.0001
Pt 209	542.561	501.989	298.459	503.812	0.0001
Pt 210	499.730	293.356	255.854	295.122	0.0010
Pt 211	637.846	273.191	393.876	275.184	0.0003
Pt 212	549.359	293.425	305.333	295.429	0.0000
Pt 213	521.003	495.822	276.978	497.906	-0.0004
Pt 214	472.699	414.847	228.872	416.822	0.0006
Pt 215	472.699	414.847	228.872	416.822	0.0006
Pt 216	404.401	573.752	160.632	575.768	0.0007
Pt 217	682.136	255.833	437.948	257.950	-0.0006
Pt 218	682.136	255.833	437.948	257.950	-0.0006
Pt 219	298.033	571.075	53.942	573.108	-0.0002
Pt 220	528.606	504.179	284.675	506.144	0.0003
Pt 221	603.353	31.134	359.455	33.156	0.0001
Pt 222	428.943	87.188	185.012	89.359	-0.0004
Pt 223	382.046	142.700	138.046	144.936	-0.0006
Pt 224	382.046	142.700	138.046	144.936	-0.0006
Pt 225	636.797	473.944	392.892	475.710	0.0011
Pt 226	399.049	144.546	154.793	146.572	-0.0006
Pt 227	399.049	144.546	154.793	146.572	-0.0006
Pt 228	526.425	532.470	282.278	534.403	-0.0004
Pt 229	328.573	323.357	84.433	326.371	-0.0023

ID	Image location of conjugate points in Image A		Image location of conjugate points in Image B		Residuals
	x (Pixels)	y (Pixels)	x (Pixels)	y (Pixels)	Signed Dist (Pixels)
Pt 230	706.051	32.652	462.038	34.623	0.0004
Pt 231	449.464	125.367	205.527	127.192	0.0005
Pt 232	409.894	154.869	165.912	156.904	-0.0001
Pt 233	577.800	558.504	333.648	560.395	-0.0003
Pt 234	533.709	610.464	289.813	612.450	0.0003
Pt 235	607.526	443.782	363.497	445.591	0.0005
Pt 236	607.526	443.782	363.497	445.591	0.0005
Pt 237	631.863	449.381	387.891	451.182	0.0008
Pt 238	631.341	481.805	387.421	483.715	0.0006
Pt 239	419.844	375.930	175.790	377.842	0.0001
Pt 240	474.025	551.772	230.109	553.534	0.0008
Pt 241	546.489	560.113	302.438	562.078	-0.0002
Pt 242	487.969	538.026	244.058	540.024	0.0002
Pt 243	419.460	340.705	175.419	342.673	0.0000
Pt 244	503.010	600.955	259.026	603.004	-0.0002
Pt 245	741.083	521.369	497.733	523.757	0.0008
Pt 246	785.176	11.614	541.722	13.554	0.0015
Pt 247	304.902	258.786	60.917	260.820	0.0001
Pt 248	304.902	258.786	60.917	260.820	0.0001
Pt 249	304.902	258.786	60.917	260.820	0.0001
Pt 250	661.229	162.047	417.272	163.995	0.0005
Pt 251	661.229	162.047	417.272	163.995	0.0005
Pt 252	297.917	178.166	53.948	180.327	-0.0002
Pt 253	320.197	219.736	76.195	221.820	-0.0001
Pt 254	537.966	201.885	293.994	203.822	0.0003
Pt 255	538.673	266.889	294.688	268.940	0.0000
Pt 256	284.880	269.731	40.883	271.708	0.0002
Pt 257	582.738	196.909	338.729	198.994	-0.0002
Pt 258	629.444	277.825	385.449	279.896	-0.0001
Pt 259	658.836	276.540	415.335	278.495	0.0015
Pt 260	373.954	289.543	129.918	291.601	-0.0001
Pt 261	373.954	289.543	129.918	291.601	-0.0001
Pt 262	499.261	308.858	255.325	310.779	0.0004
Pt 263	561.388	307.215	317.409	309.227	0.0001
Pt 264	461.084	310.553	217.074	312.589	-0.0001
Pt 265	595.278	309.876	351.292	312.017	-0.0003
Pt 266	292.157	316.131	48.191	318.042	0.0004
Pt 267	502.282	324.567	258.594	326.157	0.0019
Pt 268	607.576	326.240	363.548	328.219	0.0001

ID	Image location of conjugate points in Image A		Image location of conjugate points in Image B		Residuals
	x (Pixels)	y (Pixels)	x (Pixels)	y (Pixels)	Signed Dist (Pixels)
Pt 269	570.240	428.555	326.251	430.571	0.0000
Pt 270	320.030	334.017	75.983	335.901	0.0003
Pt 271	560.857	333.934	316.833	335.949	0.0000
Pt 272	370.005	354.232	125.972	356.232	0.0000
Pt 273	583.343	364.622	339.383	366.639	0.0001
Pt 274	457.296	408.085	213.221	410.093	-0.0002
Pt 275	358.152	375.279	114.256	377.238	0.0005
Pt 276	333.500	401.414	89.524	403.422	0.0002
Pt 277	255.314	609.669	11.271	611.578	0.0003
Pt 278	620.301	602.223	376.292	604.348	-0.0006
Pt 279	258.821	480.192	14.844	482.239	0.0003
Pt 280	474.763	390.223	230.735	392.350	-0.0004
Pt 281	787.088	563.064	543.470	564.829	0.0023
Pt 282	536.838	525.157	292.824	527.222	-0.0003
Pt 283	536.838	525.157	292.824	527.222	-0.0003
Pt 284	454.871	549.534	210.930	551.675	-0.0002
Pt 285	288.469	602.206	44.518	604.833	-0.0009
Pt 286	546.292	303.267	302.446	305.295	0.0004
Pt 287	575.895	305.219	332.009	307.231	0.0003
Pt 288	530.943	444.172	287.010	446.045	0.0006
Pt 289	381.206	131.390	137.347	133.183	0.0007
Pt 290	582.192	181.751	338.199	183.827	-0.0001
Pt 291	594.369	199.660	350.909	202.548	-0.0015
Pt 292	581.799	224.943	337.861	226.980	0.0001
Pt 293	278.807	250.346	34.852	252.269	0.0004
Pt 294	493.566	267.421	249.468	269.397	-0.0001
Pt 295	571.387	242.016	327.479	244.167	-0.0002
Pt 296	291.162	469.645	46.947	471.627	-0.0004
Pt 297	363.166	586.072	118.989	587.998	-0.0004
Pt 298	473.608	473.901	229.729	475.772	0.0007
Pt 299	494.464	473.766	250.355	475.706	-0.0002
Pt 300	494.464	473.766	250.355	475.706	-0.0002
Pt 301	643.006	189.908	399.171	192.740	-0.0022
Pt 302	562.464	386.058	318.419	387.978	0.0002
Pt 303	296.351	239.907	52.251	242.193	-0.0007
Pt 304	296.351	239.907	52.251	242.193	-0.0007
Pt 305	550.004	510.581	305.936	512.594	-0.0003
Pt 306	535.623	286.339	291.508	288.346	-0.0002
Pt 307	259.268	70.071	15.564	71.891	0.0008

ID	Image location of conjugate points in Image A		Image location of conjugate points in Image B		Residuals
	x (Pixels)	y (Pixels)	x (Pixels)	y (Pixels)	Signed Dist (Pixels)
Pt 308	564.784	525.980	320.668	527.934	-0.0003
Pt 309	450.704	152.561	206.763	154.496	0.0003
Pt 310	664.566	87.856	420.851	89.799	0.0009
Pt 311	629.369	558.998	385.567	561.054	0.0004
Pt 312	562.876	566.179	318.911	568.137	0.0001
Pt 313	380.608	103.942	136.742	105.943	0.0002
Pt 314	511.185	331.166	267.080	333.163	-0.0002
Pt 315	314.821	65.955	70.821	67.921	0.0000
Pt 316	465.028	605.111	221.000	607.233	-0.0005
Pt 317	297.167	51.806	53.228	53.790	0.0000
Pt 318	358.647	168.903	114.385	169.543	0.0025
Pt 319	577.695	286.559	333.774	288.470	0.0005
Pt 320	273.765	62.701	29.823	64.755	-0.0001
Pt 321	591.291	98.083	347.433	100.156	0.0001
Pt 322	454.785	509.175	210.799	511.017	0.0004
Pt 323	454.785	509.175	210.799	511.017	0.0004
Pt 324	326.568	59.698	82.422	62.019	-0.0010
Pt 325	391.761	10.904	147.632	13.827	-0.0025
Pt 326	514.107	433.305	270.137	435.279	0.0002
Pt 327	592.741	592.768	348.723	594.640	0.0002
Pt 328	487.131	162.243	243.328	164.095	0.0008
Pt 329	759.934	485.040	515.959	487.170	-0.0002
Pt 330	484.909	468.165	240.870	470.376	-0.0007
Pt 331	484.909	468.165	240.870	470.376	-0.0007
Pt 332	692.968	299.392	449.082	303.034	-0.0051
Pt 333	692.968	299.392	449.082	303.034	-0.0051
Pt 334	456.460	494.879	212.914	496.496	0.0024
Pt 335	289.934	161.087	46.121	163.331	0.0000
Pt 336	273.384	148.399	29.372	150.266	0.0003
Pt 337	335.799	542.795	91.834	544.966	-0.0001
Pt 338	461.728	135.352	217.908	137.646	-0.0004
Pt 339	776.352	72.114	532.556	74.494	-0.0006
Pt 340	562.279	295.823	319.193	297.326	0.0037
Pt 341	562.279	295.823	319.193	297.326	0.0037
Pt 342	574.573	92.311	330.949	93.395	0.0034
Pt 343	619.922	233.149	375.911	234.837	0.0011
Pt 344	618.449	591.945	375.830	593.014	0.0076
Pt 345	503.228	382.280	259.276	384.201	0.0004
Pt 346	632.339	407.951	387.019	409.152	-0.0011

ID	Image location of conjugate points in Image A		Image location of conjugate points in Image B		Residuals
	x (Pixels)	y (Pixels)	x (Pixels)	y (Pixels)	Signed Dist (Pixels)
Pt 347	292.762	459.819	48.891	461.709	0.0008
Pt 348	378.438	14.236	134.704	15.907	0.0010
Pt 349	732.233	99.278	488.071	101.540	-0.0008
Pt 350	623.728	112.411	379.431	114.544	-0.0008
Pt 351	335.880	126.343	91.872	128.603	-0.0006
Pt 352	536.644	554.091	292.720	556.096	0.0001
Pt 353	536.644	554.091	292.720	556.096	0.0001
Pt 354	658.157	175.583	414.233	177.484	0.0007
Pt 355	658.157	175.583	414.233	177.484	0.0007
Pt 356	607.739	199.585	363.618	201.714	-0.0005
Pt 357	721.506	533.976	477.672	535.882	0.0009
Pt 358	567.252	218.858	323.279	220.723	0.0005
Pt 359	268.169	191.246	24.322	193.239	0.0004
Pt 360	672.407	265.810	428.393	267.924	-0.0002
Pt 361	506.234	271.224	262.167	273.145	0.0001
Pt 362	643.404	272.249	399.147	274.188	-0.0002
Pt 363	277.115	281.139	33.127	283.153	0.0002
Pt 364	381.507	303.484	136.738	305.632	-0.0021
Pt 365	657.638	316.033	413.680	318.052	0.0002
Pt 366	277.663	311.622	33.673	313.472	0.0005
Pt 367	361.578	316.646	117.471	318.781	-0.0005
Pt 368	643.678	447.178	399.636	449.078	0.0003
Pt 369	421.625	139.154	177.156	141.139	-0.0009
Pt 370	573.508	440.335	330.145	442.341	0.0019
Pt 371	348.247	123.801	104.119	125.801	-0.0002
Pt 372	390.097	344.386	146.148	346.448	0.0001
Pt 373	620.027	409.159	376.024	411.147	0.0001
Pt 374	779.206	542.730	534.514	544.146	0.0000
Pt 375	460.346	349.496	216.244	351.661	-0.0007
Pt 376	607.675	389.420	363.720	391.473	0.0000
Pt 377	696.956	9.297	452.740	11.560	-0.0009
Pt 378	496.236	589.536	252.172	591.542	-0.0004
Pt 379	517.677	572.318	273.677	574.258	0.0001
Pt 380	506.775	559.425	262.809	561.409	0.0001
Pt 381	506.775	559.425	262.809	561.409	0.0001
Pt 382	514.813	527.484	270.771	529.449	-0.0001
Pt 383	354.056	512.294	110.090	514.324	0.0001
Pt 384	354.056	512.294	110.090	514.324	0.0001
Pt 385	296.045	373.281	51.994	375.141	0.0003

ID	Image location of conjugate points in Image A		Image location of conjugate points in Image B		Residuals
	x (Pixels)	y (Pixels)	x (Pixels)	y (Pixels)	Signed Dist (Pixels)
Pt 386	296.045	373.281	51.994	375.141	0.0003
Pt 387	316.082	351.555	71.890	353.544	-0.0003
Pt 388	592.867	290.933	348.921	292.914	0.0003
Pt 389	633.517	234.692	389.443	236.633	0.0002
Pt 390	633.517	234.692	389.443	236.633	0.0002
Pt 391	656.952	191.197	412.942	193.095	0.0005
Pt 392	656.952	191.197	412.942	193.095	0.0005
Pt 393	372.138	172.555	128.115	174.553	0.0000
Pt 394	540.368	598.044	296.439	600.066	0.0000
Pt 395	513.600	590.508	269.561	592.454	-0.0001
Pt 396	513.600	590.508	269.561	592.454	-0.0001
Pt 397	446.126	584.320	202.087	586.265	-0.0001
Pt 398	446.126	584.320	202.087	586.265	-0.0001
Pt 399	535.725	568.973	291.777	570.959	0.0001
Pt 400	535.725	568.973	291.777	570.959	0.0001
Pt 401	487.709	554.635	243.703	556.628	-0.0001
Pt 402	725.399	549.738	481.373	551.649	0.0003
Pt 403	738.431	535.942	494.353	537.955	-0.0002
Pt 404	502.282	540.796	258.237	542.799	-0.0002
Pt 405	611.287	467.395	367.252	469.434	-0.0002
Pt 406	625.185	442.253	381.239	444.086	0.0007
Pt 407	625.185	442.253	381.239	444.086	0.0007
Pt 408	554.742	437.388	310.789	439.412	0.0001
Pt 409	568.313	416.233	324.238	418.199	-0.0001
Pt 410	598.180	403.279	354.181	405.260	0.0001
Pt 411	379.318	389.280	135.204	391.263	-0.0002
Pt 412	379.318	389.280	135.204	391.263	-0.0002
Pt 413	622.129	321.936	378.050	323.918	0.0000
Pt 414	569.470	318.847	325.456	320.880	-0.0001
Pt 415	522.867	294.173	278.866	296.282	-0.0003
Pt 416	522.867	294.173	278.866	296.282	-0.0003
Pt 417	549.334	277.318	305.240	279.427	-0.0005
Pt 418	380.291	157.568	136.180	159.704	-0.0005
Pt 419	524.174	604.356	280.109	606.172	0.0001
Pt 420	524.174	604.356	280.109	606.172	0.0001
Pt 421	440.051	605.034	196.301	607.109	0.0006
Pt 422	366.174	129.545	122.109	131.384	0.0002
Pt 423	725.169	569.643	481.298	571.622	0.0005
Pt 424	725.666	133.649	479.699	134.763	-0.0001

ID	Image location of conjugate points in Image A		Image location of conjugate points in Image B		Residuals
	x (Pixels)	y (Pixels)	x (Pixels)	y (Pixels)	Signed Dist (Pixels)
Pt 425	388.184	116.099	144.214	117.954	0.0003
Pt 426	323.270	533.841	79.273	535.913	0.0000
Pt 427	777.415	169.242	532.485	170.546	0.0013
Pt 428	775.589	523.682	530.058	524.389	0.0000
Pt 429	598.772	517.426	354.676	519.529	-0.0007
Pt 430	642.325	182.185	398.174	184.112	0.0001
Pt 431	642.325	182.185	398.174	184.112	0.0001
Pt 432	308.490	508.791	64.373	510.898	-0.0004
Pt 433	270.023	495.564	26.052	497.564	0.0003
Pt 434	617.947	487.721	373.907	489.671	0.0000
Pt 435	617.947	487.721	373.907	489.671	0.0000
Pt 436	634.216	463.786	390.457	465.817	0.0007
Pt 437	462.026	466.436	218.228	468.421	0.0007
Pt 438	588.415	211.525	344.411	213.459	0.0003
Pt 439	434.833	463.905	190.890	465.651	0.0008
Pt 440	584.256	457.258	340.268	459.379	-0.0003
Pt 441	477.369	457.732	233.504	459.778	0.0003
Pt 442	327.552	458.204	83.651	459.922	0.0010
Pt 443	634.376	217.215	389.919	219.209	-0.0008
Pt 444	559.943	453.441	315.905	455.509	-0.0003
Pt 445	550.370	231.897	306.330	233.976	-0.0002
Pt 446	424.198	444.402	180.257	446.676	-0.0005
Pt 447	424.198	444.402	180.257	446.676	-0.0005
Pt 448	352.986	442.261	108.957	444.301	-0.0001
Pt 449	489.267	421.969	245.298	424.008	0.0000
Pt 450	768.961	15.583	525.016	18.889	-0.0043
Pt 451	432.505	404.708	188.644	406.577	0.0008
Pt 452	378.444	268.292	134.168	269.828	0.0005
Pt 453	649.770	389.591	405.904	391.767	-0.0001
Pt 454	709.806	19.241	465.659	21.374	-0.0004
Pt 455	403.329	370.271	159.388	372.003	0.0009
Pt 456	485.102	361.586	240.969	364.500	-0.0028
Pt 457	516.574	318.508	272.562	320.499	0.0000
Pt 458	434.555	341.676	190.489	343.892	-0.0007
Pt 459	573.413	96.370	329.478	98.269	0.0005
Pt 460	530.117	328.773	286.176	330.773	0.0002
Pt 461	550.353	316.330	306.406	318.344	0.0002
Pt 462	558.769	346.227	314.793	348.224	0.0001
Pt 463	589.487	347.945	345.408	349.766	0.0004

ID	Image location of conjugate points in Image A		Image location of conjugate points in Image B		Residuals
	x (Pixels)	y (Pixels)	x (Pixels)	y (Pixels)	Signed Dist (Pixels)
Pt 464	589.487	347.945	345.408	349.766	0.0004
Pt 465	541.789	360.436	297.881	362.510	0.0001
Pt 466	552.735	376.065	308.786	377.926	0.0006
Pt 467	257.202	253.819	13.270	255.453	0.0010
Pt 468	753.279	249.785	509.310	251.767	0.0005
Pt 469	489.802	379.459	245.771	381.225	0.0006
Pt 470	308.955	235.768	64.986	237.900	-0.0001
Pt 471	539.266	398.021	295.241	399.939	0.0002
Pt 472	713.650	201.238	469.828	203.075	0.0013
Pt 473	643.770	204.398	399.646	206.430	-0.0002
Pt 474	397.941	434.419	154.159	436.508	0.0005
Pt 475	373.216	109.719	129.152	111.534	0.0003
Pt 476	282.946	445.175	38.881	447.189	0.0000
Pt 477	390.989	86.342	146.863	88.264	-0.0001
Pt 478	300.180	82.693	56.419	84.735	0.0003
Pt 479	494.734	459.715	250.775	461.964	-0.0006
Pt 480	611.522	41.951	367.575	43.976	0.0001
Pt 481	281.995	28.087	38.015	30.189	-0.0003
Pt 482	281.995	28.087	38.015	30.189	-0.0003
Pt 483	306.294	21.422	62.144	22.957	0.0006
Pt 484	755.352	11.198	511.262	13.179	0.0004
Pt 485	298.127	495.257	54.046	497.205	0.0000
Pt 486	327.952	12.395	84.056	13.589	0.0017
Pt 487	640.570	602.587	396.778	604.542	0.0007
Pt 488	419.324	588.051	175.382	590.036	0.0002
Pt 489	566.206	577.169	322.446	579.187	0.0006
Pt 490	566.206	577.169	322.446	579.187	0.0006
Pt 491	637.022	568.096	393.024	569.974	0.0003
Pt 492	273.621	564.323	29.488	566.252	-0.0001
Pt 493	478.605	520.448	234.636	522.454	0.0000
Pt 494	478.605	520.448	234.636	522.454	0.0000
Pt 495	346.333	56.600	102.214	58.656	-0.0004
Pt 496	693.244	601.388	449.757	603.463	0.0015
Pt 497	573.955	541.822	330.225	543.668	0.0013
Pt 498	573.955	541.822	330.225	543.668	0.0013
Pt 499	618.529	517.158	374.488	519.331	-0.0007
Pt 500	394.294	602.154	149.999	604.090	-0.0009
Pt 501	667.252	598.270	423.005	600.266	-0.0010
Pt 502	393.627	565.996	149.615	568.109	-0.0003

ID	Image location of conjugate points in Image A		Image location of conjugate points in Image B		Residuals
	x (Pixels)	y (Pixels)	x (Pixels)	y (Pixels)	Signed Dist (Pixels)
Pt 503	393.627	565.996	149.615	568.109	-0.0003
Pt 504	746.011	586.203	501.720	588.121	-0.0007
Pt 505	638.556	584.337	394.147	586.437	-0.0018
Pt 506	657.198	584.333	413.384	586.289	0.0007
Pt 507	658.151	568.238	413.729	570.154	-0.0012
Pt 508	728.296	599.468	484.282	601.296	0.0005
Pt 509	308.053	555.110	63.999	557.149	-0.0001
Pt 510	319.503	151.976	75.511	154.630	-0.0013
Pt 511	312.919	603.938	68.427	605.965	-0.0017
Pt 512	312.919	603.938	68.427	605.965	-0.0017
Pt 513	340.070	497.419	96.228	499.607	0.0002
Pt 514	647.805	117.582	403.877	119.110	0.0018
Pt 515	280.851	536.630	36.909	538.828	0.0000
Pt 516	490.644	47.403	246.473	49.454	-0.0005
Pt 517	686.098	61.602	441.882	63.745	-0.0006
Pt 518	564.784	180.150	321.526	183.095	-0.0012
Pt 519	749.887	74.769	505.864	76.437	0.0016
Pt 520	749.887	74.769	505.864	76.437	0.0016
Pt 521	348.655	462.063	104.614	464.399	-0.0007
Pt 522	652.102	239.959	407.431	242.006	-0.0014
Pt 523	601.396	254.680	357.494	256.757	0.0001
Pt 524	567.265	115.610	322.707	117.838	-0.0016
Pt 525	377.354	47.834	133.757	50.010	0.0001
Pt 526	414.590	267.442	170.546	269.356	0.0001
Pt 527	355.623	287.793	111.616	289.862	-0.0001
Pt 528	512.538	182.502	268.305	184.606	-0.0007
Pt 529	510.938	360.378	267.234	361.920	0.0021
Pt 530	416.000	208.536	172.330	210.696	0.0003
Pt 531	426.539	40.281	182.216	42.370	-0.0008
Pt 532	659.714	254.723	415.955	256.571	0.0013
Pt 533	419.743	250.221	175.984	252.487	-0.0001
Pt 534	769.368	604.009	525.363	606.735	-0.0027
Pt 535	720.750	68.498	476.489	70.054	0.0015
Pt 536	720.750	68.498	476.489	70.054	0.0015
Pt 537	655.195	484.254	411.624	485.797	0.0029
Pt 538	740.116	468.736	495.273	471.409	-0.0048
Pt 539	526.999	457.538	283.149	460.595	-0.0025
Pt 540	665.180	38.558	421.114	40.598	0.0000
Pt 541	519.522	86.240	274.639	88.098	-0.0011

ID	Image location of conjugate points in Image A		Image location of conjugate points in Image B		Residuals
	x (Pixels)	y (Pixels)	x (Pixels)	y (Pixels)	Signed Dist (Pixels)
Pt 542	374.040	512.498	129.769	514.654	-0.0012
Pt 543	749.647	95.217	505.712	97.177	0.0007
Pt 544	665.727	346.276	421.855	347.851	0.0019
Pt 545	704.165	177.633	459.549	179.359	0.0000
Pt 546	597.452	178.708	353.289	180.962	-0.0010
Pt 547	534.672	112.238	290.906	114.283	0.0003
Pt 548	486.530	136.192	242.871	137.826	0.0016
Pt 549	713.599	318.217	469.742	320.396	0.0000
Pt 550	303.849	285.824	59.615	288.051	-0.0009
Pt 551	535.975	140.890	291.708	143.085	-0.0010
Pt 552	361.467	494.363	117.442	497.062	-0.0015
Pt 553	591.628	573.354	349.450	575.078	0.0070
Pt 554	327.084	29.566	83.023	31.565	-0.0002
Pt 555	731.421	34.245	487.354	36.268	0.0002
Pt 556	276.687	164.357	32.713	166.438	0.0000
Pt 557	276.687	164.357	32.713	166.438	0.0000
Pt 558	563.957	176.687	320.255	178.380	0.0016
Pt 559	733.608	244.503	490.022	246.603	0.0009
Pt 560	526.608	249.677	282.810	251.410	0.0013
Pt 561	472.522	294.793	228.476	296.966	-0.0005
Pt 562	664.774	294.828	420.752	296.788	0.0003
Pt 563	609.714	298.967	365.280	301.013	-0.0011
Pt 564	438.923	310.152	194.918	311.740	0.0011
Pt 565	438.923	310.152	194.918	311.740	0.0011
Pt 566	282.373	358.886	38.430	360.696	0.0007
Pt 567	412.324	458.113	168.306	460.176	-0.0002
Pt 568	767.901	488.941	524.611	491.108	0.0018
Pt 569	647.664	532.104	403.782	533.746	0.0015
Pt 570	759.709	569.974	515.378	571.956	-0.0010
Pt 571	414.663	589.536	170.663	591.470	0.0001
Pt 572	514.667	199.697	271.101	201.544	0.0014
Pt 573	554.088	207.158	309.073	210.195	-0.0051
Pt 574	759.653	210.287	512.611	212.111	-0.0053
Pt 575	397.656	271.100	153.088	272.548	0.0000
Pt 576	525.345	273.547	281.442	275.452	0.0005
Pt 577	525.345	273.547	281.442	275.452	0.0005
Pt 578	733.121	374.607	489.927	377.749	-0.0016
Pt 579	360.055	381.063	116.179	383.106	0.0004
Pt 580	547.485	414.468	303.604	416.267	0.0009

ID	Image location of conjugate points in Image A		Image location of conjugate points in Image B		Residuals
	x (Pixels)	y (Pixels)	x (Pixels)	y (Pixels)	Signed Dist (Pixels)
Pt 581	679.028	415.244	435.112	417.406	-0.0002
Pt 582	535.336	443.323	291.349	444.450	0.0025
Pt 583	512.208	470.531	268.186	472.447	0.0001
Pt 584	400.708	483.051	155.888	486.443	-0.0058
Pt 585	413.560	521.680	169.718	524.572	-0.0016
Pt 586	264.419	546.257	22.289	546.915	0.0090
Pt 587	474.265	568.130	229.961	570.101	-0.0010
Pt 588	590.002	593.553	345.866	595.383	-0.0001
Pt 589	295.843	42.962	53.521	44.822	0.0027
Pt 590	580.763	51.345	335.216	53.401	-0.0025
Pt 591	280.181	96.495	35.673	98.361	-0.0006
Pt 592	299.737	212.387	54.005	212.673	-0.0001
Pt 593	337.772	233.213	94.964	232.388	0.0087
Pt 594	304.322	327.230	61.996	329.188	0.0045
Pt 595	303.457	472.307	58.478	477.575	-0.0094
Pt 596	472.894	23.586	226.838	24.545	-0.0003
Pt 597	341.079	85.274	96.894	87.352	-0.0005
Pt 598	574.091	395.437	328.487	396.750	-0.0024
Pt 599	574.091	395.437	328.487	396.750	-0.0024
Pt 600	311.784	403.376	68.718	405.393	0.0028
Pt 601	311.784	403.376	68.718	405.393	0.0028
Pt 602	706.226	22.754	463.142	24.849	0.0013
Pt 603	396.535	50.059	153.833	52.144	0.0017
Pt 604	396.535	50.059	153.833	52.144	0.0017
Pt 605	687.883	71.785	442.585	73.910	-0.0023
Pt 606	551.169	93.627	308.968	95.721	0.0028
Pt 607	277.536	170.657	33.646	172.818	0.0000
Pt 608	397.950	171.470	154.530	173.146	0.0019
Pt 609	483.372	186.671	239.643	188.538	0.0009
Pt 610	659.285	227.989	415.615	229.453	0.0027
Pt 611	510.767	247.009	266.104	249.242	-0.0021
Pt 612	357.107	277.909	112.166	279.798	-0.0019
Pt 613	422.707	360.766	179.170	362.889	0.0010
Pt 614	708.777	356.276	463.535	358.266	-0.0030
Pt 615	329.287	369.247	82.888	371.278	-0.0064
Pt 616	329.287	369.247	82.888	371.278	-0.0064
Pt 617	435.383	501.201	191.156	503.467	-0.0014
Pt 618	687.149	494.633	444.681	496.883	0.0040
Pt 619	499.166	508.904	254.162	510.991	-0.0035

ID	Image location of conjugate points in Image A		Image location of conjugate points in Image B		Residuals
	x (Pixels)	y (Pixels)	x (Pixels)	y (Pixels)	Signed Dist (Pixels)
Pt 620	574.465	529.720	331.742	531.746	0.0040
Pt 621	403.599	538.609	158.906	540.242	-0.0014
Pt 622	688.831	563.888	444.489	565.302	0.0008
Pt 623	595.053	26.955	348.999	26.939	0.0032
Pt 624	644.246	47.016	399.726	48.870	-0.0002
Pt 625	296.932	71.253	53.636	73.261	0.0011
Pt 626	617.082	94.728	371.521	96.773	-0.0027
Pt 627	617.082	94.728	371.521	96.773	-0.0027
Pt 628	464.010	114.087	219.843	116.759	-0.0021
Pt 629	407.860	131.261	163.837	133.333	-0.0002
Pt 630	462.771	160.702	217.261	163.884	-0.0060
Pt 631	414.263	195.431	168.835	199.183	-0.0071
Pt 632	640.406	198.845	397.611	200.800	0.0028
Pt 633	276.761	252.987	33.487	254.875	0.0020
Pt 634	413.322	302.819	168.644	305.254	-0.0026
Pt 635	545.444	317.046	299.871	319.034	-0.0038
Pt 636	511.042	387.386	268.397	389.401	0.0037
Pt 637	511.042	387.386	268.397	389.401	0.0037
Pt 638	483.961	422.345	239.295	424.360	-0.0019
Pt 639	711.925	513.808	466.917	515.775	-0.0031
Pt 640	431.955	555.718	188.816	557.945	0.0023
Pt 641	431.955	555.718	188.816	557.945	0.0023
Pt 642	655.712	556.406	410.991	557.907	-0.0008
Pt 643	362.804	577.213	119.223	579.108	0.0017
Pt 644	451.388	433.398	208.273	435.453	0.0025
Pt 645	407.731	411.678	165.067	413.824	0.0035
Pt 646	574.955	477.397	331.774	479.674	0.0017
Pt 647	574.955	477.397	331.774	479.674	0.0017
Pt 648	629.879	148.850	386.243	151.380	-0.0008
Pt 649	279.611	177.746	39.406	182.403	0.0025
Pt 650	390.381	505.223	146.171	508.317	-0.0032
Pt 651	524.381	152.714	277.272	152.466	0.0004
Pt 652	319.210	533.353	71.477	531.596	-0.0043
Pt 653	319.210	533.353	71.477	531.596	-0.0043
Pt 654	507.506	389.839	262.365	394.417	-0.0102
Pt 655	507.506	389.839	262.365	394.417	-0.0102
Pt 656	659.399	541.994	414.326	544.287	-0.0045
				SUM	-0.0009

APPENDIX D

Table D1: Image coordinates of associated image pairs automatically obtained using Modified Harris Corner Detector algorithm on UAV acquired image pairs.

ID	Image location of conjugate points in Image A		Image location of conjugate points in Image B		Residuals
	x (Pixels)	y (Pixels)	x (Pixels)	y (Pixels)	Signed Dist (Pixels)
Pt 01	1472.000	1815.000	1424.000	2487.000	0.0000
Pt 02	1474.000	1807.000	1427.000	2478.000	-0.0004
Pt 03	1755.000	294.000	1710.000	904.000	0.0000
Pt 04	1860.000	1942.000	1820.000	2614.000	-0.0007
Pt 05	3846.000	417.000	3838.000	996.000	0.0002
Pt 06	1831.000	1938.000	1788.000	2614.000	0.0003
Pt 07	2102.000	1938.000	2065.000	2609.000	-0.0003
Pt 08	3827.000	624.000	3819.000	1211.000	-0.0001
Pt 09	1896.000	2199.000	1856.000	2877.000	0.0000
Pt 10	1542.000	2195.000	1496.000	2877.000	0.0002
Pt 11	1796.000	1789.000	1753.000	2460.000	-0.0001
Pt 12	1480.000	2057.000	1433.000	2735.000	0.0000
Pt 13	1904.000	2190.000	1866.000	2869.000	-0.0011
Pt 14	2538.000	881.000	2509.000	1498.000	-0.0003
Pt 15	2500.000	926.000	2469.000	1547.000	0.0002
Pt 16	1696.000	1778.000	1652.000	2445.000	0.0000
Pt 17	1531.000	1123.000	1481.000	1768.000	0.0010
Pt 18	2112.000	1278.000	2074.000	1919.000	0.0004
Pt 19	1818.000	1925.000	1776.000	2599.000	-0.0002
Pt 20	2773.000	1938.000	2746.000	2589.000	0.0008
Pt 21	1528.000	2171.000	1483.000	2853.000	-0.0006
Pt 22	1333.000	501.000	1282.000	1126.000	-0.0009
Pt 23	2487.000	934.000	2455.000	1555.000	0.0006
Pt 24	1923.000	546.000	1882.000	1164.000	-0.0003
Pt 25	1897.000	2017.000	1856.000	2695.000	-0.0001
Pt 26	1908.000	2079.000	1867.000	2757.000	0.0002
Pt 27	1808.000	284.000	1767.000	892.000	-0.0014
Pt 28	2046.000	1743.000	2008.000	2408.000	-0.0004
Pt 29	1497.000	1739.000	1449.000	2408.000	0.0002
Pt 30	1459.000	1741.000	1411.000	2416.000	-0.0007
Pt 31	1343.000	496.000	1290.000	1121.000	0.0001
Pt 32	1852.000	1438.000	1809.000	2092.000	0.0005
Pt 33	1856.000	1923.000	1814.000	2594.000	0.0003
Pt 34	2091.000	2144.000	2053.000	2819.000	0.0005
Pt 35	2098.000	2138.000	2061.000	2812.000	0.0000

ID	Image location of conjugate points in Image A		Image location of conjugate points in Image B		Residuals
	x (Pixels)	y (Pixels)	x (Pixels)	y (Pixels)	Signed Dist (Pixels)
Pt 36	1774.000	2084.000	1733.000	2761.000	-0.0007
Pt 37	2035.000	1732.000	1996.000	2394.000	0.0002
Pt 38	1501.000	1730.000	1453.000	2398.000	0.0002
Pt 39	2226.000	1976.000	2191.000	2640.000	0.0002
Pt 40	1844.000	1442.000	1801.000	2095.000	0.0005
Pt 41	2507.000	945.000	2476.000	1567.000	0.0003
Pt 42	2132.000	1258.000	2094.000	1901.000	0.0003
Pt 43	1791.000	1454.000	1747.000	2109.000	0.0005
Pt 44	1616.000	1457.000	1568.000	2116.000	0.0008
Pt 45	1735.000	1721.000	1691.000	2386.000	0.0002
Pt 46	2514.000	945.000	2483.000	1566.000	0.0004
Pt 47	1912.000	2133.000	1872.000	2811.000	-0.0001
Pt 48	1962.000	2022.000	1924.000	2698.000	-0.0010
Pt 49	1783.000	2054.000	1740.000	2735.000	-0.0001
Pt 50	1616.000	1475.000	1568.000	2132.000	0.0011
Pt 51	1787.000	1948.000	1744.000	2622.000	0.0002
Pt 52	2000.000	2123.000	1963.000	2798.000	-0.0008
Pt 53	1760.000	275.000	1716.000	883.000	-0.0003
Pt 54	1614.000	1486.000	1567.000	2144.000	0.0005
Pt 55	1733.000	275.000	1688.000	883.000	-0.0001
Pt 56	1994.000	2123.000	1956.000	2800.000	-0.0005
Pt 57	1613.000	1495.000	1566.000	2154.000	0.0004
Pt 58	2630.000	576.000	2604.000	1178.000	-0.0009
Pt 59	1764.000	1693.000	1721.000	2356.000	0.0000
Pt 60	1668.000	1870.000	1623.000	2541.000	0.0003
Pt 61	1519.000	1685.000	1472.000	2350.000	0.0000
Pt 62	1832.000	2030.000	1791.000	2710.000	-0.0008
Pt 63	1906.000	2031.000	1865.000	2709.000	0.0000
Pt 64	1610.000	1506.000	1563.000	2164.000	0.0006
Pt 65	1953.000	2028.000	1914.000	2705.000	-0.0006
Pt 66	1462.000	1874.000	1414.000	2547.000	0.0001
Pt 67	1526.000	1675.000	1478.000	2341.000	0.0004
Pt 68	1604.000	1524.000	1557.000	2184.000	0.0004
Pt 69	1603.000	1533.000	1556.000	2193.000	0.0004
Pt 70	1244.000	535.000	1189.000	1165.000	0.0000
Pt 71	1832.000	1650.000	1790.000	2311.000	0.0000
Pt 72	1470.000	1191.000	1420.000	1843.000	0.0002
Pt 73	1481.000	1189.000	1431.000	1839.000	0.0005
Pt 74	1477.000	2047.000	1430.000	2726.000	-0.0001

ID	Image location of conjugate points in Image A		Image location of conjugate points in Image B		Residuals
	x (Pixels)	y (Pixels)	x (Pixels)	y (Pixels)	Signed Dist (Pixels)
Pt 75	1824.000	1881.000	1782.000	2554.000	-0.0002
Pt 76	2052.000	1881.000	2014.000	2549.000	-0.0002
Pt 77	2047.000	1962.000	2009.000	2632.000	-0.0001
Pt 78	1318.000	506.000	1264.000	1131.000	0.0004
Pt 79	1081.000	1962.000	1028.000	2645.000	-0.0008
Pt 80	2501.000	953.000	2470.000	1576.000	0.0002
Pt 81	1473.000	2038.000	1427.000	2716.000	-0.0006
Pt 82	1558.000	1618.000	1510.000	2282.000	0.0006
Pt 83	2433.000	1960.000	2401.000	2623.000	0.0002
Pt 84	1565.000	1609.000	1517.000	2273.000	0.0006
Pt 85	1456.000	1901.000	1409.000	2575.000	-0.0005
Pt 86	1666.000	1889.000	1622.000	2561.000	-0.0003
Pt 87	1756.000	1893.000	1713.000	2568.000	-0.0004
Pt 88	1494.000	2094.000	1448.000	2774.000	-0.0004
Pt 89	1477.000	1208.000	1427.000	1860.000	0.0003
Pt 90	1486.000	1207.000	1435.000	1858.000	0.0010
Pt 91	1285.000	1595.000	1234.000	2262.000	-0.0004
Pt 92	1500.000	2103.000	1454.000	2783.000	-0.0004
Pt 93	1586.000	1205.000	1538.000	1854.000	0.0004
Pt 94	1586.000	1571.000	1538.000	2233.000	0.0008
Pt 95	2809.000	1954.000	2783.000	2608.000	0.0004
Pt 96	1578.000	1581.000	1531.000	2243.000	0.0003
Pt 97	2174.000	1731.000	2137.000	2387.000	0.0007
Pt 98	2231.000	1954.000	2196.000	2617.000	0.0003
Pt 99	1715.000	1898.000	1671.000	2571.000	0.0000
Pt 100	3248.000	1571.000	3229.000	2207.000	0.0003
Pt 101	1781.000	1890.000	1738.000	2563.000	0.0000
Pt 102	1541.000	1612.000	1493.000	2276.000	0.0004
Pt 103	2854.000	607.000	2832.000	1205.000	-0.0009
Pt 104	1871.000	2042.000	1830.000	2719.000	-0.0001
Pt 105	3021.000	438.000	3003.000	1028.000	-0.0015
Pt 106	1612.000	34.000	1565.000	638.000	-0.0007
Pt 107	3226.000	1558.000	3207.000	2185.000	0.0006
Pt 108	1647.000	264.000	1601.000	872.000	-0.0003
Pt 109	2035.000	1998.000	1996.000	2672.000	0.0001
Pt 110	1907.000	1626.000	1867.000	2284.000	-0.0003
Pt 111	2218.000	1811.000	2183.000	2470.000	0.0000
Pt 112	2219.000	1886.000	2183.000	2550.000	0.0004
Pt 113	1990.000	2108.000	1952.000	2782.000	-0.0003

ID	Image location of conjugate points in Image A		Image location of conjugate points in Image B		Residuals
	x (Pixels)	y (Pixels)	x (Pixels)	y (Pixels)	Signed Dist (Pixels)
Pt 114	3129.000	1063.000	3108.000	1674.000	0.0008
Pt 115	2022.000	2110.000	1984.000	2784.000	-0.0001
Pt 116	1161.000	1640.000	1106.000	2312.000	0.0004
Pt 117	1869.000	1637.000	1828.000	2297.000	-0.0002
Pt 118	1926.000	2003.000	1887.000	2676.000	-0.0006
Pt 119	2519.000	909.000	2488.000	1529.000	0.0004
Pt 120	2369.000	1187.000	2334.000	1820.000	0.0012
Pt 121	1664.000	1910.000	1620.000	2582.000	-0.0002
Pt 122	2271.000	1045.000	2237.000	1676.000	-0.0004
Pt 123	2240.000	1110.000	2205.000	1744.000	-0.0001
Pt 124	2214.000	1803.000	2179.000	2462.000	0.0000
Pt 125	1899.000	1643.000	1857.000	2305.000	0.0004
Pt 126	2534.000	901.000	2504.000	1520.000	0.0000
Pt 127	2066.000	1646.000	2026.000	2302.000	0.0011
Pt 128	1769.000	1880.000	1726.000	2553.000	-0.0001
Pt 129	2090.000	2115.000	2053.000	2789.000	-0.0001
Pt 130	3084.000	2089.000	3063.000	2740.000	0.0002
Pt 131	3904.000	759.000	3898.000	1347.000	-0.0004
Pt 132	2075.000	1650.000	2037.000	2306.000	0.0002
Pt 133	3232.000	1531.000	3213.000	2158.000	0.0006
Pt 134	637.000	366.000	569.000	1000.000	0.0000
Pt 135	1806.000	1663.000	1764.000	2323.000	-0.0001
Pt 136	1978.000	1667.000	1940.000	2327.000	-0.0008
Pt 137	619.000	1799.000	554.000	2488.000	0.0003
Pt 138	2000.000	1671.000	1962.000	2330.000	-0.0005
Pt 139	2213.000	1795.000	2177.000	2453.000	0.0005
Pt 140	2164.000	2030.000	2128.000	2697.000	0.0002
Pt 141	1643.000	274.000	1595.000	884.000	0.0005
Pt 142	3972.000	776.000	3965.000	1365.000	0.0005
Pt 143	1971.000	2117.000	1933.000	2790.000	-0.0004
Pt 144	2024.000	1682.000	1985.000	2342.000	0.0001
Pt 145	2035.000	1680.000	1998.000	2340.000	-0.0008
Pt 146	2053.000	122.000	2016.000	719.000	-0.0011
Pt 147	2033.000	1971.000	1994.000	2642.000	0.0003
Pt 148	1814.000	1794.000	1773.000	2461.000	-0.0006
Pt 149	2263.000	1238.000	2226.000	1876.000	0.0011
Pt 150	3984.000	783.000	3976.000	1371.000	0.0011
Pt 151	1784.000	1795.000	1743.000	2464.000	-0.0010
Pt 152	3934.000	785.000	3928.000	1374.000	-0.0002

ID	Image location of conjugate points in Image A		Image location of conjugate points in Image B		Residuals
	x (Pixels)	y (Pixels)	x (Pixels)	y (Pixels)	Signed Dist (Pixels)
Pt 153	1817.000	1819.000	1774.000	2489.000	0.0003
Pt 154	894.000	1823.000	837.000	2506.000	-0.0009
Pt 155	2123.000	1947.000	2088.000	2614.000	-0.0009
Pt 156	1566.000	1357.000	1516.000	2013.000	0.0013
Pt 157	1816.000	2060.000	1776.000	2735.000	-0.0008
Pt 158	2405.000	1090.000	2374.000	1722.000	-0.0008
Pt 159	1825.000	1701.000	1784.000	2366.000	-0.0007
Pt 160	2148.000	1702.000	2111.000	2359.000	0.0003
Pt 161	1825.000	1707.000	1783.000	2372.000	-0.0002
Pt 162	2077.000	1943.000	2040.000	2612.000	-0.0004
Pt 163	1669.000	1860.000	1625.000	2531.000	-0.0003
Pt 164	1770.000	1823.000	1727.000	2493.000	-0.0001
Pt 165	1489.000	989.000	1439.000	1630.000	0.0005
Pt 166	3180.000	199.000	3164.000	779.000	-0.0012
Pt 167	2720.000	1154.000	2693.000	1776.000	0.0004
Pt 168	2238.000	1916.000	2203.000	2578.000	0.0003
Pt 169	1977.000	2134.000	1939.000	2809.000	-0.0004
Pt 170	1799.000	1726.000	1755.000	2393.000	0.0005
Pt 171	2168.000	1723.000	2132.000	2380.000	0.0000
Pt 172	2116.000	2132.000	2079.000	2807.000	0.0001
Pt 173	1275.000	490.000	1220.000	1118.000	0.0002
Pt 174	2216.000	1975.000	2181.000	2642.000	-0.0001
Pt 175	1255.000	488.000	1200.000	1116.000	0.0000
Pt 176	2208.000	1786.000	2172.000	2444.000	0.0005
Pt 177	1435.000	828.000	1383.000	1462.000	0.0010
Pt 178	1577.000	1439.000	1528.000	2098.000	0.0009
Pt 179	2236.000	1072.000	2200.000	1702.000	0.0005
Pt 180	2072.000	1781.000	2034.000	2447.000	-0.0002
Pt 181	2698.000	1974.000	2672.000	2630.000	-0.0005
Pt 182	3829.000	540.000	3821.000	1123.000	0.0000
Pt 183	3064.000	1141.000	3043.000	1755.000	0.0003
Pt 184	2269.000	1054.000	2233.000	1685.000	0.0006
Pt 185	2648.000	637.000	2621.000	1240.000	-0.0002
Pt 186	2715.000	1995.000	2687.000	2652.000	0.0007
Pt 187	1608.000	1437.000	1560.000	2095.000	0.0008
Pt 188	418.000	336.000	347.000	973.000	-0.0009
Pt 189	1539.000	1143.000	1490.000	1789.000	0.0006
Pt 190	2261.000	1266.000	2225.000	1904.000	0.0007
Pt 191	2236.000	1092.000	2200.000	1725.000	0.0003

ID	Image location of conjugate points in Image A		Image location of conjugate points in Image B		Residuals
	x (Pixels)	y (Pixels)	x (Pixels)	y (Pixels)	Signed Dist (Pixels)
Pt 192	3167.000	198.000	3150.000	779.000	-0.0009
Pt 193	2556.000	1100.000	2526.000	1725.000	0.0004
Pt 194	1816.000	1850.000	1773.000	2522.000	0.0002
Pt 195	1962.000	2158.000	1925.000	2834.000	-0.0011
Pt 196	3040.000	1118.000	3019.000	1732.000	0.0001
Pt 197	2181.000	1740.000	2144.000	2396.000	0.0008
Pt 198	2582.000	174.000	2555.000	762.000	-0.0010
Pt 199	3913.000	402.000	3906.000	980.000	0.0002
Pt 200	2079.000	2156.000	2042.000	2830.000	0.0000
Pt 201	3039.000	410.000	3021.000	998.000	-0.0013
Pt 202	2134.000	1922.000	2097.000	2588.000	0.0002
Pt 203	3084.000	2078.000	3064.000	2730.000	-0.0004
Pt 204	2492.000	1424.000	2460.000	2062.000	0.0009
Pt 205	2186.000	1747.000	2149.000	2404.000	0.0008
Pt 206	1673.000	1842.000	1628.000	2512.000	0.0003
Pt 207	1931.000	2075.000	1891.000	2751.000	0.0000
Pt 208	1712.000	1752.000	1668.000	2417.000	0.0002
Pt 209	2455.000	2011.000	2424.000	2674.000	0.0000
Pt 210	2226.000	1838.000	2191.000	2497.000	0.0002
Pt 211	1760.000	325.000	1715.000	936.000	0.0001
Pt 212	3301.000	1983.000	3285.000	2626.000	-0.0006
Pt 213	2199.000	1769.000	2163.000	2427.000	0.0003
Pt 214	1855.000	2173.000	1816.000	2852.000	-0.0010
Pt 215	1905.000	1770.000	1864.000	2436.000	0.0001
Pt 216	1712.000	1988.000	1669.000	2663.000	-0.0003
Pt 217	1798.000	1837.000	1756.000	2508.000	-0.0004
Pt 218	2512.000	866.000	2482.000	1482.000	0.0000
Pt 219	3447.000	1009.000	3432.000	1611.000	0.0005
Pt 220	1054.000	1840.000	1000.000	2520.000	-0.0008
Pt 221	3043.000	2074.000	3021.000	2725.000	0.0005
Pt 222	2234.000	1926.000	2200.000	2589.000	-0.0003
Pt 223	1820.000	1720.000	1778.000	2385.000	-0.0002
Pt 224	474.000	1787.000	406.000	2477.000	0.0005
Pt 225	3937.000	762.000	3929.000	1352.000	0.0007
Pt 226	2871.000	711.000	2849.000	1314.000	-0.0008
Pt 227	3696.000	2016.000	3689.000	2656.000	-0.0023
Pt 228	2935.000	641.000	2912.000	1240.000	0.0002
SUM:					0.0004

APPENDIX E

Table E1: Image coordinates of associated image pairs automatically obtained using Speeded Up Robust Features algorithm on UAV acquired image pairs.

ID	Image location of conjugate points in Image A		Image location of conjugate points in Image B		Residuals
	x (Pixels)	y (Pixels)	x (Pixels)	y (Pixels)	Signed Dist (Pixels)
Pt 01	3980.213	689.823	3986.292	1284.916	0.0004
Pt 02	2330.302	173.564	2312.204	754.364	-0.0002
Pt 03	1410.835	235.351	1371.241	828.151	0.0000
Pt 04	3635.278	1408.854	3624.883	2033.501	0.0015
Pt 05	1635.850	1326.869	1589.167	1968.758	0.0004
Pt 06	2445.925	2314.158	2406.836	2981.595	0.0002
Pt 07	1711.045	1242.449	1667.195	1879.884	0.0002
Pt 08	1644.639	1698.690	1594.846	2355.266	0.0002
Pt 09	2029.565	550.976	1999.936	1154.402	0.0001
Pt 10	1802.408	1165.766	1761.042	1798.875	0.0003
Pt 11	1223.097	1965.485	1163.022	2634.864	-0.0003
Pt 12	1223.097	1965.485	1163.022	2634.864	-0.0003
Pt 13	1211.612	1970.512	1152.338	2639.415	-0.0007
Pt 14	3692.909	324.208	3697.968	906.058	0.0005
Pt 15	3692.909	324.208	3697.968	906.058	0.0005
Pt 16	3692.909	324.208	3697.968	906.058	0.0005
Pt 17	2706.786	1222.389	2684.064	1848.787	-0.0001
Pt 18	2237.983	659.961	2211.076	1266.922	0.0003
Pt 19	3939.693	672.354	3945.710	1266.236	0.0003
Pt 20	3939.693	672.354	3945.710	1266.236	0.0003
Pt 21	3939.693	672.354	3945.710	1266.236	0.0003
Pt 22	2276.458	621.317	2251.140	1225.475	0.0002
Pt 23	2276.458	621.317	2251.140	1225.475	0.0002
Pt 24	2959.416	1909.005	2934.295	2556.071	0.0004
Pt 25	1370.484	614.120	1325.719	1225.802	0.0002
Pt 26	2201.523	696.727	2173.620	1305.790	0.0002
Pt 27	3980.773	699.891	3986.841	1295.325	0.0003
Pt 28	1117.904	2013.905	1056.227	2686.351	-0.0007
Pt 29	1117.904	2013.905	1056.227	2686.351	-0.0007
Pt 30	1770.083	1192.884	1727.896	1827.172	0.0002
Pt 31	1770.083	1192.884	1727.896	1827.172	0.0002
Pt 32	1491.290	1607.456	1439.990	2258.708	-0.0001
Pt 33	1491.290	1607.456	1439.990	2258.708	-0.0001
Pt 34	2089.087	611.745	2059.661	1218.092	0.0003

ID	Image location of conjugate points in Image A		Image location of conjugate points in Image B		Residuals
	x (Pixels)	y (Pixels)	x (Pixels)	y (Pixels)	Signed Dist (Pixels)
Pt 35	1998.760	726.305	1966.145	1338.592	0.0003
Pt 36	1998.760	726.305	1966.145	1338.592	0.0003
Pt 37	2083.433	600.873	2054.782	1206.800	-0.0001
Pt 38	1651.167	1702.718	1602.041	2359.075	-0.0001
Pt 39	2294.260	599.859	2269.631	1203.256	0.0001
Pt 40	1631.689	1707.183	1581.922	2364.044	0.0000
Pt 41	1631.689	1707.183	1581.922	2364.044	0.0000
Pt 42	1663.698	1706.396	1614.614	2362.930	0.0000
Pt 43	2821.779	243.179	2812.633	825.371	0.0000
Pt 44	1851.599	1565.766	1808.758	2215.000	-0.0004
Pt 45	2437.023	17.858	2422.430	592.211	0.0000
Pt 46	2437.023	17.858	2422.430	592.211	0.0000
Pt 47	1230.849	2071.463	1170.998	2741.527	-0.0007
Pt 48	1737.532	1207.535	1694.160	1845.008	0.0003
Pt 49	1709.954	1714.943	1661.845	2371.187	0.0000
Pt 50	1709.954	1714.943	1661.845	2371.187	0.0000
Pt 51	2258.433	212.316	2238.048	795.733	0.0000
Pt 52	1656.461	1726.908	1606.930	2383.974	0.0001
Pt 53	2085.124	572.983	2056.178	1177.437	0.0002
Pt 54	1646.155	1729.157	1596.850	2387.719	-0.0002
Pt 55	3879.670	839.560	3883.259	1439.576	0.0002
Pt 56	2000.883	565.180	1970.532	1169.730	0.0001
Pt 57	2067.745	862.595	2035.186	1480.947	0.0002
Pt 58	3918.805	168.801	3927.688	746.161	0.0010
Pt 59	1732.215	1223.151	1688.591	1859.508	0.0004
Pt 60	3925.901	159.919	3935.413	737.194	0.0007
Pt 61	2472.777	161.247	2457.934	742.022	-0.0003
Pt 62	2472.777	161.247	2457.934	742.022	-0.0003
Pt 63	2472.777	161.247	2457.934	742.022	-0.0003
Pt 64	2661.050	156.877	2650.635	735.584	-0.0005
Pt 65	1697.454	1743.828	1649.053	2400.889	-0.0001
Pt 66	1397.970	138.722	1359.446	726.660	-0.0002
Pt 67	1718.224	1231.281	1674.575	1867.875	0.0002
Pt 68	3598.122	970.333	3595.603	1578.266	-0.0002
Pt 69	2354.455	507.713	2333.019	1106.358	-0.0003
Pt 70	2291.873	474.694	2269.871	1072.307	-0.0005
Pt 71	1648.526	1306.657	1602.420	1947.544	0.0003
Pt 72	1648.526	1306.657	1602.420	1947.544	0.0003
Pt 73	2343.192	500.855	2320.946	1098.762	0.0001

ID	Image location of conjugate points in Image A		Image location of conjugate points in Image B		Residuals
	x (Pixels)	y (Pixels)	x (Pixels)	y (Pixels)	Signed Dist (Pixels)
Pt 74	2313.447	1057.348	2283.566	1680.227	0.0005
Pt 75	2844.860	428.320	2834.323	1019.117	-0.0003
Pt 76	1700.423	1249.913	1656.244	1889.065	0.0001
Pt 77	1786.191	1179.063	1744.545	1812.260	0.0002
Pt 78	3230.449	1671.527	3213.188	2308.034	0.0002
Pt 79	2587.385	800.925	2566.412	1409.898	0.0003
Pt 80	2057.245	569.359	2027.876	1173.417	0.0002
Pt 81	2057.245	569.359	2027.876	1173.417	0.0002
Pt 82	3093.690	811.498	3082.739	1417.979	0.0001
Pt 83	2174.147	153.114	2153.582	742.950	-0.0012
Pt 84	2519.276	1553.392	2488.992	2193.332	0.0002
Pt 85	2221.613	255.629	2199.856	842.232	0.0000
Pt 86	3207.782	926.002	3199.864	1538.164	-0.0013
Pt 87	3564.147	230.652	3568.420	808.174	0.0005
Pt 88	2021.704	572.784	1991.230	1177.665	0.0003
Pt 89	2051.674	300.724	2027.722	894.861	-0.0014
Pt 90	2593.482	124.893	2581.886	702.388	-0.0004
Pt 91	2819.774	2121.696	2790.229	2777.268	0.0003
Pt 92	1327.786	177.038	1287.463	767.854	-0.0003
Pt 93	2537.570	807.646	2515.229	1418.047	0.0003
Pt 94	2537.570	807.646	2515.229	1418.047	0.0003
Pt 95	2928.718	1966.051	2902.253	2615.840	0.0004
Pt 96	2126.609	598.712	2098.305	1203.633	0.0002
Pt 97	2126.609	598.712	2098.305	1203.633	0.0002
Pt 98	2960.379	202.176	2955.580	781.773	-0.0006
Pt 99	2096.897	608.152	2067.819	1214.017	0.0002
Pt 100	3435.811	449.820	3437.251	1037.308	-0.0006
Pt 101	1888.453	1041.011	1849.441	1669.381	0.0006
Pt 102	2924.222	133.320	2919.833	709.175	-0.0007
Pt 103	1541.891	68.884	1505.642	658.165	0.0005
Pt 104	2091.135	640.048	2061.224	1247.988	0.0004
Pt 105	3254.183	1402.466	3240.993	2029.406	-0.0003
Pt 106	2853.874	1673.012	2828.908	2313.655	0.0003
Pt 107	3151.883	777.246	3143.021	1381.846	-0.0002
Pt 108	1600.593	508.534	1561.785	1112.502	0.0004
Pt 109	2557.537	397.962	2539.792	990.500	0.0005
Pt 110	2195.584	256.123	2173.266	843.598	-0.0001
Pt 111	1105.325	1828.359	1045.512	2492.470	-0.0009
Pt 112	2863.084	422.296	2852.564	1011.967	0.0001

ID	Image location of conjugate points in Image A		Image location of conjugate points in Image B		Residuals
	x (Pixels)	y (Pixels)	x (Pixels)	y (Pixels)	Signed Dist (Pixels)
Pt 113	2863.084	422.296	2852.564	1011.967	0.0001
Pt 114	3117.629	771.115	3107.931	1375.961	-0.0001
Pt 115	2833.248	2120.235	2803.605	2775.743	0.0004
Pt 116	2833.248	2120.235	2803.605	2775.743	0.0004
Pt 117	2110.170	605.444	2081.606	1211.326	0.0001
Pt 118	3365.419	1511.242	3353.364	2141.531	-0.0004
Pt 119	1096.193	825.881	1043.932	1448.349	-0.0001
Pt 120	1991.885	1509.544	1951.680	2155.859	-0.0001
Pt 121	3104.559	1794.433	3082.588	2436.109	0.0007
Pt 122	3627.901	1765.184	3620.190	2400.883	-0.0010
Pt 123	1462.243	241.845	1424.344	834.493	-0.0003
Pt 124	1462.243	241.845	1424.344	834.493	-0.0003
Pt 125	2119.544	621.622	2090.400	1227.382	0.0005
Pt 126	2831.964	2137.217	2802.501	2793.178	0.0003
Pt 127	2868.310	2090.223	2839.751	2744.452	0.0004
Pt 128	1306.300	2284.156	1245.752	2962.412	-0.0006
Pt 129	2166.086	558.025	2139.214	1160.108	0.0002
Pt 130	2166.086	558.025	2139.214	1160.108	0.0002
Pt 131	1295.499	2252.086	1234.468	2927.795	-0.0003
Pt 132	1991.888	724.192	1960.793	1337.146	-0.0006
Pt 133	2210.490	728.393	2182.654	1338.319	0.0002
Pt 134	2822.730	1029.190	2805.130	1650.397	-0.0009
Pt 135	2627.660	1286.878	2602.045	1916.693	0.0002
Pt 136	2072.064	750.755	2039.793	1362.680	0.0008
Pt 137	2839.288	1043.211	2821.000	1665.318	-0.0005
Pt 138	2919.622	2008.913	2893.783	2662.050	-0.0003
Pt 139	3515.300	502.396	3516.970	1090.637	-0.0001
Pt 140	1729.851	785.612	1690.857	1402.458	0.0003
Pt 141	2954.862	1946.750	2929.507	2593.111	0.0006
Pt 142	2913.680	1937.972	2887.579	2586.126	0.0004
Pt 143	2220.403	93.522	2202.767	677.747	-0.0017
Pt 144	2120.561	637.097	2095.128	1246.357	-0.0017
Pt 145	1535.156	811.419	1491.863	1431.042	0.0003
Pt 146	2910.484	1259.639	2892.642	1884.796	-0.0006
Pt 147	2910.484	1259.639	2892.642	1884.796	-0.0006
Pt 148	2081.118	586.754	2052.583	1191.395	-0.0001
Pt 149	1640.434	841.232	1599.272	1460.756	0.0002
Pt 150	1643.453	862.786	1602.268	1483.222	0.0001
Pt 151	1340.059	408.382	1297.624	1009.352	-0.0003

ID	Image location of conjugate points in Image A		Image location of conjugate points in Image B		Residuals
	x (Pixels)	y (Pixels)	x (Pixels)	y (Pixels)	Signed Dist (Pixels)
Pt 152	2079.019	859.800	2047.027	1478.749	0.0000
Pt 153	478.146	1853.231	401.536	2527.691	0.0004
Pt 154	1229.652	2084.945	1169.377	2756.702	-0.0006
Pt 155	1229.652	2084.945	1169.377	2756.702	-0.0006
Pt 156	3071.862	1223.880	3057.104	1846.948	-0.0005
Pt 157	1476.648	896.897	1430.632	1521.127	0.0006
Pt 158	2145.768	368.237	2120.667	962.270	0.0001
Pt 159	1220.511	2060.958	1160.338	2732.378	-0.0006
Pt 160	1220.511	2060.958	1160.338	2732.378	-0.0006
Pt 161	2753.799	1241.951	2730.945	1867.771	0.0004
Pt 162	3135.722	1791.680	3114.370	2433.150	0.0007
Pt 163	1532.985	937.630	1488.343	1563.347	0.0003
Pt 164	3926.801	147.187	3936.656	725.161	0.0004
Pt 165	1188.294	1989.864	1127.432	2658.479	-0.0003
Pt 166	2733.267	1226.368	2710.178	1852.049	0.0004
Pt 167	2733.267	1226.368	2710.178	1852.049	0.0004
Pt 168	2752.343	289.614	2741.614	873.444	-0.0001
Pt 169	2752.343	289.614	2741.614	873.444	-0.0001
Pt 170	1180.200	1974.141	1120.660	2643.625	-0.0009
Pt 171	2729.355	269.257	2718.879	852.587	-0.0004
Pt 172	2706.912	253.068	2695.799	836.045	-0.0003
Pt 173	1156.131	1926.431	1096.198	2594.790	-0.0008
Pt 174	2810.510	228.391	2800.926	810.513	0.0001
Pt 175	2485.400	210.366	2469.958	797.519	-0.0006
Pt 176	1343.244	336.286	1301.589	934.308	-0.0003
Pt 177	3133.926	1558.829	3116.735	2191.978	-0.0001
Pt 178	3884.146	199.559	3892.545	776.671	0.0011
Pt 179	3884.146	199.559	3892.545	776.671	0.0011
Pt 180	3055.936	192.597	3052.727	771.483	-0.0005
Pt 181	1409.661	306.063	1369.234	902.131	0.0000
Pt 182	3438.671	1592.948	3427.822	2224.731	-0.0005
Pt 183	2723.093	286.220	2711.711	869.902	-0.0001
Pt 184	1383.833	279.401	1343.632	873.580	-0.0002
Pt 185	3471.531	1573.556	3461.996	2204.285	-0.0007
Pt 186	3471.531	1573.556	3461.996	2204.285	-0.0007
Pt 187	3406.625	1101.898	3398.702	1718.129	-0.0002
Pt 188	1120.377	1856.099	1061.737	2523.600	-0.0014
Pt 189	2753.656	1188.314	2731.739	1813.941	0.0000
Pt 190	3099.568	1484.723	3082.387	2116.696	-0.0002

ID	Image location of conjugate points in Image A		Image location of conjugate points in Image B		Residuals
	x (Pixels)	y (Pixels)	x (Pixels)	y (Pixels)	Signed Dist (Pixels)
Pt 191	3607.709	1422.292	3601.985	2046.309	-0.0006
Pt 192	2971.845	58.383	2967.313	633.030	0.0000
Pt 193	2971.845	58.383	2967.313	633.030	0.0000
Pt 194	3607.337	1467.392	3601.166	2093.229	-0.0007
Pt 195	1491.019	936.161	1444.647	1561.494	0.0007
Pt 196	2527.994	447.522	2510.767	1041.860	-0.0003
Pt 197	2952.929	322.469	2945.908	906.134	-0.0001
Pt 198	2056.701	601.739	2027.112	1208.301	0.0000
Pt 199	1830.166	608.860	1795.499	1216.575	0.0002
Pt 200	3506.778	442.811	3508.625	1029.071	0.0000
Pt 201	2516.201	822.854	2493.104	1433.126	0.0005
Pt 202	2776.426	1132.890	2755.395	1755.120	0.0002
Pt 203	3401.356	1117.765	3393.490	1733.699	-0.0002
Pt 204	2894.593	1950.007	2868.877	2598.887	0.0000
Pt 205	1996.108	531.889	1965.706	1134.171	0.0003
Pt 206	3517.709	470.323	3519.999	1057.555	-0.0003
Pt 207	3177.665	1667.655	3159.978	2304.735	0.0000
Pt 208	1785.219	668.695	1748.727	1279.771	0.0003
Pt 209	2162.638	366.598	2138.481	958.836	-0.0001
Pt 210	2786.278	1089.757	2765.537	1710.350	0.0004
Pt 211	3039.769	1366.282	3022.394	1993.707	0.0000
Pt 212	3039.769	1366.282	3022.394	1993.707	0.0000
Pt 213	1403.130	224.495	1363.635	816.444	-0.0001
Pt 214	2799.365	2182.669	2769.026	2840.601	0.0002
Pt 215	3639.240	483.761	3642.801	1071.431	0.0000
Pt 216	3017.542	1906.007	2993.734	2552.432	0.0003
Pt 217	1434.432	214.331	1396.074	806.308	-0.0003
Pt 218	3087.663	761.388	3077.742	1365.717	-0.0002
Pt 219	2159.647	311.538	2136.072	902.405	-0.0002
Pt 220	1282.389	2215.617	1221.700	2891.887	-0.0004
Pt 221	1354.557	299.479	1315.329	896.232	-0.0012
Pt 222	2191.374	278.510	2167.969	867.241	0.0003
Pt 223	3171.095	1465.586	3155.668	2095.866	-0.0003
Pt 224	3577.090	1567.658	3569.658	2197.593	-0.0008
Pt 225	3315.269	168.242	3315.634	743.851	0.0006
Pt 226	1414.278	274.236	1374.953	868.639	-0.0003
Pt 227	3126.024	1455.861	3109.812	2085.825	-0.0002
Pt 228	2931.116	261.028	2924.316	844.569	-0.0004
Pt 229	1380.604	218.967	1341.247	809.243	-0.0004

ID	Image location of conjugate points in Image A		Image location of conjugate points in Image B		Residuals
	x (Pixels)	y (Pixels)	x (Pixels)	y (Pixels)	Signed Dist (Pixels)
Pt 230	2593.454	1211.798	2568.089	1839.477	0.0001
Pt 231	2593.454	1211.798	2568.089	1839.477	0.0001
Pt 232	2928.085	84.583	2923.681	659.441	-0.0005
Pt 233	1043.734	575.464	992.414	1187.987	0.0000
Pt 234	1971.479	952.497	1934.963	1575.875	0.0007
Pt 235	2946.251	206.174	2941.059	786.110	-0.0006
Pt 236	1334.066	322.615	1293.137	922.693	-0.0007
Pt 237	2638.080	1274.145	2611.693	1901.752	0.0009
Pt 238	3446.678	1077.182	3439.335	1691.860	0.0000
Pt 239	1832.680	628.780	1798.076	1236.969	0.0001
Pt 240	1832.680	628.780	1798.076	1236.969	0.0001
Pt 241	2756.615	1158.396	2733.640	1781.537	0.0009
Pt 242	1811.876	608.556	1775.083	1215.681	0.0011
Pt 243	1736.793	316.450	1702.614	913.792	0.0004
Pt 244	1354.129	319.793	1312.445	916.516	0.0000
Pt 245	1354.129	319.793	1312.445	916.516	0.0000
Pt 246	1402.307	321.617	1361.472	918.269	0.0001
Pt 247	3225.734	1428.668	3211.607	2056.644	-0.0002
Pt 248	3598.831	1490.672	3591.969	2117.120	-0.0005
Pt 249	3135.387	831.468	3124.826	1437.849	0.0002
Pt 250	3623.651	1337.486	3618.925	1958.343	-0.0006
Pt 251	2949.391	1968.086	2923.763	2617.306	0.0003
Pt 252	1365.879	284.135	1325.605	879.931	-0.0005
Pt 253	2501.705	217.881	2486.331	808.777	-0.0009
Pt 254	3804.591	78.062	3812.680	653.034	0.0008
Pt 255	3597.527	1685.464	3590.393	2319.797	-0.0014
Pt 256	3187.904	1688.399	3169.357	2326.006	0.0003
Pt 257	3836.865	100.083	3844.430	675.965	0.0012
Pt 258	3445.111	1715.562	3433.451	2352.234	-0.0007
Pt 259	1952.499	462.164	1922.214	1061.809	0.0001
Pt 260	1952.499	462.164	1922.214	1061.809	0.0001
Pt 261	1393.754	258.962	1354.948	853.001	-0.0008
Pt 262	1384.506	356.372	1343.266	954.399	-0.0001
Pt 263	3679.321	124.493	3685.203	698.860	0.0011
Pt 264	1423.670	252.266	1383.947	845.429	0.0001
Pt 265	1423.670	252.266	1383.947	845.429	0.0001
Pt 266	1624.866	851.473	1583.292	1471.542	0.0002
Pt 267	3154.510	1776.581	3134.131	2417.391	0.0005
Pt 268	3154.510	1776.581	3134.131	2417.391	0.0005

ID	Image location of conjugate points in Image A		Image location of conjugate points in Image B		Residuals
	x (Pixels)	y (Pixels)	x (Pixels)	y (Pixels)	Signed Dist (Pixels)
Pt 269	1434.438	735.995	1389.468	1352.016	0.0004
Pt 270	2181.987	296.083	2158.641	886.162	0.0000
Pt 271	2181.987	296.083	2158.641	886.162	0.0000
Pt 272	1645.035	742.473	1604.228	1356.582	0.0006
Pt 273	3153.649	823.789	3143.374	1430.542	0.0002
Pt 274	2615.564	1300.505	2589.600	1930.990	0.0002
Pt 275	1452.108	723.893	1407.539	1339.730	0.0005
Pt 276	3915.899	161.724	3925.784	739.795	0.0003
Pt 277	2517.858	231.590	2501.237	821.377	0.0001
Pt 278	1750.906	303.234	1715.874	900.390	0.0011
Pt 279	1554.775	797.025	1512.222	1415.499	0.0002
Pt 280	3892.202	119.997	3901.982	697.812	0.0001
Pt 281	3539.679	396.320	3542.918	980.421	-0.0001
Pt 282	3221.852	1951.382	3203.247	2597.052	-0.0003
Pt 283	3221.852	1951.382	3203.247	2597.052	-0.0003
Pt 284	1387.059	334.578	1346.644	931.338	-0.0004
Pt 285	3682.349	429.379	3687.319	1014.946	0.0000
Pt 286	3682.349	429.379	3687.319	1014.946	0.0000
Pt 287	2773.108	233.531	2763.542	815.434	-0.0003
Pt 288	2476.715	608.037	2456.501	1210.131	-0.0002
Pt 289	2476.715	608.037	2456.501	1210.131	-0.0002
Pt 290	3476.842	429.631	3479.150	1015.854	-0.0005
Pt 291	1977.810	983.857	1941.254	1606.463	0.0007
Pt 292	2759.253	1215.070	2736.968	1840.723	0.0002
Pt 293	2759.253	1215.070	2736.968	1840.723	0.0002
Pt 294	3444.681	1019.951	3438.842	1630.678	-0.0001
Pt 295	3707.434	159.471	3713.446	735.827	0.0009
Pt 296	3707.434	159.471	3713.446	735.827	0.0009
Pt 297	1615.393	381.234	1578.097	979.325	0.0004
Pt 298	2794.968	1245.526	2774.584	1872.745	-0.0006
Pt 299	3655.748	436.124	3660.281	1020.782	0.0001
Pt 300	1752.671	726.438	1714.482	1340.567	0.0005
Pt 301	3184.014	841.107	3176.777	1450.402	-0.0014
Pt 302	3179.851	2168.755	3156.275	2826.674	-0.0001
Pt 303	2693.303	1608.132	2666.248	2247.691	0.0002
Pt 304	897.181	864.712	839.492	1490.094	0.0002
Pt 305	1921.251	1540.527	1879.648	2188.487	-0.0003
Pt 306	1921.251	1540.527	1879.648	2188.487	-0.0003
Pt 307	2595.145	782.412	2574.569	1390.165	0.0003

ID	Image location of conjugate points in Image A		Image location of conjugate points in Image B		Residuals
	x (Pixels)	y (Pixels)	x (Pixels)	y (Pixels)	Signed Dist (Pixels)
Pt 308	2293.307	791.020	2265.908	1402.524	0.0005
Pt 309	2540.328	1536.025	2510.930	2177.024	-0.0001
Pt 310	1108.188	1507.903	1048.842	2163.282	0.0002
Pt 311	3080.404	763.542	3070.640	1368.896	-0.0005
Pt 312	1625.909	759.039	1585.352	1374.737	0.0002
Pt 313	1625.909	759.039	1585.352	1374.737	0.0002
Pt 314	1525.731	763.472	1484.246	1383.562	-0.0006
Pt 315	2319.365	931.753	2291.831	1548.861	0.0001
Pt 316	2319.365	931.753	2291.831	1548.861	0.0001
Pt 317	1747.679	754.943	1710.575	1369.015	-0.0002
Pt 318	3141.521	1417.378	3125.153	2046.248	0.0001
Pt 319	3203.652	1342.717	3192.318	1965.588	-0.0009
Pt 320	3474.339	1023.680	3469.047	1637.756	-0.0007
Pt 321	3474.339	1023.680	3469.047	1637.756	-0.0007
Pt 322	3637.921	105.239	3643.066	679.376	0.0012
Pt 323	3393.296	1265.486	3383.172	1885.138	0.0003
Pt 324	2995.957	1910.368	2972.012	2558.940	0.0000
Pt 325	3615.066	1059.027	3612.160	1670.011	-0.0002
Pt 326	2927.403	116.017	2922.990	691.818	-0.0007
Pt 327	2927.403	116.017	2922.990	691.818	-0.0007
Pt 328	3027.191	1885.714	3005.070	2531.216	-0.0002
Pt 329	3856.856	1072.892	3860.756	1682.323	-0.0014
Pt 330	3422.635	1090.551	3417.081	1705.919	-0.0011
Pt 331	3422.635	1090.551	3417.081	1705.919	-0.0011
Pt 332	3634.734	1192.618	3630.794	1807.975	-0.0002
Pt 333	1398.544	148.942	1359.132	737.008	0.0002
Pt 334	1307.110	1817.339	1250.493	2481.350	-0.0004
Pt 335	2207.557	1130.442	2172.723	1756.533	0.0015
Pt 336	2964.147	185.628	2959.309	764.408	-0.0005
Pt 337	2964.147	185.628	2959.309	764.408	-0.0005
Pt 338	3581.835	1062.971	3577.893	1674.658	-0.0001
Pt 339	3581.835	1062.971	3577.893	1674.658	-0.0001
Pt 340	2474.726	1059.842	2447.552	1682.010	0.0007
Pt 341	1640.087	204.310	1604.166	793.702	0.0010
Pt 342	2853.954	197.581	2846.330	775.785	0.0000
Pt 343	3663.788	1177.432	3660.539	1792.021	-0.0002
Pt 344	3663.788	1177.432	3660.539	1792.021	-0.0002
Pt 345	2581.256	1181.573	2556.054	1806.947	0.0002
Pt 346	2581.256	1181.573	2556.054	1806.947	0.0002

ID	Image location of conjugate points in Image A		Image location of conjugate points in Image B		Residuals
	x (Pixels)	y (Pixels)	x (Pixels)	y (Pixels)	Signed Dist (Pixels)
Pt 347	2801.379	1889.758	2772.911	2537.943	0.0006
Pt 348	2801.379	1889.758	2772.911	2537.943	0.0006
Pt 349	1950.105	1010.222	1916.429	1633.380	-0.0010
Pt 350	3506.114	1004.657	3500.571	1616.033	0.0001
Pt 351	2701.670	1207.472	2678.655	1833.254	0.0001
Pt 352	1022.143	977.448	967.607	1607.387	-0.0005
Pt 353	2900.763	1919.341	2873.948	2567.932	0.0005
Pt 354	2900.763	1919.341	2873.948	2567.932	0.0005
Pt 355	2047.945	576.450	2021.018	1182.642	-0.0013
Pt 356	2047.945	576.450	2021.018	1182.642	-0.0013
Pt 357	2681.156	267.987	2670.279	851.112	-0.0007
Pt 358	3519.166	920.964	3514.370	1527.967	0.0004
Pt 359	2732.489	304.570	2720.943	888.893	0.0000
Pt 360	1380.782	2004.728	1324.144	2676.394	-0.0005
Pt 361	1380.782	2004.728	1324.144	2676.394	-0.0005
Pt 362	2032.668	336.564	2008.715	933.009	-0.0018
Pt 363	2679.395	298.973	2667.641	882.865	-0.0003
Pt 364	2652.361	1291.829	2628.478	1921.115	-0.0003
Pt 365	3625.315	1302.154	3621.107	1921.432	-0.0006
Pt 366	3625.315	1302.154	3621.107	1921.432	-0.0006
Pt 367	2905.280	372.037	2895.293	960.645	0.0003
Pt 368	1056.000	516.977	1005.326	1128.386	0.0001
Pt 369	2447.855	2027.429	2410.709	2683.634	0.0007
Pt 370	1999.974	379.340	1971.390	979.888	-0.0001
Pt 371	3176.698	803.732	3167.953	1410.592	-0.0004
Pt 372	3956.269	420.957	3964.812	1006.184	0.0003
Pt 373	1469.600	747.493	1425.716	1363.430	0.0002
Pt 374	1326.783	477.820	1283.246	1082.397	-0.0002
Pt 375	2556.391	2249.043	2520.216	2912.508	0.0003
Pt 376	1433.964	2136.507	1376.644	2811.910	-0.0003
Pt 377	1993.493	1524.267	1952.601	2170.877	0.0001
Pt 378	2586.320	2158.353	2551.576	2819.047	0.0002
Pt 379	3180.712	1421.508	3163.675	2050.698	0.0006
Pt 380	3734.728	646.053	3739.682	1243.501	-0.0015
Pt 381	2871.798	384.986	2861.952	971.948	0.0001
Pt 382	3619.984	1439.916	3614.333	2063.976	-0.0006
Pt 383	1861.025	1466.714	1818.014	2112.898	0.0001
Pt 384	2979.451	402.474	2972.828	988.753	-0.0004
Pt 385	2205.310	818.860	2175.496	1433.435	0.0005

ID	Image location of conjugate points in Image A		Image location of conjugate points in Image B		Residuals
	x (Pixels)	y (Pixels)	x (Pixels)	y (Pixels)	Signed Dist (Pixels)
Pt 386	2205.310	818.860	2175.496	1433.435	0.0005
Pt 387	1593.090	578.342	1552.461	1185.482	0.0008
Pt 388	1878.700	615.554	1844.446	1224.257	0.0004
Pt 389	1382.232	636.102	1337.403	1248.289	0.0003
Pt 390	2725.308	2257.024	2692.051	2918.390	0.0005
Pt 391	3641.552	508.438	3645.007	1096.732	0.0000
Pt 392	2047.449	663.225	2015.566	1273.142	0.0007
Pt 393	2768.930	1565.521	2742.009	2202.980	0.0009
Pt 394	3608.594	488.827	3611.675	1076.599	0.0000
Pt 395	3608.594	488.827	3611.675	1076.599	0.0000
Pt 396	2493.802	873.515	2470.145	1487.263	0.0002
Pt 397	1607.793	704.740	1566.384	1317.573	0.0007
Pt 398	2436.775	2134.070	2400.081	2796.304	-0.0002
Pt 399	3695.726	708.963	3697.319	1306.184	0.0001
Pt 400	3695.187	455.129	3700.810	1041.202	-0.0003
Pt 401	3564.404	1658.644	3556.461	2291.920	-0.0011
Pt 402	3327.795	348.148	3327.995	933.437	-0.0007
Pt 403	3263.653	1364.124	3251.396	1988.836	-0.0003
Pt 404	1695.801	909.351	1655.663	1532.140	-0.0001
Pt 405	3236.385	1349.630	3221.813	1976.614	0.0002
Pt 406	1410.927	2073.510	1354.647	2747.068	-0.0007
Pt 407	2116.446	769.802	2087.864	1382.094	-0.0007
Pt 408	3517.444	1685.165	3508.713	2319.397	-0.0012
Pt 409	3340.339	1571.319	3327.706	2202.939	-0.0004
Pt 410	1398.764	2044.854	1341.353	2715.491	-0.0002
Pt 411	1808.958	328.120	1776.204	924.070	0.0005
Pt 412	3079.052	799.777	3067.733	1404.268	0.0004
Pt 413	984.090	747.179	929.553	1365.584	0.0001
Pt 414	2791.347	2012.630	2761.890	2665.023	0.0004
Pt 415	2798.739	331.280	2787.465	916.517	0.0004
Pt 416	1455.247	1287.864	1404.123	1928.397	0.0009
Pt 417	2382.522	860.553	2355.356	1473.598	0.0010
Pt 418	1005.850	1982.074	940.845	2654.123	-0.0002
Pt 419	992.020	974.824	936.002	1602.859	-0.0001
Pt 420	2581.454	904.749	2558.400	1518.815	0.0006
Pt 421	3787.685	975.636	3787.568	1580.393	0.0007
Pt 422	1014.058	1009.297	959.002	1640.140	-0.0005
Pt 423	1164.736	569.196	1116.101	1179.514	0.0001
Pt 424	1814.250	566.079	1784.723	1171.704	-0.0024

ID	Image location of conjugate points in Image A		Image location of conjugate points in Image B		Residuals
	x (Pixels)	y (Pixels)	x (Pixels)	y (Pixels)	Signed Dist (Pixels)
Pt 425	3599.076	1326.806	3594.768	1944.826	-0.0005
Pt 426	2487.319	721.410	2464.443	1325.585	0.0009
Pt 427	3650.354	1314.796	3645.809	1936.429	-0.0007
Pt 428	3650.354	1314.796	3645.809	1936.429	-0.0007
Pt 429	3646.547	1752.047	3639.761	2388.259	-0.0014
Pt 430	2872.431	1204.636	2850.767	1830.039	0.0009
Pt 431	2305.635	707.580	2279.601	1315.199	0.0004
Pt 432	2305.635	707.580	2279.601	1315.199	0.0004
Pt 433	2730.876	238.849	2722.968	824.251	-0.0020
Pt 434	1089.005	238.921	1043.461	834.144	-0.0008
Pt 435	2453.609	1742.522	2420.542	2390.688	0.0000
Pt 436	3645.655	1050.392	3642.767	1661.571	-0.0001
Pt 437	2834.682	1898.441	2806.929	2546.750	0.0005
Pt 438	2820.793	187.922	2812.603	767.540	-0.0002
Pt 439	1351.761	202.506	1312.960	793.895	-0.0010
Pt 440	3455.432	1772.932	3443.858	2409.799	-0.0006
Pt 441	3455.432	1772.932	3443.858	2409.799	-0.0006
Pt 442	2293.286	1150.663	2263.034	1777.774	0.0000
Pt 443	3464.233	1206.848	3459.274	1823.522	-0.0011
Pt 444	2502.608	1838.517	2469.406	2489.873	0.0000
Pt 445	1523.549	1839.796	1471.854	2504.328	-0.0007
Pt 446	2572.952	1807.803	2543.282	2452.400	-0.0002
Pt 447	1395.572	577.480	1351.440	1186.235	0.0004
Pt 448	2264.898	1113.599	2233.715	1739.166	0.0003
Pt 449	2594.570	1484.800	2567.316	2122.777	-0.0003
Pt 450	1502.399	915.227	1456.609	1538.737	0.0007
Pt 451	1502.399	915.227	1456.609	1538.737	0.0007
Pt 452	1705.345	975.428	1664.489	1602.252	0.0000
Pt 453	1083.558	1473.858	1024.017	2128.465	0.0002
Pt 454	2591.058	2115.047	2557.028	2772.272	0.0003
Pt 455	3536.560	431.731	3537.944	1015.088	0.0010
Pt 456	1806.355	1349.941	1763.511	1988.993	0.0002
Pt 457	2924.628	177.987	2918.540	754.911	0.0001
Pt 458	1890.952	1518.109	1848.895	2164.991	-0.0002
Pt 459	2510.743	1178.067	2484.193	1804.339	0.0001
Pt 460	1157.758	2186.938	1095.493	2866.721	-0.0008
Pt 461	2847.019	1775.313	2819.601	2420.025	0.0008
Pt 462	1054.901	606.654	1003.855	1220.486	-0.0001
Pt 463	1594.074	246.685	1557.869	840.506	0.0003

ID	Image location of conjugate points in Image A		Image location of conjugate points in Image B		Residuals
	x (Pixels)	y (Pixels)	x (Pixels)	y (Pixels)	Signed Dist (Pixels)
Pt 464	2263.040	289.494	2242.043	876.588	-0.0001
Pt 465	2704.087	2128.883	2672.309	2784.673	0.0004
Pt 466	1372.961	370.814	1332.436	970.193	-0.0007
Pt 467	2928.728	1884.312	2904.208	2528.107	0.0004
Pt 468	3387.820	1124.633	3379.400	1739.472	0.0001
Pt 469	3508.115	457.487	3510.973	1044.292	-0.0006
Pt 470	2252.446	794.411	2224.182	1405.596	0.0005
Pt 471	2784.584	1105.567	2765.353	1726.894	-0.0004
Pt 472	1544.313	923.679	1500.261	1548.221	0.0002
Pt 473	1544.313	923.679	1500.261	1548.221	0.0002
Pt 474	1573.800	818.971	1532.027	1439.841	-0.0001
Pt 475	1689.713	819.300	1649.631	1437.526	0.0003
Pt 476	1619.672	820.013	1577.928	1439.243	0.0004
Pt 477	2633.548	900.126	2616.142	1515.467	-0.0018
Pt 478	2864.522	341.401	2855.519	929.712	-0.0005
Pt 479	3310.710	1858.289	3295.155	2499.128	-0.0004
Pt 480	2452.617	927.092	2426.244	1543.461	0.0008
Pt 481	3636.925	935.272	3638.317	1538.785	-0.0010
Pt 482	3030.424	215.148	3025.968	795.013	-0.0002
Pt 483	3651.108	1396.561	3645.680	2019.922	-0.0004
Pt 484	3582.927	516.674	3584.561	1104.844	0.0005
Pt 485	2428.023	1496.331	2397.024	2135.875	-0.0001
Pt 486	1262.951	84.260	1222.771	671.172	-0.0007
Pt 487	1472.979	376.438	1433.758	974.156	-0.0002
Pt 488	2089.200	1217.420	2052.969	1849.874	0.0004
Pt 489	2572.880	1132.259	2548.982	1756.114	-0.0003
Pt 490	2572.880	1132.259	2548.982	1756.114	-0.0003
Pt 491	1427.891	382.104	1388.301	981.627	-0.0006
Pt 492	3270.267	1616.570	3254.658	2250.953	0.0000
Pt 493	2655.407	441.549	2640.835	1033.689	-0.0002
Pt 494	1600.893	529.773	1561.720	1135.221	0.0004
Pt 495	2457.431	520.360	2438.461	1116.340	-0.0003
Pt 496	1089.026	1102.751	1030.839	1737.762	0.0014
Pt 497	3592.630	1777.419	3584.628	2416.968	-0.0017
Pt 498	3251.072	1353.467	3237.613	1978.730	0.0001
Pt 499	1316.418	550.058	1271.666	1159.616	-0.0001
Pt 500	944.932	610.651	891.846	1225.297	-0.0004
Pt 501	1725.232	714.372	1690.702	1327.702	-0.0016
Pt 502	2330.358	748.272	2309.984	1357.578	-0.0024

ID	Image location of conjugate points in Image A		Image location of conjugate points in Image B		Residuals
	x (Pixels)	y (Pixels)	x (Pixels)	y (Pixels)	Signed Dist (Pixels)
Pt 503	2688.180	1583.890	2661.757	2223.752	-0.0002
Pt 504	2766.375	1543.683	2740.296	2183.483	0.0003
Pt 505	3393.119	1591.805	3381.492	2221.410	-0.0001
Pt 506	3393.119	1591.805	3381.492	2221.410	-0.0001
Pt 507	2328.854	1519.165	2294.182	2160.100	0.0006
Pt 508	2822.604	1508.983	2801.151	2146.058	-0.0010
Pt 509	3446.755	1486.477	3434.068	2118.897	0.0001
Pt 510	3446.755	1486.477	3434.068	2118.897	0.0001
Pt 511	3300.211	1479.061	3282.937	2105.820	0.0020
Pt 512	1436.489	336.256	1396.813	931.898	-0.0002
Pt 513	1561.777	442.673	1524.954	1045.133	-0.0008
Pt 514	1561.777	442.673	1524.954	1045.133	-0.0008
Pt 515	1885.586	1408.350	1842.182	2046.534	0.0011
Pt 516	1673.794	462.365	1636.166	1065.037	0.0008
Pt 517	2614.902	500.417	2600.017	1095.785	-0.0008
Pt 518	1007.482	592.574	954.383	1207.423	0.0004
Pt 519	1993.410	1656.483	1951.492	2307.262	0.0001
Pt 520	1663.323	692.957	1622.763	1306.237	0.0009
Pt 521	1002.963	732.109	948.873	1349.526	0.0002
Pt 522	2270.193	740.887	2242.793	1351.686	0.0004
Pt 523	2495.802	742.255	2473.543	1350.170	0.0002
Pt 524	2495.802	742.255	2473.543	1350.170	0.0002
Pt 525	3130.669	796.757	3119.645	1402.426	0.0005
Pt 526	1749.733	1346.323	1706.272	1985.524	0.0000
Pt 527	1749.733	1346.323	1706.272	1985.524	0.0000
Pt 528	2505.142	893.980	2481.407	1504.742	0.0006
Pt 529	1877.274	1678.766	1831.871	2331.470	0.0005
Pt 530	3533.342	1045.566	3530.332	1658.826	-0.0012
Pt 531	2421.673	1228.956	2395.541	1858.945	-0.0012
Pt 532	3493.598	1670.030	3482.539	2301.967	0.0001
Pt 533	3660.751	1133.660	3657.018	1744.503	0.0006
Pt 534	2789.949	1172.989	2767.488	1798.721	0.0006
Pt 535	2143.058	1694.931	2102.548	2346.678	0.0005
Pt 536	2230.510	1196.101	2197.155	1825.691	0.0006
Pt 537	3719.103	1158.974	3715.545	1776.125	-0.0002
Pt 538	2729.012	1157.144	2707.685	1782.198	-0.0004
Pt 539	2729.012	1157.144	2707.685	1782.198	-0.0004
Pt 540	1793.645	1276.153	1752.289	1913.559	-0.0003
Pt 541	2112.418	1294.210	2078.354	1928.249	-0.0006

ID	Image location of conjugate points in Image A		Image location of conjugate points in Image B		Residuals
	x (Pixels)	y (Pixels)	x (Pixels)	y (Pixels)	Signed Dist (Pixels)
Pt 542	2112.418	1294.210	2078.354	1928.249	-0.0006
Pt 543	606.728	1305.871	535.875	1951.265	0.0012
Pt 544	2381.208	1316.702	2350.647	1950.602	0.0000
Pt 545	2843.276	1311.613	2824.907	1942.745	-0.0016
Pt 546	3136.927	1342.740	3120.520	1971.245	0.0001
Pt 547	2470.069	1135.825	2442.896	1759.982	0.0003
Pt 548	1818.237	1368.890	1775.142	2011.388	0.0002
Pt 549	3578.021	1091.239	3573.871	1701.226	0.0003
Pt 550	722.033	1426.148	656.453	2079.263	-0.0004
Pt 551	1679.104	1430.860	1631.428	2076.887	0.0007
Pt 552	3204.578	1420.313	3193.069	2048.410	-0.0015
Pt 553	3160.312	1488.574	3143.979	2118.932	0.0001
Pt 554	2908.136	1733.415	2884.361	2375.636	0.0000
Pt 555	3456.132	1561.810	3446.357	2194.099	-0.0010
Pt 556	2341.847	1594.055	2308.845	2239.190	-0.0005
Pt 557	3842.667	981.844	3840.487	1587.211	0.0020
Pt 558	3842.667	981.844	3840.487	1587.211	0.0020
Pt 559	3166.969	1627.329	3151.342	2263.344	-0.0009
Pt 560	3423.732	1656.408	3412.264	2289.534	-0.0005
Pt 561	1941.897	1681.803	1898.489	2330.919	0.0003
Pt 562	1941.897	1681.803	1898.489	2330.919	0.0003
Pt 563	3544.948	1738.416	3535.863	2374.657	-0.0011
Pt 564	2188.969	910.267	2158.036	1530.478	0.0003
Pt 565	1635.665	1787.815	1584.748	2447.293	0.0002
Pt 566	3660.374	1805.362	3652.984	2442.288	-0.0010
Pt 567	3670.020	877.435	3668.217	1481.936	0.0005
Pt 568	2288.902	870.811	2261.159	1486.075	0.0002
Pt 569	2998.573	1898.604	2973.324	2545.103	0.0008
Pt 570	1873.045	1909.330	1824.829	2569.992	0.0007
Pt 571	1551.750	1927.864	1498.763	2590.186	-0.0001
Pt 572	2431.364	828.367	2406.719	1439.855	0.0004
Pt 573	1752.748	820.928	1713.798	1438.164	0.0004
Pt 574	3168.434	2024.107	3148.521	2671.057	-0.0002
Pt 575	1232.227	784.870	1180.168	1404.362	0.0015
Pt 576	3136.332	2138.369	3114.143	2791.249	-0.0002
Pt 577	3136.332	2138.369	3114.143	2791.249	-0.0002
Pt 578	2187.419	766.402	2160.445	1376.614	-0.0006
Pt 579	2593.536	1801.943	2560.580	2449.213	0.0010
Pt 580	2436.499	713.186	2413.377	1319.964	0.0003

ID	Image location of conjugate points in Image A		Image location of conjugate points in Image B		Residuals
	x (Pixels)	y (Pixels)	x (Pixels)	y (Pixels)	Signed Dist (Pixels)
Pt 581	2246.018	2225.709	2205.130	2897.562	-0.0008
Pt 582	3032.104	1804.067	3009.260	2449.305	0.0001
Pt 583	2432.427	2218.819	2393.390	2883.734	0.0004
Pt 584	2310.840	2226.025	2270.339	2895.673	-0.0003
Pt 585	670.230	671.698	608.113	1287.880	0.0006
Pt 586	1101.921	2201.994	1037.262	2883.563	-0.0004
Pt 587	1352.259	639.440	1303.465	1253.430	0.0019
Pt 588	1671.872	1855.155	1623.118	2517.227	-0.0007
Pt 589	2568.758	2165.174	2535.115	2823.588	-0.0001
Pt 590	2696.375	1872.160	2664.295	2524.323	0.0009
Pt 591	2444.978	2136.044	2406.226	2796.977	0.0008
Pt 592	2311.216	534.096	2287.354	1135.961	0.0002
Pt 593	3188.220	2093.596	3164.081	2745.039	0.0011
Pt 594	1590.682	1879.798	1537.481	2542.873	0.0004
Pt 595	3757.558	432.243	3763.055	1019.098	0.0001
Pt 596	2944.604	372.566	2936.281	962.682	-0.0004
Pt 597	1616.492	380.366	1577.982	978.737	0.0011
Pt 598	3586.591	356.727	3590.829	941.258	-0.0004
Pt 599	3422.422	356.979	3421.531	939.143	0.0013
Pt 600	2337.236	1990.109	2299.225	2650.918	-0.0002
Pt 601	1173.991	328.604	1128.631	928.070	-0.0003
Pt 602	3870.411	304.502	3880.102	883.482	0.0001
Pt 603	3870.411	304.502	3880.102	883.482	0.0001
Pt 604	2791.350	303.301	2780.281	886.471	0.0005
Pt 605	726.363	1972.613	653.866	2647.757	0.0004
Pt 606	3475.563	1950.070	3460.447	2593.711	0.0002
Pt 607	3929.659	238.701	3937.202	818.820	0.0014
Pt 608	1281.858	225.393	1240.396	822.349	-0.0006
Pt 609	1342.417	143.590	1302.920	733.203	-0.0004
Pt 610	2980.926	124.960	2977.281	702.650	-0.0008
Pt 611	3271.857	1913.341	3253.959	2554.577	0.0004
Pt 612	3539.321	185.010	3544.160	760.010	0.0004
Pt 613	1104.853	100.941	1056.385	691.499	0.0017
Pt 614	1104.853	100.941	1056.385	691.499	0.0017
Pt 615	2206.527	264.867	2185.370	855.123	-0.0008
Pt 616	3574.372	971.023	3569.822	1578.537	0.0007
Pt 617	2539.475	1039.951	2515.671	1661.238	-0.0003
Pt 618	2971.163	1293.443	2953.454	1922.256	-0.0006
Pt 619	1616.595	1306.605	1569.105	1949.011	0.0006

ID	Image location of conjugate points in Image A		Image location of conjugate points in Image B		Residuals
	x (Pixels)	y (Pixels)	x (Pixels)	y (Pixels)	Signed Dist (Pixels)
Pt 620	3361.365	1523.010	3348.918	2150.785	0.0002
Pt 621	3213.167	1687.005	3194.052	2321.029	0.0013
Pt 622	3213.167	1687.005	3194.052	2321.029	0.0013
Pt 623	2973.939	1759.826	2950.684	2401.747	0.0003
Pt 624	2973.939	1759.826	2950.684	2401.747	0.0003
Pt 625	543.073	1961.763	464.557	2638.751	0.0013
Pt 626	2768.463	2118.984	2737.606	2774.386	0.0005
Pt 627	683.210	2223.702	607.089	2911.519	0.0006
Pt 628	3563.823	2236.067	3544.669	2888.291	0.0015
Pt 629	3223.587	1784.262	3205.405	2421.744	0.0006
Pt 630	3223.587	1784.262	3205.405	2421.744	0.0006
Pt 631	1822.300	1553.738	1780.192	2204.165	-0.0010
Pt 632	2762.088	175.166	2752.052	754.914	0.0002
Pt 633	2088.783	530.435	2061.441	1135.103	-0.0005
Pt 634	1321.711	775.571	1275.964	1394.109	-0.0006
Pt 635	2390.603	1419.992	2359.211	2057.306	0.0001
Pt 636	1580.425	1115.494	1535.395	1742.189	0.0003
Pt 637	1529.237	1266.618	1481.920	1908.237	-0.0001
Pt 638	1917.661	1198.827	1879.217	1828.935	0.0001
Pt 639	3459.259	1142.132	3450.794	1754.954	0.0010
Pt 640	1093.338	654.979	1042.693	1269.996	-0.0001
Pt 641	1203.331	2108.712	1140.564	2779.640	0.0001
Pt 642	1411.079	353.555	1371.647	951.388	-0.0007
Pt 643	1411.079	353.555	1371.647	951.388	-0.0007
Pt 644	1014.533	571.528	963.650	1183.548	-0.0005
Pt 645	1440.140	684.151	1395.518	1297.763	0.0006
Pt 646	2183.467	1187.463	2151.790	1815.701	-0.0005
Pt 647	2472.859	1323.208	2445.225	1956.457	-0.0005
Pt 648	1912.462	1587.770	1869.937	2236.488	-0.0001
Pt 649	1912.462	1587.770	1869.937	2236.488	-0.0001
Pt 650	2357.295	1612.068	2320.809	2256.614	0.0012
Pt 651	2508.252	1786.029	2481.586	2434.285	-0.0024
Pt 652	2652.519	2123.144	2619.285	2780.677	0.0004
Pt 653	2082.179	328.907	2059.465	922.407	-0.0017
Pt 654	1942.488	623.057	1909.455	1228.776	0.0006
Pt 655	1437.099	800.594	1392.722	1416.370	-0.0001
Pt 656	3755.278	1119.684	3753.857	1733.795	-0.0004
Pt 657	3496.911	1480.126	3487.299	2107.246	-0.0001
Pt 658	3233.860	1551.824	3215.810	2185.867	0.0008

ID	Image location of conjugate points in Image A		Image location of conjugate points in Image B		Residuals
	x (Pixels)	y (Pixels)	x (Pixels)	y (Pixels)	Signed Dist (Pixels)
Pt 659	2271.178	2082.251	2230.679	2748.579	-0.0002
Pt 660	3841.012	451.093	3844.012	1039.706	0.0017
Pt 661	1736.377	1104.943	1695.464	1734.092	-0.0002
Pt 662	1736.377	1104.943	1695.464	1734.092	-0.0002
Pt 663	1359.576	2143.370	1297.647	2815.947	0.0010
Pt 664	2015.046	1143.525	1981.039	1773.019	-0.0009
Pt 665	3500.148	1298.894	3490.499	1920.521	0.0006
Pt 666	1594.476	701.190	1554.101	1315.521	0.0000
Pt 667	1157.975	968.678	1101.154	1596.557	0.0021
Pt 668	2687.606	1451.986	2665.350	2087.204	-0.0015
Pt 669	2256.315	1856.810	2216.917	2511.385	0.0005
Pt 670	2996.132	1530.977	2974.134	2166.506	0.0007
Pt 671	2996.132	1530.977	2974.134	2166.506	0.0007
SUM:					-0.0002

APPENDIX F

Table F1: Image coordinates of associated image pairs automatically obtained using Scale Invariant Feature Transform algorithm on UAV acquired image pairs.

ID	Image location of conjugate points in Image A		Image location of conjugate points in Image B		Residuals
	x (Pixels)	y (Pixels)	x (Pixels)	y (Pixels)	Signed Dist (Pixels)
Pt 01	2074.789	751.900	2043.112	1364.626	0.0004
Pt 02	1326.860	176.477	1286.811	767.173	-0.0007
Pt 03	1366.201	176.087	1326.434	766.763	-0.0003
Pt 04	1905.858	476.847	1874.114	1077.540	0.0001
Pt 05	1387.533	229.697	1347.245	822.328	-0.0001
Pt 06	1894.987	472.872	1863.095	1073.410	0.0001
Pt 07	1049.606	473.227	999.865	1081.626	0.0000
Pt 08	2291.928	476.127	2268.339	1072.846	0.0002
Pt 09	3875.245	1775.162	3872.942	2412.460	-0.0013
Pt 10	1697.225	1743.938	1649.026	2400.850	-0.0002
Pt 11	2062.107	574.306	2032.343	1179.297	0.0002
Pt 12	1362.153	340.916	1320.843	939.060	-0.0004
Pt 13	1919.742	994.687	1882.605	1622.355	0.0002
Pt 14	1475.172	885.106	1429.691	1508.837	0.0004
Pt 15	1802.091	581.054	1766.969	1187.527	0.0001
Pt 16	2706.427	1221.995	2683.818	1848.559	-0.0003
Pt 17	2107.201	585.093	2078.247	1189.912	0.0002
Pt 18	3136.031	1477.990	3119.947	2108.725	-0.0002
Pt 19	2856.391	1335.661	2835.800	1963.785	-0.0002
Pt 20	2082.624	759.024	2051.828	1371.567	0.0000
Pt 21	2024.122	572.284	1993.099	1176.915	0.0005
Pt 22	1651.728	1702.408	1602.452	2358.928	0.0000
Pt 23	2239.493	659.445	2212.409	1266.025	0.0003
Pt 24	1210.596	1970.470	1151.651	2639.415	-0.0006
Pt 25	1433.448	305.856	1393.807	901.568	-0.0003
Pt 26	3114.167	1523.909	3096.784	2156.591	-0.0001
Pt 27	1650.781	1722.848	1601.096	2380.897	0.0001
Pt 28	3443.061	1789.901	3432.161	2428.209	-0.0007
Pt 29	2519.808	1553.744	2488.955	2193.235	0.0002
Pt 30	2624.103	1287.401	2598.192	1917.317	0.0001
Pt 31	2057.431	568.641	2028.623	1172.622	-0.0003
Pt 32	2827.145	1991.137	2798.777	2642.568	0.0001
Pt 33	1369.374	261.368	1329.118	855.451	-0.0005
Pt 34	1700.661	1249.904	1656.238	1888.982	0.0004

ID	Image location of conjugate points in Image A		Image location of conjugate points in Image B		Residuals
	x (Pixels)	y (Pixels)	x (Pixels)	y (Pixels)	Signed Dist (Pixels)
Pt 35	2751.878	1232.943	2729.448	1859.673	0.0000
Pt 36	2348.451	497.103	2327.086	1096.764	-0.0006
Pt 37	3165.782	844.730	3155.812	1451.983	0.0002
Pt 38	2784.974	1075.113	2764.913	1695.667	0.0000
Pt 39	1491.393	1607.425	1439.828	2258.681	-0.0001
Pt 40	3476.012	1004.335	3470.924	1616.402	-0.0002
Pt 41	1410.967	235.195	1371.562	827.703	-0.0003
Pt 42	2197.781	255.910	2175.507	843.471	-0.0003
Pt 43	3622.890	1409.469	3617.021	2033.508	0.0000
Pt 44	1378.794	257.910	1338.294	851.477	-0.0002
Pt 45	2099.759	643.709	2070.087	1251.224	0.0002
Pt 46	1925.368	1006.099	1889.591	1634.220	-0.0005
Pt 47	2112.362	593.605	2084.345	1198.184	-0.0002
Pt 48	2473.043	160.310	2458.386	740.273	-0.0006
Pt 49	1602.936	506.645	1563.362	1111.105	0.0007
Pt 50	3160.272	834.819	3149.962	1441.477	0.0004
Pt 51	3256.000	1333.467	3243.149	1957.248	0.0002
Pt 52	2091.112	641.230	2061.640	1248.457	0.0000
Pt 53	2661.213	156.854	2650.908	735.319	-0.0007
Pt 54	2451.911	157.245	2436.579	736.831	-0.0004
Pt 55	3605.706	440.813	3609.157	1026.179	0.0008
Pt 56	2149.331	639.108	2121.026	1245.926	0.0001
Pt 57	1331.969	736.720	1284.698	1354.186	0.0005
Pt 58	1696.482	511.196	1659.354	1114.861	0.0004
Pt 59	1355.263	254.383	1314.646	848.305	-0.0004
Pt 60	1118.023	2013.891	1056.486	2686.221	-0.0004
Pt 61	2895.915	1951.011	2870.247	2598.938	0.0000
Pt 62	2313.795	1057.572	2282.952	1680.341	0.0007
Pt 63	3777.696	1883.839	3772.350	2524.486	-0.0009
Pt 64	2126.975	598.165	2098.927	1202.485	-0.0001
Pt 65	2161.776	558.167	2134.373	1160.253	0.0002
Pt 66	3144.882	1555.148	3127.245	2188.172	0.0002
Pt 67	1264.338	42.669	1223.500	629.361	-0.0002
Pt 68	2036.442	555.127	2006.777	1158.891	0.0000
Pt 69	1992.417	519.967	1962.204	1122.053	0.0000
Pt 70	2083.920	601.852	2054.809	1207.190	0.0000
Pt 71	2073.946	607.665	2044.316	1213.877	0.0001
Pt 72	1881.323	408.077	1849.664	1006.148	0.0001
Pt 73	2094.531	606.854	2064.942	1212.125	0.0003

ID	Image location of conjugate points in Image A		Image location of conjugate points in Image B		Residuals
	x (Pixels)	y (Pixels)	x (Pixels)	y (Pixels)	Signed Dist (Pixels)
Pt 74	2029.540	551.164	1999.608	1154.806	0.0001
Pt 75	1709.440	550.152	1671.993	1155.676	0.0005
Pt 76	1206.019	1977.287	1146.972	2646.135	-0.0006
Pt 77	3093.842	811.249	3082.844	1417.984	0.0001
Pt 78	2844.665	428.756	2834.063	1020.121	-0.0003
Pt 79	1388.942	202.654	1349.316	793.843	-0.0003
Pt 80	1398.610	138.934	1359.965	726.844	-0.0004
Pt 81	1659.364	1700.703	1610.320	2357.170	0.0000
Pt 82	1644.667	1698.859	1595.134	2355.788	0.0001
Pt 83	1305.122	99.730	1265.218	687.268	-0.0006
Pt 84	2959.356	203.906	2954.799	783.621	-0.0007
Pt 85	2070.337	624.201	2039.973	1231.179	0.0004
Pt 86	1987.118	939.176	1951.324	1564.098	0.0005
Pt 87	2819.881	2122.716	2789.292	2778.512	0.0004
Pt 88	2926.258	1937.995	2899.098	2586.195	0.0007
Pt 89	2894.009	1320.682	2873.906	1948.940	-0.0001
Pt 90	1599.769	804.653	1558.415	1423.219	0.0000
Pt 91	2523.994	34.935	2511.500	609.810	-0.0004
Pt 92	3230.819	1671.303	3213.175	2308.483	0.0004
Pt 93	3022.358	1188.368	3005.777	1811.129	0.0000
Pt 94	2276.951	620.427	2250.942	1225.030	0.0004
Pt 95	2960.142	1909.257	2934.094	2555.952	0.0007
Pt 96	1998.449	725.749	1965.886	1338.040	0.0001
Pt 97	2087.764	620.080	2057.917	1226.367	0.0003
Pt 98	1123.851	804.311	1072.794	1425.321	-0.0002
Pt 99	1987.504	723.857	1954.211	1336.508	0.0004
Pt 100	1631.879	1707.482	1582.038	2364.297	0.0001
Pt 101	2587.313	801.066	2566.106	1409.889	0.0003
Pt 102	1663.260	1706.514	1614.279	2363.055	0.0000
Pt 103	2071.557	614.607	2041.762	1220.350	0.0001
Pt 104	2091.440	613.565	2062.056	1219.720	0.0001
Pt 105	1325.749	32.044	1286.490	616.368	-0.0004
Pt 106	3125.231	1631.931	3106.111	2268.526	0.0002
Pt 107	2780.048	375.007	2768.806	962.663	-0.0001
Pt 108	1969.964	967.862	1934.469	1590.787	0.0000
Pt 109	2008.750	674.519	1977.690	1284.329	-0.0002
Pt 110	1635.019	180.441	1600.485	769.451	0.0001
Pt 111	1196.124	179.062	1152.980	773.407	-0.0004
Pt 112	3598.130	970.255	3594.905	1578.228	0.0007

ID	Image location of conjugate points in Image A		Image location of conjugate points in Image B		Residuals
	x (Pixels)	y (Pixels)	x (Pixels)	y (Pixels)	Signed Dist (Pixels)
Pt 113	2593.493	125.196	2581.722	702.946	-0.0005
Pt 114	1195.078	1977.069	1135.788	2645.884	-0.0006
Pt 115	3037.214	1362.635	3019.313	1990.728	0.0001
Pt 116	2964.834	169.850	2960.560	748.111	-0.0006
Pt 117	2977.280	181.158	2973.438	760.005	-0.0008
Pt 118	1888.608	1041.065	1849.584	1669.265	0.0006
Pt 119	2537.385	807.680	2515.305	1418.020	0.0001
Pt 120	2959.866	202.249	2955.348	782.121	-0.0008
Pt 121	935.048	753.631	881.299	1380.683	0.0002
Pt 122	3436.808	1085.520	3429.278	1700.321	0.0003
Pt 123	2588.647	2054.005	2554.903	2709.290	0.0001
Pt 124	1651.163	1720.047	1601.617	2376.473	0.0000
Pt 125	2051.947	300.805	2027.969	895.121	-0.0015
Pt 126	1411.947	308.189	1371.951	904.534	-0.0003
Pt 127	2040.177	315.933	2014.502	910.841	-0.0008
Pt 128	2030.332	327.238	2005.625	924.222	-0.0015
Pt 129	3181.420	643.250	3176.093	1244.115	-0.0011
Pt 130	2109.671	606.651	2080.230	1212.117	0.0004
Pt 131	2099.208	634.931	2070.195	1241.868	-0.0001
Pt 132	2088.567	611.801	2059.125	1217.430	0.0002
Pt 133	3446.043	1666.425	3434.907	2301.218	-0.0004
Pt 134	2138.615	630.911	2110.648	1237.938	-0.0002
Pt 135	2571.858	382.648	2556.147	972.273	-0.0002
Pt 136	2195.384	256.233	2173.238	843.790	-0.0004
Pt 137	2866.991	1949.869	2839.267	2598.239	0.0005
Pt 138	3402.882	1115.843	3394.125	1730.960	0.0006
Pt 139	3640.688	1224.808	3636.304	1842.015	0.0003
Pt 140	805.997	1392.656	742.044	2043.908	0.0006
Pt 141	3156.763	793.639	3147.578	1398.655	0.0001
Pt 142	2951.019	1951.187	2924.102	2600.237	0.0007
Pt 143	2556.284	398.147	2540.433	990.665	-0.0006
Pt 144	1710.127	796.399	1671.083	1413.477	0.0000
Pt 145	2941.180	1945.972	2917.078	2592.289	-0.0001
Pt 146	2427.182	1286.829	2398.056	1918.628	-0.0002
Pt 147	2773.562	1205.797	2752.642	1832.362	-0.0005
Pt 148	1453.191	217.251	1414.920	808.591	-0.0003
Pt 149	2851.838	373.065	2841.548	960.612	0.0002
Pt 150	2854.015	1672.685	2829.671	2313.353	-0.0001
Pt 151	3252.982	1403.941	3240.055	2030.311	-0.0001

ID	Image location of conjugate points in Image A		Image location of conjugate points in Image B		Residuals
	x (Pixels)	y (Pixels)	x (Pixels)	y (Pixels)	Signed Dist (Pixels)
Pt 152	2242.236	65.312	2222.605	650.091	-0.0004
Pt 153	2097.178	607.511	2067.987	1213.994	0.0001
Pt 154	1318.447	507.305	1274.713	1113.367	-0.0004
Pt 155	1404.498	229.132	1365.093	821.743	-0.0004
Pt 156	1703.961	1690.817	1656.145	2346.588	-0.0001
Pt 157	2756.095	348.109	2744.413	934.731	0.0000
Pt 158	538.171	1117.870	471.078	1758.750	0.0005
Pt 159	872.723	1474.811	808.339	2126.750	0.0007
Pt 160	1659.943	1698.357	1610.509	2355.045	0.0002
Pt 161	1600.594	508.941	1561.769	1112.880	0.0002
Pt 162	1372.065	232.854	1331.832	825.685	-0.0003
Pt 163	2990.262	236.626	2985.322	817.187	-0.0003
Pt 164	1746.244	595.544	1709.828	1202.877	0.0001
Pt 165	2872.246	1302.285	2851.140	1930.200	0.0002
Pt 166	1106.077	1827.876	1046.694	2493.224	-0.0006
Pt 167	2027.118	681.504	1995.967	1291.225	0.0000
Pt 168	1306.150	2283.465	1246.182	2962.631	-0.0007
Pt 169	2801.375	1099.683	2781.603	1720.880	-0.0001
Pt 170	863.917	1462.435	800.793	2115.351	0.0003
Pt 171	1228.329	2081.075	1168.888	2752.843	-0.0008
Pt 172	2521.135	1563.317	2490.308	2204.052	0.0001
Pt 173	2857.116	2074.780	2828.800	2728.529	0.0001
Pt 174	1638.230	1714.101	1588.261	2371.589	0.0002
Pt 175	1986.443	553.560	1956.205	1157.367	-0.0002
Pt 176	2924.293	132.840	2919.912	708.578	-0.0007
Pt 177	1986.167	984.494	1950.629	1608.311	0.0001
Pt 178	2716.268	1219.119	2692.886	1845.931	0.0001
Pt 179	1876.005	519.073	1843.443	1121.819	-0.0001
Pt 180	1282.917	2213.825	1222.330	2889.980	-0.0005
Pt 181	1110.054	2007.401	1048.823	2679.086	-0.0005
Pt 182	2989.250	1792.466	2966.227	2435.215	0.0002
Pt 183	3105.853	1794.349	3082.920	2436.100	0.0010
Pt 184	2178.329	251.851	2155.123	839.998	-0.0001
Pt 185	2920.302	2003.180	2892.515	2654.937	0.0005
Pt 186	2720.884	1228.947	2698.379	1853.232	0.0000
Pt 187	1994.564	531.380	1964.210	1133.474	0.0001
Pt 188	2819.596	1290.206	2797.783	1918.089	0.0001
Pt 189	2976.060	181.495	2972.077	760.460	-0.0008
Pt 190	2034.503	559.745	2004.684	1163.673	0.0000

ID	Image location of conjugate points in Image A		Image location of conjugate points in Image B		Residuals
	x (Pixels)	y (Pixels)	x (Pixels)	y (Pixels)	Signed Dist (Pixels)
Pt 191	2049.817	560.303	2020.159	1164.658	0.0001
Pt 192	2080.097	586.425	2053.175	1191.696	-0.0011
Pt 193	2948.653	190.643	2943.448	769.820	-0.0004
Pt 194	3518.047	470.510	3519.544	1056.953	0.0009
Pt 195	3055.517	192.484	3052.257	771.518	-0.0003
Pt 196	3017.753	1904.914	2995.157	2551.669	-0.0002
Pt 197	2110.036	605.645	2081.566	1211.254	-0.0001
Pt 198	2960.341	200.125	2955.653	779.995	-0.0007
Pt 199	2789.608	452.987	2777.987	1045.209	-0.0004
Pt 200	980.470	1813.927	918.648	2481.033	-0.0004
Pt 201	2120.672	623.626	2091.641	1229.609	0.0002
Pt 202	2732.360	1223.911	2708.762	1849.746	0.0004
Pt 203	2095.361	635.936	2066.237	1244.080	-0.0001
Pt 204	1403.736	224.624	1364.166	816.510	-0.0003
Pt 205	1189.473	1989.781	1128.301	2657.587	-0.0002
Pt 206	2863.587	422.238	2853.286	1012.559	-0.0001
Pt 207	3454.416	1676.430	3442.729	2311.088	0.0000
Pt 208	2589.252	2053.590	2555.255	2708.746	0.0002
Pt 209	1222.358	2062.731	1162.033	2732.788	-0.0005
Pt 210	3314.868	168.281	3315.659	744.023	0.0008
Pt 211	3037.601	1364.018	3019.968	1991.698	0.0000
Pt 212	2752.701	1188.006	2730.584	1813.585	0.0000
Pt 213	1371.601	232.903	1331.182	825.522	-0.0002
Pt 214	2867.515	408.496	2855.649	996.195	0.0011
Pt 215	2964.354	170.467	2960.181	749.324	-0.0008
Pt 216	2809.820	229.301	2800.227	811.318	0.0001
Pt 217	3577.813	1568.390	3570.243	2198.551	-0.0003
Pt 218	1462.473	241.957	1423.833	834.209	-0.0002
Pt 219	3132.899	1557.243	3115.650	2190.544	-0.0001
Pt 220	1229.445	2082.286	1169.017	2753.786	-0.0005
Pt 221	3203.639	1692.840	3185.498	2330.476	0.0003
Pt 222	2913.904	386.304	2906.342	976.256	-0.0010
Pt 223	2858.910	384.039	2848.614	972.042	0.0002
Pt 224	2708.127	254.657	2697.233	837.272	-0.0004
Pt 225	2867.800	2090.383	2839.414	2744.942	0.0001
Pt 226	2568.872	382.175	2553.579	972.146	-0.0005
Pt 227	3088.582	761.466	3078.978	1365.962	-0.0003
Pt 228	3254.681	1402.159	3241.741	2029.077	-0.0002
Pt 229	3116.899	771.629	3107.749	1375.816	-0.0002

ID	Image location of conjugate points in Image A		Image location of conjugate points in Image B		Residuals
	x (Pixels)	y (Pixels)	x (Pixels)	y (Pixels)	Signed Dist (Pixels)
Pt 230	3150.918	778.151	3142.220	1382.514	-0.0001
Pt 231	1729.397	787.614	1690.019	1404.519	0.0005
Pt 232	3405.289	1102.817	3397.598	1719.145	-0.0001
Pt 233	191.086	795.966	120.186	1426.435	0.0003
Pt 234	3434.271	1085.750	3427.510	1700.866	-0.0001
Pt 235	1709.684	794.928	1670.347	1412.017	0.0002
Pt 236	2729.700	268.965	2719.241	851.857	-0.0005
Pt 237	1666.032	161.406	1629.822	755.726	0.0017
Pt 238	1096.281	826.088	1044.118	1448.493	0.0000
Pt 239	3722.034	1955.812	3716.266	2598.501	-0.0011
Pt 240	2191.363	278.296	2168.118	867.234	0.0000
Pt 241	3366.422	1511.998	3354.387	2142.157	-0.0001
Pt 242	1384.097	285.488	1343.857	881.117	-0.0004
Pt 243	1888.243	1041.378	1849.399	1669.725	0.0005
Pt 244	2722.680	285.885	2712.614	868.763	-0.0008
Pt 245	1654.500	1714.473	1604.838	2371.654	0.0001
Pt 246	3487.982	1018.104	3483.289	1631.356	-0.0005
Pt 247	1644.665	862.988	1603.572	1482.883	0.0000
Pt 248	1991.844	1509.783	1951.608	2155.848	-0.0002
Pt 249	2832.304	2120.132	2802.552	2775.708	0.0002
Pt 250	3714.597	1833.339	3706.779	2471.712	-0.0001
Pt 251	3171.010	1466.290	3154.474	2097.238	0.0002
Pt 252	1639.605	1715.925	1590.473	2373.348	-0.0002
Pt 253	2829.682	340.207	2819.686	926.294	0.0000
Pt 254	1411.854	307.387	1371.615	903.239	-0.0002
Pt 255	1344.252	337.180	1302.239	935.505	-0.0002
Pt 256	2030.311	329.102	2005.680	925.944	-0.0016
Pt 257	3098.725	1487.529	3082.218	2119.080	-0.0004
Pt 258	2830.534	2136.301	2801.740	2792.145	-0.0001
Pt 259	2913.579	1938.683	2886.890	2587.707	0.0003
Pt 260	3152.397	1792.765	3132.425	2433.987	0.0003
Pt 261	1532.164	938.304	1487.361	1564.078	0.0004
Pt 262	1600.964	509.521	1561.824	1113.576	0.0004
Pt 263	1469.211	320.866	1429.986	916.607	-0.0002
Pt 264	2707.918	320.164	2695.740	905.512	-0.0001
Pt 265	2124.910	1303.649	2089.571	1939.715	-0.0002
Pt 266	1969.759	953.953	1933.465	1577.163	0.0005
Pt 267	2867.948	1948.359	2841.161	2597.839	0.0000
Pt 268	1647.308	498.376	1609.118	1102.029	0.0005

ID	Image location of conjugate points in Image A		Image location of conjugate points in Image B		Residuals
	x (Pixels)	y (Pixels)	x (Pixels)	y (Pixels)	Signed Dist (Pixels)
Pt 269	2004.247	554.636	1974.034	1158.956	-0.0001
Pt 270	707.883	1285.989	643.633	1934.053	0.0004
Pt 271	2204.719	114.354	2187.116	695.339	-0.0021
Pt 272	816.338	335.903	763.511	942.788	0.0000
Pt 273	871.827	1473.733	808.115	2125.821	0.0005
Pt 274	2749.767	336.204	2738.351	921.943	-0.0001
Pt 275	2952.732	1950.180	2927.965	2598.458	0.0000
Pt 276	2970.587	60.427	2966.505	634.583	0.0000
Pt 277	2059.233	602.893	2030.172	1208.548	-0.0003
Pt 278	1830.063	609.207	1795.338	1216.565	0.0001
Pt 279	3124.450	1457.339	3108.499	2087.327	-0.0003
Pt 280	2755.041	1241.557	2732.726	1869.239	-0.0002
Pt 281	2105.777	626.018	2076.199	1232.063	0.0003
Pt 282	1081.820	860.581	1027.779	1485.434	0.0007
Pt 283	2974.158	204.073	2969.458	783.682	-0.0005
Pt 284	2124.891	291.742	2100.512	882.254	-0.0003
Pt 285	2367.771	856.054	2341.214	1469.480	0.0003
Pt 286	2811.465	1021.963	2791.860	1641.228	0.0002
Pt 287	769.213	1348.883	703.319	1997.805	0.0012
Pt 288	2353.286	842.618	2326.281	1456.160	0.0004
Pt 289	464.077	1046.077	395.130	1685.040	0.0011
Pt 290	3470.521	1044.899	3464.386	1658.378	0.0001
Pt 291	1435.380	216.248	1396.451	807.580	-0.0002
Pt 292	2181.594	143.498	2156.964	732.543	0.0013
Pt 293	2593.379	1213.857	2567.624	1841.592	0.0001
Pt 294	457.539	1057.634	390.294	1696.295	0.0000
Pt 295	2586.843	1055.216	2563.558	1675.835	-0.0002
Pt 296	2774.899	1203.974	2753.292	1830.505	-0.0002
Pt 297	3607.615	1422.247	3601.521	2046.846	-0.0001
Pt 298	467.759	1068.152	400.370	1708.284	0.0003
Pt 299	3276.197	1355.685	3263.976	1980.040	0.0000
Pt 300	2785.467	1089.979	2765.571	1710.207	-0.0001
Pt 301	2027.475	681.695	1995.858	1291.719	0.0002
Pt 302	1799.118	262.548	1766.135	860.047	0.0008
Pt 303	2850.002	371.761	2839.971	959.534	0.0000
Pt 304	535.885	1114.995	470.229	1757.565	0.0002
Pt 305	923.990	1543.781	860.752	2197.616	0.0003
Pt 306	1499.104	764.720	1455.717	1381.913	0.0002
Pt 307	1105.981	1826.874	1047.151	2492.673	-0.0007

ID	Image location of conjugate points in Image A		Image location of conjugate points in Image B		Residuals
	x (Pixels)	y (Pixels)	x (Pixels)	y (Pixels)	Signed Dist (Pixels)
Pt 308	2193.961	256.078	2171.247	843.584	-0.0001
Pt 309	2570.689	397.035	2553.037	986.432	0.0008
Pt 310	2178.722	251.421	2155.853	839.620	-0.0002
Pt 311	2929.517	84.106	2925.687	658.720	-0.0007
Pt 312	2184.316	724.815	2156.399	1335.303	-0.0003
Pt 313	2893.020	390.996	2885.919	980.195	-0.0014
Pt 314	1660.572	1695.460	1611.401	2351.722	0.0001
Pt 315	3366.274	1460.782	3355.658	2088.714	-0.0004
Pt 316	2613.717	857.934	2591.003	1467.565	0.0011
Pt 317	1641.375	839.586	1599.557	1458.388	0.0005
Pt 318	3764.094	1816.636	3759.827	2454.008	-0.0009
Pt 319	3627.993	1765.780	3622.048	2401.965	-0.0011
Pt 320	1365.307	285.843	1323.312	880.642	0.0003
Pt 321	2737.655	1224.926	2714.254	1850.640	0.0004
Pt 322	2145.423	371.790	2120.581	965.480	-0.0003
Pt 323	3519.502	978.455	3514.061	1589.026	0.0006
Pt 324	1414.538	272.883	1375.035	866.669	-0.0005
Pt 325	2420.501	1102.729	2391.784	1726.731	0.0005
Pt 326	3154.954	1779.378	3134.869	2420.070	0.0004
Pt 327	2562.890	381.783	2547.740	970.740	-0.0006
Pt 328	1452.834	723.953	1407.845	1340.255	0.0007
Pt 329	3002.843	1918.511	2975.180	2563.613	0.0018
Pt 330	2921.480	2011.864	2894.044	2662.211	0.0005
Pt 331	1991.846	724.169	1959.128	1336.788	0.0002
Pt 332	1797.888	683.316	1761.555	1294.678	0.0002
Pt 333	2888.349	365.663	2877.631	952.351	0.0009
Pt 334	2162.860	365.094	2138.688	957.966	-0.0004
Pt 335	2125.015	367.253	2100.067	960.663	-0.0004
Pt 336	313.917	682.067	247.408	1309.076	0.0004
Pt 337	3470.655	1574.230	3461.250	2204.481	-0.0003
Pt 338	1411.457	731.735	1366.248	1348.250	0.0003
Pt 339	3058.330	1782.250	3035.890	2424.198	0.0005
Pt 340	1763.845	672.565	1726.762	1284.174	0.0003
Pt 341	1393.748	259.831	1354.010	853.470	-0.0005
Pt 342	1971.238	949.975	1934.444	1573.801	0.0007
Pt 343	3637.938	482.459	3641.698	1070.044	0.0006
Pt 344	1646.220	742.833	1605.988	1357.927	0.0002
Pt 345	3399.520	1119.775	3391.709	1736.086	-0.0001
Pt 346	2642.225	737.863	2623.404	1342.929	0.0001

ID	Image location of conjugate points in Image A		Image location of conjugate points in Image B		Residuals
	x (Pixels)	y (Pixels)	x (Pixels)	y (Pixels)	Signed Dist (Pixels)
Pt 347	2773.723	288.352	2762.571	872.202	0.0003
Pt 348	2189.529	254.944	2166.183	843.531	0.0001
Pt 349	1422.763	251.470	1383.427	845.727	-0.0002
Pt 350	1662.340	1740.711	1612.458	2398.356	0.0002
Pt 351	3397.381	1085.040	3389.674	1701.317	-0.0002
Pt 352	2910.263	1258.735	2892.079	1883.978	-0.0005
Pt 353	2797.164	2182.347	2766.638	2840.283	0.0001
Pt 354	3599.647	1491.784	3593.122	2118.409	-0.0001
Pt 355	1489.085	936.409	1443.657	1561.838	0.0003
Pt 356	2168.546	1126.060	2135.748	1753.686	-0.0001
Pt 357	1698.420	362.036	1663.578	957.194	-0.0001
Pt 358	2046.671	1491.313	2009.685	2135.707	-0.0010
Pt 359	2460.061	1260.730	2430.769	1891.284	0.0003
Pt 360	1646.734	1716.949	1597.654	2373.576	-0.0002
Pt 361	3133.875	1771.987	3113.949	2411.905	0.0003
Pt 362	2179.316	297.882	2156.140	887.472	-0.0003
Pt 363	2953.088	81.674	2949.687	656.067	-0.0007
Pt 364	3361.312	1478.330	3349.845	2106.583	-0.0001
Pt 365	3509.080	443.626	3510.479	1030.088	0.0008
Pt 366	2685.297	296.952	2672.935	881.170	-0.0001
Pt 367	528.829	1131.030	460.340	1769.949	0.0006
Pt 368	3308.589	758.382	3303.070	1359.895	0.0001
Pt 369	2770.734	233.861	2765.193	816.918	-0.0028
Pt 370	2637.391	1274.051	2611.828	1903.542	0.0001
Pt 371	1385.584	356.247	1344.183	954.434	-0.0002
Pt 372	2419.586	633.367	2398.419	1236.087	-0.0006
Pt 373	2832.325	232.955	2822.948	814.995	0.0003
Pt 374	2641.887	1201.369	2617.950	1827.474	-0.0002
Pt 375	1831.427	631.056	1796.464	1240.087	0.0001
Pt 376	2517.666	232.054	2500.938	822.228	0.0001
Pt 377	1752.345	303.251	1717.454	901.879	0.0011
Pt 378	3134.675	1790.279	3112.979	2433.427	0.0005
Pt 379	3599.961	1439.441	3594.174	2063.114	0.0000
Pt 380	3403.678	1077.394	3395.255	1693.434	0.0002
Pt 381	2792.515	1073.657	2772.704	1693.635	0.0000
Pt 382	2459.040	619.811	2437.526	1221.602	0.0001
Pt 383	3224.146	1429.921	3209.885	2057.964	0.0000
Pt 384	3539.232	396.717	3542.470	980.841	0.0004
Pt 385	1475.997	894.564	1430.209	1519.177	0.0006

ID	Image location of conjugate points in Image A		Image location of conjugate points in Image B		Residuals
	x (Pixels)	y (Pixels)	x (Pixels)	y (Pixels)	Signed Dist (Pixels)
Pt 386	2135.369	612.810	2106.607	1218.931	0.0003
Pt 387	2096.613	614.611	2067.801	1220.506	-0.0001
Pt 388	1380.265	216.498	1340.291	808.764	-0.0003
Pt 389	3741.730	1816.507	3737.685	2454.241	-0.0012
Pt 390	2614.112	1298.747	2588.227	1928.759	0.0000
Pt 391	3223.315	1951.521	3204.511	2597.235	0.0000
Pt 392	1642.744	786.062	1600.540	1403.883	0.0010
Pt 393	1809.895	608.090	1775.363	1216.381	-0.0002
Pt 394	3126.651	2149.287	3104.065	2803.528	-0.0002
Pt 395	2972.508	211.814	2967.645	791.509	-0.0004
Pt 396	3374.026	1141.506	3365.693	1756.940	0.0002
Pt 397	1553.912	796.630	1511.776	1414.681	-0.0001
Pt 398	2797.794	436.777	2786.229	1028.170	-0.0003
Pt 399	2076.916	603.263	2047.867	1209.453	-0.0002
Pt 400	2858.124	405.469	2849.120	994.630	-0.0007
Pt 401	2185.702	142.518	2163.493	732.335	-0.0001
Pt 402	2116.479	316.067	2092.307	907.675	-0.0007
Pt 403	2161.721	314.100	2137.902	904.703	-0.0003
Pt 404	3359.919	1307.730	3347.958	1929.175	0.0009
Pt 405	1338.990	408.045	1296.606	1008.736	-0.0005
Pt 406	2573.714	808.343	2549.399	1416.277	0.0018
Pt 407	3596.869	1687.482	3590.689	2321.604	-0.0011
Pt 408	1535.915	812.565	1492.805	1431.569	0.0002
Pt 409	2754.232	1155.600	2732.932	1780.263	-0.0002
Pt 410	1332.985	321.779	1290.855	918.455	-0.0003
Pt 411	1940.722	982.207	1902.987	1605.788	0.0008
Pt 412	1352.775	318.224	1311.641	914.856	-0.0005
Pt 413	2902.031	155.556	2896.192	733.251	-0.0003
Pt 414	1373.517	321.925	1333.402	919.169	-0.0008
Pt 415	2137.955	193.950	2117.414	785.149	-0.0019
Pt 416	3040.440	1367.707	3023.174	1995.245	-0.0001
Pt 417	3682.160	429.971	3687.580	1015.503	0.0004
Pt 418	2078.589	860.593	2047.484	1479.253	-0.0005
Pt 419	1044.177	575.907	993.404	1188.321	-0.0001
Pt 420	2515.947	822.841	2493.052	1433.973	0.0002
Pt 421	3153.667	825.393	3143.345	1431.588	0.0004
Pt 422	1625.686	851.052	1584.025	1470.020	0.0001
Pt 423	2770.021	1169.156	2749.005	1793.154	-0.0002
Pt 424	3134.779	830.491	3124.621	1437.388	0.0001

ID	Image location of conjugate points in Image A		Image location of conjugate points in Image B		Residuals
	x (Pixels)	y (Pixels)	x (Pixels)	y (Pixels)	Signed Dist (Pixels)
Pt 425	1386.103	334.835	1345.979	932.956	-0.0007
Pt 426	2868.555	170.901	2861.381	749.433	-0.0001
Pt 427	3623.369	1337.649	3618.163	1957.886	0.0003
Pt 428	2883.780	423.949	2873.880	1013.922	-0.0001
Pt 429	2086.206	841.637	2055.791	1455.810	-0.0006
Pt 430	2890.068	175.751	2884.078	754.159	-0.0005
Pt 431	1404.430	324.042	1364.355	920.756	-0.0005
Pt 432	2441.830	1037.119	2413.987	1658.240	0.0006
Pt 433	2572.428	1221.541	2547.061	1850.897	-0.0004
Pt 434	2980.466	1936.076	2955.874	2585.251	0.0000
Pt 435	2595.367	780.381	2574.706	1388.525	0.0002
Pt 436	2258.474	788.738	2231.333	1399.718	-0.0001
Pt 437	1756.699	781.368	1718.612	1396.435	0.0001
Pt 438	1553.752	796.774	1512.253	1416.399	-0.0003
Pt 439	1656.896	800.342	1615.440	1418.881	0.0007
Pt 440	3137.176	776.946	3128.563	1380.778	-0.0002
Pt 441	1500.174	775.027	1456.614	1391.877	0.0002
Pt 442	2294.532	791.354	2266.240	1402.773	0.0008
Pt 443	2898.907	1922.313	2875.327	2568.435	-0.0005
Pt 444	3023.371	1333.841	3005.722	1960.725	0.0000
Pt 445	2201.520	1100.727	2169.684	1727.486	-0.0002
Pt 446	3304.847	760.825	3298.396	1360.757	0.0009
Pt 447	3080.629	796.554	3070.985	1403.260	-0.0007
Pt 448	3358.120	1309.077	3347.564	1929.728	0.0005
Pt 449	1625.261	756.182	1585.005	1372.093	0.0000
Pt 450	452.129	806.844	385.091	1438.313	0.0015
Pt 451	2074.947	751.456	2042.962	1362.773	0.0005
Pt 452	1749.661	752.955	1709.757	1368.103	0.0011
Pt 453	1471.909	744.292	1428.321	1359.018	0.0000
Pt 454	1722.698	809.643	1683.571	1426.955	0.0001
Pt 455	3116.018	812.294	3104.999	1419.170	0.0003
Pt 456	3172.847	808.293	3163.701	1413.776	0.0001
Pt 457	1647.731	741.422	1607.401	1356.168	0.0003
Pt 458	1433.396	739.334	1388.917	1355.391	0.0001
Pt 459	2542.144	727.647	2520.794	1334.333	0.0002
Pt 460	2792.824	1896.579	2764.727	2545.052	0.0001
Pt 461	3424.677	1087.601	3417.709	1702.721	-0.0001
Pt 462	1452.732	720.974	1408.117	1336.824	0.0005
Pt 463	1409.766	729.985	1366.163	1344.548	-0.0006

ID	Image location of conjugate points in Image A		Image location of conjugate points in Image B		Residuals
	x (Pixels)	y (Pixels)	x (Pixels)	y (Pixels)	Signed Dist (Pixels)
Pt 464	3041.133	1372.167	3024.137	1999.378	-0.0002
Pt 465	3623.641	1301.826	3619.577	1920.675	0.0000
Pt 466	3030.607	1886.978	3007.458	2532.175	0.0003
Pt 467	2191.781	1124.842	2159.295	1752.231	-0.0001
Pt 468	2952.255	82.853	2948.792	657.961	-0.0007
Pt 469	3165.539	1388.412	3149.663	2016.254	0.0002
Pt 470	2306.765	705.263	2280.448	1313.078	0.0004
Pt 471	2985.257	1872.885	2961.172	2517.768	0.0003
Pt 472	3022.393	1392.785	3004.712	2020.587	-0.0001
Pt 473	1586.324	836.609	1544.005	1455.849	0.0002
Pt 474	1066.284	1977.654	1003.472	2647.773	-0.0003
Pt 475	1799.709	682.119	1763.567	1293.637	0.0001
Pt 476	2556.906	2249.235	2520.693	2913.296	-0.0001
Pt 477	2538.919	826.713	2515.920	1438.130	0.0004
Pt 478	3133.766	834.338	3123.743	1441.034	0.0000
Pt 479	2168.067	671.856	2135.900	1276.951	0.0022
Pt 480	2016.053	674.064	1984.482	1283.811	0.0001
Pt 481	2952.943	1968.479	2925.409	2617.368	0.0009
Pt 482	1758.994	672.055	1722.956	1282.784	-0.0003
Pt 483	2796.397	1072.902	2776.602	1693.046	0.0000
Pt 484	2657.096	1289.555	2631.206	1918.745	0.0004
Pt 485	499.708	847.669	433.120	1478.309	0.0012
Pt 486	2045.887	669.008	2013.139	1276.369	0.0011
Pt 487	1009.922	1861.000	947.358	2529.184	-0.0001
Pt 488	1005.116	1981.426	940.500	2653.347	0.0001
Pt 489	1662.076	844.031	1621.573	1464.228	0.0000
Pt 490	3179.503	1422.179	3164.721	2051.894	-0.0004
Pt 491	3228.523	1425.683	3213.107	2054.826	0.0003
Pt 492	1123.772	663.511	1072.920	1279.196	0.0004
Pt 493	2950.985	1851.085	2928.097	2493.863	-0.0001
Pt 494	2928.899	118.319	2924.425	694.414	-0.0006
Pt 495	3613.152	1059.013	3611.129	1671.950	-0.0006
Pt 496	3581.294	1061.220	3578.501	1673.628	-0.0004
Pt 497	2445.137	638.186	2423.399	1241.207	-0.0001
Pt 498	3424.324	1056.133	3416.238	1670.946	0.0004
Pt 499	2804.269	1129.069	2782.018	1745.628	0.0016
Pt 500	1623.312	854.951	1582.317	1474.845	-0.0002
Pt 501	3772.474	1835.279	3768.754	2473.279	-0.0011
Pt 502	2489.299	633.560	2468.469	1236.627	-0.0001

ID	Image location of conjugate points in Image A		Image location of conjugate points in Image B		Residuals
	x (Pixels)	y (Pixels)	x (Pixels)	y (Pixels)	Signed Dist (Pixels)
Pt 503	2781.142	2213.442	2751.101	2871.748	-0.0002
Pt 504	2889.982	1837.317	2864.278	2482.337	0.0002
Pt 505	3595.813	1443.186	3589.932	2065.122	0.0004
Pt 506	2379.779	859.589	2352.428	1472.734	0.0008
Pt 507	2459.229	619.422	2437.378	1220.608	0.0003
Pt 508	1511.354	620.685	1467.684	1232.338	0.0012
Pt 509	3150.057	1458.047	3135.340	2087.964	-0.0006
Pt 510	1831.655	601.233	1796.772	1208.409	0.0002
Pt 511	1862.832	1466.568	1820.493	2111.535	-0.0002
Pt 512	1026.694	164.177	979.794	760.560	-0.0001
Pt 513	1076.015	2000.059	1014.665	2671.649	-0.0007
Pt 514	2035.232	597.432	2006.335	1203.646	-0.0007
Pt 515	1540.010	594.431	1497.491	1203.973	0.0011
Pt 516	1642.887	872.211	1600.936	1493.120	0.0004
Pt 517	2984.704	158.846	2980.057	737.629	-0.0002
Pt 518	992.287	1828.891	929.859	2496.072	-0.0002
Pt 519	3480.118	165.188	3483.763	740.942	0.0009
Pt 520	2053.211	579.022	2023.784	1184.265	-0.0001
Pt 521	2356.016	872.946	2328.650	1485.916	0.0006
Pt 522	1043.472	574.104	992.719	1187.747	0.0001
Pt 523	2947.004	1991.040	2919.878	2639.855	0.0008
Pt 524	2031.390	567.620	2000.867	1171.525	0.0003
Pt 525	2894.720	171.768	2887.788	752.032	-0.0001
Pt 526	3599.598	1492.678	3592.444	2120.040	0.0000
Pt 527	3176.181	2171.772	3153.008	2827.521	0.0001
Pt 528	1511.070	883.250	1467.155	1506.202	0.0000
Pt 529	3347.978	1503.873	3335.391	2134.420	-0.0001
Pt 530	2057.656	881.345	2025.564	1499.833	-0.0003
Pt 531	1902.387	1516.967	1860.123	2164.108	-0.0001
Pt 532	1965.380	1514.906	1924.820	2162.359	-0.0003
Pt 533	2495.211	875.325	2470.906	1487.775	0.0004
Pt 534	2590.080	2158.515	2555.411	2816.418	0.0001
Pt 535	3638.302	1791.478	3631.820	2428.634	-0.0009
Pt 536	2850.388	195.194	2842.467	774.834	0.0000
Pt 537	1919.254	1542.124	1878.384	2190.332	-0.0006
Pt 538	2545.285	1536.878	2516.016	2177.410	-0.0003
Pt 539	3117.399	1543.827	3100.282	2176.186	-0.0001
Pt 540	3613.155	1779.626	3604.977	2417.761	-0.0007
Pt 541	2980.374	209.973	2973.007	791.621	0.0009

ID	Image location of conjugate points in Image A		Image location of conjugate points in Image B		Residuals
	x (Pixels)	y (Pixels)	x (Pixels)	y (Pixels)	Signed Dist (Pixels)
Pt 542	1949.361	1567.828	1908.802	2216.578	-0.0006
Pt 543	2835.689	1240.178	2815.576	1867.179	-0.0004
Pt 544	2793.123	1244.097	2772.764	1872.187	-0.0008
Pt 545	3443.933	1019.149	3438.901	1630.523	-0.0003
Pt 546	3531.870	485.508	3532.981	1074.332	0.0007
Pt 547	3480.136	1765.724	3469.968	2403.426	-0.0007
Pt 548	3131.492	1769.769	3111.156	2409.739	0.0005
Pt 549	1325.728	477.295	1282.733	1082.937	-0.0005
Pt 550	3644.613	1754.355	3638.037	2391.786	-0.0011
Pt 551	683.942	1020.901	619.641	1661.193	0.0017
Pt 552	1954.412	463.012	1923.186	1062.245	0.0005
Pt 553	2705.831	226.293	2693.311	807.857	0.0007
Pt 554	2775.428	229.001	2765.144	811.691	0.0001
Pt 555	2839.987	231.868	2834.388	811.820	-0.0016
Pt 556	2739.911	1224.700	2717.912	1850.024	-0.0002
Pt 557	3702.552	452.423	3707.453	1037.525	0.0011
Pt 558	435.539	1180.455	366.804	1826.958	0.0005
Pt 559	1056.672	923.438	1003.394	1551.943	-0.0002
Pt 560	3655.194	434.653	3660.099	1019.846	0.0005
Pt 561	3506.754	1006.403	3501.222	1618.129	0.0003
Pt 562	2733.347	240.462	2722.418	823.062	-0.0001
Pt 563	1803.460	1620.941	1759.033	2273.504	-0.0004
Pt 564	3059.506	2097.470	3036.227	2749.426	-0.0001
Pt 565	2452.866	1742.606	2420.188	2391.176	-0.0005
Pt 566	3538.838	396.889	3542.191	980.594	0.0005
Pt 567	1394.268	259.076	1353.929	852.432	-0.0002
Pt 568	1423.400	251.407	1383.870	844.150	-0.0002
Pt 569	2978.478	403.524	2970.464	990.950	0.0003
Pt 570	2899.915	403.859	2888.435	991.634	0.0013
Pt 571	2850.593	405.438	2843.438	995.354	-0.0019
Pt 572	2757.614	1215.449	2736.439	1842.821	-0.0006
Pt 573	2583.040	1179.744	2558.414	1804.882	-0.0002
Pt 574	2449.456	2027.690	2411.829	2684.256	0.0004
Pt 575	2868.856	382.819	2859.099	970.757	0.0000
Pt 576	1134.289	1212.224	1078.300	1852.922	0.0006
Pt 577	3362.567	379.402	3362.829	963.757	0.0002
Pt 578	1667.041	268.940	1631.630	862.913	0.0005
Pt 579	2795.253	377.801	2783.776	965.392	0.0002
Pt 580	2144.347	378.758	2120.014	970.726	-0.0005

ID	Image location of conjugate points in Image A		Image location of conjugate points in Image B		Residuals
	x (Pixels)	y (Pixels)	x (Pixels)	y (Pixels)	Signed Dist (Pixels)
Pt 581	1615.039	381.778	1577.718	981.235	0.0003
Pt 582	1957.081	1001.911	1920.392	1625.798	0.0003
Pt 583	3661.016	1176.432	3656.572	1791.419	0.0008
Pt 584	2735.573	1203.788	2713.796	1830.217	-0.0004
Pt 585	3562.310	1660.438	3555.442	2294.379	-0.0011
Pt 586	1383.775	276.544	1344.129	871.469	-0.0007
Pt 587	1567.589	281.081	1530.826	875.588	-0.0001
Pt 588	2155.234	284.872	2130.290	875.755	0.0004
Pt 589	1398.939	2042.551	1340.481	2713.356	0.0003
Pt 590	2801.565	335.151	2791.423	920.527	-0.0002
Pt 591	2775.621	291.601	2764.458	876.240	0.0002
Pt 592	1806.902	329.191	1774.899	924.724	-0.0001
Pt 593	1408.827	327.086	1367.985	923.626	-0.0001
Pt 594	3187.209	1687.515	3168.702	2324.592	0.0005
Pt 595	1405.251	301.387	1365.045	897.652	-0.0003
Pt 596	2137.060	307.289	2112.574	898.767	-0.0002
Pt 597	1977.550	983.498	1941.824	1607.753	0.0001
Pt 598	2684.377	298.571	2672.421	882.416	-0.0003
Pt 599	1939.980	983.939	1904.642	1604.638	-0.0004
Pt 600	2115.782	320.220	2091.107	911.680	-0.0004
Pt 601	3637.578	1194.731	3633.284	1809.457	0.0007
Pt 602	1734.461	319.053	1702.474	914.863	-0.0009
Pt 603	1632.474	311.218	1596.016	906.307	0.0004
Pt 604	3232.852	1352.141	3221.760	1976.771	-0.0009
Pt 605	1606.629	700.363	1566.259	1314.426	0.0001
Pt 606	3307.669	1856.296	3290.171	2497.496	0.0005
Pt 607	3625.253	1847.663	3617.684	2487.623	-0.0010
Pt 608	3037.844	1384.649	3022.978	2011.982	-0.0011
Pt 609	2617.096	1119.348	2593.348	1742.363	-0.0001
Pt 610	3388.534	1123.402	3380.466	1739.170	0.0001
Pt 611	2694.394	1606.291	2666.932	2246.463	0.0001
Pt 612	2097.502	622.934	2067.695	1228.970	0.0004
Pt 613	1386.956	632.331	1341.776	1244.461	0.0005
Pt 614	2206.718	1128.714	2173.297	1756.346	0.0005
Pt 615	1879.308	618.354	1844.398	1226.343	0.0007
Pt 616	1053.661	607.171	1001.798	1220.405	0.0004
Pt 617	2797.625	1887.364	2768.780	2535.608	0.0004
Pt 618	1157.670	2189.364	1093.067	2868.103	0.0004
Pt 619	1550.878	595.727	1507.773	1206.034	0.0015

ID	Image location of conjugate points in Image A		Image location of conjugate points in Image B		Residuals
	x (Pixels)	y (Pixels)	x (Pixels)	y (Pixels)	Signed Dist (Pixels)
Pt 620	2453.579	726.517	2431.264	1332.894	-0.0001
Pt 621	2035.656	574.875	2005.436	1178.110	0.0002
Pt 622	1590.998	582.660	1550.708	1190.413	0.0005
Pt 623	2450.773	927.847	2423.210	1543.341	0.0013
Pt 624	2993.729	1903.862	2969.519	2550.503	0.0002
Pt 625	2318.769	930.999	2291.571	1548.065	-0.0003
Pt 626	3007.019	1365.789	2987.647	1994.279	0.0004
Pt 627	3621.106	1431.149	3615.896	2054.554	-0.0001
Pt 628	1919.788	572.992	1887.377	1179.402	0.0001
Pt 629	1306.445	1817.514	1249.415	2481.124	0.0000
Pt 630	1539.307	922.273	1494.231	1547.320	0.0007
Pt 631	2199.654	2153.105	2156.721	2819.825	-0.0001
Pt 632	3203.569	1347.824	3188.615	1974.885	0.0002
Pt 633	3224.268	920.501	3212.943	1531.174	0.0009
Pt 634	2612.570	1168.289	2589.626	1794.315	-0.0008
Pt 635	1056.679	517.631	1007.836	1127.942	-0.0006
Pt 636	2932.077	163.061	2929.041	740.648	-0.0016
Pt 637	1434.614	2136.592	1377.618	2811.972	-0.0002
Pt 638	1530.262	761.856	1487.677	1380.225	0.0002
Pt 639	2832.094	2124.618	2802.730	2780.747	0.0000
Pt 640	2702.731	2125.796	2669.905	2781.089	0.0005
Pt 641	3450.829	1065.611	3444.764	1678.912	0.0000
Pt 642	2723.626	2255.156	2689.208	2919.362	0.0003
Pt 643	2819.402	185.212	2811.358	764.946	-0.0003
Pt 644	2920.304	181.985	2914.320	759.732	-0.0001
Pt 645	3637.455	471.502	3641.544	1058.475	0.0005
Pt 646	2472.614	1062.162	2447.016	1682.737	-0.0002
Pt 647	3508.171	457.070	3511.154	1044.127	-0.0002
Pt 648	1577.031	776.079	1536.358	1395.336	-0.0004
Pt 649	3597.007	1325.174	3591.772	1944.741	0.0002
Pt 650	3385.239	1321.604	3376.063	1940.872	0.0004
Pt 651	2550.565	777.985	2529.428	1387.016	-0.0001
Pt 652	3152.131	1788.958	3132.212	2428.849	0.0005
Pt 653	3652.247	1317.000	3646.502	1936.834	0.0007
Pt 654	3390.490	1306.217	3380.178	1927.061	0.0006
Pt 655	2989.716	209.538	2984.816	789.257	-0.0002
Pt 656	3645.795	1051.657	3643.755	1663.477	-0.0001
Pt 657	1664.812	783.875	1626.837	1397.381	-0.0010
Pt 658	1936.808	1665.715	1894.671	2319.083	-0.0005

ID	Image location of conjugate points in Image A		Image location of conjugate points in Image B		Residuals
	x (Pixels)	y (Pixels)	x (Pixels)	y (Pixels)	Signed Dist (Pixels)
Pt 659	2774.701	218.747	2765.737	800.820	-0.0006
Pt 660	1512.321	796.514	1469.231	1415.865	0.0000
Pt 661	2251.629	793.842	2224.476	1405.403	-0.0003
Pt 662	1088.239	236.456	1041.634	835.835	0.0001
Pt 663	2699.838	1211.485	2676.315	1836.327	0.0003
Pt 664	2725.428	234.037	2716.346	817.169	-0.0013
Pt 665	1396.050	243.624	1356.009	836.399	-0.0002
Pt 666	2895.828	1231.357	2877.506	1856.604	-0.0005
Pt 667	2003.863	384.925	1976.027	985.285	-0.0004
Pt 668	3774.588	2065.090	3765.879	2713.590	-0.0006
Pt 669	1382.492	371.286	1339.606	970.306	0.0005
Pt 670	3474.306	1025.945	3472.481	1632.107	-0.0005
Pt 671	1572.632	825.135	1530.999	1445.798	-0.0002
Pt 672	1617.480	821.053	1576.090	1440.668	0.0001
Pt 673	1687.243	818.300	1647.102	1436.332	0.0002
Pt 674	1954.951	1013.178	1916.793	1638.069	0.0009
Pt 675	2909.680	368.573	2900.082	956.790	0.0003
Pt 676	1733.620	814.711	1694.271	1432.163	0.0003
Pt 677	2678.723	265.083	2667.104	848.478	-0.0004
Pt 678	2804.929	268.847	2794.636	850.371	0.0005
Pt 679	2649.515	1291.841	2625.521	1921.363	-0.0005
Pt 680	2712.088	1245.640	2689.094	1872.431	-0.0001
Pt 681	2875.883	1244.240	2856.084	1869.810	-0.0001
Pt 682	883.308	281.845	832.829	884.975	-0.0004
Pt 683	2983.800	335.976	2976.399	924.391	-0.0001
Pt 684	3539.019	1769.109	3529.576	2405.876	-0.0004
Pt 685	1405.449	289.035	1364.944	884.876	0.0000
Pt 686	2264.447	290.592	2244.033	877.825	-0.0007
Pt 687	2650.584	329.140	2635.320	917.180	0.0007
Pt 688	3119.991	1763.428	3098.323	2404.406	0.0007
Pt 689	2952.301	1771.797	2928.511	2414.567	0.0002
Pt 690	1894.271	1518.481	1852.018	2167.014	-0.0002
Pt 691	1724.807	318.909	1689.940	915.632	0.0006
Pt 692	2212.640	301.811	2187.062	895.002	0.0013
Pt 693	2726.096	303.261	2714.589	887.333	-0.0001
Pt 694	3187.753	844.016	3177.571	1450.826	0.0006
Pt 695	3394.800	1266.107	3384.619	1886.079	0.0006
Pt 696	2454.752	840.813	2430.530	1453.421	0.0001
Pt 697	940.191	300.136	891.038	903.305	-0.0006

ID	Image location of conjugate points in Image A		Image location of conjugate points in Image B		Residuals
	x (Pixels)	y (Pixels)	x (Pixels)	y (Pixels)	Signed Dist (Pixels)
Pt 698	2553.352	1279.865	2527.622	1910.383	-0.0006
Pt 699	2469.526	659.571	2448.530	1263.080	-0.0003
Pt 700	2266.097	1115.780	2236.483	1742.195	-0.0006
Pt 701	1097.277	2205.475	1031.108	2887.176	0.0006
Pt 702	2489.799	624.359	2468.826	1225.438	0.0002
Pt 703	3638.428	936.191	3638.631	1538.711	0.0004
Pt 704	2571.954	1129.467	2548.045	1753.167	-0.0004
Pt 705	3261.228	1711.089	3244.224	2348.105	0.0004
Pt 706	246.393	600.425	180.736	1223.511	-0.0007
Pt 707	3656.746	1241.371	3653.752	1859.065	-0.0002
Pt 708	2929.596	1883.339	2904.648	2528.616	0.0002
Pt 709	3362.848	1244.731	3353.516	1863.692	0.0001
Pt 710	2428.195	1287.758	2399.227	1919.738	-0.0003
Pt 711	2807.906	1292.405	2785.976	1919.216	0.0002
Pt 712	1661.513	1776.143	1613.345	2434.235	-0.0006
Pt 713	2790.109	369.773	2779.829	957.440	-0.0005
Pt 714	2787.115	2008.965	2756.790	2661.196	0.0005
Pt 715	1393.379	579.847	1349.855	1189.161	0.0000
Pt 716	2832.993	1900.810	2806.129	2546.454	0.0002
Pt 717	1474.556	374.238	1435.313	971.489	-0.0004
Pt 718	3634.220	1904.190	3624.760	2546.806	-0.0005
Pt 719	1424.050	383.792	1382.438	983.333	0.0003
Pt 720	3782.847	977.499	3783.884	1582.944	0.0007
Pt 721	1600.215	244.611	1563.899	835.789	0.0002
Pt 722	2427.144	1495.314	2395.767	2135.421	-0.0002
Pt 723	1805.385	1345.562	1762.850	1985.820	0.0000
Pt 724	1373.775	404.555	1331.811	1005.075	-0.0003
Pt 725	2863.987	156.491	2856.766	736.813	-0.0003
Pt 726	2888.362	156.757	2881.952	736.221	-0.0004
Pt 727	1018.816	503.297	969.227	1116.045	-0.0003
Pt 728	1446.654	179.638	1407.835	769.039	0.0001
Pt 729	2603.266	1005.709	2580.299	1624.818	0.0000
Pt 730	2179.825	2132.464	2136.841	2800.392	-0.0002
Pt 731	3691.129	458.830	3695.840	1044.259	0.0010
Pt 732	2117.715	769.208	2088.409	1379.496	-0.0004
Pt 733	2426.836	992.571	2400.212	1611.638	0.0002
Pt 734	492.061	233.025	433.507	836.303	-0.0004
Pt 735	1539.928	876.498	1496.375	1498.911	0.0001
Pt 736	2770.478	1563.931	2744.682	2201.468	0.0002

ID	Image location of conjugate points in Image A		Image location of conjugate points in Image B		Residuals
	x (Pixels)	y (Pixels)	x (Pixels)	y (Pixels)	Signed Dist (Pixels)
Pt 737	1115.062	2105.971	1050.993	2781.522	0.0001
Pt 738	2160.729	2098.303	2117.329	2764.032	-0.0001
Pt 739	3159.019	1704.561	3139.746	2343.106	0.0004
Pt 740	1538.561	267.240	1501.104	860.475	0.0000
Pt 741	2199.690	344.140	2176.218	935.505	-0.0002
Pt 742	3187.788	1532.592	3171.462	2164.343	0.0002
Pt 743	2287.523	1154.685	2256.181	1782.181	0.0002
Pt 744	2875.177	135.657	2868.114	714.847	-0.0001
Pt 745	1552.340	538.905	1512.106	1144.042	0.0002
Pt 746	2758.560	452.298	2746.215	1044.371	-0.0004
Pt 747	1648.410	1732.405	1599.621	2390.057	-0.0003
Pt 748	2724.309	1827.159	2697.104	2473.333	-0.0005
Pt 749	1801.779	715.226	1765.421	1327.549	0.0001
Pt 750	1923.974	485.653	1891.597	1087.464	0.0006
Pt 751	1003.117	1005.729	948.350	1636.988	-0.0005
Pt 752	2638.259	237.221	2625.996	819.432	-0.0004
Pt 753	2783.300	1398.214	2759.760	2029.806	0.0001
Pt 754	3370.439	239.858	3372.096	818.299	0.0005
Pt 755	3065.872	1354.515	3049.240	1981.566	-0.0001
Pt 756	2341.263	957.296	2312.650	1575.622	0.0005
Pt 757	2143.792	714.638	2112.555	1321.101	0.0012
Pt 758	2738.378	1241.515	2715.998	1866.898	0.0000
Pt 759	3160.111	1672.735	3140.575	2310.685	0.0005
Pt 760	2615.631	266.350	2602.894	849.718	-0.0005
Pt 761	3162.707	872.907	3151.962	1478.789	0.0008
Pt 762	2544.466	647.358	2525.458	1249.203	-0.0004
Pt 763	1704.135	761.498	1665.202	1376.949	0.0001
Pt 764	1890.260	619.369	1855.359	1226.636	0.0008
Pt 765	2494.004	1730.239	2461.286	2377.387	0.0000
Pt 766	2915.980	1735.739	2892.579	2376.667	0.0000
Pt 767	3038.751	1747.605	3015.747	2388.712	0.0007
Pt 768	3424.090	1650.911	3413.013	2282.925	0.0000
Pt 769	3168.202	1623.496	3150.630	2259.323	0.0000
Pt 770	3114.054	1757.406	3095.393	2396.485	-0.0002
Pt 771	2692.867	1588.455	2665.689	2231.570	-0.0004
Pt 772	2790.895	1774.330	2764.714	2415.839	0.0001
Pt 773	3397.168	1578.376	3385.068	2209.563	0.0001
Pt 774	3147.760	1790.033	3129.958	2431.172	-0.0005
Pt 775	3590.799	1775.560	3583.917	2413.140	-0.0012

ID	Image location of conjugate points in Image A		Image location of conjugate points in Image B		Residuals
	x (Pixels)	y (Pixels)	x (Pixels)	y (Pixels)	Signed Dist (Pixels)
Pt 776	3733.306	1774.464	3726.480	2409.858	0.0001
Pt 777	3504.679	1801.285	3495.262	2440.668	-0.0011
Pt 778	1736.249	1833.744	1687.823	2491.887	-0.0003
Pt 779	2004.854	1523.193	1964.944	2169.894	-0.0003
Pt 780	1887.610	1516.491	1846.709	2164.350	-0.0008
Pt 781	3153.801	1487.596	3137.935	2115.949	0.0002
Pt 782	3307.313	1858.159	3290.465	2498.233	0.0005
Pt 783	2862.432	142.138	2853.462	724.163	0.0005
Pt 784	3619.278	1427.120	3613.232	2051.284	0.0001
Pt 785	2998.281	1901.065	2972.044	2547.997	0.0009
Pt 786	3216.134	1908.245	3198.204	2552.438	-0.0002
Pt 787	3655.507	1400.193	3650.280	2024.445	-0.0001
Pt 788	3039.349	1391.307	3022.832	2018.733	-0.0004
Pt 789	3274.029	1893.045	3256.468	2535.896	0.0002
Pt 790	3623.667	1366.472	3620.422	1987.460	-0.0006
Pt 791	3247.903	1356.054	3238.084	1977.563	-0.0008
Pt 792	1645.758	203.313	1607.143	795.633	0.0025
Pt 793	3589.211	1330.573	3584.677	1947.564	0.0004
Pt 794	2848.497	1320.159	2830.074	1950.557	-0.0015
Pt 795	3662.023	1312.453	3656.262	1934.759	0.0002
Pt 796	490.514	222.134	435.106	826.557	-0.0019
Pt 797	3624.108	1282.507	3617.882	1904.332	0.0002
Pt 798	1090.880	226.145	1043.862	825.632	0.0005
Pt 799	2893.808	1985.171	2868.588	2634.695	-0.0003
Pt 800	2240.047	1281.471	2206.434	1915.160	0.0001
Pt 801	2101.891	2001.821	2058.091	2663.365	0.0001
Pt 802	915.358	247.642	866.345	850.173	-0.0005
Pt 803	1397.213	245.792	1357.735	838.700	-0.0005
Pt 804	2846.188	2026.603	2817.097	2682.820	-0.0001
Pt 805	3471.964	1209.718	3464.383	1826.414	0.0005
Pt 806	2582.740	1188.442	2557.768	1814.921	-0.0002
Pt 807	2754.490	264.506	2743.514	847.442	0.0001
Pt 808	2513.800	1183.137	2487.178	1808.497	0.0001
Pt 809	2320.305	1183.872	2289.398	1811.642	0.0002
Pt 810	2141.632	291.747	2117.296	882.598	-0.0001
Pt 811	2265.730	294.653	2247.099	882.734	-0.0018
Pt 812	2656.612	1162.160	2632.775	1786.105	0.0002
Pt 813	1058.221	2097.691	995.326	2774.106	-0.0005
Pt 814	2153.804	2098.721	2113.127	2766.478	-0.0011

ID	Image location of conjugate points in Image A		Image location of conjugate points in Image B		Residuals
	x (Pixels)	y (Pixels)	x (Pixels)	y (Pixels)	Signed Dist (Pixels)
Pt 815	3663.464	1134.797	3659.958	1746.524	0.0010
Pt 816	2562.627	1136.488	2540.734	1759.593	-0.0014
Pt 817	3041.804	2101.639	3018.019	2754.153	-0.0001
Pt 818	2694.441	2129.653	2663.735	2785.857	-0.0004
Pt 819	2778.114	1105.074	2758.423	1727.574	-0.0005
Pt 820	2623.777	1119.941	2600.698	1742.733	-0.0003
Pt 821	2830.384	2123.706	2801.030	2779.891	0.0000
Pt 822	2443.560	2136.037	2405.702	2798.097	0.0000
Pt 823	2585.375	337.953	2570.617	930.085	-0.0007
Pt 824	1730.159	1094.141	1686.822	1722.136	0.0008
Pt 825	3011.499	2148.099	2986.689	2802.162	-0.0001
Pt 826	3134.895	2136.475	3111.941	2790.666	0.0000
Pt 827	1463.503	2211.614	1405.512	2886.032	-0.0001
Pt 828	2604.490	1008.679	2579.628	1624.849	0.0012
Pt 829	2318.443	2238.373	2278.091	2908.783	-0.0006
Pt 830	2425.879	2230.409	2386.307	2896.279	0.0001
Pt 831	2011.632	385.447	1984.140	983.436	-0.0005
Pt 832	2543.860	2247.152	2506.346	2911.928	0.0002
Pt 833	2142.842	398.822	2118.803	992.046	-0.0008
Pt 834	2225.593	390.664	2201.975	984.426	-0.0001
Pt 835	2943.440	381.065	2934.167	971.997	0.0001
Pt 836	2683.443	2234.825	2650.974	2895.741	-0.0003
Pt 837	2456.948	922.826	2431.242	1538.888	0.0004
Pt 838	1545.188	923.132	1501.526	1547.364	0.0000
Pt 839	2553.021	447.654	2538.605	1041.969	-0.0017
Pt 840	3665.914	876.303	3666.865	1480.704	-0.0003
Pt 841	3752.808	437.310	3758.640	1022.869	0.0009
Pt 842	2055.953	461.638	2026.764	1061.812	0.0005
Pt 843	3232.930	832.225	3222.818	1436.671	0.0013
Pt 844	3679.518	458.406	3686.221	1045.859	-0.0007
Pt 845	1692.451	820.233	1652.845	1438.560	0.0000
Pt 846	1623.763	817.409	1582.948	1438.887	0.0000
Pt 847	1569.249	826.209	1527.853	1445.903	-0.0004
Pt 848	909.813	826.710	853.274	1450.297	0.0001
Pt 849	3189.711	797.773	3180.406	1404.020	0.0002
Pt 850	3130.887	794.474	3122.495	1400.258	-0.0007
Pt 851	2249.060	799.089	2219.558	1409.417	0.0009
Pt 852	1507.762	798.086	1462.321	1415.838	0.0011
Pt 853	1665.635	778.646	1625.900	1395.302	0.0000

ID	Image location of conjugate points in Image A		Image location of conjugate points in Image B		Residuals
	x (Pixels)	y (Pixels)	x (Pixels)	y (Pixels)	Signed Dist (Pixels)
Pt 854	2458.450	514.210	2439.146	1112.266	-0.0005
Pt 855	2327.081	750.117	2300.670	1358.706	0.0004
Pt 856	1604.106	529.631	1565.622	1135.650	0.0000
Pt 857	1791.895	530.380	1757.050	1134.453	0.0001
Pt 858	1318.433	550.515	1273.853	1159.141	-0.0002
Pt 859	3739.327	658.800	3744.438	1250.565	0.0004
Pt 860	2215.814	662.468	2188.600	1270.281	0.0001
Pt 861	1426.679	650.043	1381.365	1260.511	0.0008
Pt 862	2048.976	631.825	2020.868	1240.599	-0.0011
Pt 863	1060.690	609.915	1007.031	1223.962	0.0015
Pt 864	1552.422	601.939	1511.930	1209.425	0.0000
Pt 865	3151.343	1678.220	3132.606	2313.473	0.0006
Pt 866	904.487	1701.695	841.157	2363.237	-0.0002
Pt 867	1186.819	642.773	1138.340	1256.411	-0.0001
Pt 868	2571.339	593.834	2554.044	1193.164	-0.0007
Pt 869	2516.145	592.103	2495.527	1193.129	0.0004
Pt 870	2339.137	82.669	2323.082	660.386	-0.0010
Pt 871	2765.153	86.090	2757.427	661.578	-0.0005
Pt 872	1803.382	585.326	1766.088	1189.690	0.0012
Pt 873	672.502	669.795	616.602	1294.832	-0.0011
Pt 874	2271.856	673.638	2242.877	1283.811	0.0014
Pt 875	2376.608	674.658	2352.585	1281.058	0.0001
Pt 876	2346.456	1591.884	2313.046	2237.460	-0.0005
Pt 877	962.323	1790.683	898.389	2455.338	0.0001
Pt 878	2618.611	1775.292	2587.566	2422.275	0.0002
Pt 879	990.902	738.690	936.547	1361.526	0.0007
Pt 880	3280.144	1561.298	3265.749	2193.589	0.0000
Pt 881	2135.674	720.228	2107.967	1329.428	-0.0008
Pt 882	2394.417	722.359	2370.378	1331.588	0.0000
Pt 883	761.727	749.912	704.167	1376.118	0.0001
Pt 884	2190.864	760.580	2162.439	1369.213	0.0000
Pt 885	2621.730	507.609	2607.045	1102.720	-0.0010
Pt 886	3455.390	1810.824	3444.887	2451.706	-0.0012
Pt 887	2720.875	1827.904	2690.133	2475.424	0.0007
Pt 888	1229.528	781.282	1178.744	1400.579	0.0009
Pt 889	2819.070	134.183	2810.399	712.117	0.0003
Pt 890	1349.542	150.325	1310.312	741.702	-0.0006
Pt 891	749.915	811.065	695.028	1437.997	-0.0019
Pt 892	3558.746	1853.752	3550.173	2493.899	-0.0010

ID	Image location of conjugate points in Image A		Image location of conjugate points in Image B		Residuals
	x (Pixels)	y (Pixels)	x (Pixels)	y (Pixels)	Signed Dist (Pixels)
Pt 893	3710.159	1461.401	3705.978	2089.081	-0.0007
Pt 894	3447.152	1481.033	3436.300	2108.260	0.0004
Pt 895	2147.827	807.797	2119.753	1419.416	-0.0009
Pt 896	494.725	1884.777	421.265	2556.990	0.0000
Pt 897	1543.770	489.931	1503.415	1093.921	0.0005
Pt 898	1089.362	482.984	1041.189	1091.285	-0.0005
Pt 899	1153.059	819.238	1103.366	1441.210	-0.0006
Pt 900	1908.911	1472.127	1865.848	2116.637	0.0005
Pt 901	1447.291	166.404	1408.055	757.648	0.0005
Pt 902	2588.070	1427.449	2559.685	2062.521	0.0003
Pt 903	2742.619	1908.365	2712.811	2558.411	0.0002
Pt 904	2116.716	474.655	2087.259	1073.955	0.0013
Pt 905	3385.434	1388.278	3374.719	2014.435	-0.0001
Pt 906	1284.997	462.719	1238.828	1065.451	0.0006
Pt 907	2310.099	1390.949	2276.017	2027.607	0.0004
Pt 908	3548.747	433.587	3550.813	1020.220	0.0007
Pt 909	3296.979	1384.745	3285.408	2009.128	-0.0001
Pt 910	560.612	889.503	497.487	1524.524	0.0005
Pt 911	1084.445	896.958	1029.268	1522.556	0.0010
Pt 912	1823.784	1365.598	1780.717	2007.083	0.0003
Pt 913	1750.495	1345.172	1702.168	1983.936	0.0019
Pt 914	2077.305	1962.816	2034.151	2623.599	-0.0002
Pt 915	3177.433	1945.161	3158.900	2591.666	-0.0005
Pt 916	2620.338	1333.472	2592.763	1960.232	0.0010
Pt 917	3458.975	1941.835	3447.321	2583.838	-0.0005
Pt 918	3343.456	195.374	3342.981	773.886	0.0014
Pt 919	3335.245	1313.900	3323.184	1938.203	0.0003
Pt 920	1613.042	1986.771	1560.548	2651.377	-0.0002
Pt 921	2341.807	1980.650	2304.330	2640.847	-0.0005
Pt 922	2409.096	942.035	2381.777	1561.181	0.0005
Pt 923	2232.519	222.554	2210.164	807.076	0.0004
Pt 924	1706.867	962.999	1664.684	1589.127	0.0007
Pt 925	282.050	1271.553	210.819	1922.603	-0.0002
Pt 926	3049.444	2007.348	3025.793	2654.939	0.0004
Pt 927	2262.461	967.568	2230.209	1588.133	0.0013
Pt 928	3655.899	1246.297	3653.264	1862.687	-0.0001
Pt 929	3368.321	242.065	3369.338	818.894	0.0011
Pt 930	2431.075	1233.967	2402.869	1863.624	-0.0003
Pt 931	3349.180	2018.494	3331.591	2664.818	0.0004

ID	Image location of conjugate points in Image A		Image location of conjugate points in Image B		Residuals
	x (Pixels)	y (Pixels)	x (Pixels)	y (Pixels)	Signed Dist (Pixels)
Pt 932	2426.218	997.516	2398.485	1616.573	0.0007
Pt 933	2482.422	2234.051	2446.278	2898.887	-0.0006
Pt 934	998.294	1010.050	943.447	1641.061	-0.0005
Pt 935	2545.887	1218.696	2519.630	1847.582	-0.0002
Pt 936	2228.972	1198.923	2193.896	1825.675	0.0012
Pt 937	2091.617	1218.934	2057.506	1849.923	-0.0006
Pt 938	1132.954	2064.366	1070.848	2736.055	-0.0005
Pt 939	1154.723	2187.677	1091.872	2867.099	-0.0002
Pt 940	2217.333	303.059	2195.958	894.479	-0.0010
Pt 941	2402.978	1072.444	2375.041	1695.980	0.0001
Pt 942	1419.540	2178.117	1362.391	2854.348	-0.0004
Pt 943	1173.418	328.752	1127.681	927.512	-0.0002
Pt 944	2755.399	2153.714	2723.131	2810.340	0.0005
Pt 945	2747.342	350.077	2735.103	938.230	0.0000
Pt 946	1085.312	1107.560	1032.429	1743.421	-0.0009
Pt 947	2730.626	409.876	2719.493	1001.143	-0.0012
Pt 948	1099.831	104.252	1055.150	697.070	-0.0002
Pt 949	2996.043	122.519	2991.446	700.405	0.0000
Pt 950	1462.544	149.622	1424.047	737.985	0.0003
Pt 951	3639.093	169.761	3646.660	745.307	0.0004
Pt 952	811.685	222.373	759.171	823.723	0.0003
Pt 953	1278.489	224.603	1236.375	819.126	-0.0003
Pt 954	1176.565	258.588	1131.336	856.526	0.0001
Pt 955	1073.772	289.605	1027.057	889.615	-0.0005
Pt 956	2800.937	304.363	2789.049	887.612	0.0011
Pt 957	2603.147	345.781	2588.262	931.658	0.0001
Pt 958	1622.979	379.900	1589.026	977.812	-0.0015
Pt 959	2266.197	377.261	2245.256	969.726	-0.0010
Pt 960	2942.202	362.944	2932.797	952.473	0.0004
Pt 961	1381.303	439.996	1338.857	1040.668	-0.0002
Pt 962	1570.998	438.087	1532.289	1040.234	0.0002
Pt 963	2582.791	439.716	2567.505	1030.623	-0.0006
Pt 964	1256.892	465.022	1213.848	1069.859	-0.0013
Pt 965	2537.072	486.113	2519.310	1082.798	-0.0003
Pt 966	2465.422	532.422	2448.903	1128.433	-0.0018
Pt 967	1547.642	619.300	1506.859	1226.666	0.0000
Pt 968	1690.323	597.729	1652.011	1204.389	0.0004
Pt 969	2202.413	646.883	2173.473	1251.885	0.0010
Pt 970	2322.770	648.041	2300.845	1249.716	-0.0012

ID	Image location of conjugate points in Image A		Image location of conjugate points in Image B		Residuals
	x (Pixels)	y (Pixels)	x (Pixels)	y (Pixels)	Signed Dist (Pixels)
Pt 971	2078.440	688.987	2047.736	1293.703	0.0004
Pt 972	1400.252	698.117	1353.503	1314.222	0.0012
Pt 973	2433.180	715.363	2409.785	1322.141	0.0002
Pt 974	2269.312	738.676	2241.356	1348.958	0.0006
Pt 975	2556.349	742.963	2535.550	1351.498	-0.0001
Pt 976	1611.053	775.403	1567.928	1392.820	0.0012
Pt 977	2092.871	767.975	2060.622	1380.971	0.0008
Pt 978	1760.292	822.688	1721.545	1438.881	0.0002
Pt 979	2343.009	822.295	2314.572	1432.399	0.0013
Pt 980	2426.740	833.017	2398.990	1444.080	0.0017
Pt 981	1574.234	859.118	1534.117	1481.495	-0.0011
Pt 982	2286.544	873.419	2260.829	1490.988	-0.0012
Pt 983	269.289	913.328	203.768	1549.320	-0.0017
Pt 984	1432.656	945.389	1385.643	1568.990	0.0003
Pt 985	3559.687	970.297	3555.394	1578.798	0.0007
Pt 986	1766.797	999.226	1727.903	1627.536	-0.0004
Pt 987	1500.323	1018.808	1452.987	1648.085	0.0009
Pt 988	2403.429	1016.065	2375.263	1634.426	0.0007
Pt 989	1952.357	1048.073	1917.692	1669.231	-0.0009
Pt 990	2536.900	1035.347	2513.438	1653.950	-0.0004
Pt 991	2114.900	1056.530	2079.915	1681.648	0.0007
Pt 992	3577.153	1099.599	3574.433	1711.415	-0.0002
Pt 993	1897.641	1107.378	1858.517	1737.145	0.0004
Pt 994	2464.604	1138.067	2435.966	1763.181	0.0007
Pt 995	2724.389	1148.752	2702.724	1772.779	-0.0002
Pt 996	2246.512	2219.074	2205.175	2890.020	-0.0007
Pt 997	3724.902	1167.918	3719.983	1778.326	0.0025
Pt 998	2628.998	2197.073	2592.596	2862.351	0.0003
Pt 999	3222.103	2172.906	3200.541	2828.417	-0.0001
Pt 1000	3079.740	2178.576	3056.404	2832.294	0.0000
Pt 1001	2676.595	1209.055	2653.701	1834.210	-0.0002
Pt 1002	3372.552	1199.820	3363.332	1818.560	0.0001
Pt 1003	2625.948	1223.544	2601.114	1852.567	-0.0002
Pt 1004	3671.618	1232.702	3668.659	1846.239	0.0008
Pt 1005	3423.866	1254.917	3412.495	1876.194	0.0011
Pt 1006	2768.446	2142.732	2738.055	2799.524	-0.0001
Pt 1007	669.846	1282.118	605.700	1928.963	-0.0002
Pt 1008	1791.398	1274.906	1748.988	1911.623	0.0001
Pt 1009	3040.965	2120.284	3016.108	2772.239	0.0004

ID	Image location of conjugate points in Image A		Image location of conjugate points in Image B		Residuals
	x (Pixels)	y (Pixels)	x (Pixels)	y (Pixels)	Signed Dist (Pixels)
Pt 1010	2718.308	1288.548	2694.303	1915.220	0.0004
Pt 1011	1856.770	1312.781	1814.174	1952.668	0.0006
Pt 1012	2762.095	2112.427	2731.243	2766.964	0.0003
Pt 1013	3682.598	1314.612	3678.651	1930.247	0.0011
Pt 1014	2454.138	2123.660	2415.226	2784.334	0.0005
Pt 1015	3568.883	1325.907	3564.124	1946.488	-0.0004
Pt 1016	2374.250	2130.661	2335.133	2795.267	-0.0002
Pt 1017	1686.544	2122.750	1634.118	2792.469	-0.0002
Pt 1018	3195.383	2090.210	3177.348	2741.639	-0.0010
Pt 1019	381.186	1375.052	307.584	2028.934	0.0012
Pt 1020	789.952	1410.312	727.552	2062.080	-0.0003
Pt 1021	1889.488	1400.817	1847.475	2044.133	0.0002
Pt 1022	2823.735	2051.938	2793.357	2706.043	0.0005
Pt 1023	3206.259	1428.258	3192.674	2054.224	-0.0001
Pt 1024	3161.925	2025.466	3139.966	2673.533	0.0005
Pt 1025	2932.624	2035.106	2904.590	2688.445	0.0005
Pt 1026	2389.670	2020.322	2352.152	2681.234	-0.0003
Pt 1027	2136.178	2030.626	2092.498	2695.704	0.0001
Pt 1028	2719.310	1474.330	2694.001	2111.518	-0.0003
Pt 1029	3290.593	1471.639	3279.493	2101.206	-0.0010
Pt 1030	2576.649	1496.359	2549.709	2134.561	-0.0008
Pt 1031	3533.342	1504.764	3524.841	2133.170	-0.0001
Pt 1032	2769.532	1531.541	2743.390	2168.962	0.0004
Pt 1033	3364.018	1520.330	3352.083	2151.424	-0.0003
Pt 1034	2415.141	1947.128	2378.352	2603.096	0.0000
Pt 1035	3455.504	1553.267	3444.811	2184.773	-0.0002
Pt 1036	2842.583	1937.564	2815.607	2585.781	0.0001
Pt 1037	1550.938	1938.049	1497.795	2602.246	-0.0002
Pt 1038	2985.513	1904.149	2961.322	2549.359	0.0004
Pt 1039	1835.955	1557.236	1793.359	2208.106	-0.0006
Pt 1040	918.895	1586.541	856.717	2240.607	-0.0005
Pt 1041	3387.051	1600.075	3377.031	2230.469	-0.0006
Pt 1042	2608.143	1612.798	2580.384	2252.602	-0.0004
Pt 1043	3174.371	1850.547	3152.003	2492.505	0.0013
Pt 1044	2721.670	1639.742	2691.166	2282.762	0.0011
Pt 1045	1496.909	1672.844	1446.239	2329.262	-0.0005
Pt 1046	1874.983	1675.179	1833.247	2329.605	-0.0011
Pt 1047	2693.384	1852.224	2663.357	2500.732	0.0001
Pt 1048	2674.049	1663.257	2648.974	2304.008	-0.0011

ID	Image location of conjugate points in Image A		Image location of conjugate points in Image B		Residuals
	x (Pixels)	y (Pixels)	x (Pixels)	y (Pixels)	Signed Dist (Pixels)
Pt 1049	3027.286	1663.092	3007.014	2302.076	-0.0003
Pt 1050	1816.779	1676.405	1772.147	2328.947	-0.0005
Pt 1051	2136.333	1696.343	2095.756	2347.664	0.0003
Pt 1052	2942.403	1684.856	2920.001	2325.060	-0.0002
Pt 1053	3213.165	1698.752	3196.516	2334.452	0.0002
Pt 1054	1674.898	1854.786	1625.886	2515.485	-0.0005
Pt 1055	2824.741	1712.647	2799.736	2353.566	-0.0001
Pt 1056	3541.497	1737.710	3533.815	2374.979	-0.0013
Pt 1057	2540.431	1764.317	2512.727	2410.808	-0.0016
Pt 1058	2976.099	1766.571	2953.253	2408.944	0.0000
Pt 1059	3668.967	1808.288	3655.157	2446.348	0.0019
Pt 1060	3039.644	1808.524	3014.516	2452.083	0.0012
Pt 1061	1632.751	1786.514	1582.982	2445.899	-0.0003
Pt 1062	2858.041	1798.198	2833.235	2440.468	0.0000
Pt 1063	2600.022	1810.314	2568.267	2457.255	0.0003
Pt 1064	416.580	1539.603	343.959	2203.250	0.0011
Pt 1065	3888.181	1255.725	3888.157	1871.662	0.0006
Pt 1066	631.500	485.517	570.336	1098.567	0.0014
Pt 1067	2915.164	1424.110	2896.357	2057.461	-0.0011
				SUM:	0.0010

APPENDIX G

EXTRACT OF JAVA CODES IMPLEMENTED FOR THE DEVELOPED IMAGE REGISTRATION MODULE

The extract of the JAVA codes of the implemented algorithms for the development of the automatic image registration scheme is herewith attached. Due to the voluminous nature of the Java codes which is around 1000 pages, the full code could not be annexed in this thesis. The complete codes are as contained in the attached CD.

EXTRACTION OF ASSOCIATED PAIRS

```
package FeaturesExtractionModel;
import boofcv.abst.feature.associate.AssociateDescription;
import boofcv.abst.feature.detdesc.DetectDescribePoint;
import boofcv.alg.descriptor.UtilFeature;
import boofcv.io.image.ConvertBufferedImage;
import boofcv.struct.feature.TupleDesc;
import boofcv.struct.image.ImageGray;
import georegression.struct.point.Point2D_F64;
import org.ddogleg.struct.FastQueue;
import java.awt.image.BufferedImage;
import java.util.ArrayList;
import java.util.List;
/**
 * Created by BEATA on 7/25/2016.
 */
public class AssociatePoints<T extends ImageGray, TD extends TupleDesc> {
    // algorithm used to detect and describe interest points
    private DetectDescribePoint<T, TD> detDesc;
    // Associated descriptions together by minimizing an error metric
    private AssociateDescription<TD> associate;
```

```

// Associated Matches
// location of interest points
public List<Point2D_F64> pointsA;
public List<Point2D_F64> pointsB;
Class<T> imageType;
public AssociatePoints(DetectDescribePoint<T, TD> detDesc,
    AssociateDescription<TD> associate,
    Class<T> imageType) {
    this.detDesc = detDesc;
    this.associate = associate;
    this.imageType = imageType;
}
/**
 * Detect and associate point features in the two images. Display the results.
 */
public void associate(BufferedImage imageA, BufferedImage imageB) {
    T inputA = ConvertBufferedImage.convertFromSingle(imageA, null, imageType);
    T inputB = ConvertBufferedImage.convertFromSingle(imageB, null, imageType);
    // stores the location of detected interest points
    pointsA = new ArrayList<Point2D_F64>();
    pointsB = new ArrayList<Point2D_F64>();
    // stores the description of detected interest points
    FastQueue<TD> descA = UtilFeature.createQueue(detDesc, 100);
    FastQueue<TD> descB = UtilFeature.createQueue(detDesc, 100);
    // describe each image using interest points
    describeImage(inputA, pointsA, descA);
    describeImage(inputB, pointsB, descB);
    // Associate features between the two images
    associate.setSource(descA);
    associate.setDestination(descB);
}

```

```

    associate.associate();

/*    // display the results
    AssociationPanel panel = new AssociationPanel(20);
    panel.setAssociation(pointsA, pointsB, associate.getMatches());
    panel.setImages(imageA, imageB);
    ShowImages_OutPut.showWindow(panel, "Associated Features", true);*/
}
/**
 * Detects features inside the two images and computes descriptions at those points.
 */
private void describeImage(T input, List<Point2D_F64> points, FastQueue<TD> descs) {
    detDesc.detect(input);
    for (int i = 0; i < detDesc.getNumberOfFeatures(); i++) {
        points.add(detDesc.getLocation(i).copy());
        descs.grow().setTo(detDesc.getDescription(i));
    }
}
}
}
package FeaturesExtractionModel;
/**
 * Created by BEATA on 4/15/2016.
 */
public class ConjugatePoint {
    private int x,y; // conjugate points position
    private double Intensity; // Intensity Value
    public ConjugatePoint(){
        // Nothing Here
    }
    public ConjugatePoint(int x, int y, double intensity){

```

```

        this.x=x;
        this.y=y;
        this.Intensity=intensity;
    }
    public int getX() {
        return x;
    }
    public int getY() {
        return y;
    }
    public double getIntensity() {
        return Intensity;
    }
    public void setX(int x) {
        this.x = x;
    }
    public void setY(int y) {
        this.y = y;
    }
    public void setIntensity(double intensity) {
        Intensity = intensity;
    }
}

```

MODIFIED HARRIS CORNER DETECTOR

```

package FeaturesExtractionModel;
import georegression.struct.point.Point2D_F64;
import java.util.ArrayList;
import java.util.Iterator;
import java.util.List;

```



```

/**
 * Harris Corner Detector
 *
 *  $k = \det(A) - k * \text{trace}(A)^2$ 
 *
 * Where A is the second-moment matrix
 *
 * 
$$A = \sum_{dx,dy} \begin{vmatrix} Lx^2(x+dx,y+dy) & Lx.Ly(x+dx,y+dy) \\ Lx.Ly(x+dx,y+dy) & Ly^2(x+dx,y+dy) \end{vmatrix} * \text{Gaussian}(dx,dy)$$

 *
 * and  $k = a/(1+a)^2$ ,
 *
 * where "a" is the minimum ratio between the two eigenvalues
 * for a point to be considered as a corner.
 *
 * @author Oluibukun Ajayi
 */
public class HarrisFast {

    // corner class
    public class Corner extends Point2D_F64 {
        int x,y; // corner position
        float h; // harris measure
        public Corner(int x, int y, float h) {
            this.x=x; this.y=y; this.h=h;
        }
    }

    // corners list

```

```

private List<Corner> corners = new ArrayList<Corner>();
public List<Corner> corners_sort = new ArrayList<Corner>();

// image
private int[][] image;
int width,height;

// precomputed values of the derivatives
private float[][] Lx2,Ly2,Lxy;
/**
 * Constructor
 */
public HarrisFast(int[][] image, int width, int height) {
    this.image = image;
    this.width = width;
    this.height = height;
}
/**
 * Gaussian function
 */
private double gaussian(double x, double y, double sigma) {
    double sigma2 = sigma*sigma;
    double t = (x*x+y*y)/(2*sigma2);
    double u = 1.0/(2*Math.PI*sigma2);
    double e = u*Math.exp( -t );
    return e;
}
/**
 * Sobel gradient 3x3
 */

```

```

private float[] sobel(int x, int y) {
    int v00=0,v01=0,v02=0,v10=0,v12=0,v20=0,v21=0,v22=0;
    int x0 = x-1, x1 = x, x2 = x+1;
    int y0 = y-1, y1 = y, y2 = y+1;
    if (x0<0) x0=0;
    if (y0<0) y0=0;
    if (x2>=width) x2=width-1;
    if (y2>=height) y2=height-1;
    v00=image[x0][y0]; v10=image[x1][y0]; v20=image[x2][y0];
    v01=image[x0][y1];          v21=image[x2][y1];
    v02=image[x0][y2]; v12=image[x1][y2]; v22=image[x2][y2];
    float sx = ((v20+2*v21+v22)-(v00+2*v01+v02))/(4*255f);
    float sy = ((v02+2*v12+v22)-(v00+2*v10+v20))/(4*255f);
    return new float[] {sx,sy};
}

```

/**

* Compute the 3 arrays Ix, Iy and Ixy

*/

```
private void computeDerivatives(double sigma){
```

```
    this.Lx2 = new float[width][height];
```

```
    this.Ly2 = new float[width][height];
```

```
    this.Lxy = new float[width][height];
```

```
    // gradient values: Gx,Gy
```

```
    float[][][] grad = new float[width][height][3];
```

```
    for (int y=0; y<height; y++)
```

```
        for (int x=0; x<width; x++)
```

```
            grad[x][y] = sobel(x,y);
```

```
    // precomputed the coefficients of the gaussian filter
```

```

int radius = (int)(2*sigma);
int window = 1+2*radius;
float[][] gaussian = new float[window][window];
for(int j=-radius;j<=radius;j++)
    for(int i=-radius;i<=radius;i++)
        gaussian[i+radius][j+radius]=(float)gaussian(i,j,sigma);

// Convolve gradient with gaussian filter:
//
// Ix2 = (F) * (Gx^2)
// Iy2 = (F) * (Gy^2)
// Ixy = (F) * (Gx.Gy)
//
for (int y=0; y<height; y++) {
    for (int x=0; x<width; x++) {
        for(int dy=-radius;dy<=radius;dy++) {
            for(int dx=-radius;dx<=radius;dx++) {
                int xk = x + dx;
                int yk = y + dy;
                if (xk<0 || xk>=width) continue;
                if (yk<0 || yk>=height) continue;
                // gaussian weight
                double gw = gaussian[dx+radius][dy+radius];
                // convolution
                this.Lx2[x][y]+=gw*grad[xk][yk][0]*grad[xk][yk][0];
                this.Ly2[x][y]+=gw*grad[xk][yk][1]*grad[xk][yk][1];
                this.Lxy[x][y]+=gw*grad[xk][yk][0]*grad[xk][yk][1];
            }
        }
    }
}

```

```

    }
}
/**
 * compute harris measure for a pixel
 */
private float harrisMeasure(int x, int y, float k) {

    // matrix elements (normalized)
    float m00 = this.Lx2[x][y];
    float m01 = this.Lxy[x][y];
    float m10 = this.Lxy[x][y];
    float m11 = this.Ly2[x][y];

    // Harris corner measure = det(M)-k.trace(M)^2
    return m00*m11 - m01*m10 - k*(m00+m11)*(m00+m11);
}
/**
 * return true if the measure at pixel (x,y) is a local spatial Maxima
 */
private boolean isSpatialMaxima(float[][] hmap, int x, int y) {
    int n=8;
    int[] dx = new int[] { -1,0,1,1,1,0,-1,-1 };
    int[] dy = new int[] { -1,-1,-1,0,1,1,1,0 };
    double w = hmap[x][y];
    for(int i=0;i<n;i++) {
        double wk = hmap[x+dx[i]][y+dy[i]];
        if (wk>=w) return false;
    }
    return true;
}
}

```

```

/**
 * compute the Harris measure for each pixel of the image
 */
private float[][] computeHarrisMap(double k) {

    // Harris measure map
    float[][] harrismap = new float[width][height];
    // for each pixel in the image
    for (int y=0; y<height; y++) {
        for (int x=0; x<width; x++) {
            // compute the harris measure
            double h = harrisMeasure(x,y,(float)k);
            if (h<=0) continue;
            // log scale
            h = 255 * Math.log(1+h) / Math.log(1+255);
            // store
            harrismap[x][y]=(float)h;
        }
    }
    return harrismap;
}

/**
 * Perform the Harris Corner Detection
 *
 * @param sigma gaussian filter parameter
 * @param k parameter of the harris measure formula
 * @param minDistance minimum distance between corners
 * @param threshold harris fast response measure
 * @return the original image marked with cross sign at each corner
 */

```

```

public int[][] filter(double sigma, double k, int minDistance, double threshold) {

    // precompute derivatives
    computeDerivatives(sigma);

    // Harris measure map
    float[][] harrismap = computeHarrisMap(k);
    // for each pixel in the harrismap
    for (int y=1; y<height-1; y++) {
        for (int x=1; x<width-1; x++) {

            // thresholding : harris measure > epsilon
            float h = harrismap[x][y];
            if (h<=1E-3) continue;

            // keep only a local maxima
            if (!isSpatialMaxima(harrismap, x, y)) continue;

            // add the corner to the list
            corners.add( new Corner(x,y,h) );
        }
    }
    for (int i=0;i<corners.size();i++) {
        if(corners.get(i).h>= threshold){
            corners_sort.add(corners.get(i));
        }
    }

    // remove corners to close to each other (keep the highest measure)
    Iterator<Corner> iter = corners_sort.iterator();

```

```

while(iter.hasNext()) {
    Corner p = iter.next();
    for(Corner n:corners_sort) {
        if (n==p) continue;
        int dist = (int)Math.sqrt( (p.x-n.x)*(p.x-n.x)+(p.y-n.y)*(p.y-n.y) );
        if(dist>minDistance) continue;
        if (n.h<p.h) continue;
        iter.remove();
        break;
    }
}

// output
int[][] output =new int[width][height];
for (int y=0; y<height; y++)
    for (int x=0; x<width; x++)
        output[x][y]=(int)(image[x][y]*0.75); // original image (darker)

// for each corner
for (Corner p: corners_sort) {

    // add the cross sign over the image
    for (int dt=-3; dt<=3; dt++) {
        if (p.x+dt>=0 && p.x+dt<width ) output[p.x+dt][p.y]=255;
        if (p.y+dt>=0 && p.y+dt<height) output[p.x][p.y+dt]=255;
    }
}
return output;
}
}

```


GEOMETRIC TRANSFORMATION

```
package FeaturesExtractionModel;
import ApplicationTools.Matrix;
import java.util.ArrayList;
import java.util.List;

/**
 * Created by BEATA on 29/04/2016.
 */
public class GeometricTransformation {

    // Variable for storing conjugate points from two overlapping photography
    private List<HarrisFast.Corner> conjugatePointsOne = new ArrayList<>();
    private List<HarrisFast.Corner> conjugatePointsTwo = new ArrayList<>();
    private int numPoints;

    // Orthogonal Transformation Parameter
    private double scale ;
    private double rotation;
    private double translationX;
    private double translationY;

    // Affine Transformation Parameter
    private double aff_A;
    private double aff_B;
    private double aff_C;
    private double aff_D;
    private double aff_E;
    private double aff_F;
```

```

// Projective Transformation Parameters Approximate Value
private double a1,a2,a3,b1,b2,b3,c1,c2;

//Class Constructor
public GeometricTransformation(List<HarrisFast.Corner> conjugatePointsOne,
                               List<HarrisFast.Corner> conjugatePointsTwo){
    this.conjugatePointsOne = conjugatePointsOne;
    this.conjugatePointsTwo = conjugatePointsTwo;
    this.numPoints = conjugatePointsOne.size();
} // End of Class Constructor

// Method for orthogonal transformation parameter computation
public void orthogonalTransform(){
    double[][] a1 = new double[numPoints*2][4];
    double[][] l1 = new double[numPoints*2][1];
    int countI =0;
    for (int i=0; i<numPoints; i++){
        a1[countI][0]= conjugatePointsTwo.get(i).x;
        a1[countI+1][0]= conjugatePointsTwo.get(i).y;
        a1[countI][1]= -conjugatePointsTwo.get(i).y;
        a1[countI+1][1]= conjugatePointsTwo.get(i).x;
        a1[countI][2]= 1;
        a1[countI+1][2]=0;
        a1[countI][3]= 0;
        a1[countI+1][3]= 1;
        l1[countI][0]= conjugatePointsOne.get(i).x;
        l1[countI+1][0]= conjugatePointsOne.get(i).y;
        countI=countI+2;
    }
}

```

```

Matrix A = new Matrix(a1);
Matrix L = new Matrix(l1);

//Perform Least Square analysis
Matrix A_tran= Matrix.transpose(A);
Matrix AA = Matrix.multiply(A_tran, A);
Matrix invAA = Matrix.inverse(AA);
Matrix AL = Matrix.multiply(A_tran, L);
Matrix matrix = Matrix.multiply(invAA, AL);
// Assigning Transformation parameters
this.scale =
Math.sqrt((Math.pow(matrix.getValueAt(0,0),2)+Math.pow(matrix.getValueAt(1,0),2)));
    this.rotation = Math.toRadians(Math.atan(matrix.getValueAt(1, 0) /
matrix.getValueAt(0, 0)));
    this.translationX = matrix.getValueAt(2, 0);
    this.translationY = matrix.getValueAt(3,0);
}

public void affineTransformation() {
    double[][] a1 = new double[numPoints * 2][6];
    double[][] l1 = new double[numPoints * 2][1];
    int countI =0;
    for (int i = 0; i < numPoints; i++) {
        a1[countI][0] = conjugatePointsTwo.get(i).x;
        a1[countI + 1][0] = 0;
        a1[countI][1] = conjugatePointsTwo.get(i).y;
        a1[countI + 1][1] = 0;
        a1[countI][2] = 1;
        a1[countI + 1][2] = 0;
        a1[countI][3] = 0;
        a1[countI + 1][3] = conjugatePointsTwo.get(i).x;
        a1[countI][4] = 0;

```

```

    a1[countI + 1][4] = conjugatePointsTwo.get(i).y;
    a1[countI][5] = 0;
    a1[countI + 1][5] = 1;
    l1[countI][0]= conjugatePointsOne.get(i).x;
    l1[countI+1][0]= conjugatePointsOne.get(i).y;
    countI=countI+2;
}
/* for (int r =0; r<a1.length;r++) {
    for (int c = 0; c < 6; c++) {
        System.out.print(a1[r][c] + " ");
    }
    System.out.println();
}*/
Matrix A = new Matrix(a1);
Matrix L = new Matrix(l1);

//Perform Least Square analysis
Matrix A_tran= Matrix.transpose(A);
Matrix AA = Matrix.multiply(A_tran, A);
Matrix invAA = Matrix.inverse(AA);
Matrix AL = Matrix.multiply(A_tran, L);
Matrix matrix = Matrix.multiply(invAA, AL); // Transformation Result

// Assigning Transformation parameters
this.aff_A = matrix.getValueAt(0, 0);
this.aff_B = matrix.getValueAt(1, 0);
this.aff_C = matrix.getValueAt(2, 0);
this.aff_D = matrix.getValueAt(3, 0);
this.aff_E = matrix.getValueAt(4, 0);
this.aff_F = matrix.getValueAt(5, 0);

```

```

}

public void projectiveTransformation(){

    // Getting approximate parameter
    double[][] a1 = new double[numPoints * 2][8];
    double[][] l1 = new double[numPoints * 2][1];
    int countI =0;
    for (int i = 0; i < numPoints; i++) {
        a1[countI][0] = conjugatePointsTwo.get(i).x;
        a1[countI][1] = conjugatePointsTwo.get(i).y;
        a1[countI][2] = 1;
        a1[countI][3] = 0;
        a1[countI][4] = 0;
        a1[countI][5] = 0;
        a1[countI][6] = -(conjugatePointsTwo.get(i).x *conjugatePointsOne.get(i).x );
        a1[countI][7] = -(conjugatePointsTwo.get(i).x *conjugatePointsOne.get(i).y );
        a1[countI+1][0]=0;
        a1[countI+1][1]=0;
        a1[countI+1][2]=0;
        a1[countI+1][3] = conjugatePointsTwo.get(i).x;
        a1[countI+1][4] = conjugatePointsTwo.get(i).y;
        a1[countI+1][5] = 1;
        a1[countI+1][6] = -(conjugatePointsTwo.get(i).y *conjugatePointsOne.get(i).x );
        a1[countI+1][7] = -(conjugatePointsTwo.get(i).y *conjugatePointsOne.get(i).y );
        l1[countI][0]= conjugatePointsOne.get(i).x;
        l1[countI+1][0]= conjugatePointsOne.get(i).y;
        countI=countI+2;
    }

    // for (int r =0; r<l1.length;r++){

```

```

//      for (int c=0; c<1;c++){
//          System.out.print(l1[r][c]+" ");
//      }
//      System.out.println();
//  }

Matrix A = new Matrix(a1);
Matrix L = new Matrix(l1);
//Perform Least Square analysis
Matrix A_tran= Matrix.transpose(A);
Matrix AA = Matrix.multiply(A_tran, A);
Matrix invAA = Matrix.inverse(AA);
Matrix AL = Matrix.multiply(A_tran, L);
Matrix matrix = Matrix.multiply(invAA, AL);
this.getProjectiveParameter(matrix);
}

public double getScale() {
    return scale;
}

public double getRotation() {
    return rotation;
}

public double getTranslationX() {
    return translationX;
}

public double getTranslationY() {
    return translationY;
}

public List<HarrisFast.Corner> getConjugatePointsOne() {
    return conjugatePointsOne;
}

```

```
public double getAff_F() {
    return aff_F;
}
public double getAff_E() {
    return aff_E;
}

public double getAff_D() {
    return aff_D;
}
public double getAff_C() {
    return aff_C;
}
public double getAff_B() {
    return aff_B;
}
public double getAff_A() {
    return aff_A;
}
public double getA1() {
    return a1;
}
public double getA2() {
    return a2;
}
public double getA3() {
    return a3;
}
public double getB1() {
    return b1;
}
```

```

    }
    public double getB2() {
        return b2;
    }
    public double getB3() {
        return b3;
    }
    public double getC1() {
        return c1;
    }
    public double getC2() {
        return c2;
    }
    private void getProjectiveParameter(Matrix matrix){
        this.a1=matrix.getValueAt(0,0);
        this.a2=matrix.getValueAt(3,0);
        this.a3=matrix.getValueAt(6,0);
        this.b1=matrix.getValueAt(1,0);
        this.b2=matrix.getValueAt(4,0);
        this.b3=matrix.getValueAt(7,0);
        this.c1=matrix.getValueAt(2,0);
        this.c2=matrix.getValueAt(5,0);
    }
}

```

INTEGRATED EPIPOLAR MODEL

```
package EpipolarGeometric;
```

```
/**
```

```
* Created by BEATA on 3/12/2017.
```

```
*/
```



```

import ApplicationTools.AlertBox;
import CameraModels.CameraMatrix;
import boofcv.abst.feature.associate.AssociateDescription;
import boofcv.abst.feature.associate.ScoreAssociation;
import boofcv.abst.feature.describe.ConfigBrief;
import boofcv.abst.feature.describe.DescribeRegionPoint;
import boofcv.abst.feature.detdesc.ConfigCompleteSift;
import boofcv.abst.feature.detdesc.DetectDescribePoint;
import boofcv.abst.feature.detect.interest.ConfigFastHessian;
import boofcv.abst.feature.detect.interest.ConfigGeneralDetector;
import boofcv.abst.feature.detect.interest.InterestPointDetector;
import boofcv.abst.geo.Estimate1ofEpipolar;
import boofcv.alg.descriptor.UtilFeature;
import boofcv.alg.distort.ImageDistort;
import boofcv.alg.distort.PixelTransformHomography_F32;
import boofcv.alg.distort.impl.DistortSupport;
import boofcv.alg.feature.detect.interest.GeneralFeatureDetector;
import boofcv.alg.filter.derivative.GImageDerivativeOps;
import boofcv.alg.interpolate.InterpolatePixelS;
import boofcv.core.image.border.BorderType;
import boofcv.factory.feature.associate.FactoryAssociation;
import boofcv.factory.feature.describe.FactoryDescribeRegionPoint;
import boofcv.factory.feature.detdesc.FactoryDetectDescribe;
import boofcv.factory.feature.detect.interest.FactoryDetectPoint;
import boofcv.factory.feature.detect.interest.FactoryInterestPoint;
import boofcv.factory.geo.*;
import boofcv.factory.interpolate.FactoryInterpolation;
import boofcv.io.image.ConvertBufferedImage;
import boofcv.struct.feature.AssociatedIndex;
import boofcv.struct.feature.BrightFeature;

```

```

import boofcv.struct.feature.TupleDesc;
import boofcv.struct.geo.AssociatedPair;
import boofcv.struct.image.GrayF32;
import boofcv.struct.image.ImageGray;
import boofcv.struct.image.Planar;
import georegression.struct.homography.Homography2D_F64;
import georegression.struct.point.Point2D_F64;
import georegression.struct.point.Point2D_I32;
import georegression.transform.homography.HomographyPointOps_F64;
import org.ddogleg.fitting.modelset.ModelFitter;
import org.ddogleg.fitting.modelset.ModelMatcher;
import org.ddogleg.struct.FastQueue;
import org.ejml.data.DenseMatrix64F;
import org.ejml.factory.DecompositionFactory;
import org.ejml.interfaces.decomposition.SingularValueDecomposition;
import org.ejml.ops.CommonOps;
import javax.imageio.ImageIO;
import java.awt.*;
import java.awt.geom.Rectangle2D;
import java.awt.image.BufferedImage;
import java.io.File;
import java.util.ArrayList;
import java.util.List;
import java.util.SortedSet;
import java.util.TreeSet;
/**
 * Created by BEATA on 10/6/2016.
 */
public class FittingStereoModel2<T extends ImageGray, FD extends TupleDesc, TD extends
TupleDesc> {
    /**

```

* Using abstracted code, find a transform which minimizes the difference between corresponding features

* in both images. This code is completely modelled independent and is the core algorithms.

*/

```
private List<AssociatedPair> rawPairs = new ArrayList<>();
```

```
private List<AssociatedPair> pairsInlier = new ArrayList<>();
```

```
private Class<T> imageType = (Class<T>) GrayF32.class;
```

```
private BufferedImage outputWithPoints;
```

```
private Homography2D_F64 fromWorkToB;
```

```
private int modelType;
```

```
private int ransacIteration;
```

```
private int width;
```

```
private int height;
```

```
/**
```

```
* Class Constructor for Un-Calibrated Mode
```

```
* Estimating the homography, fundamental matrix, and orienting the stereo-pair
```

```
* @param modelType
```

```
*/
```

```
public FittingStereoModel2(int modelType, int ransacIteration) {
```

```
    this.modelType = modelType;
```

```
    this.ransacIteration = ransacIteration;
```

```
}
```

```
public Homography2D_F64 computeTransform(T imageA , T imageB ,  
DetectDescribePoint<T,FD> detDesc ,
```

```
AssociateDescription<FD> associate)
```

```
{
```

```
    // get the length of the description
```

```
    List<Point2D_F64> pointsA = new ArrayList<>();
```

```
    FastQueue<FD> descA = UtilFeature.createQueue(detDesc, 200);
```

```
    List<Point2D_F64> pointsB = new ArrayList<>();
```

```

FastQueue<FD> descB = UtilFeature.createQueue(detDesc,200);

// extract feature locations and descriptions from each image
describeImage(imageA, detDesc, pointsA, descA);
describeImage(imageB, detDesc, pointsB, descB);

//System.out.println(descA.data[0].getDouble(0));
// Associate features between the two images
associate.setSource(descA);
associate.setDestination(descB);
associate.associate();

// create a list of AssociatedPairs that tell the model matcher how a feature moved
FastQueue<AssociatedIndex> matches = associate.getMatches();
for( int i = 0; i < matches.size(); i++ ) {
    AssociatedIndex match = matches.get(i);
    Point2D_F64 a = pointsA.get(match.src);
    Point2D_F64 b = pointsB.get(match.dst);
    rawPairs.add( new AssociatedPair(a,b,false));
}

// fit the images using a homography. This works well for rotations and distant objects.
ModelMatcher<Homography2D_F64,AssociatedPair> modelMatcher =
    FactoryMultiViewRobust.homographyRansac(null, new
ConfigRansac(ransacIteration,3));

// find the best fit model to describe the change between these images
// Estimate the homography matrix while removing outliers
if( !modelMatcher.process(rawPairs) )
    throw new RuntimeException("Model Matcher failed!");

```

```

// Store the Inliers pairs
List<AssociatedPair> pairsInlier = modelMatcher.getMatchSet();

// Compute Homography using the inliers with RANSAC
Estimate1ofEpipolar estimateH = FactoryMultiView.computeHomography(true);
DenseMatrix64F H = new DenseMatrix64F(3, 3);
if (!estimateH.process(pairsInlier, H))
    throw new IllegalArgumentException("Failed");
return denseMatrix64F_To_homography2D_f64(H);
}
/**
 * Any arbitrary implementation of InterestPointDetector, OrientationImage,
DescribeRegionPoint
 * can be combined into DetectDescribePoint. The syntax is more complex, but the end
result is more flexible.
 * This should only be done if there isn't a pre-made DetectDescribePoint.
 */
public DetectDescribePoint <T, TD> createFromComponents(Class<T> imageType ) {
    // create a corner detector
    Class derivType = GImageDerivativeOps.getDerivativeType(imageType);
    GeneralFeatureDetector corner = FactoryDetectPoint.createShiTomasi(new
ConfigGeneralDetector(1000,5, .001f), false, derivType);
    InterestPointDetector detector = FactoryInterestPoint.wrapPoint(corner, 1, imageType,
derivType);

    // describe points using BRIEF
    DescribeRegionPoint describe = FactoryDescribeRegionPoint.brief(new
ConfigBrief(true), imageType);

    // Combine together.
    // NOTE: orientation will not be estimated
    return FactoryDetectDescribe.fuseTogether(detector, null, describe);
}

```

```

}
/**
 * Detects features inside the two images and computes descriptions at those points.
 */
private void describeImage(T image, DetectDescribePoint<T,FD> detDesc,
                           List<Point2D_F64> points, FastQueue<FD> listDescs) {
    detDesc.detect(image);
    listDescs.reset();
    for( int i = 0; i < detDesc.getNumberOfFeatures(); i++ ) {
        points.add( detDesc.getLocation(i).copy() );
        listDescs.grow().setTo(detDesc.getDescription(i));
    }
} // End describeImage
/**
 * Harris Corner detection model used in detecting
 * describing and computing a refine homography that exist
 * between conjugate points in a stereo pair
 */
public Homography2D_F64 using_HarrisModel(BufferedImage imageA, BufferedImage
imageB){
    T inputA = ConvertBufferedImage.convertFromSingle(imageA, null, this.imageType);
    T inputB = ConvertBufferedImage.convertFromSingle(imageB, null, this.imageType);

    // Detect using the standard Harris Corner descriptor and describer
    DetectDescribePoint detDesc = createFromComponents(imageType);
    ScoreAssociation scorer =
FactoryAssociation.defaultScore(detDesc.getDescriptionType());
    AssociateDescription associate = FactoryAssociation.greedy(scorer,
Double.POSITIVE_INFINITY, true);
    return computeTransform(inputA,inputB,detDesc,associate);
}

```

```

/**
 * SURF model used in detecting
 * describing and computing a refine homography that exist
 * between conjugate points in a stereo pair
 */
public Homography2D_F64 stitchUsing_SURF(BufferedImage imageA, BufferedImage
imageB)
{
    T inputA = ConvertBufferedImage.convertFromSingle(imageA, null, imageType);
    T inputB = ConvertBufferedImage.convertFromSingle(imageB, null, imageType);

    // Detect using the standard SURF feature descriptor and describer
    DetectDescribePoint detDesc = FactoryDetectDescribe.surfStable(
        new ConfigFastHessian(1, 2, 1000, 1, 9, 4, 4), null, null,imageType);

    ScoreAssociation<BrightFeature> scorer =
FactoryAssociation.scoreEuclidean(BrightFeature.class, true);

    AssociateDescription<BrightFeature> associate =
FactoryAssociation.greedy(scorer,2,true);

    // fit the images using a homography. This works well for rotations and distant objects.
    return computeTransform(inputA,inputB,detDesc, (AssociateDescription<FD>)
associate);
}
/**
 * SURF model used in detecting
 * describing and computing a refine homography that exist
 * between conjugate points in a stereo pair
 */
public Homography2D_F64 stitchUsing_SIFT(BufferedImage imageA, BufferedImage
imageB)
{
    T inputA = ConvertBufferedImage.convertFromSingle(imageA, null, imageType);

```

```

T inputB = ConvertBufferedImage.convertFromSingle(imageB, null, imageType);

// Detect using the standard SIFT feature descriptor and describer
DetectDescribePoint detDesc = FactoryDetectDescribe.sift(new
ConfigCompleteSift(0,5,1000));

ScoreAssociation<BrightFeature> scorer =
FactoryAssociation.scoreEuclidean(BrightFeature.class, true);

AssociateDescription<BrightFeature> associate =
FactoryAssociation.greedy(scorer,2,true);

// fit the images using a homography. This works well for rotations and distant objects.
return computeTransform(inputA,inputB,detDesc, (AssociateDescription<FD>)
associate);
}
/**
 * Renders and displays the stitched together images
 */
public BufferedImage renderStitching( BufferedImage imageA, BufferedImage imageB ,
Homography2D_F64 fromAtoB )
{
// specify size of output image
double scale = 0.5;
// Convert into a BoofCV color format
Planar<GrayF32> colorA =
    ConvertBufferedImage.convertFromMulti(imageA, null, true, GrayF32.class);
Planar<GrayF32> colorB =
    ConvertBufferedImage.convertFromMulti(imageB, null,true, GrayF32.class);

// Where the output images are rendered into
Planar<GrayF32> work = colorA.createSameShape();
//Planar<GrayF32> work
=colorA._createNew((int)(colorA.width*1.8),(int)(colorA.height*1.8));

```



```

//System.out.println(work.getHeight()+" "+work.getWidth());
//System.out.println(colorA.getHeight()+" "+colorA.getWidth());

// Adjust the transform so that the whole image can appear inside of it
Homography2D_F64 fromAToWork = new
Homography2D_F64(scale,0,colorA.width/4,0,scale,colorA.height/4,0,0,1);
Homography2D_F64 fromWorkToA = fromAToWork.invert(null);

// Used to render the results onto an image
PixelTransformHomography_F32 model = new PixelTransformHomography_F32();
InterpolatePixelS<GrayF32> interpolatePixelS =
FactoryInterpolation.bilinearPixelS(GrayF32.class, BorderType.ZERO);
ImageDistort<Planar<GrayF32>,Planar<GrayF32>> distort =
    DistortSupport.createDistortPL(GrayF32.class, model, interpolatePixelS, false);
distort.setRenderAll(false);

// Render first image
model.set(fromWorkToA);
distort.apply(colorA,work);

// Render second image
fromWorkToB = fromWorkToA.concat(fromAtoB,null);
model.set(fromWorkToB);
distort.apply(colorB,work);
//Homography2D_F64 fromWorkToB = fromAtoB.concat(fromAtoB,null);

// Convert the rendered image into a BufferedImage
BufferedImage output = new
BufferedImage(work.width,work.height,imageA.getType());
ConvertBufferedImage.convertTo(work,output,true);

```

```

outputWithPoints = new BufferedImage(work.width,work.height,imageA.getType());
ConvertBufferedImage.convertTo(work,outputWithPoints,true);
return output;
}

// Mosaic output with conjugate points drawn on it
public void output_with_conjugatePointDraw(){
    List<AssociatedPair> points2drw = getPairsInlier();
    Graphics2D g1 = outputWithPoints.createGraphics();
    Graphics2D g2 = outputWithPoints.createGraphics();
    g1.setColor(Color.red);
    g2.setColor(Color.blue);

    // draw the position of the conjugate points on the image to make it visible to see
    Homography2D_F64 fromBtoWork = fromWorkToB.invert(null);
    for (int i =0; i<points2drw.size();i++){
        Point2D_I32 corners[] = new Point2D_I32[1];
        corners[0] =
renderPoint(points2drw.get(i).getP2().x,points2drw.get(i).getP2().y,fromBtoWork);
        g1.fill(new Rectangle2D.Float((float)(corners[0].x - 2), (float)(corners[0].y - 2), 5,
5));
        g2.drawString(i+" ",(float)(corners[0].x-18 ), (float)(corners[0].y+5));
    }
}

private static Point2D_I32 renderPoint(double x0 , double y0 , Homography2D_F64
fromBtoWork )
{
    Point2D_F64 result = new Point2D_F64();
    HomographyPointOps_F64.transform(fromBtoWork, new Point2D_F64(x0, y0), result);
    return new Point2D_I32((int)result.x,(int)result.y);
}

```

```

public static double[] transformPoint(double x,double y,Homography2D_F64 H){
    double[] result = new double[2];
    double h = ((H.get(2,0)*x)+( H.get(2,1)*y) + (H.get(2,2)));
    double x1 = ((H.get(0,0)*x) + (H.get(0,1)*y) + (H.get(0,2))) / h;
    double y1 = ((H.get(1,0)*x) + (H.get(1,1)*y) + (H.get(1,2))) / h;
    result[0]=x1;
    result[1]=y1;
    return result;
}

// Convert Homography2D_f64 dataType to DenseMatrix64F
private DenseMatrix64F homography2D_f64_To_denseMatrix64F(Homography2D_F64
Homo){
    DenseMatrix64F E_init = new DenseMatrix64F(3,3);
    E_init.set(0, 0,Homo.get(0, 0));
    E_init.set(0, 1,Homo.get(0, 1));
    E_init.set(0, 2,Homo.get(0, 2));
    E_init.set(1, 1,Homo.get(1, 1));
    E_init.set(1, 2,Homo.get(1, 2));
    E_init.set(2, 0,Homo.get(2, 0));
    E_init.set(2, 1,Homo.get(2, 1));
    E_init.set(2, 2,Homo.get(2, 2));
    return E_init;
}

// Convert DenseMatrix64F dataType to DenseMatrix64FHomography2D_f64 dataType
private Homography2D_F64 denseMatrix64F_To_homography2D_f64(DenseMatrix64F
H){
    Homography2D_F64 result = new Homography2D_F64();

```

```

    result.a11 = H.get(0, 0);
    result.a12 = H.get(0, 1);
    result.a13 = H.get(0, 2);
    result.a21 = H.get(1, 0);
    result.a22 = H.get(1, 1);
    result.a23 = H.get(1, 2);
    result.a31 = H.get(2, 0);
    result.a32 = H.get(2, 1);
    result.a33 = H.get(2, 2);
    return result;
}
/**
 * Compute Singular Value Decomposition of matrix A
 * and return an instance of SingularValueDecomposition class
 * @param A Matrix A to be decompose using svd
 * @return SingularValueDecomposition object instance
 */
public SingularValueDecomposition<DenseMatrix64F> computeSVD(DenseMatrix64F
A) {
    SingularValueDecomposition<DenseMatrix64F> svd =
DecompositionFactory.svd(A.numRows,A.numCols,true,true,false);
    if( !svd.decompose(A) )
        MessageBox.display("Decomposition fail","SINGULAR VALUE DECOMPOSITION
FAIL !!!");
    if( DecompositionFactory.quality(A,svd) > 1e-3 )
        MessageBox.display("Decomposition Quality","Bad Quality Of Decomposition ");
    return svd;
}
public BufferedImage mosaic_from_multiFile(List<String> multi_fileName,
List<Homography2D_F64> list_of_Homo){

```

```

// initial homography that exist between images
Homography2D_F64 init_Homography = new Homography2D_F64(1,0,0,0,1,0,0,0,1);

// Sort and transform corner points for each image
SortedSet<Integer> xs = new TreeSet<>();
SortedSet<Integer> ys = new TreeSet<>();
if (modelType==1){
    for (int i=0; i<multi_fileName.size()-1; i++){
        try {
            BufferedImage imageA = ImageIO.read(new File(multi_fileName.get(i)));
            BufferedImage imageB= ImageIO.read(new File(multi_fileName.get(i+1)));
            xs.add(0);
            xs.add(imageA.getWidth());
            ys.add(0);
            ys.add(imageA.getHeight());

            // Compute Homography and concatenate it with initial homography
            Homography2D_F64 H = using_HarrisModel(imageA,imageB);

            // Compute Homography and concatenate it with initial homography
            Homography2D_F64 combine_Homography = init_Homography.concat(H,null);
            init_Homography = combine_Homography;

            // Add homography to the list
            list_of_Homo.add(H);

            Point2D_I32 point2D_i32_1 =
renderPoint(imageB.getWidth(),imageB.getHeight(),combine_Homography);
            Point2D_I32 point2D_i32_2 = renderPoint(0,0,combine_Homography);

            xs.add(point2D_i32_1.x);
            xs.add(point2D_i32_2.x);

```

```

        ys.add(point2D_i32_1.y);
        ys.add(point2D_i32_2.y);
    } catch (Exception err_readingFile){
        err_readingFile.getMessage();
    }
} // End for
} else if (modelType==2){
    for (int i=0; i<multi_fileName.size()-1; i++){
        try {
            BufferedImage imageA = ImageIO.read(new File(multi_fileName.get(i)));
            BufferedImage imageB= ImageIO.read(new File(multi_fileName.get(i+1)));
            xs.add(0);
            xs.add(imageA.getWidth());
            ys.add(0);
            ys.add(imageA.getHeight());

            // Compute Homography and concatenate it with initial homography
            Homography2D_F64 H = stitchUsing_SIFT(imageA,imageB);

            // Compute Homography and concatenate it with initial homography
            Homography2D_F64 combine_Homography = init_Homography.concat(H,null);
            init_Homography = combine_Homography;

            // Add homography to the list
            list_of_Homo.add(H);

            Point2D_I32 point2D_i32_1 =
renderPoint(imageB.getWidth(),imageB.getHeight(),combine_Homography);
            Point2D_I32 point2D_i32_2 = renderPoint(0,0,combine_Homography);
            xs.add(point2D_i32_1.x);
            xs.add(point2D_i32_2.x);
            ys.add(point2D_i32_1.y);

```

```

        ys.add(point2D_i32_2.y);
    } catch (Exception err_readingFile){
        err_readingFile.getMessage();
    }
} // End for
} else if (modelType==3){
    for (int i=0; i<multi_fileName.size()-1; i++){
        try {
            BufferedImage imageA = ImageIO.read(new File(multi_fileName.get(i)));
            BufferedImage imageB= ImageIO.read(new File(multi_fileName.get(i+1)));
            xs.add(0);
            xs.add(imageA.getWidth());
            ys.add(0);
            ys.add(imageA.getHeight());

            // Compute Homography and concatenate it with initial homography
            Homography2D_F64 H = stitchUsing_SURF(imageA,imageB);

            // Compute Homography and concatenate it with initial homography
            Homography2D_F64 combine_Homography = init_Homography.concat(H,null);
            init_Homography = combine_Homography;

            // Add homography to the list
            list_of_Homo.add(H);

            Point2D_I32 point2D_i32_1 =
renderPoint(imageB.getWidth(),imageB.getHeight(),combine_Homography);
            Point2D_I32 point2D_i32_2 = renderPoint(0,0,combine_Homography);
            xs.add(point2D_i32_1.x);
            xs.add(point2D_i32_2.x);
            ys.add(point2D_i32_1.y);
            ys.add(point2D_i32_2.y);

```

```

        }catch (Exception err_readingFile){
            err_readingFile.getMessage();
        }
    } // End for
}

// Mosaic Dimension declared
int lowest_x = xs.first();
int lowest_y = ys.first();
int highest_x = xs.last();
int highest_y = ys.last();
double hh = Math.pow((highest_y-lowest_y),2);
double ww = Math.pow(((highest_x-lowest_x)),2);
double work_Width = Math.sqrt(ww)+ Math.sqrt(ww)*0.5;
double work_Height = Math.sqrt(hh)+ Math.sqrt(hh)*0.5;
return renderStitching(multi_fileName,list_of_Homo,work_Width,work_Height);

//return stitch(imageA,imageB, GrayF32.class);
}

private BufferedImage renderStitching(List<String> multi_fileName,
                                     List<Homography2D_F64> counting_Homography,
                                     double work_Width, double work_Height ){
    BufferedImage output = new BufferedImage((int)work_Width,(int)work_Height,5);
    Homography2D_F64 fromAToWork;
    Homography2D_F64 fromWorkToA;
    Planar<GrayF32> work;

    // Used to render the results onto an image
    PixelTransformHomography_F32 model = new PixelTransformHomography_F32();
    InterpolatePixelS<GrayF32> interp =
    FactoryInterpolation.bilinearPixelS(GrayF32.class, BorderType.ZERO);
    ImageDistort<Planar<GrayF32>,Planar<GrayF32>> distort =

```



```

        DistortSupport.createDistortPL(GrayF32.class, model, interp, false);
distort.setRenderAll(false);
try{
    BufferedImage imageA = ImageIO.read(new File(multi_fileName.get(0)));

    // Convert into a BoofCV color format
    Planar<GrayF32> colorA =
        ConvertBufferedImage.convertFromMulti(imageA, null, true, GrayF32.class);

    // Where the output images are rendered into
    work = colorA.createSameShape()._createNew((int)work_Width,(int)work_Height);

    // Adjust the transform so that the whole image can appear inside of it
    fromAToWork = new
Homography2D_F64(1,0,work.width/4,0,1,work.height/2,0,0,1);
    fromWorkToA = fromAToWork.invert(null);

    // Render first image
    model.set(fromWorkToA);
    distort.apply(colorA,work);
    Homography2D_F64 fromWorkToB =
fromWorkToA.concat(counting_Homography.get(0),null);
    for (int i=1; i<multi_fileName.size(); i++){
        try{
            BufferedImage imageB= ImageIO.read(new File(multi_fileName.get(i)));
            Planar<GrayF32> colorB =
                ConvertBufferedImage.convertFromMulti(imageB, null,true,
GrayF32.class);

            // Render second image
            model.set(fromWorkToB);

```

```

        distort.apply(colorB,work);
        fromWorkToB = fromWorkToB.concat(counting_Homography.get(i),null);
    }catch (Exception err2){
    }
}
// Convert the rendered image into a BufferedImage
ConvertBufferedImage.convertTo(work,output,true);
}catch (Exception err){

}
return output;
}
private DenseMatrix64F getNormalized_to_centroidMatrix(){

//The matrix for normalization(Centroid)
double[][] array = {{2./width,0.,-1.},{0.,2./height, -1},{0.,0.,1}};
return new DenseMatrix64F(array);
}

// Matches comprises of both inliers and outliers
public List<AssociatedPair> getRawPairs() {
    return rawPairs;
}

// Matches comprises of inliers alone
public List<AssociatedPair> getPairsInlier() {
    return pairsInlier;
}
}

```